On the recyclability of liquid organic hydrides: Hydrogenation of 9-ethylcarbazole and other heterocyclic compounds for application in hydrogen storage

By

Katarzyna Anna Morawa Eblagon

Linacre College

MSc in Materials Science and Engineering,
AGH-University of Science and Technology,
Krakow, Poland

A dissertation submitted for the degree of Doctor of Philosophy (Inorganic Chemistry) at the Chemistry Department, University of Oxford
2011

Declaration

This thesis is the record of the research carried out by the author that has not been submitted for any previous degree or award. This work is wholly original, unless otherwise stated and where due acknowledgement is made.

Katarzyna Morawa Eblagon

April 2011, Oxford

Abstract

The main focus of the present work is the recovery process for spent fuels based on catalytic hydrogenation of liquid organic hydrides (LOH). To gain the knowledge about the possible hurdles of hydrogen loading process, the hydrogenation of 9-ethylcarbazole as a model compound was elected to be studied in more detail. The structures of the intermediates and products of this reaction were characterized for the first time using combined GC-MS and NMR analysis with reference to DFT calculations. The fully saturated product was found to be a mixture of stereoisomers. A reaction model was developed which agreed well with the experimental results. The combined theoretical and experimental approaches were also undertaken to identify catalytic sites on the metal surface and their role in the hydrogenation of 9-ethylcarbazole. Kinetically stable intermediate (Plus 8 [H]) containing a central unsaturated "pyrrole" ring was found to be accumulated in the solution over a ruthenium black catalyst. Its further hydrogenation was found to involve its unusual shuttling from terraced sites to higher indexed sites. The stability of Plus 8 [H] was found to be influenced by the type of active sites present on the surface of the catalyst, as well as by the electronic structure of the metal. In addition, the kinetics of the hydrogenation was analyzed experimentally and the activation energies were obtained for all of the intermediate steps. Further understanding of how the molecules interact with the catalyst surface was provided by examining the hydrogenation activity and selectivity of a series of LOH. The general factors involved in LOH structure-catalyst –activity trend were outlined. Overall, due to a number of defined challenges in the LOH spent fuel recharging, it is believed that this complex H_2 storage strategy is not likely to meet the targets for wide scale applications.

Acknowledgements

Writing up of this thesis was undoubtedly one of the greatest scientific challenges in my life. Several people have assisted me in this study and I wish to show my deepest gratitude to those outstanding individuals both from within university and outside, without whom this work would not have been completed.

First and foremost, I would like to thank my supervisor, Prof. S.C. Edman Tsang for accepting me as a DPhil student and providing for me an exceptional opportunity to study at University of Oxford. Additionally his guidance and academic experience have been invaluable during my research as well as in the preparation of this thesis.

I owe my deepest gratitude to Dr. K.M. Kerry Yu for his fantastic help and suggestions in analysis of the heaps of my data, correcting the manuscript of this thesis as well as for providing technical support of this project.

Mr. Daniel Rentsch from Laboratory for Functional Polymers at EMPA for his patience and enormous amount of help in obtaining the NMR analysis of the structures of reaction products and intermediates, as well as for useful corrections, discussions, comments and criticism with regard to scientific publications and the manuscript of this thesis.

I would like to thank Dr. Kin Tam from AstraZeneca for providing numerous useful discussions and help regarding data analysis, modeling of the reaction kinetics and for solving sheer endless computer problems.

I am also grateful to Dr. A.J. Timmy Ramirez-Cuesta from Rutherford Appleton Laboratory for providing his expertise in DFT calculations, sourcing a quality workstation for me and first and foremost organizing the funding for this research.

I thank Dr. Peter Harris from University of Reading for his friendship and for allowing me to use the TEM and SEM facilities at University of Reading as well as for providing his expertise in microscopy and helping me to obtain fantastically sharp TEM images.

I am grateful to Prof. Heyong He of Fudan University, China for inviting me to work alongside with his group. Climbing Great Wall was an unforgettable experience for me. I thank Prof. He for his kindness and assistance in every way during experiments, including TPR, HRTEM and XPS data collection. I am also very grateful to the members of Prof. He group; particularly to Ms. Lin Ye for her friendliness and great help during my stay in China. Additionally, I would also like to acknowledge Dr Lu-Cun Wang from Fudan University for providing his expertise during IR-CO chemisorption experiments.

Mr Shu-Lei Zhao and Prof. Xue-Quing Gong from East China University of Science and Technology are acknowledged for their DFT calculations of the enthalpies of adsorption and their help in analyzing the results.

Prof. Andreas Zuettel is thanked for inviting me to work at EMPA Swiss Federal Laboratories for Materials Testing and Research in Switzerland and for funding my stay there. I would also like to thank Dr. Oliver Friedrichs from Department of Hydrogen and Energy in EMPA for his comments on analysis of the hydrogen absorption curves and technical assistance during the high pressure hydrogenation experiments.

Dr. Teresa Valdes-Solis from Instituto Nacional del Carbon in Spain is thanked for for her friendship, support and guidance in my experiments, corrections of my presentations and publications, as well as very fruitful discussions concerning data analysis.

Dr. Sarah Lee from CRL for her time, friendliness and detailed discussions on separation techniques as well as for the endless TLC tries. She indeed impressed me with her

knowledge and determination during otherwise very frustrating, tedious and at the end disappointing set of experiments.

Dr. Stewart Parker from Rutherford Appleton Laboratory for his expert comments on DFT calculations using Gaussian software and his help during my visits at RAL and also

Dr. Chris Stain from University of Reading is thanked for his assistance in TEM imaging.

Thanks to Dr Adam T.S.Kong and Dr Connie M.Yu Yeung for their help in the lab and their comments concerning data analysis during my first year of studies at Reading University.

I would like to thank University of Oxford and STFC for financial support. UK e-science centre STFC (Scarf) is acknowledged for providing computing resources for this project.

I am also indebted to my friends who supported my four years of this research in many ways. I would like to thank Wiliam Owusu Oduro and Igor Curcic for their friendship, guidance, advice on my results, careful and patient ear and encouragement and for helping me to survive all of the difficult times during this project. Thank you guys for being there for me!

I am also grateful to my colleagues from Tsang Group at ICL Oxford; J. Xu for helping in TPR analysis, Nadia Acerbi for her help in chemisorption experiments, K. Tedsree for useful comments concerning IR assignments, T. Chapman for his help in the lab and for reviewing my papers and W. Tong for his kind help with the BET measurements.

I would like to thank Mr Tom Bradshaw from the Chemistry IT Support Team from University of Oxford for his kindness and for significant help in the ‘last minute’ corrections and formatting of the present thesis.

Dr Nick Brown from Linacre College, Dr Nicholas Green and Ms. Aga Borkowska from Inorganic Chemistry Laboratory at Oxford for their friendliness, support and kind advice before, during and after my maternity leave.

I would like to thank my examiners, Prof. Ian S Metcalfe from Newcastle University and Prof. John Foord from University of Oxford in advance for their time spent in reviewing this work and for finding time to examine me during summer hollidays.

Outside the lab many people have kept me sane and happy. Among them, I thank specially Tugce Eralp, Magda Balonis, Marta Krysmann, Ula Kacprzak, Martin Arraigada, Jonathan Morrell and Magda Pawelkiewicz.

Specjalne podziękowania należą sie moim najbliższym; Rodzicom i mojej kochanej Babci Irenie za ich nieopisaną pomoc, miłość i wsparcie.

Special thanks to my biggest gift from life, my little angel Mateusz Alejandro, for being such a very special 'low impact' baby and a constant source of joy and motivation for writing up of this thesis.

On a special note, I would like to thank my husband, Fernando for being my shadow and my light. He has always loved me, supported me, encouraged me at every step and has been able to make me laugh when the times were rough. Thanks to his support I have managed to concentrate my efforts on writing up this thesis. He provided me with academic guidance and advice and I am intellectually indebted to many of his ideas and insights. This thesis is dedicated to him.

Contents

1. Introduction

1.1. Hydrogen as a future energy carrier

Mobility has always been a crucial and fundamental need of the society. Unfortunately, most of the today's used light duty cars are powered by internal combustion engine (ICE), thus they are heavily dependent on fossil-fuels derived energy (1). Finding an abundant and inexpensive alternative energy supply is inevitable for sustaining the further development of worldwide economy. It is also vital to take into consideration the fact that fossil fuels are not renewable sources of energy and therefore will be soon depleted. In addition, burning fossil fuels has detrimental environmental effects such as increasing the concentration of carbon dioxide and other pollutions in the atmosphere. It is clear that for stationary applications, the produced CO_2 can be cheaply sequestered (2) nevertheless for portable energy, carbon dioxide capture is impractical (3). With this scope, hydrogen is proposed as an alternative, independent, clean and recyclable energy carrier for the future.

1.1.1. Hydrogen- physical and chemical properties of the fuel

The name 'hydrogen' comes from the greek words meaning water generator. Hydrogen is the most abundant and the lightest natural element on Earth. Due to its low mass, it has the highest chemical energy to mass ratio of all the elements. Since chemical energy is based on the energy of unpaired valence electrons (4), compared to petroleum, the energy content of hydrogen is almost three times higher on the weight basis (120 MJ kg^{-1} for hydrogen versus 44 MJ kg^{-1} for petroleum) (3). Furthermore, hydrogen is a renewable, ecologically clean and carbon free energy carrier that can be produced directly from solar light or indirectly via electricity from a renewable sources. In addition, hydrogen can be used directly to power fuel-cells, which greatly increases efficiency over ICE (increase of 32 %

for diesel-electric, 90% potential efficiency for fuel cell with heat capture, 85% for electric motor, 77% overall efficiency) (3). In addition, direct comparison of gasoline and hydrogen shows that 3 kg of gasoline liberates upon combustion; 9 kg of CO_2, whereas 1 kg of hydrogen liberates the same amount of energy without any emissions of carbon dioxide (5).

1.1.2. Are there any drawbacks of hydrogen economy?

Hydrogen is the smallest, lightest element and one of the first building blocks of life (6). However, like electricity, hydrogen is an energy carrier, not an energy source and therefore needs to be produced. In order to fully release the benefits of hydrogen, it has to be produced from renewable energy sources. Therefore, there are many technical and economic barriers to overcome before hydrogen economy can be implemented. Firstly, in order to implement the hydrogen economy, the society has to be ready to pay for the energy content of the fuel (7). Furthermore, there are some technical problems associated with using hydrogen as a fuel such as: safe and efficient storage and effective combustion (8). Hydrogen has a very low boiling point and a high low heating value which make it inherently expensive to transport and distribute (9). In addition, hydrogen has a reputation of being dangerously explosive. This concern arose from the reported controversial accident of the German airship Hindenburg in 1937 and the explosion of American Challenger space shuttle in 1986 (7). It is clear that hydrogen has to be handled with extreme care because of the fact that a broad range of its mixtures with air would burn (from 4% -75% of the volume of hydrogen in air as compared to only 1% -8% by volume of petrol in air) (10). In addition, hydrogen is a colourless gas that burns with odourless, invisible flames (11). However, the main problem with hydrogen as a fuel for transportation is that it has extremely low volumetric density (5). Hydrogen has only 1/10 of energy compared with gasoline in the same volume (12). As a result, a minimal amount

of 5 kg of hydrogen sufficient to cover a driving range of 300 miles, under normal conditions (atmospheric pressure and room temperature) takes over a space equal to the balloon with 4.8 metres in diameter (10). Therefore, in order to fit the necessary amount of hydrogen on-board of a car, the hydrogen gas would have to be pressurised up to 700 bar. Additionally, the low melting (-259 °C) and boiling (- 253 °C) points of hydrogen add complexity to its use as a fuel (13). Therefore, clearly one of the greatest technological challenges in the mobile application of hydrogen fuel cell technologies is on-board storage of hydrogen in the most compact way.

1.2. Hydrogen storage

In order to reduce the great volume of hydrogen gas, work has to be applied to either compress it, liquefy it or the repulsion between hydrogen molecules can be minimised by interaction of hydrogen with other material (8). The main approaches to the storage of hydrogen are depicted in Figure 1.1.

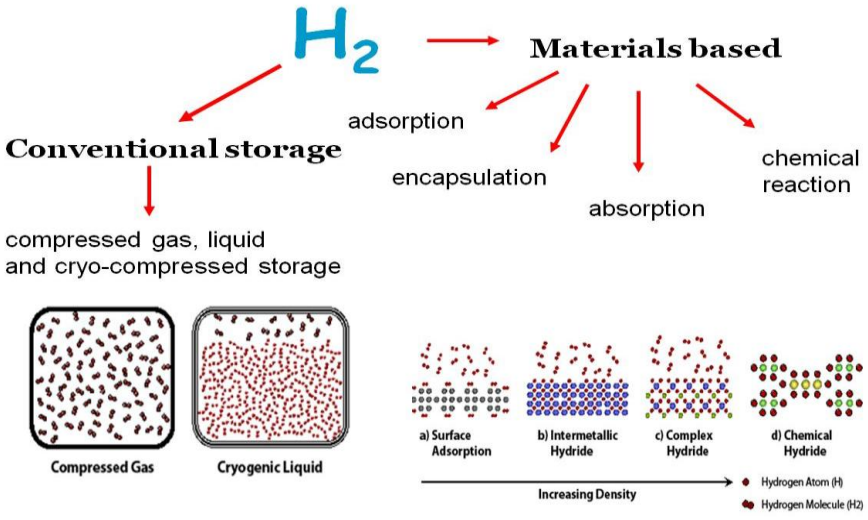

Figure 1.1. Main mechanisms of hydrogen storage (8) (7) (10) (14).

Apart from conventional storage techniques such as compressed gas or liquid, there are four generic mechanisms to store hydrogen such as absorption, encapsulation, adsorption

and chemical reaction. In absorption (chemisorption), hydrogen molecule interacts chemically with the host material, dissociates on its surface (10) and subsequently the hydrogen atoms are absorbed into the bulk of the material where they can form different types of bonds as shown in Figure 1.1. On the other hand, in encapsulation, the hydrogen molecule is contained within the solid structure of another material and can be released upon a change in the thermodynamic conditions (15), whereas in adsorption, the hydrogen molecule is weakly bonded to the surface of the material (16). Additionally, the chemical reaction route of storing hydrogen involves reversible chemical reaction where hydrogen is produced or stored by modest changes in temperature and pressure (17). In this mode of hydrogen storage, the hydrogen can be generated on-board, but the loading of the material is bound to take place off-board of the car.

1.2.1. Challenges of onboard hydrogen storage for transportation

Finding a sufficiently compact way of storing enough hydrogen on-board of the vehicle is the most complicated demand still awaiting solution. The comparison of weight and volume of different fuels and tank systems required to store enough energy for a light-duty passenger car to travel 500 km is shown in Figure 1.2.

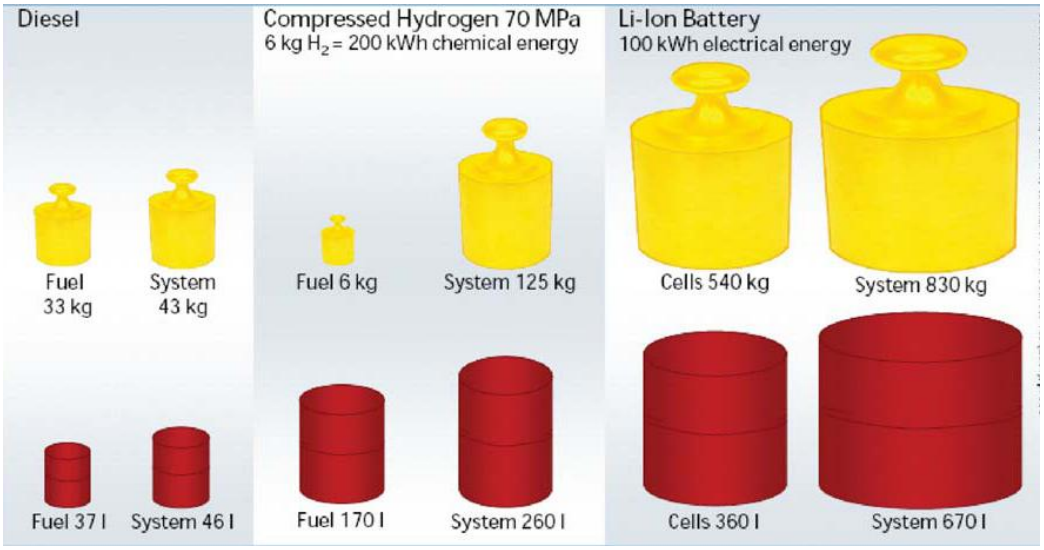

Figure 1.2. Comparison of a weight and volume specifications of different energy storage systems for mobile applications for equivalent driving ranges (18) (19).

To guide the efforts of the emerging technologies, the US Department of Energy (DOE) in collaboration with the automotive industry has established a revised set of technical targets for onboard hydrogen storage systems in 2009 (20). A list of selected DOE targets for onboard hydrogen storage in light-duty vehicles is shown in Table 1.1. It is essential that all of these targets are met simultaneously by the same storage media. Moreover, it should be underlined that the set of targets is outlined for a complete system, including tank, material, valves, regulators etc. Thus, in order to completely replace gasoline in ICE cars across the entire light duty vehicles, about double of the values listed in Table 1.1 would be required (21).

Table 1.1 DOE technical targets for onboard hydrogen storage systems set in 2009 (1) (22) (23).

Storage parameter	2010	2015	Ultimate
System gravimetric capacity [wt % H_2]	4.5	5.5	7.5
System volumetric capacity [g H_2/L]	28	40	70
H_2 max/min delivery temp [°C]	-40/85	-40/85	-40/95
System fill time (for 5 kg H_2) [min]	4.2	3.3	2.5
Operational cycle lifetime (from ¼ to full tank) [cycles]	1000	1500	1500
Loss of useable H_2 [(g/h)/kg stored]	0.1	0.05	0.05

The operating temperatures of the storage are dictated by the operating temperature of a fuel cell and the weather conditions. Therefore, the preferable temperature of hydrogen desorption from the storage media is in the range of maximum 70-80 °C. The refuelling time of a storage system is also an important factor and must be similar to the time required for gasoline powered cars for the hydrogen to be widely accepted as a fuel (24). Thus kinetics and thermodynamics of the system have to allow fast reversible loading and unloading. On the other hand, the hydrogen loss factor protects against the decrease of driving range of the FCV (fuel cell vehicle) after extended periods of rest like parking of the vehicle. At the loss of 0.1g of hydrogen per hour, a full tank will require more than a year to empty (16). However, apart from the material performance, the cost of the storage system is the most important driving factor in the development of hydrogen storage technology.

1.2.2. How far are the DOE targets?

The targets outlined by DOE represent hydrogen storage system performance that could result in the full FCV penetration into light duty market across all the range of manufacturers and cars designs (22). The current status in terms of weight and volume of various hydrogen storage technologies is shown in Figure 1.3 together with the revised DOE targets and estimated cost.

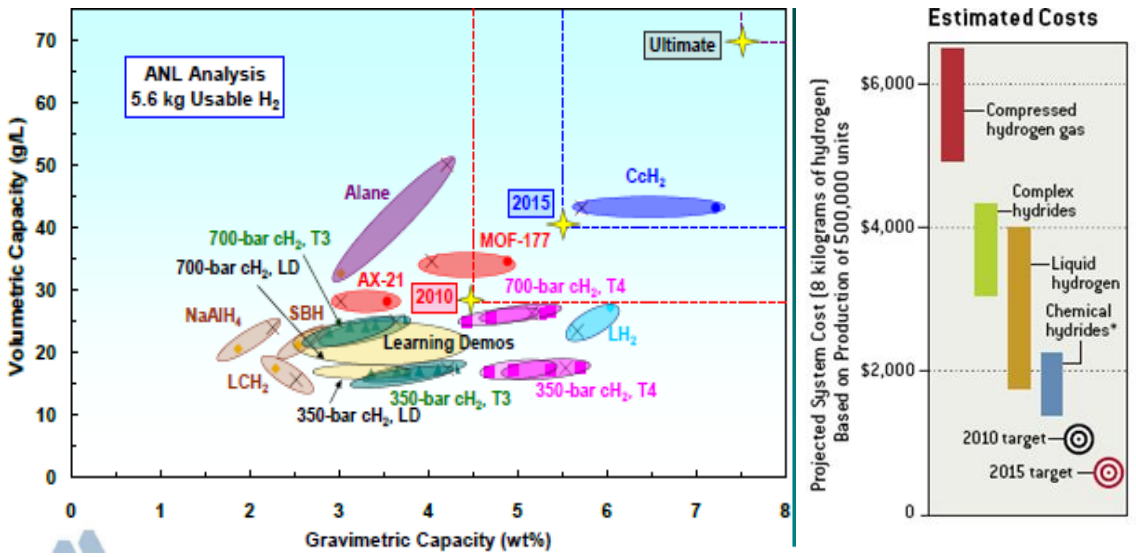

Figure 1.3. Current state of the art for on-board hydrogen storage technologies versus revised DOE targets (left) and estimated cost of the different ways of hydrogen storage (right). The values are estimated from storage system developers and R&D communities that cooperate with DOE. (Learning Demo' data shows a range of 138 vehicles with 350-700 bar systems) (16) (25).

As it can be seen from Figure 1.3, the only technology close to meeting the DOE targets for 2015 is storage of hydrogen as a cryo-compressed gas. However, due to the complexity of the design of high pressure hydrogen tanks and the quality of materials required, this method is not likely to meet the cost targets as it is depicted in Figure 1.3 (right).

1.2.3. Physical storage of hydrogen

The conventional methods to store hydrogen are the most advanced in development and the most appealing due to their simplicity and familiarity of the concept (21). These techniques include storage of hydrogen as a compressed gas (GH_2) at 35-70 MPa and at room temperature (26), and cryogenic storage of hydrogen as liquid (LH_2) at 20 K- 30 K and 0.1-1 MPa (8). Another physical way of storing hydrogen is using insulated cryogenic vessels operating at 20 K and high pressure of at least 24 MPa. These vessels can be filled with liquid hydrogen, cryogenic GH_2, or ambient temperature GH_2 (27).

1.2.4. Materials based hydrogen storage

The safe and compact storage of hydrogen in a solid medium has the potential to be a superior option to compressed gas storage or liquid hydrogen storage (28). The biggest challenge is to find a material for hydrogen storage that would simultaneously fulfil three competing targets: high hydrogen density (which requires strong chemical bonds and close atomic packing), reversibility at moderate temperatures (weak, breakable bonds) and fast hydrogen charge and release (loose atomic packing and adequate thermal conductivity to prevent decomposition) (29). Unfortunately none of the considered materials up to the date was capable to satisfy all of the criteria simultaneously. The following sections will briefly summarize the state-of–the-art of some of the most promising material based hydrogen storage solutions and the general progress of technology towards meeting the DOE goals set for 2015.

1.2.4.1. Physical adsorption

Physical adsorption is the weakest possible interaction between hydrogen molecule and the surface of the material and it is governed by resonant fluctuations of the charge distributions, known as Van der Waals forces. Thus, the heat of adsorption of hydrogen on the surface of porous materials is in the range of 4-10 $kJ/mol^{-1}H_2$ (24). In general, the amount of hydrogen adsorbed is proportional to the specific surface area of the adsorbent defined by BET measurements.

Storage in carbon materials

Carbon materials are interesting sorbents to consider for hydrogen storage due to their low densities, high porosities and high specific surface areas, good chemical stability and great variety of possible structural forms (30). Carbon nanotubes can take up to 8 wt % of hydrogen at 120 bar and cryogenic temperatures, but the binding energy is far too low to allow any significant uptakes at ambient conditions (21). For single wall carbon nanotubes (SWNT), hydrogen uptakes of 1% were reported at 80 bar and at room temperature. The uptake was decreased to only 0.1% with decreased pressure to 2 bar (24). For the low density charcoal, reversible uptakes of 4-5 wt % at 4 bar and 65-78 K were reported (31). Carbon nanofibres showed hydrogen storage capacities of 5-10 wt % at room temperature and moderate pressures (32). To sum up, it is very unlikely that technical targets for mobile hydrogen storage materials will be reached by carbon based sorbents.

Zeolites

Zeolites are aluminosilicates or aluminophosphates, possessing microporous framework, with a pore size around the size of the hydrogen molecule. For the highest micropore zeolite to the date (ITQ-33), the maximum storage capacity of 2.5 wt % at liquid nitrogen temperature was reported (38). Thus, it can be expected that zeolites will not be suitable for storage of hydrogen in transportation. Nonetheless, there is a new direction emerging from this field, which is using zeolites as a template structures to form carbon networks. Recently, promising results have been reported for zeolite like materials achieving 6.9 wt % at 77 K and 20 bar (3).

Metal organic frameworks (MOFS)

Metal organic frameworks consist of metal ions as vertices connected by organic molecules, which are often polyvalent carboxylic acids or nitrogen donor linkers (18). Similarly to carbon based materials, only low hydrogen uptakes were reported for MOFS at 77 K and 1 bar of pressure, reaching a maximum of 1.32 wt % (33). Further research on this group of materials is ongoing, focusing mainly on the influence of the framework structure on the mechanism of hydrogen sorption.

Polymers with intrinsic microporosity (PIMS)

In PIMS, pores are formed as a result of inefficient packing of rigid polymer subunits. These polymers are generally structures similar to large pieces of broken glass (34). The gravimetric storage capacities of PIMS are similar to those obtained by MOFS and reach up to 3 wt % at 77 K and 15 bar (3). Slightly more promising values were reported for polymeric material based on a triptycene monomer that is capable of storing 2.7 wt % of hydrogen at 1 bar and 77 K (1). Overall, the obtained values of hydrogen uptake by PIMS are not outstanding, however with the wide possibility of synthesis methods and high BET surface areas, further developments in this field can be anticipated.

1.2.4.2. Encapsulation

Encapsulation is a rather new approach towards hydrogen storage that is receiving increasing attention. It is based on the idea of trapping hydrogen gas molecules inside the guest (solid) structure that results in the formation of a clathrate. The hydrogen can be released from such structures by a change in temperature and pressure (15). The main drawback of this class of materials is that they are only stable at very high pressures of 2000 bar at 280 K (35). In general, clathrates do not seem to be able to reach the targets of DOE hydrogen storage materials due to their slow kinetics and low hydrogen capacity.

Nevertheless, valuable information gained from studying the behaviour of confined hydrogen molecules will be helpful tool in the design of new inclusion materials for this application (36).

1.2.4.3. Chemical storage

Chemical storage of hydrogen is based on the use of materials that bond hydrogen via strong chemisorption process (typically >10 kJ/mol H_2) (5). Many metals, alloys and intermetallic compounds are capable of reversibly absorbing large amounts of hydrogen, forming hydrides (8). There are two types of metal hydrides; reversible- in which hydrogen uptake and release is taking place on-board of the vehicle and 'non-reversible'- in which the hydrogen upload (fuel regeneration) must take place in a chemical plant. Furthermore, within metal hydrides there are generally two groups of compounds: elemental metal hydrides (10) and complex metal hydrides (5). Apart from metal hydrides, there are boron and nitrogen based compounds, that have also demonstrated the potential of meeting DOE requirements in the near future.

Metal hydrides

One of the most studied conventional metal hydride is MgH_2 (8) (15). It has high hydrogen content of 7.6 wt % along with the highest energy density of all reversible hydrides (9MJ/kg Mg) (1). Nevertheless, practical application of magnesium is hindered by the fact that the hydrogenation/dehydrogenation reactions are very slow. In addition, because of the high bond formation enthalpy value (75 kJ/mol), it requires unacceptably high hydrogen release temperatures (350°C- 400°C). Moreover, magnesium is not stable in air and oxidizes exothermically to form MgO or $Mg(OH)_2$ which do not adsorb hydrogen and additionally effectively block its diffusion into the bulk of the hydride (37). However, very recently, a significant breakthrough towards using magnesium as a hydrogen storage

material has been achieved by Jeon et all (38) who developed a new, simple method of producing air-stable magnesium based composite material for hydrogen storage. The measured absorption isotherm showed the maximum hydrogen uptake of 4 wt % based on the overall composite mass with considerably rapid kinetics (hydrogen absorption in 30 min at 200 °C).

Aluminium hydride AlH_3 (alane) is also widely investigated for the possible applications in vehicular hydrogen storage because of its high hydrogen uptake capacity of 10.1 wt % and high hydrogen density of 1.48 g/ml (39). However, due to weak binding energy (1), the pressures required to regenerate alane at room temperature approached 700 bar (40). In addition, aluminium hydride is very reactive towards air and water, which results in several difficulties in handling and regenerating the spent fuel off-board of the vehicle.

Complex hydrides

Complex hydrides generally consist of lightweight alkali/alkaline earth cations such as Li, Mg, Ca and hydrogen containing complex anions such as borohydrides (BH_4^-), alanates (AlH_4^-) and amides (NH_2^-) (1).

Borohydrides

Among borohydrides, $LiBH_4$ is definitely the most attractive candidate for hydrogen storage due to its very high theoretical gravimetric and volumetric hydrogen capacities of 18.5 wt % H_2 and 120 g H_2/L (8). $LiBH_4$ decomposition produces lithium hydride, boron and releases 13.5 wt % of hydrogen (5). However, hydrogen desorption from this compound is highly endothermic and requires higher temperature than 380 °C to take place.

Another example of complex borohydrides is the most commonly used $NaBH_4$ with 10.8 wt % of theoretical hydrogen uptake capacity. The thermal decomposition of sodium borohydride is at the region of 400 °C which is also too high for mobile applications (24). $NaBH_4$ additionally produces $NaBO_4$ as a byproduct during hydrogen release which poisons the fuel cell catalyst and destroys the membrane (41).

Aluminum hydrides (alanates).

The most studied lightweight complex aluminium hydride is $NaAlH_4$ having reversible hydrogen uptake capacity of 5.6 wt %. Like most of the other complex aluminum hydrides, $NaAlH_4$ decomposes in three steps mechanism; first step takes place at 30 °C and releases 3.7 wt % of hydrogen, and the second step releases 1.9 wt % at 130 °C. The decomposition temperature of a third step (around 500 °C) is far too high for mobile application (18). The main problems associated with commercial application of $NaAlH_4$ for hydrogen storage are: unfavourable thermodynamics (24) and its lack of reversibility under moderate conditions (42). Overall, it is clear that the theoretical gravimetric capacity of this hydride is too low for applications in transport. However, it could be used to power smaller scale electronic units such as mobile phones or laptops.

Amides

Another interesting approach towards hydrogen storage is using amide/imide compounds of lightweight elements. Li_3N can theoretically store 10.3 wt % of a reversible reaction. In addition, more than 11 wt % of hydrogen was recorded to desorb from a mixture of $LiNH_2$ and $LiBH_4$ at temperature range of 250-350 °C (43). The attempts are undertaken to decrease the temperature of hydrogen release from these systems by applying catalysts such as Pd, Pt and ball milling (43), or substitution with more electronegative elements such as Mg^{2+} cations (18). One of the biggest issues concerning the use of amides based

storage systems which may hinder their commercial application is the production of trace amounts of ammonia during the decomposition step, which is known to have detrimental effect on PEM fuel cell.

Boron-nitrogen compounds

B-N compounds are very attractive candidates for hydrogen storage due to the fact that these lightweight elements are capable of holding multiple hydrogen atoms.

Amonia-borane

Ammonia-borane (NH_3BH_3) has a high hydrogen content of 19.6 wt %- which exceeds even that of gasoline (28). The hydrogen from NH_3BH_3 can be released at temperatures from

90 °C- 500 °C (41) in a multistep process (18), which produces several intermediates such as iminoboranes, traces of diborane and small fractions of borazine. The biggest disadvantages of ammonia-borane system are: a long induction time before the release of hydrogen (200 min at 80 °C), high decomposition temperatures (3) (5) (18) (41), expensive production process and a lack of recycling methods of the spent fuel (reaction products) back to hydrides (44).

1.2.4.4. Hydrogen storage via chemical reaction

Some metals and alloys are capable of producing hydrogen in water or alcoholic based solutions. The reported systems include: aluminium powder, scraps of magnesium waste, MgH_2-X (X= Ca, Li) composites and Mg-La systems (45). The hydrolysis reaction can be initiated on demand by contacting the substrate with a catalyst in the basic solution. The highest expected capacity of the fuel based on $NaBH_4$-H_2O is 10.8 wt % of hydrogen and

H_2O provides half of the hydrogen. The main hurdle of this reaction is the fact that the rate of hydrogen evolution decreases drastically with time leading to only a percentage of theoretical yields being produced. Another significant drawback is a lack of an efficient way to recycle the $NaBH_4$ fuel.

Using liquid hydrogen carriers known as liquid organic hydrides (LOH) is a relatively novel approach towards hydrogen storage by means of chemical reaction. The present work is focused on the aspects of possible utilization of these systems for hydrogen storage; therefore this approach will be described in more detail in the following chapter.

1.3. Hydrogen storage using liquid organic hydrides (LOH)

LOH rely on storing hydrogen during reversible hydrogenation / dehydrogenation of pairs of cycloalkanes and arenes (46). It was estimated that with a weight capacity of 7 wt % of the organic carrier, 5 kilograms of hydrogen could be contained in 70 litres of a liquid carrier, offering a very attractive solution for hydrogen powered vehicles (47). The cycloalkanes mostly studied in the literature include; cyclohexane, decalin, bicyclohexyl, methylcyclohexane, methyldecalin etc (48). Some of the typical reactions together with endothermic energy requirements are shown in Figure 1.4. These systems are attractive due to good gravimetric and reasonable volumetric storage capacities as listed in Table 1.2.

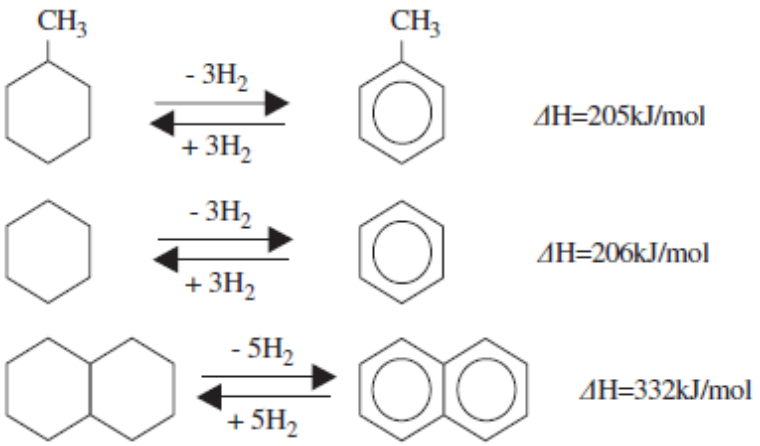

Figure 1.4. Hydrogenation and dehydrogenation of the most typical organic chemical hydrides : from the top- methylcyclohexane- toluene, middle: cyclohexane-benzene, bottom; decalin-naphtalene (49).

Table 1.2 Hydrogen storage capacity of selected organic liquids.

Liquid organic carrier	Hydrogen content	
	wt %	***mol/L***
Cyclohexane	7.2	27.77
Methylcyclohexane	6.2	23.29
cis-decalin	7.3	32.44
trans-decalin	6.6	31.46
cis—syn-1-methyldecalin	6.6	29.31
trans-anti-1-methyldecalin	6.6	28.52

Furthermore, most of these carriers are liquid under ambient conditions. Therefore, they offer a cost effective solution, due to the fact that the existing gasoline infrastructure can be used for utilization of these fuels (18). In addition, liquid organic hydrides are easier and safer to handle than metal hydrides, since they are relatively inert to air and moisture (50).

1.3.1. Liquid hydrogen carriers in powering PEMFC cars

Liquid organic carriers are not considered to be reversible on-board of the vehicle, but will require an off-board regeneration in the power plant, preferably the same that would be

handling hydrogen production (refinery) (51). In the LOH approach, liquid organic carriers such as decalin will be produced using sustainable technology based on biogas derived from sewage or biomass (52). Subsequently, the hydrogen rich liquid carrier will be supplied on-board of the vehicle. The hydrogen will be produced on-board of the vehicle using a catalytic converter and will eventually yield hydrogen-poor material. The dehydrogenated carrier will be transported back to the centralized facility to be recharged (47). The novel hydrogen storage infrastructure based on delivery of liquid hydrogen carrier, fuelling and onboard dehydrogenation process is shown in Figure 1.5.

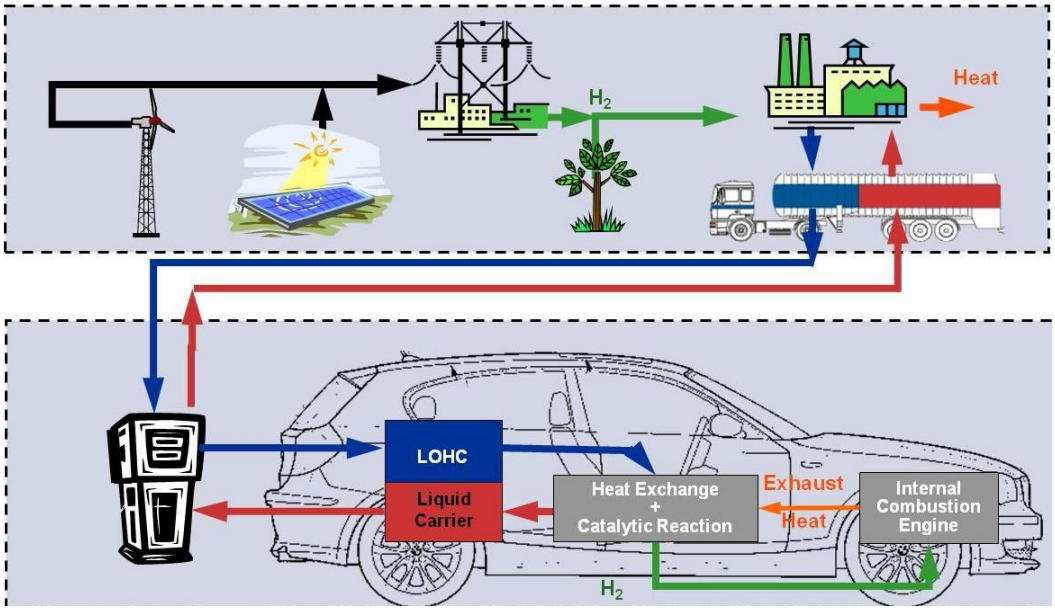

Figure 1.5. Vision of a sustainable hydrogen economy utilizing LOH as an alternative solution for hydrogen economy (53). LOHC- liquid organic hydrogen carrier.

1.3.2. Catalytic hydrogen release

The use of catalysis was considered to improve the kinetics of the hydrogen release step of typical cycloalkanes such as cyclohexane. Finding the appropriate catalytic system for this application is not easy due to the possibility of coke formation (18). Furthermore, rapid removal of the hydrogen atom and aromatics has to take place in order to avoid the reverse reaction on the surface of the catalyst (54). The reported catalysts for hydrogen release from organic hydride include: molybdenum based catalysts (55), noble metals catalysts

such as Pt, Rh., Ru, Ir, Pd (56), bimetallic catalysts such as Pt-Pd (57) supported on variety of different carriers including alumina, zeolites, carbon nanofibres (58) and activated carbon (48). Nevertheless, research showed that despite the presence of the active noble metal catalyst, the endothermic nature of the arene formation from cycloalkanes is such that the temperatures required for hydrogen to be released are prohibitively elevated (50). The temperatures obtained in catalytic reactions were in the range of 250-500°C for typical cycloalkanes (59), (55), (49). This range of temperatures is still greatly exceeding the working temperatures of the traditional PEM fuel-cells (± 80 °C) (60) as well as the DOE targets for the hydrogen carrier (see Table 1.1). In order to increase the rate of hydrogen production, several different experimental set-ups for dehydrogenation reactions have been explored, such as non-equilibrium "liquid film state" (61), or spray-pulsed reactor (62).

1.3.3. Rational design of the structure of the carrier

Another possible way of lowering the endothermicity of hydrogen liberation is to modify the structure of the liquid organic carrier (50). This approach was first undertaken by Pez, Scott and Cheng from Air Products and resulted in a series of patents and presentations (63) (51) (64) (65). Hydrogen release from a wide range of aza and poly-aza heterocycles has been studied both experimentally and computationally (47) (65) (66) in order to establish the relationships between the structure of the compounds and kinetics and thermodynamics of hydrogen liberation. This extensive research led to discoveries of the general trends in the carrier structures that govern the dehydrogenation step in liquid organic carriers. The ideal interaction between hydrogen and the carrier has to be in the range of weak to moderate chemisorption (ΔH= 40-60 kJ/mol H_2), for the dehydrogenation step to be feasible at moderate temperatures (67). The enthalpy of dehydrogenation was found to decrease with the increasing number of fused aromatic rings. Additionally, it was found that the heteroatom substitution, particularly by nitrogen (50), favours lower

temperature for hydrogen release, both thermodynamically and kinetically, permitting the dehydrogenation to take place even at 110 °C (66). However, placing a heteroatom within the conjugated rings was suggested to be the most powerful technique towards lowering the enthalpy of dehydrogenation (67) (68). In addition; the thermodynamics of dehydrogenation of a liquid carrier can be improved by the addition of electron donating groups and/or by the presence of conjugated external substituent (68). Nevertheless, the largest difference in dehydrogenation temperature was found to be introduced by moving from a 6-member ring towards a 5-member ring due to the fact that in a 5 member rings, aromaticity can be achieved much easier (66). Taking into consideration these findings, several compounds were taken into account as candidates for liquid organic carriers. Selected LOH are gathered in

Table 1.3. As it can be seen from this table, the gravimetric capacity of hydrogen uptake of most of these liquid organic carriers is satisfactory, however in order to meet the targets for mobile applications, new carriers should be discovered with the possibility of absorbing more hydrogen atoms per one heavy atom (50).

Table 1.3. Selected heterocycles considered as candidates for liquid hydrogen carriers (67) (63) (47) (3) (18) (69) (70). (t) theoretically possible capacity, (e) experimentaly obtained capacity, operating temperature for hydrogen liberation step.

Hydrogen carrier	***Capacity (wt %)***	***Catalyst***	***Operating temperature (°C)***
Coronene	5.1 (t) 3.6 (e)	Rh/C	150
Phenylenecarbazole	6.9 (t) 6.2 (e)	Pd/Al	225
Phenanthroline	7.2(t) 6.8 (e)	Pd/C	230
Dibenzofuran	6.7 (t) 4.0 (e)	Pt/Al_2O_3	225
1,2 dihydro-1,2-azaborine	7.1(t) 4.0(e)	Pd/C	>80
9-ethyl-carbazole	5.7(t) 4.5 (e)	Ru/C	197
9-methyl-carbazole	6.2 (t) 6.0 (e)	Pt/γ-alumina	200
Terphenyl	6.0 (t) 2-2.9 (e)	Pt/C	320

The present work will be focused on hydrogenation step in hydrogen storage approach using LOH. Therefore, a short overview of state-of –art of hydrogenation of arenes will be presented next.

1.4. Hydrogenation of aromatics

The study of hydrogenation of organic molecules have recently gained increased attention not only in LOH hydrogen storage applications but mainly because of the fact that reduction of aromatics can drastically improve the cetane number of the fuel and eliminate or decrease the harmful emissions of particulates from diesel fuels (71).

1.4.1. A quick glance at the structure of heterocycles

Interpretation of the reactivity of any aromatic compound is tightly dependant on its molecular structure. The most common aromatic; benzene is known for its extraordinary stability towards substitution reactions and extremely low reactivity towards any addition reactions under moderate conditions. It is well known that the difference in reactivity between benzene and alkenes is due to the cyclic arrangement of the six π-electrons, which forms an extremely stable conjugated molecular-orbital system. In addition, the geometry of the benzene ring with the angles of 120 ° results in assembly of a δ-skeleton of six sp^2 hybridized carbon atoms in a completely strain-free planar ring (72). The electrons of the double Π-bonds oscillate between adjoined carbon bonds. This delocalization of the charge leads to a resonant stabilisation of the structure. Therefore, the geometry of the benzene ring can be described as "resonance hybrid". It should be noted that the resonant energy of bicyclic aromatic compounds such as naphthalene is considerably lower than resonance of a corresponding monocyclic compounds, making the polycyclic compounds more reactive (73). There is a group of heterocyclic compounds with a structure analogous to that of benzene. One of the typical compounds of six-Π-electron heterocycles is pyridine.

However, there are some distinct differences between the structure of benzene and pyridine, the most important being: the replacement of carbon with nitrogen results in distorted geometry from regular hexagonal arrangement, replacement of the hydrogen in the plane of the ring with a lone pair of electrons and the appearance of strong permanent dipoles as a result of differences in electronegativity (72). The permanent dipole towards the nitrogen atom makes the carbon atom electron-deficient; therefore pyridine is referred as an 'electron-poor' heterocyclic molecule. The electronic structure of pyridine as compared to benzene is shown in Figure 1.6. In general, the degree of aromatic character of the monocyclic analogous of benzene decreases with increasing number of ring heteroatoms (74). Therefore, pyridine is easier to hydrogenate than benzene.

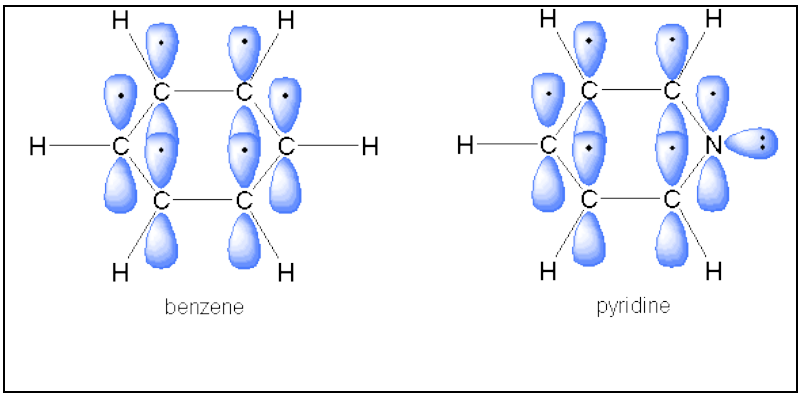

Figure 1.6. Comparison of the electronic structures of benzene and pyridine (75)

Apart from the six-Π-electron heterocycles, there are also planar structures containing five atoms having an uninterrupted cycle of p-orbitals forming a Π-orbital with a total of six electrons. An example of the five member aromatic heterocycles is pyrrole. Pyrrole has one carbon atom substituted with an sp^2 hybridized nitrogen. In the geometry of pyrrole (see Figure 1.7), three δ-bond of nitrogen are situated in the plane of the molecule, whereas the remaining lone pair of electrons from nitrogen is situated on the p-orbital, orthogonal to the plane. However, unlike in the case of pyridine, the lone pair of electrons on nitrogen interacts with four p-orbitals on the carbon atoms leading to the formation of a cyclic Π-electron system. The perturbation of the system brought about by the introduction of

nitrogen results in the electron density being higher on all of the carbon atoms as compared to benzene, but highest around nitrogen. Due to this electron distribution, pyrrole unlike pyridine, is considered a Π-excessive aromatic heterocycle (73). Generally, within the five membered ring heterocycles, the aromaticity of the compound decreases with increasing electronegativity of the heteroatom. In addition, all five-membered ring heterocycles show some signs of bond delocalization, however this delocalization is smaller than in the case of six-membered ring heterocycles (72) (74).

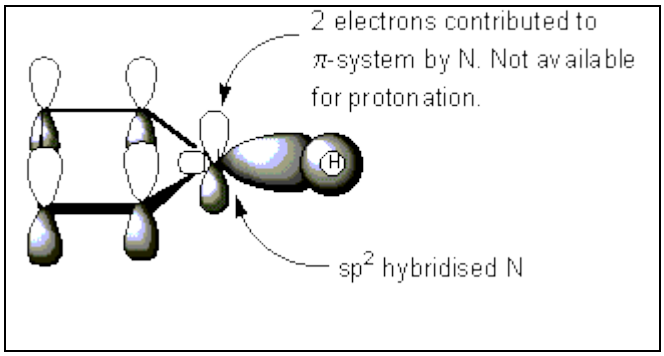

Figure 1.7. Electronic structure of pyrrole (76)

The structure of the model molecule 9-ethylcarbazole-studied in the present work contains the 'pyrrole' ring fused between two six-membered aromatic rings. The aromaticity of the system is decreased by the conjugation of multiple rings as well as by the presence of the heteroatom in the structure. Therefore, 9-ethylcarbazole is more reactive to hydrogen than benzene or naphthalene.

1.4.2. Hydrogenation of arenes - general considerations

Mainly due to stabilization by resonance, as well as thermodynamic limitations, aromatic molecules are generally very difficult to hydrogenate. These reactions are exothermic, which means that the conversion at equilibrium decreases with increasing temperature. Normally, high pressures are unavoidable in order to achieve considerable conversions in hydrogenation reactions of typical aromatic compounds (77). It is known that in the hydrogenation of polycyclic compounds, the saturation of the first ring is much easier than

the saturation of the final ring. This can be explained by higher resonance stabilization of the monoaromatic and/or competition for active sites where the compound with higher number of aromatic rings prevails (78). In addition, the hydrogenation of aromatic C-C double bonds in arenes is known to result in mixtures of isomers of the intermediates and main products. The number of isomers increases with the increasing number of fused rings (79). The selectivity of the hydrogenation of aromatic compounds is governed by a combination of factors such as: reactivity of the respective positions in the rings of the substrate and favourable modes of adsorption of intermediates and products on the metal surface.

1.4.3. Hydrogenation mechanism

The hydrogenation reaction mechanism is normally best described by the classical work of Horuti and Polanyi (80) which is shown in Figure 1.8, for hydrogenation of benzene in liquid phase. In accordance with this model, during the hydrogenation reaction, the hydrogen molecule has to be activated in non-competitive chemisorptions (dissociative adsorption) on the surface of the metal catalyst. Subsequently, the chemisorbed H atoms can interact with the double bonds of the activated aromatic compound.

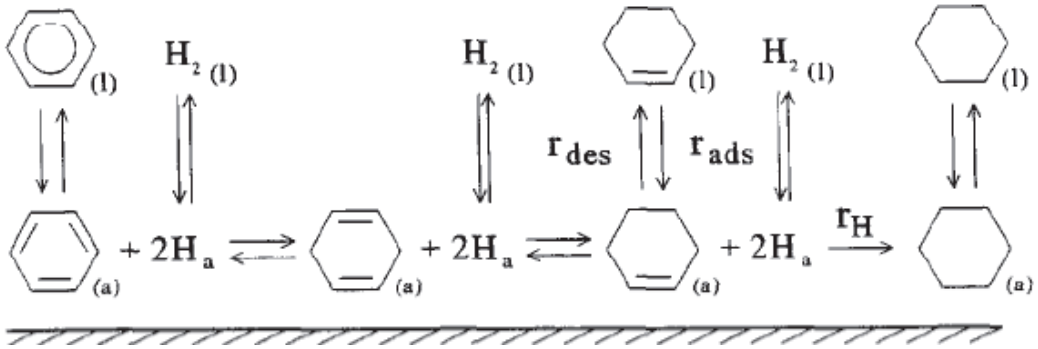

Figure 1.8. The stepwise mechanism of hydrogenation of benzene over transition metal catalysts developed by Horiuti-Polanyi (81)

There are generally three modes of adsorption of aromatic compounds on the surface of metal catalyst. Associative adsorption modes include Π-adsorption and adsorption through

a transition state Π/δ complex, whereas dissociative mode is δ- adsorption (82). In all modes of adsorption, the interaction of the aromatic double bond with the surface of the metal results in the opening of the former and formation of so called 'Π-complexes' with the surface of the catalyst. These complexes are created by the transfer of electrons from the highest occupied molecular orbital (HOMO) of the arene to an unoccupied d-orbital on the metal. Subsequently, the interaction between activated hydrogen and aromatic compound takes place, which involves the transfer of the hydrogen atom to one of the carbon atoms of the 'Π-complexes' and forming a partially hydrogenated state. This is followed by subsequent attachment of hydrogen atoms to the remaining carbons giving rise to hydrogenation (83).

1.4.4. Catalytic hydrogenation of aromatics

Development of an effective heterogeneous catalyst for the hydrogenation of aromatic nuclei under moderate conditions is a challenging task. The hydrogenation of monoaromatics has been extensively studied using noble metal catalysts (84) (85) (86) and bimetallic catalyst containing combinations of Pt, Pd, Rh, Ru or Re. In the hydrogenation of tricyclic compounds, rhodium catalyst was found to be the most active but the least selective out of the noble metals. However, noble metal catalysts exhibit low-resistance towards sulphur and nitrogen poisoning (87). In liquid phase hydrogenation of aromatic compounds over noble metals, generally higher hydrogenation rates and better sulfur resistance were reported over highly acidic supports such as SiO_2-Al_2O_3 or TiO_2.

1.4.5. Catalytic hydrogenation of nitrogen containing heterocycles

Most of the reported hydrogenation reactions in the literature are focused on the typical aromatic compounds such as benzene, toluene, xylene, naphthalene and tetralin. However, there are only a few reports of the hydrogenation of heterocyclic compounds. It is well known that the hydrogenation of heterocyclic compounds leads to several partially

hydrogenated intermediates. The hydrogenation pathway depends on the structure of the substrate and the type of bonds formed between the intermediate and the catalyst surface. Nitrogen containing heterocyclic compounds generally fall into two classes: basic compounds for which the lone pair of electrons is localized on the nitrogen atom and it is available for donation to a Lewis acid and nonbasic where the lone pair is delocalized in the aromatic system (77). Furthermore, nitrogen containing heterocycles, depending on their structure, can reversibly deactivate noble metal catalysts as it was mentioned before. Therefore the hydrogenation of these compounds over noble metal catalyst is not facile. Hydrogenation of nitrogen containing heterocycles was reported to take place over platinum metals (Pt, Ru, Rh, Pd). The nitrogen heterocyclic compounds such as pyridine, pyrridazine, quinoline and isoquinoline were found to adsorb via lone pair of electrons of nitrogen on the cobalt catalyst which results in the vertical position of the substrate on the surface of the metal. However, while moving towards platinum metals, there is an increase contribution of the Π-electrons to the adsorption, which results in the flat geometry of the substrate on the metal catalyst (88). Okazaki et al. (89) have pointed out that in case of hydrogenation of isoquinoline over ruthenium catalyst, the heterocyclic ring is preferably hydrogenated, leaving the benzene ring intact. This is explained by the fact that the Π-electrons are more localized in the ring containing more electronegative nitrogen atom. In general, the reactivity to hydrogen of the nitrogen containing heterocyclic intermediates is proportional to the degree of their unsaturation.

1.5. Scope of the research

In light of the previously described findings concerning the influence of the structure of the liquid organic hydride (LOH) hydrogen carrier on the kinetics and thermodynamics of hydrogen release step, 9-ethylcarbazole seems to be a perfect prototype material for hydrogen storage (67) (65) (90). This heterocyclic compound can uptake reversibly up to 6

moles of equivalent hydrogen (5.7 wt %). This capacity is lower than the revised storage targets for mobile applications for 2015 set by DOE in early 2009 (22), however it can serve as a simple model compound to define the remaining unresolved challenges and problems in this area. 9-ethylcarbazole is an interesting compound due to the fact that it has a very favourable structure that involves incorporation of the nitrogen atom in the five member ring as well as the presence of three conjugated aromatic rings.

Taking into consideration a hydrogen storage system based on liquid organic carriers, the hydrogen loading step (hydrogenation reaction) is assumed to be taking place off-board in the refinery plant. Therefore, most of the research efforts concerning LOH are focused on optimisation of dehydrogenation step, whereas in our opinion, there is not enough attention devoted to the hydrogen loading step. It is therefore very important to take into consideration the issue of effective recovery of the spent fuel back to the fully charged regenerated material. Ideally, the optimised process should take place under mild conditions of temperature and pressure, with a minimum amount of catalyst used and preferably in solvent-free environment. It is clear that the use of solvent makes the process less economically attractive and environmentally friendly. Lack of appropriate optimisation of the hydrogen charging step can raise the need of an additional purification step or result in accumulation of a non-rechargeable fraction in the fuel tank on-board of the vehicle. Severe problems in recyclability could end up with a necessity to newly manufacture the LOH from starting substrates which would bring about an enormous economic penalty.

Therefore, the main objective of the present work is to study the recyclability of LOH-fuels based on the 9-ethylcarbazole as a model compound. The knowledge obtained in this research is meant to provide a groundwork for developing a highly efficient recovery process for the spent LOH fuels.

The main objectives of the present work are:

- to demonstrate the direct and integrated system of catalytic hydrogenation and dehydrogenation of the molten reactant without the unnecessary use of solvent
- to study the reaction pathway of 9-ethylcarbazole hydrogenation, develop the reaction model and to determine the influence of the catalytic active sites on the metal surface on the activity and selectivity obtained in this reaction using experimental and theoretical approaches
- understand the interaction of the substrate and intermediates with the active sites of the catalyst which would lead to rational design of superior catalysts for reversible reaction
- determine the kinetics of the 9-ethylcarbazole hydrogenation and influence of the thermodynamic parameters on yield and selectivity in this reaction, in order to optimise the conditions of fuel recycling process
- to gain knowledge about the influence of the catalytic system and analyse the electronic and geometric influence of the metal-support system on the reaction selectivity and conversion, which would aid in designing an effective catalyst
- to study the influence of the chemical structure of the substrate on the recyclability of its spent form in order to obtain guidelines for designing LOH with higher gravimetric capacities and improved hydrogenation kinetics and thermodynamics.

1.6. References

1. *High capacity hydrogen storage materials: attributes for automotive applications and techniques for materials discovery.* **J. Yang, A. Sudlik, C. Wolverton, D.J. Siegel**, Chem. Soc. Rev, 2010, Vol. 39.
2. *Carbon dioxide capture: Prospects for new materials.* **D.M. D'Alessndro, B. Smit, J.R. Long**, Angew. Chem. Int. Ed, 2010, Vol. 49.
3. *B-N compounds for chemical hydrogen storage.* **C.W. Hamilton, R.T Baker, A. Staubitz, I. Manners**, Chem. Soc. Rev., 2009, Vol. 38.
4. *Hydrogen-storage materials for mobile applications.* **L. Schlapbach, A. Zuettel**, Nature, 2001, Vol. 414.
5. *New approaches to hydrogen storage.* **J. Graetz**, Chem. Soc. Rev., 2008, Vol. 38.
6. *http://www.autos.ca/tech-and-environment/special-report-the-future-of-hydrogen.* [Online]
7. *Hydrogen as a future energy carrier.***A. Zuettel, A. Borgchulte, L. Schlapbach,** Weinheim Germany : Wiley-VCH, 2008.
8. *Hydrogen storage materials.* **A. Zuettel**, Naturwissenschaften, 2004, Vol. 91.
9. *Rethinking hydrogen cars.* **D.W. Keith, A.E. Farrell,** Science, 2003, Vol. 301.
10. *Hydrogen-fuelled vehicles.* **L. Schlapbach**, Nature, 2009, Vol. 460.
11. http://www.hydrogenhighway.ca.gov/facts/einsafety.pdf. *How safe is hydrogen/.* [Online]
12. *Recent challenges of hydrogen storage technologies for fuel vehicles.* **D.Mori, K.Hirose,** Int. J. Hydrogen Energy, 2009, Vol. 34.
13. *Thermodynamics of gaseous and liquid hydrogen storage-conference proceedings.* **M. Klell, H. Kindermann, C. Jogl,** Istambul, Turkey : IHEC 2007, 2007.
14. *http://www1.eere.energy.gov.* [Online]
15. *Materials for hydrogen storage: current reserch trends and perspectives.* **A.W.C.Van der Berg, C.O.Arean,** Chem. Commun, 2008.
16. http://www.eia.doe.gov. [Online]
17. http://www.eoearth.org/article/Hydrogen_storage. [Online]
18. *Chemical and physical solutions for hydrogen storage.* **U. Eberle, M. Felderhoff, F. Schuth,** Angew.Chem.Int.Ed., 2009, Vol. 48.
19. *Challenges in hydrogen storage.* **F. Schutz,** Eur. Phys. J. Special Topics, 2009, Vol. 176.
20. *The U.S.Department of Energy's National Hydrogen Storage Project: Progress towards meeting hydrogen-powered vehicle requirements.* **S. Satyapal, J. Petrovic, C. Read, G. Thomas, G. Ordaz,** Cat. Today, 2007, Vol. 120.
21. *Bottling the hydrogen Genie.* **F.E. Pinkerton, B.G. Wicke,** The industrail physicist, 2004
22. *Targets for onboard hydrogen storage systems for light-duty veicles.* Freedom Car and Fuel Partners, 2009.
23. *Automotive hydrogen storage system using cryo-adsorption on activated carbon.* **R.K. Ahluwalia, J.K. Peng,** Int. J. Hydrogen Energy, 2009, Vol. 34.
24. *Hydrogen storage : the remaining scientific and technological challenges.* **M. Felderhoff, C. Weidenthaler, R. von Helmot, U. Eberle,** Phys. Chem. Chem. Phys, 2007, Vol. 9.
25. *System level analysis of hydrogen storage option.* **R.K. Ahluwalia, T.Q. Hua,J.K. Peng, R. Kumar,**Washington DC, 2010.

26. *Hydrogen storage: state-of-the-art and future perspective.* **E. Tzimas, C. Filiou, S.D. Peteves, J-B. Veyret,** Luxembourg, 2003.
27. *Vehicular storage of hydrogen in insulated pressure vessels.* **S.M. Aceves, G.D. Berry, J. Martinez-Fias, F. Espinosa-Loza,** Lawrence Livermore National Laboratory, 2005.
28. *Hydrogen: a future energy vector for sustainable development.* **T.K. Mandal, D.H. Gregory,** J. Mech. Engineering Science, 2009, Vol. 224.
29. *The hydrogen fuel alternative.* **G.W. Crabtree, M.S. Dresselhaus,** MRS Bull., 2008, Vol. 33.
30. *Hydrogen adsorption and storage on porous materials.* **T.K. Mark,** Cat. Today, 2007, Vol. 120.
31. *Problem of hydrogen storage and prospective uses of hydrides for hydrogen accumulation.* **B.P. Tarasov, M.V. Lototskii, V.A. Yartys,** Russ. Journ. Gen. Chem, 2007, Vol. 77.
32. *Hydrogen storage in carbon nanotubes.* **H.M. Cheng, Q-H. Yang, Ch. Liu**, Carbon, 2001, Vol. 39.
33. *Improved designs of metal-organic frameworks for hydrogen storage.* **S.S. Han, W-Q Deng, W.A. Goddard,** Angew. Chem. Int. Ed., 2007, Vol. 46.
34. *Nanoporous polymers for hydrogen storage.* **J. Germain, J.M.J. Frechet, F. Svec,** Small, 2009, Vol. 5.
35. http://www.techconnectworld.com/Cleantech2010/a.html?i=915 [Online]
36. *Hydrogen storage properties of clathrate hydrate materials.* **T.A. Strobel, C.A. Koh, E.D. Sloan,** Fluid Phase Equilib, 2007, Vol. 261.
37. *Hydrogen storage in Mg: A most promising material.* **I.P. Jain, C. Lal, A. Jain,** Int. J. Hydrogen Energy, 2010, Vol. 35.
38. *Air -stable magnesium nanocomposite provide rapid and high -capacity hydrogen storage without using heavy-metal catalysts.* **K.J. Jeon, H.R. Moon, A.M. Ruminski, B. Jiang, C. Kisielowski, R. Bardhan, J. J. Urban**, Nature Materials, 2011.
39. *Metal hydrides for vehicular applications: The state of art.* **D. Chandra, J.J. Reilly, R. Chellappa,** JOM, 2006, Vol. 58.
40. *Automotive storage of hydrogen in alane.* **R.K. Ahluwalia, T.Q. Hua and J.K. Peng,** Int J. Hydrogen Energy, 2009, Vol. 34.
41. *Novel hydrogen storage materials: A review of lightweight complex hydrides.* **I.P. Jain, P. Jain, A. Jain,** J. Alloys Compd, 2010, Vol. 503.
42. *Complex aluminium hydrides.* **B. Bogdanovic, U. Eberle, M. Felderhoff, F. Schuth,** Scr. Mater, 2007, Vol. 56.
43. *Recent progress in hydrogen storage.* **P. Cheng, M. Zhu,** Mater.Today, 2008, Vol. 11.
44. *Sodim borohydride versus amonia borane, in hydrogen storage and direct fuel cell applications.* **U. B. Demirci, P. Miele,** Energy Environ.Sci, 2009, Vol. 2.
45. *Production of hydrogen via hydrolysis of hydrides in Mg-La systems.* **L.Z. Ouyang, Y.J. Xu, H.W. Dong, L.X. Sun, M. Zhu,** Int. J. Hydrogen Energy, 2009, Vol. 34.
46. *Chemical recuperation of low-quality waste heats by catalytic dehydrogenation of organic chemical hydrides and its energy analysis.* **S. Hodoshima, A. Shono, Y. Saito,** Energy Fuels, 2008, Vol. 22.
47. *Hydrogen storage by reversible hydrogenation of liquid -phase hydrogen carriers.* **A. Cooper, A. Scott, D. Fowler, J. Cunningham, M. Ford, F. Wilhelm, V. Monk, H. Cheng, G. Pez.** DOE hydrogen program/Air Products, 2007.
48. *Chemical hydrides: A solution to high capacity hydrogen storage and supply.* **R.B. Binwale, S. Rayalu, S. Devotta, M. Ichikawa,** Int. J. Hydrogen Energy, 2008, Vol. 33.

49. *Development of dehydrogenation catalyst for hydrogen generation in organic chemical hydride method.* **Y. Okada, E. Sasaki, E. Watanabe, S. Hyodo, H. Nishijima,** Int. J. Hydrogen Energy, 2006, Vol. 31.
50. *Hydrogen storage in liquid organic hydrides.* **R.H. Crabtree,** Energy Environ. Sci., 2008, Vol. 1.
51. *Hydrogen storage and delivery in a liquid carrier infrastructure- presentation.* **G.Pez, A.C. Cooper, H. Cheng, B.A. Toseland, K. Cambell,** Allentown, 2006.
52. *Novel zero-CO_2 emission technology of catalytic production of hydrogen and aromatics from methane and biogas fo fuel cell society.* **M. Ichikawa, J.** Am. Chem. Soc., 2004, Vol. 49.
53. *Liquid organic hydrogen carriers (LOHC): An auspicious alternative to conventional hydrogen storage technologies.* **J. von Wild, T. Friedrich, A. Cooper, B. Toseland, G. Muraro, W. Tegrotenhuis, Y. Wang, P. Humble, A. Karim.** Essen : 18 th World Hydrogen Energy Conference 2010- WHEC 2010/ Conference procedings, 2010.
54. *A feasibility analysis of hydrogen delivery system using liquid organic hydrides.* **A.U. Pradhan, A. Shukla, J.V. Pande, S. Karmarkar, R.B. Biniwale,** Int. J. Hydrogen Energy, 2011, Vol. 36.
55. *Dehydrogenation of cyclohexane over molybdenum/mixed oxide catalysts.* **M. Raid, S. Mikhail,** Catal.Commun, 2008, Vol. 9.
56. *US patent 7351395.* **G.P. Pez, A.R. Scott, A.C. Cooper, H. Cheng, F.C. Wilhel, A. Abdourazak.** 2008.
57. *Ni/Al_2O_3 catalysts and their activity in dehydrogenation of methylcyclohexane for hydrogen production.* **S. Yolcular, O. Olgun,** Cat. Today, 2008, Vol. 138.
58. *In situ hydrogen generation from cyclohexanes using Pt/CNF catalyst.* **M.P. Lazara, E. Garcia-Bordeje, D. Sebastian, M.J. Lazaro, R. Molier,** Cat. Today, 2008, Vol. 138.
59. *Kinetic modelling of pure hydrogen production from decalin.* **B. Wang, D.W. Goodman, G.F. Froment,** J. Catal, 2007, Vol. 253.
60. http://www.geifuelcells.com/innovation/ht-pem. [Online]
61. *Hydrogen storage in organic hydrides at low energy consumption-conference proceedings.***Y. Saito, S. Hodoshima, A. Shono,** Lyon France, 2006.
62. *Thermal imaging of catalyst surface during catalystic dehydrogenation of cyclohexane under spray-pulsed conditions.* **R.B. Biniwale, M. Ichikawa,** Chem. Eng. Sci., 2007, Vol. 62.
63. http://www.hydrogen.energy.gov.
64.http://www.hydrogen.energy.gov/pdfs/review05/pd34_pez.pdf. [Online]
65.http://www.iphe.net/docs/Meetings/Lucca_Italy_05/Cooper.pdf. [Online]
66. *Computational structure-activity relationship in H_2 storage : How a placement of N atoms affects release temperatures in organic liquid storage materials.* **E. Clot, O. Eisenstein, R.H. Crabtree.** Chem. Commun., 2007, Vol. 22.
67.*An integrated hydrogen storage and delivery approach using organic liquid -phase carriers.* **A.C. Cooper, K.M. Campbell, G.P. Pez** Lyon, France : WHEC 13-16 June, 2006.
68. *The effect of substitution on the utility of piperidines and octaindoles for reversible hydrogen storage.* **Y. Cui, S. Kwok, A. Bucholtz, B. Davis, R.A. Whitney, P.G. Jessop,** New J. Chem, 2008, Vol. 32.
69. *Hydrogen storage by novel CBN heterocycle materials.* **S-Y Liu,** University of Oregon, 2009.
70. *A new hydrogen storage system based on efficient reversible catalytic hydrogenation/dehydrogenation of terphenyl.* **J.S. Sung, K.Y. Choo, T.H. Kim,A.L. Tarasov, O.P. Tkachenko, L.M. Kustov,** Int. J. Hydrogen Enrgy, 2008, Vol. 33.

71. *Investigation of hydrodearomatization of gas oils on noble metal/support catalysts.* **G. Polczmann, D. Kallo, J. Hancsok,** Chem. Eng. J, 2009, Vol. 154.
72. *Heterocycle chemistry.* **J.A. Joule, K. Mills.** West Sussex : Blackwell publishing Ltd, 2010.
73. *Organic chemistry* **J. Clayden, N. Geeves, S. Warren,** Oxford : Oxford Univesity Press, 2000.
74. *The chemistry of heterocycles.* **T. Eicher, S. Hauptman,** Wiley-VCH, 2003.
75. www.chemgapedia.d**.** [Online]
76. http://www.uea.ac.uk. [Online]
77. *Reactivities, reaction networks and kinetics in high-pressure catalystic hydroprocessing.* **M.J. Girgis, B.C. Gates,** Ind. Eng. Chem. Res, 1991, Vol. 30.
78. *Comperative study of the hydrogenation of tetralin on supported Ni, Pt, and Pd catalysts.* **S. Dokjampa, T. Rirksomboon, S. Osuwan, S. Jongpatiwut, D.E. Resasco.** Catal. Today, 2007, Vol. 123.
79. *Aromatic stability of heterocyclic conjugated systems.* **M. Randic, N. Trinajstic, J.V. Knoop, Z. Jericevic,** J. Am. Chem.Soc., 1985, Vol. 107.
80. *Catalytic interchange of hydrogen between water and ethylene and between water and benzene.* **J.Horiuti, M.Polanyi,** Nature, 1934, Vol. 134.
81. *Partial liquid phase hydrogenation of benzene to cyclohexane over ruthenium catalysts in the presence of an aqueous salt solution.* **J. Struijk, M.d'Angremond, W.J.M. Lucas-de Regt, J.J.F. Scholten,** Apl. Catal, 1992, Vol. 83.
82. *Liquid-phase hydrogenation of naphthalene and tetralin on Ni/Al_2O_3 : Kinetic modelling.* **P.A. Rautinen, M.S. Lylykangas, J.R. Atimamaa, A. Outi, I. Krause,** Ind. Eng.Chem.Res, 2002, Vol. 41.
83. *In Horiuti's footsteps: links between catalysis and electrolysis.* **G. Horanyi**, J. Appl. Catal, 2003, Vol. 199.
84. *Rhodium nanoparticles intercalated into montmorillonite for hydrogenation of aromatic compounds in the presence of thiophene.* **K.B. Sidhpuria, H.A. Patel, P.A. Parikh, P. Bahadur, H.C. Bajaj, R.V. Jasr,** Appl. Clay. Sci., 2009, Vol. 42.
85. *Ring hydrogenation of naphtalene and 1-naphtol over supported metal catalyst in supercritical carbon dioxide solvent.* **M. Shirai, C.V. Rode, E. Mine, A. Sasaki, O. Sato, N. Hiyoshi,** Catal. Today, 2006, Vol. 115.
86. *Catalytically active sites of supported Pt catalysts for hydrogenation of tetralin in the presence of dibenzothiophene and qunoline.* **M.F. Wiliams, B. Fonte, A. Jentys, C. Breitkopf, J.A.R.van Veen, J.A.Lercher,** J. Phys. Chem, 2010, Vol. 114.
87. *Aromatic saturation of distillates: an overview.* **B.H. Cooper, B.B.L. Donnis,** Appl. Catal., 1996, Vol. 37.
88. *Cobalt as a catalyst for specific iothopic hydrogen labelling in heterocyclic compounds.* **G.E. Calf, J.L. Garnett,** Chem. Comm., 1967.
89. *Kinetic study on hydrogenation of isoquinoline over supported ruthenium catalysts.* **H. Okazaki, M. Soeda, Y. Ikefuji, R. Tamura, I. Mochida,** Bull. Chem. Soc. Jpn., 1989, Vol. 62.
90. *Hydrogen storage by reversible hydrogenation of liquid-phase carriers.* **A.Cooper, A. Scott, D. Fowler, J.Cunningham, M. Ford, F. Wilhelm, V. Monk, H. Cheng, G. Pez.** Air Products, 2008.

Chapter 2. Analytical techniques

2.1. Characterization of the surface and morphology of a solid state catalyst

The principle of Sabatier adsorption states that a good heterogeneous catalyst is a material that exhibits intermediate strengths of adsorption of reactants in the catalyzed process (1). Therefore, interactions of the substrate with the catalysts that are too weak (no reaction) or too strong (catalyst poisoning), both result in a low catalytic activity. In order to fully understand the mechanism of any catalytic reaction, it is necessary to characterize primarily the surface of the catalyst. In the present work, several techniques described in this chapter were used to determine the physical and chemical characteristics of the catalytic surfaces.

2.1.1. Determination of surface area using the Brunauer- Emmett –Teller (BET) method

The BET method is based on the physisorption phenomena, that occurs if gas (adsorptive) is brought in contact with a solid surface (adsorbent) (2). This method is based on an extension of the Langmuir monolayer model to multilayer adsorption (3). The forces of the interaction involve the long range, but weak Van der Waals –type interactions and a short range intermolecular repulsion. There is a negligible exchange of electrons and hence the enthalpy of physisorption is lower than 34 kJ/mol (3). The concept of the BET method is based on the fact that the molecules of the first layer act as the sites for the molecules of the second-layer, which in turn provide sites for the adsorption of molecules in the higher layers. Equlibration is achieved at a certain temperature, where the rate of condensation is equal to the rate of evaporation (4). The general assumptions of this method are that the adsorption of the first layer takes place on surface sites with identical energy and that when

$P=P_0$ (the saturated vapour pressure of the adsorbate), an infinite numbers of layers will form (3). The sumation of the amount adsorbed in all of the layers gives the genaral BET equation, expressed in linear form in Equation.2.1. (5):

$$\frac{P}{V_{ads}(P_0-P)} = \frac{1}{V_{mC}} + \frac{C-1}{V_{mC}}\left(\frac{P}{P_0}\right) \qquad \text{Equation 2.1}$$

where: V_{ads} is the volume of gas adsorbed at pressures P, P_0 is the saturation pressure, commonly 200-390 Torr, V_m is the volume of the gas adsorbed at monolayer coverage and C is the BET constant that depends on the enthalpy of adsorption.

The BET surface area of the sample is given by Equation.2.2 (3) (5) (6).

$$S_A = \frac{V_m \times N \times A_m}{m \times 22400} \qquad \text{Equation 2.2}$$

where; S_A is the surface area [m^2g^{-1}], N is the Avogadros's number, A_m is the effective cross sectional area of the adsorbate molecule in square meters (0.162 nm^2 for nitrogen), m is a mass of test powder in grams and V_m is the volume of the nitrogen adsorbed at monolayer coverage in cubic meters and 22400 is the volume occupied by 1 mole of the adsorbate gas at standard temperature and pressure (3) (5) (6).

2.1.2 CO pulse -chemisorption

Chemisorption can be distinguished from physisorption based on the magnitude of the enthalpy of adsorption which is greater than 34 kJ/mol (3) and normally between 200-390 kJ/mol (7). During chemisorption, the exchange of electrons takes place and therefore the strength of the interaction can be analyzed in terms of the traditional bonding (covalent, ionic or metallic) and spectroscopic methods can be used to determine the nature of the interaction (3). The chemisorption process can take place in two ways:

dissociatively (e.g. chemisorption of H_2 on a metal surface) and non-dissociatively (e.g. ethane on metal surface) (8). Transition metal catalysts are most frequently characterized by using selective chemisorptions. The measurement of the quantity of gas adsorbed on the metal at the monolayer coverage gives the metal surface area and metal dispersion, if the stochiometry is known (2). In the chemisorption experiment, from the volume of the chemisorbed gas required to form a monolayer V_m, the specific metal surface area A can be calculated from Equation.2.3 (2).

$$A = \frac{V_m}{22414} \times N \times \mathrm{n}\frac{1}{\mathrm{m}} \times s_a \frac{100}{wt} \quad (\mathrm{m^2 g^{-1} metal}) \qquad \text{Equation 2.3.}$$

where; n is chemisorption stoichiometry, m is the mass of the sample, S_a is the surface area occupied by a metal atom and wt is weight percentage of the metal loading.

The catalyst (metal) dispersion can be defined as the ratio between the number of surface atoms and the total number of atoms (5). The dispersion (D) can be directly obtained from Equation 2.4 (2) where M is the atomic mass of metal

$$D = \frac{V_m \times n}{22414\, m} \Big/ \frac{wt}{100\, M} \ (\%) \qquad \text{Equation 2.4.}$$

2.1.3. CO chemisorption and Infra- Red (IR) analysis of surface species

Heterogeneous catalysis typically contains different types of surface sites and this is a result of the crystalline anisotropy of the solids. Therefore, different crystallographic planes which expose sites with different coordination environments, posses various properties for chemisorption and catalytic reactions (9). Thus, catalysis can take place differently on the different crystallographic faces and locations on the transition metal nanoparticle, hence many reactions are known to be sensitive to the structure of the metal catalyst (10). The main types of active sites identified on the surface of the nanoparticle

are planar (face) sites, corner and edge sites, which are shown in Figure 2.1. Additionally, the active sites on the surface of the nanoparticles are associated with terraces, kinks and vacancies (11). CO is one of the most used molecules for probing the surface of the supported metal catalyst (12), due to the fact that it is able to reveal the oxidation and the coordination state of the sites to which it is bonded to (13).

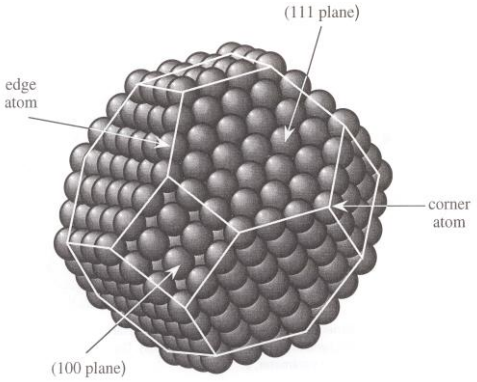

Figure 2.1. The types of active sites on the surface of metal nanoparticle (13)

It is well known that CO can be chemisorbed in various forms on the noble metals such as Pd, Pt, Rh and non-noble metals such as Fe, Co, Ni (2). Additionally, the chemisorption of carbon monoxide can be dissociative (CO/metal $\leq$ 2) or associative in the linear or bridging mode and less frequently in capped form (14). The representative resonance structures of various forms of the chemisorbed carbon monoxide on the surface of metal are shown in Figure 2.2.

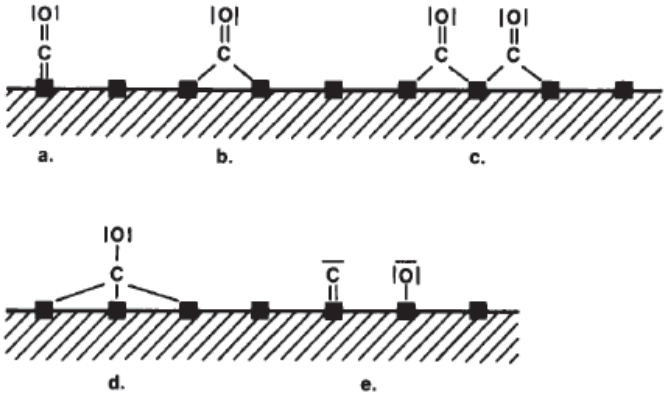

Figure 2.2. A schematic representation of the various modes of binding of CO on the metal surface (14). a- lineral, b-bridging, c-multicarbonyl, d-capped, e-dissociative bonding (14).

There is a vast amount of literature concerning the study of CO adsorption on ruthenium with Infra-Red analysis (13) (14) (15). The most widely observed bands for carbon monoxide adsorbed on ruthenium metal are: a high frequency 1 (2110-2129 cm^{-1}) band assigned to linear mode, a high frequency 2 (2039-2100 cm^{-1}) band assigned to multicarbonyl mode and additional low frequency 3 (1975-2025 cm^{-1}) band assigned to bridging mode (13) (16).

IR is a non-destructive spectroscopic method based on the interaction of the radiation with matter in the range of frequencies from 10^{12} to 10^{14} Hz (17). This frequency range corresponds with the energy required for stretching and bending of the bonds in most covalent molecules. Thus, in the adsorption process, those frequencies of infrared radiation which match the natural vibrational frequencies of the molecule being analyzed are adsorbed and the energy adsorbed serves to increase the amplitude of the vibrational motions of the bonds in the molecule. It should be noted that not all of the bonds in the molecule are capable of adsorbing IR radiation, but only those having a dipole moment that changes as a function of time (18). The fundamental adsorptions arise from excitation from the ground state to the lowest-energy excited state. The basic infrared active modes of vibrational motion in the molecule are: stretching (higher energy) and bending modes (lower energy) (19).

Diffuse Reflectance Fourier Transform Infrared Spectroscopy (DRIFT)

The most widely used technique for studying and characterization of the surfaces of metal nanocatalysts is diffuse reflectance (DR) IR spectroscopy (DRIFT). In the DR technique, the radiation intensity scattered at a given wavelength from infinitely thick, closely packed catalyst layer is compared with that scattered from an infinitely thick layer of nonabsorbing highly scattering (white) reference (20). The ratio of the light intensity scattered form the catalyst to that from the reference is recorded as a function of wavenumber (21). The reflectance of the sample (R) is defined as a ratio of backward and forward fluxes at the illuminated front surface (2). The isotopic scattering can be described using absorption and scattering coefficients according to the Schuster-Kubelka-Munk theory (21).

2.1.4. Temperature Programmed Reduction (TPR)

TPR belongs to the thermal analysis methods that rely on recording the changes in the sample with a change in temperature. The first useful information provided by TPR experiment is the temperature range needed for complete reduction of a catalyst. Additionally, peak temperatures observed during TPR of unsupported compound and supported precursors can be used to assess the strength of metal-support interactions for supported noble metals (2). Furthermore, the TPR profile of bimetallic systems (metal alloys) can reveal whether the two metals are in contact or not. The influence of the additives, dopants and promoters on the reduction temperature can also be obtained from TPR experiments (20).

Reduction is a crucial step in preparation of well dispersed, active metallic catalysts. The reduction of a metal oxide MO_n by H_2 is well described by Equation 2.5 (20):

$$MO_n + n\,H_2 \longrightarrow M + n\,H_2O$$ Equation. 2.5

The standard Gibbs free energy ΔG^0 change for many of the metal oxides such as cobalt, nickel or noble metals is negative and thus for these oxides, the reductions are thermodynamically feasible (22). Equation 2.6 (22), shows the dependence of Gibbs free energy ΔG, on pressure and temperature;

$$\Delta G = \Delta G^0 + nRT \ln \left[\frac{p_{H_2O}}{p_{H_2}}\right]$$ Equation. 2.6

where:, R- is the gas constant, T- is the temperature, p- is the partial pressure, n- number of moles.

It should be noted that the reduction of a solid catalyst by flowing hydrogen gas is a complex process that can be limited by many factors such as; transport of reducing gases or gaseous products from the reaction interface, or adsorption –desorption processes.

2.1.5. X-Ray Powder Diffraction (XRD)

The basis of the X-ray diffraction geometry is described by Bragg's Law. Bragg showed that every diffracted beam produced by an appropriate orientation of the crystal in an X-ray beam, can be regarded geometrically as if it was a reflection from sets of parallel planes passing through the lattice points (23). For the reflection to occur, constructive interference must take place. The path difference of the two rays is shown in Figure 2.3. and described by Equation 2.7. where; θ is the Bragg angle and d is the distance between two lattice planes (24).

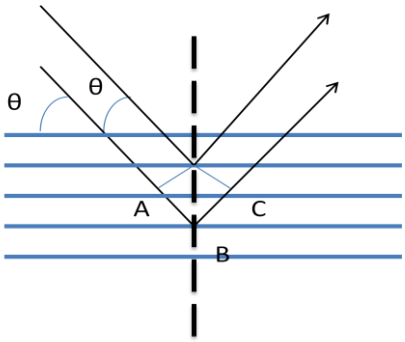

Figure 2.3. The conventional derivation of the Bragg law. Constructive interference occurs when AB + BC is equal to an integral number of wavelengths (25).

$$AB + BC = 2dsin\theta \qquad \text{Equation. 2. 7}$$

Thus, for the reflected waves to be in phase and to interfere constructively, the path-length difference has to be an integral number of wavelengths (AB+BC = nλ). Therefore, the bright reflection can only be observed when the glancing angle follows the Bragg law, shown in Equation 2.8 (25) where; n is an integer, λ is a wavelength of incident wave and d is the distance between two lattice planes. Thus, by measuring the angles at which the constructively interfering X-rays leave the crystal, the corresponding d– spacing can be calculated using Equation.2.8.

$$n\,\lambda = 2\mathrm{d}\,\sin\theta \qquad \text{Equation.2.8}$$

The width and the shape of the XRD peaks carry information about the dimensions of the reflecting planes. One of the important limitations of XRD technique is that clear peaks can be obtained only from samples possessing long-range order (20). Due to incomplete destructive interference in scattering directions where X-rays are out of phase, line broadening occurs especially for crystallites with small sizes. In addition, the X-ray diffraction broadening analysis is widely used for quick, but not always reliable estimate of the particle size of catalysts following Scherrer equation (20), which is shown in Equation.2.9.

$$< L >= \frac{K\lambda}{\beta \cos\theta}$$ Equation. 2.9

where; <L> is a measure of the dimensions of the particle in the direction perpendicular to the reflecting plane, K is a constant and β is the peak width (9).

2.1.6. X-Ray Photoelectron Spectroscopy (XPS)

The chemical composition obtained with the aid of XPS experiment refers to the identification of the species present on the outermost one or two atomic layers on the surface (9). XPS can also provide information about the different chemical states of the elements present on the catalyst's surface (20). In this technique, the electrons are expelled from their original orbitals by a photoelectric effect shown in Figure 2.4, using X-rays as a primary radiation to eject the electrons (21).

For the analysis of XPS spectra, the atomic core level binding energies are used, which are not only element specific, but also depend on the chemical state of an atom. In the case of heterogeneous catalysis, the binding energy (E_b) can be calculated using measured kinetic energy of the photoelectron (E_k) as shown in Equation. 2.10.

$$E_b = h\nu - E_k \ - \Phi_{SP} - E_C$$ Equation.2.10

Where; $h\nu$ is an energy of the radiation used, Φ_{SP} is the work function of the spectrometer and E_c is the positive charge that exists on the sample surface (21). The elements can be identified via XPS by comparing their binding energies of the electronic levels with the standard tables available in the literature (26), which have been obtained by theoretical calculations on single atoms, or determined experimentally from X-ray spectroscopy data.

The schematic XPS experiment set up is shown in Figure 2.5.

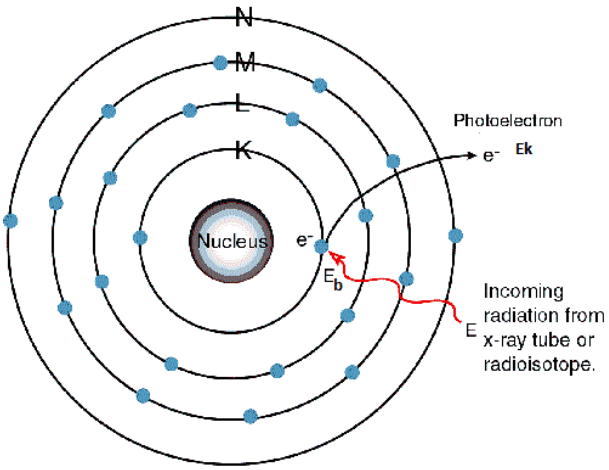

Figure 2.4. Photoelectric effect in XPS technique. An incident X-ray beam is absorbed and a photoelectron is emitted. From the measurement of the E_k (kinetic energy) of this electron, the binding energy of the photoelectron can be calculated (26). The atom after the ejection of the photoelectron stays as an unstable ion with a hole in one of the core levels.

The XPS measurements can only be carried out under ultra-high vacuum (UHV) conditions (9). The X-ray tube- which is the beam source is separated from the photoelectron chamber by a thin aluminium foil that adsorbs the electrons emitted by the anode (21). In standard UHV experiments, X-ray sources with Mg K_α and Al K_α, together with a crystal monochromator are used (9). The ejected photoelectrons from the sample are directed to the electron analyzer which separately counts them according to their kinetic energy (21).

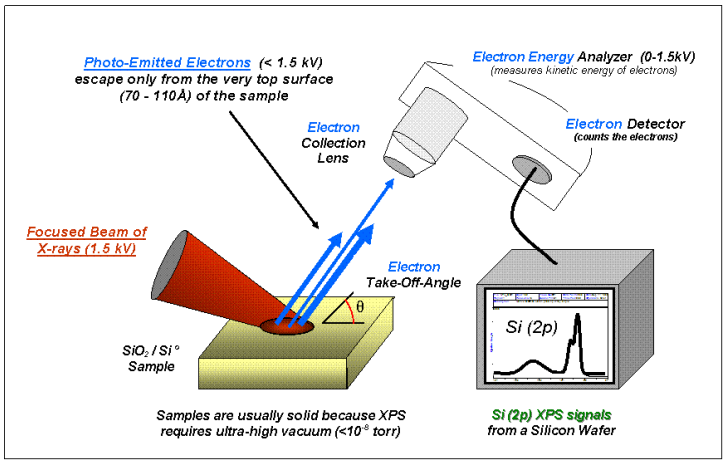

Figure 2.5. General set up for XPS measurements (27).

2.1.7. Scanning Electron Microscopy (SEM) and Energy Dispersive X-ray analysis (EDAX)

Scanning electron microscopy (SEM) is a technique designed for studying bulk samples and it is mostly used to provide a topographic image of the surface of the sample (28). A resolution of down to 10 nm is available with the most machines available in the laboratories (21).

In the present work, the SEM was used in conjunction with EDAX for the compositional analysis of the catalysts surfaces. The EDAX technique is a type of spectroscopy, closely related to the previously described XPS technique, which analyses the photoelectrons ejected from the specimen. The principle of EDAX is very similar to XPS but instead of the electrons ejected from the specimen, the characteristic X-ray released from the sample is measured (21).

2.1.8. Transmission Electron Microscopy (TEM)

Most applications of transmission electron microscopy in catalysis research are focused on obtaining the size, dispersion and shape of the active species or phases in the catalysts (21). The TEM techniques use the information carried by transmitted electrons or the forward scattered beams to produce an image of the specimen. There are two operating modes of TEM that can be distinguished: conventional TEM (CTEM) and high-resolution TEM (HRTEM) (9). In CTEM the transmitted beam is focused by the objective lens, than it propagates through several lenses, which can form two types of images; the image of the back –focal plane (diffraction pattern of the sample) or of the image plane (image of the sample) (21). On the other hand, the HRTEM uses the transmitted and the scattered beams to create an interference image (9).

2.2. Hydrogen sorption measurements

A crucial part of the search for the adequate material for hydrogen storage is an accurate determination of the hydrogen sorption or hydrogen storage characteristics of new or modified materials (29). The reliable measurements of the amount of hydrogen sorbed in a various materials facilitate the meaningful comparison between them (30) and lead to easier optimisation of their composition.

2.2.1. Volumetry or Sievert's method

The Sievert's type apparatus is mainly used for measuring the hydrogen uptake of metal hydrides by recording the variations of hydrogen pressure in the reaction chamber (31). This apparatus allows measuring the hydrogen absorption and desorption kinetics as well as the determination of pressure-composition diagrams (P-C). Standard instruments of this type can operate in the range of temperatures from 290 K up to 700 K and pressures from 1-80 bar (31).

The set-up of the Sievert's method consists of an adsorption sample chamber and a reservoir of a calibrated volume. The sample chamber can be additionally heated up using an oil bath or a heating mantle connected to the thermocouple. From the registered pressure drop, knowing the volume of the system, the volume of the sample and temperature, the amount of hydrogen absorbed by the sample can be calculated.

2.3. Gas Chromatography-Mass Spectrometry (GC-MS) technique

Most of the catalytic reactions result in a mixture of different products and intermediates, which requires separation. With the aid of a combined GC-MS mode, all the components of the complex mixtures, even those present at trace levels (as low as 10^{-12}g) can be separated, identified and quantified (32).

Gas Chromatography (GC)

In gas chromatography (GC) the sample is introduced with a syringe at a heated injection port (32). Subsequently, it is vaporised and carried along by a mobile phase over a fixed bed of a stationary phase. Depending on the interaction of the compounds with the bed of the stationary phase, they will move through the stationary phase at different rates. Those with a greater adsorption on the stationary phase will take longer to emerge than those with lesser affinity. The qualitative information about the component is provided by its retention time. A detector is attached directly to the exit of the column and a visual recording of its response with time forms a chromatogram (32). The area of the peaks present in the chromatogram carries quantitative information of the components. The main features of the GC set-up are shown in Figure 2.6.

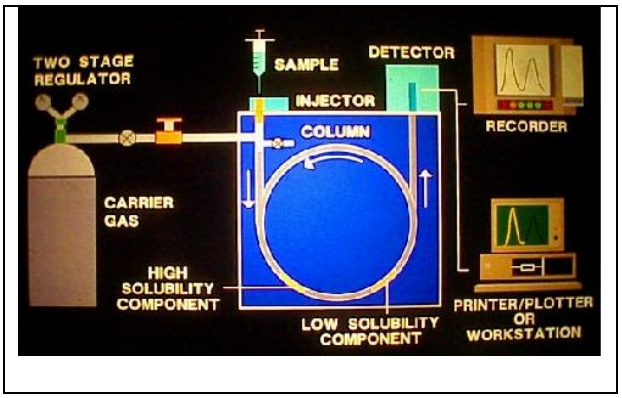

Figure 2.6. Schematic diagram of the gas chromatograph (33).

Gas chromatography- Mass spectrometry (GC-MS)

The two analytical techniques joined together allow excellent degree of separation and identification of the most complex mixtures of components. Moreover, the possibility of two components of the reaction mixture showing the same behaviour and therefore not being distinguishable is very unlikely in GC-MS. Thus, the certainty of this method is very high (34). The GC-MS instrument is built up from two parts; a gas chromatograph in which the mixture of components is separated and a mass spectrometer in which the

individual compounds are quantified and identified based on their structure (35). In a mass spectrometer, the molecules converted into ions are firstly accelerated in an electric field. These accelerated ions are separated according to their mass-to-charge ratio in a magnetic or electric field. Finally, the number of ions with specific mass/charge ratio are counted by the detector and registered in a mass spectrum (36). A schematic diagram of the main parts of the mass spectrometer system is shown in Figure 2.7 (37). Additionally, the most commonly used mass spectrometers are: single or double focusing mass spectrometers, quadrupole and time-of-flight mass spectrometers (19). Furthermore, there are several ionisation techniques available such as electron impact ionisation (EI), or chemical ionisation (CI) which is normally used for highly labile molecules (32) (38).

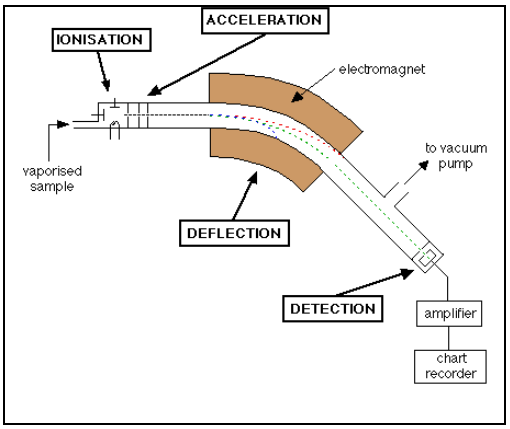

Figure 2.7. A diagram of the main parts of the mass spectrometer system (19).

2.4. Nuclear Magnetic Resonance (NMR) techniques as a tool for assignment of organic structures

The part of electromagnetic radiation spectra with a radio frequency, typically between 60-600 MHz, is used to identify compounds with the nuclear magnetic resonance (NMR) spectroscopy (39). The NMR experiment involves interaction of energy from the external

source with the magnetic properties of nucleus and allows obtaining information about the number and the type of connectivity between atoms being analyzed (39).

2.4.1 Basic concepts of NMR technique

Any atomic nucleus which has an odd mass or odd atomic number has a quantized spin angular momentum and a magnetic moment (18). For each of the nuclei possessing spin, the number of spin states that can be adopted is determined by the constant called nuclear spin number. In the absence of an external magnetic field, all the magnetic spin states of that nucleus are degenerated. However, the spin states stop being of equivalent energy in the applied magnetic field. As a result, a number of allowed orientations can be adopted. For example, the nuclear spins of ^{1}H or ^{13}C, having a spin quantum number of ½ can adopt two positions in the external magnetic field, which are; either spin aligned or opposed spin. These positions are shown schematically in Figure 2.8.

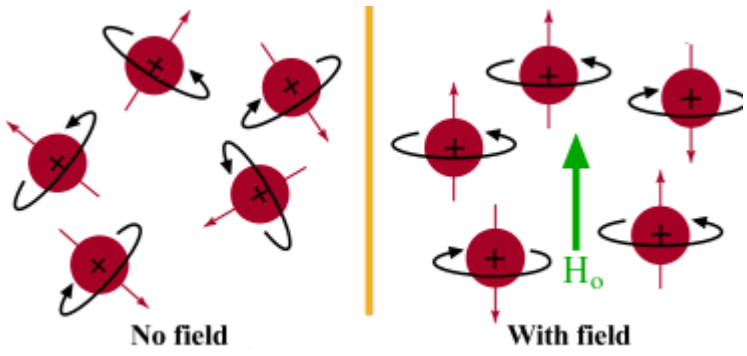

Figure 2.8. Randomly orientated spins of the nuclei in the absence of the external field (on the left) and lined up spins in the external magnetic field (on the right) (40).

The more populated state is the lower energy state called alpha spin state (α), with spin aligned parallel to the applied magnetic field. The beta spin state (β) exists when the magnetic component of the spin state is oriented against an external applied field (39). The nuclear magnetic resonance phenomenon occurs when nuclei aligned with an applied field are induced to absorb energy and change their spin orientation with respect to the applied field (41). The energy is adsorbed by the nuclei because they begin to precess in an applied

magnetic field. The frequency corresponding to this energy is called the resonance frequency (17). Moreover, if the frequency of the incomming radiation matches the electric field generated by precessing nucleus, the two fields can couple and the energy can be transferred. Transferred energy causes a spin change and this condition is referred as a resonance (40).

2.4.2. Shielding and chemical shift

One of the main reasons of wide utility of the NMR techniques lays in the fact that not every proton in a molecule resonates at equal frequency (36). This is the result of the fact that the effective magnetic field (B_{eff}) experienced by the nucleus is not always the same as the magnetic field (B_0) applied to a sample (17). Some nuclei are shielded by the electrons surrounding them. These electrons in the presence of the magnetic field B_0, generate counter magnetic fields that oppose it. Therefore, the B_{eff} experienced by the nuclei is diminished by the counter field that shields it. Because of the fact that the nuclei experiences lower applied magnetic field, it will be able to precess in lower applied field and adsorb radiofrequency radiation at lower frequency (18). The separation of the resonance frequencies resulting from the different environments of the nucleus is called chemical shift (δ) and it is expressed in dimensionless terms, as parts per million (ppm).

2.4.3. ^{1}H NMR spectroscopy

^{1}H NMR spectroscopy is known as proton NMR spectroscopy, and allows observation of hydrogen protons H^+ (39). ^{1}H NMR spectroscopy usually covers the range from 0 to 10 ppm. The main pieces of information that can be obtained from the ^{1}H NMR experiment are: number of protons with different environments (chemical shift), the relative number of protons with the same chemical shift (integrals) and the number of protons on adjacent atoms (coupling constants) (38). The factors affecting chemical shift

of the protons are: electronegativity of the elements substituted on the same carbon to which the protons of interest are attached, hybridization of the adjacent carbon atom, exchangeable protons or hydrogen bonding and magnetic anisotropy.

Chemical and magnetic equivalence of nuclei in ^{1}HNMR

In NMR experiments, two nuclei are considered *chemically equivalent*, if they resonate at the same chemical shift and have the same chemical and physical properties (42). Furthermore, two chemically equivalent nuclei can be *magnetically equivalent*, if they both demonstrate the same couplings to all other nuclei.

Spin-spin splitting (coupling)

Most of the ^{1}H-NMR signals are associated with more than a single line and usually contain several lines (splitting patterns). This is the result of the fact that magnetic field arising from one nucleus can influence the magnetic field experienced by other, non-equivalent, nuclei situated in the close proximity in the same molecule. The coupling between protons on the adjacent carbons is called *vicinal coupling* and the coupling between the protons on the same carbon is called *geminal coupling* (17). The magnetic field of adjacent protons is transmitted through the bonding electrons. In general, three bonds (vicinal coupling) is the most useful in identifying the structure of the compounds, as it identifies the heteroatom groups attached to protons. The frequency difference between the lines in multiplets is called the coupling constant (***J***) and it is independent of the external field (19).

2.4.4. ^{13}C-NMR spectroscopy

^{13}C is the only NMR active isotope of carbon, however its resonances are not easy to be observed mainly owing to its very low abundance (only 1.1 %). Nevertheless, with pulse-FT (Fourier transform approach, higher magnetic field strengths, higher sample quantities

and longer measuring times, ^{13}C-NMR experiments can be successfully performed. The ^{13}C-NMR spectrum is normally very simple, due to the fact that the spin-splitting interaction between adjacent carbon atoms is very unlikely (38). Additionally, ^{13}C spectra have very high dispersion due to the great chemical shift range (0-250 ppm). Thus, generally the only complexity stands from the coupling of hydrogen nuclei to the carbon nuclei to which they are directly bonded. However, it is customary to decouple all the protons during acquisition of the carbon spectrum to obtain noise decoupled spectrum (41). The chemical shift values in carbon NMR spectrum are affected by electronegativity, carbon hybridization and neighboring groups and stereochemistry (42). Additionally, the number of signals in carbon NMR is strongly reduced by any symmetry of the molecule. As a result, any carbons that can be transformed into another by a symmetry operation (rotation, translation, reflection), will give rise to only a single line in the spectrum.

Decoupling

A technique that eliminates all hydrogen-carbon spin-spin coupling interaction is called broadband decoupling (39). This process is carried out by applying radiofrequency irradiation at the frequency of one resonance during recording of the spectrum. This induces very rapid transitions between two spin states for the irradiated proton, so that the coupled partner experiences only an average of the spin states. As a consequence, the coupled partner resonates only at a single frequency in the absence of other protons and the present multiplets collapse into a single peak (36).

2.4.5. Two dimensional NMR experiments

Two dimensional NMR spectra contain two frequency axes. The third axis is representing the intensities and it is usually displayed as a contour plots. Two dimensional NMR plot provides a correlation of resonances between first and second axis and this provides

information on how the spins are related to each other within the molecule. In general 2D correlations present scalar coupling, dipolar coupling (a NOE) or chemical exchange between spins. There are two types of two dimensional NMR spectra: *resolved spectra* and *correlated spectra* (42). If both dimensions contain chemical shift, the experiment is called shift-correlated 2D NMR, if one dimension denotes scalar couplings, the spectra are called *J*-resolved (41). Generally, all 2D NMR experiments consist of a series of 1D experiments in which a single delay has been altered in length. When a 2D NMR spectrum is recorded, the same NMR experiment is repeated many times, changing the evolution time value from 1D spectrum to another. However, 2 D NMR experiments apart from displaying correlations between signals, allow easier extraction of the chemical shifts from better dispersed spectrum (41), thus this technique can be particularly useful when signals on 1D NMR spectrum overlap.

The 2 D NMR spectroscopy includes the following techniques (41):

Homonuclear with interactions through bond: COSY – Chemical Shift Correlation Spectroscopy, TOCSY – Total Correlation Spectroscopy, INADEQATE- Incredible Natural Abundance Double Quantum Transition Experiment

Homonuclear with interaction through space*:* NOESY – Nuclear Overhouser Effect Spectroscopy, ROESY – Rotating Frame Overhauser Effect Spectroscopy

Heteronuclear with one bond correlation*:* HSQC – Heteronuclear Single Quantum Coherence, HMQC- Heteronuclear Multiple Quantum Coherence

Heteronuclear with long-range correlation: HMBC - Heteronuclear Multiple Bond Correlation

In the present work, in order to elute the chemical structures of the products and intermediates of 9-ethylcarbazole hydrogenation, the following 2D NMR methods were used: COSY, NOESY, HSQC, TOCSY and HMBC. The COSY experiment provides a

map of all coupling networks between protons in a molecule. This experiment allows to rapidly determine the coupling pathways within even complicated molecules, by correlating the chemical shifts in a stepwise manner (19). In the NOESY experiment, the cross peaks originate from dipolar interaction between spins. In TOCSY experiment the coherence takes place via scalar couplings and the cross-peaks contain both passive and active couplings in–phase. Using this technique, the protons belonging to the same spin system can be determined. Finally, the HMBC experiment gives heteronuclear shift-correlation spectra in which the coherences are transferred through much smaller long–range couplings as compared to HSQC experiment. Additionally, the HMBC experiment is very useful because it contains the correlations to quaternary carbons.

2.5. Density Functional Theory (DFT) calculations

Computational chemistry is an independent research branch that can add information and help understand and analyze the experimental data. There are two main areas of research in computational chemistry which are: molecular mechanics (uses the laws of classical physics to predict structures and properties of molecules) and electronic structure theory (uses the laws of quantum mechanics as the basis for the computations) (43). Both of these methods can perform basic calculations of: the energy of a particular molecular structure, geometry optimization and vibrational frequencies of the molecules (44).

Within the electronic structure methods there are three major classes of methods:

- semi-empirical methods (use parameters derived from experimental data)
- ab-initio methods (do not use experimental data, solely based on the laws of quantum mechanics and on the values of physical constants)
- DFT methods

DFT methods are very attractive because they include the effects of electron correlation (the interaction between electrons in the molecular system) in their model, whereas the other methods consider this effect in the average sense only (44). However, the major problem of DFT calculations is that the accurate functional for exchange and correlations are not known except for the free electron gas. Even though various approximations exist, most of the calculations are only valid for systems in the gas phase (45).

Basis set

Quantum chemical calculations are usually done using a finite set of basic functions. A basis set is a mathematical representation of the molecular orbitals within a molecule and it can be understood as restricting each electron to a particular region in space. The larger the basis-set, the less restrictions it imposes on electrons and therefore makes the approximation of the molecular orbitals more accurate (44). There are three main types of basis set: minimal basis sets (uses fixed –size atomic –type orbitals), split valence basis set (has two or more sizes of basis function for each valence orbital and allows orbitals to change size but not shape) and polarized basis set (adds orbitals with angular momentum beyond requirements of the ground state to the description of each of the atoms) (44).

Geometry optimization

Structural changes in the molecule usually produce differences in their energy. The way the energy varies with the structural changes is described by the potential energy surface. The potential energy surface is a mathematical function linking the molecular structure and the resulting energy. Geometry optimizations usually are performed to locate the equilibrium structures of molecular systems. A geometry optimization begins with the structure specified as an input and then calculates the gradient at that point and indicates

the directions in which the energy decreases most rapidly (44). It should be noted that the geometry optimisation must be performed prior to any frequency calculations (44).

DFT calculations of thermochemistry and adsorption energy

Frequency calculations that can be done on the previously optimised structures include the analysis of the thermochemistry of the system (44). The thermodynamic quantities of the system can be obtained at the specified temperature and pressure to calculate the thermal energy of the system (43). The thermal energy of the system takes into account rotational, translational and vibrational modes. Subsequently, the total enthalpy of the system can be computed, which is the sum of electronic energies that are calculated during geometry calculations and thermal energies of the system. The electronic energies of the system have to be corrected using zero-point energy values. The zero-point energy accounts for the effects of the molecular vibrations which are present even at 0 K (44). Additionally, it is well known that the calculated harmonic vibrational frequencies carry a systematic error when they are compared to the experimental fundamental vibrational frequencies (46). Thus, for computed zero-point energies and frequencies, the adequate scaling factors must be used to match the experimental data. One should be aware that the optimum scaling factors differ with the basis set used and the scaling factor for zero-point energy and the frequencies might be slightly different (44)(46) (47) (48).

2.6. References

1. Stochiometric number and reaction mechanism of amonia synthesis**. C. Bokhoven, M. J. Gorgels, P. Mars,** *Trans.Faraday Soc.*, 1959, Vol. 55.
2. *Handbook of heterogenous catalysis volume 2.* **G. Ertl, H. Knozinger, F. Schuth, J. Weitkamp,**. Weinheim, Wiley-Vch Verlag, 2007.
3. *Surfaces.* **G. Attard, C. Barnes,** Oxford, Oxford University Press, 1998.
4. *Adsorption by powders and porous solids.* **E. Rouquerol, J. Rouquerol, K. Sing,** London: Academic Press, 1999.
5. *Heterogenous catalysis for the synthetic chemist.* **R. L. Augustine,** New York : Marcel Dekker, 1996.
6. Adsorption and co-ordination of unsaturated hydrocarbons with metal surfaces and metal atoms. **G. C. Bond,** *Disc.Faraday Soc,* 1966, Vol. 40.
7. *http://www.tutorvista.com.*
8. *Surface chemistry.* **E. M. McCash,** New York : Oxford University Press Inc., 2001.
9. *Handbook of heterogenous catalysis volume 1.* **G. Ertl, H. Knozinger, F. Schuth, J. Weitkamp,** Weinheim, Wiley-VCH Verlag, 2007
10. *Catalysis with transition metal nanoparticles in colloidal solution: Nanoparticle shape dependence and stability.* **R. Narayanan, M. A. El-Sayed,** *J. Phys. Chem.,* 2005, Vol. 109.
11. *Nanoparticles: building blocks for nanotechnology.* **V. Rotello,** London, Springer Science, 2004.
12. Structure and reactivity of Pt–Ru/SiO_2 catalysts for the preferential oxidation of CO under excess H_2. **S. Y. Chin, C. T. Williams, M. D. Amiridis,** *J. Phys. Chem. B,* 2006, Vol. 110.
13. *FTIR Study of CO interaction with Ru/TiO_2 catalyst.* **K. Hadjiivanov, J.-C. Lavalley, J. Lamotte, F. Maug, J. Saint-Just, M. Che,** *J. Catal.*, 1998, Vol. 176.
14. *Characterization of supported and nonsupported hydrogenation catalysts.* **J. J. F. Scholten, A. P. Pijpers, A. M. L. Hustings.** *Catal. Rev. Sci. Eng*., 1985, Vol. 26.
15. Infrared spectroscopy on size-controlled synthesized Pt-based nano-catalysts, **E. A. Baranova, C. Bock , D. Ilin, D. Wang, B. MacDougall,** *Surf. Sci.*, 2006, Vol. 600.
16. *Formate as a surface probe for ruthenium nanoparticles in solution 13C NMR spectroscopy.* **K. Tedsree, A. T. S. Kong, S. C. Tsang,** *Angewandte Chemie*, 2009, Vol. 47.
17. *Inorganic spectroscopic methods.* **A. K. Brisdon,** Oxford, Oxford University Press, 1998.
18. *Intoduction to spectroscopy. A guide for students of organic chemistry.* **D. L. Pavia, G. M. Lampman, G. S. Kriz,** London**,** Thomson Learning, 2001.
19. *Introduction to organic spectroscopy* **L. M. Harwood, T. D. W. Claridge,** Oxford University Press, 1997.
20. *Spectroscopy in catalysis. An introduction.* **J. W. Niemantsverdriet,** Weinheim, Wiley-VCH, 2007.
21. *Characterisation of heterogenous catalysts.* **F. Delannay,** New York, Marcel Dekker, 1984.
22. *Temperature programmed reduction for solid materials characterization.* **A. Jones, B. D. McNicol,** New York, Marcel Decker, Inc, 1986.
23. *Crystal structure determination.* **W. Clegg,** Oxford, Oxford University Press, 2004.
24. *Elements of X-ray diffraction.* **B. D. Cullity,** New York, Addison-Wesley Publishing Co, 1956.

25. *Physical chemistry.* **P. W. Atkins,** Oxford : Oxford University Press, 1995.
26. *Photoelectron and Auger Spectroscopy.***T. A. Carlson,** New York : Plenum Press, 1975.
27. http://upload.wikimedia.org/wikipedia/commons/f/f2/System2.gif. [Online]
28. *Materials chemistry.* **B. D. Fahlman,** Dordrecht, Springer, 2007.
29. *Hydrogen sorption measurements.* **D. P. Broom,** JRC Scientific and Technical Reports- The Institute for Energy, 2008.
30. *Sieverts apparatus and methodology for accurate determination of hydrogen uptake by light-atoms hosts.* **T. P. Blach, E. Mac, A. Gray.** J. Al. Comp, Vol. 436.
31. *Sievert-type apparatus for the study of hydrogen storage in solids.* **R. Checchetto, G. Trettel, A Miotello.** Meas. Sci. Technol., 2004, Vol. 15.
32. *Hydrogen as a future energy carrier.* **A. Zuettel, A. Borgschulte, L. Schlapbach.** Weinheim, Wiley-VCH Verlag , 2008.
33. *Basic gas chromatography mass spectrometry principles and techniques.* **F. W. Karasek, R. E. Clement,** Amsterdam, Elseviewer, 1987.
34. http://www.umd.umich.edu/casl/natsci/slc/slconline/GC/sld004.htm. [Online]
35. http://en.wikipedia.org/wiki/Gas_chromatography-mass_spectrometry. [Online]
36. http://www.unsolvedmysteries.oregonstate.edu/MS_05. [Online]
37. *Introduction to spectroscopy.* **D. L. Pavia, G. M. Lampman, G. S. Kriz Jr,** Orlando, Sounders College Publishing, 1996.
38. www.chemguide.co.uk. *Chemguide.* [Online] 2000.
39. *Practical skills in chemistry.* **J. R. Dean, A. M. Jones, D. Holmes, R. Reed, J. Weyers, A. Jones,** Essex, Pearson Education Limited, 2002.
40. *Organic chemistry.* **J. Clayden, N. Greeves, S. Warren, P. Wothers,** Oxford, Oxford University Press, 2001.
41. http://www.chem.ucalgary.ca. [Online]
42. *NMR and chemistry. An introduction to modern NMR spectroscopy.* **J. W. Akitt, B. E. Mann,** London, Chapman and Hall, 1992.
43. *Nuclear magnetic Resonance Spectroscopy.* **R. K. Harris,** London, Longman Scientific and Technical, 1986.
44. *help@gaussian.com.* [Online] Gaussian Inc., 2000.
45. *Exploring chemistry with electronic structure methods.* **J. B. Foresman, E. Frish,** Pittsburgh, PA, Gaussian, Inc, 1996.
46. http://arxiv.org/abs/physics/9806013. [Online]
47. *New scale factors for harmonic vibrational frequencies using the B3LYP density functional method with the triple basis set 6-311+G(d,p).* **M. P. Andersson, P. Uvdal,** J. Phys. Chem. A, 2005, Vol. 109.
48. *Scaling factors for vibrational frequencies and zero-point vibrational.* **Y. Tantirungrotechai, K. Phanasant, S. Roddecha, P. Surawatanawong, V. Sutthikhum, J. Limtrakul,** Teochem 760 , 2006, Vol. 760.

3. Experimental methods

3.1. Materials and methods

This chapter contains the details of the synthesis of the catalysts and the preparation of the samples for characterization and catalytic tests. Additionally, it includes the experimental parameters during reaction monitoring, product characterization and analysis.

3.1.1. Preparation of the supported metal catalysts

Supported noble metal and nickel catalysts were prepared using mainly two methods in the present work. The single step method used was mild chemical reduction of metal precursor impregnated on the support and two–step method was based on modified polyol process developed by Sun et al. (1) and subsequent impregnation of the metal colloid on the support.

3.1.2. Materials

All the materials were used as received, without further purification. Sodium borohydride (99%) and ruthenium (III) chloride hydrate (38-42%), platinum (III) chloride, nickel (II) chloride, tris (acetylacetonato) ruthenium (III) (Ru-70, 24.59%), rhodium (III) acetylacetonate (97%), oleic acid, dioctyl ether (99%), oleylamine (70%) were purchased from Sigma-Aldrich. Graphite, activated carbon (activated, ash 4% max), alumina, silica-alumina and zeolite were received from Johnson Matthey. The HPLC grade solvents (acetone, hexane and ethanol) were supplied by Fisher-Scientific.

3.1.3. Mild chemical reduction

The mild chemical reduction used in the preparation of the catalyst was a modified version of the method described by Shinohara et al. in (2). In short, an appropriate amount of ruthenium (III) chloride hydrate salt (0.3g),platinum (III) chloride (0.4g), or nickel (II) chloride (0.2g) was dissolved in 10 ml of distilled water. This solution was then added

drop-wise to the aqueous slurry of the support (typically 2.9 g of support in 15 ml of distilled water). After 48 hours of stirring, the mixture was reduced by solution of sodium borohydride (0.4 g in 10 ml of distilled water) at 90°C. Subsequently, the catalyst was washed five times with distilled water and acetone and centrifuged at 8,000 rpm/min for 10 minutes each time. Then it was left to dry overnight at room temperature under ambient atmosphere.

3.1.4. Modified polyol process followed by wet impregnation.

Step 1

In step one, the sol of metal nanoparticles was produced following the polyol process. Mainly, appropriate amount of Tris (acetylacetonato) ruthenium (III) / rhodium (III) acetylacetonate (0.16g/0.11g) were dissolved in 10 ml of dioctyl ether (99% Aldrich). Then the appropriate amount of oleic acid and of oleylamine (65µl/68µl) for ruthenium, and (42µl/45µl) for rhodium were added to the solution of the precursor, followed by 0.14g / 0.9g for ruthenium / rhodium of 1, 2-hexadecanediol as a reducing agent. The mixture was stirred continuously under nitrogen atmosphere for 30 minutes in a refluxing set-up without heating. Then it was refluxed at 240^{o}C for 40 minutes under nitrogen to form a black sol. After cooling down to room temperature, the catalysts were washed five times with 50% / 50% mixture of ethanol and hexane and centrifuged at 5,000 rpm/min for 10 minutes each time. After washing was completed, the catalysts were left to dry at ambient conditions for 12 h.

Step 2

In the second step of this synthesis method, the produced metal catalyst was wet-impregnated onto the support. Briefly, 0.015g of dried metal nanoparticles was dissolved in 5 ml of ethanol, using ultrasonic bath. Concurrently, 0.285 g of support was dissolved in 10 ml of ethanol. Then, whilst vigorously stirring, the sol of metal nanoparticles was added

drop-wise to the solution of the support. The solvent was then slowly evaporated. Finally, the supported nanocatalyst was dried at ambient conditions for 12 hours before testing. The dry powder was used for catalyst testing without any further pre-treatment.

3.2. Sample preparation and material characterisation

The representative samples of the prepared materials together with some commercial catalyst samples were characterised to gain an insight into the correlation of the catalyst's preparation method on its properties and subsequently the influence of the catalyst properties on its catalytic performance.

3.2.1. Surface area determination (BET)

In a typical experiment, the appropriate amount of sample, (not less then 100 mg) was weighted and placed in the quartz tube of known volume. Subsequently, the sample was outgassed and dried under vacuum at 100°C for 12 hours to remove the adsorbed water from the surface. Then the sample tube was cooled down using liquid nitrogen and a known amount of nitrogen gas was introduced. After the equilibrium was achieved, the pressure was measured with successive pulses of nitrogen. From the volume of the system, the temperature and the amount of nitrogen gas added with each pulse, the empty tube was calibrated in the absence of the adsorbent. Finally, from the difference between the pressure of the nitrogen gas in the empty tube and the pressure observed in the presence of the sample in the tube, the amount of the nitrogen adsorbed was calculated. After the adsorption was completed, the vacuum was applied to the system to measure the rate of the nitrogen desorption to obtain the pore volume of the material and the pore size distribution.

3.2.2. CO –pulse chemisorption

CO chemisorption was used to determine the metal surface. The measurements were performed using a Coulter Omnisorp 360 CX apparatus. According to the chemisorption

procedure, a known amount of catalyst (0.05g) was placed in the reactor and pre-reduced in 300 °C for 1 hour in pure hydrogen at a ramping rate of 10°C / min and then cooled to room temperature before the CO chemisorption was conducted. Subsequently, 99.9% purity CO gas was introduced in pulses and passed through the catalyst bed. The amount of CO gas that was not adsorbed was measured by on-line gas chromatography. The subsequent pulses were introduced until no further adsorption could be observed

3.2.3. CO- chemisorption and Diffuse Reflection Infrared Spectroscopy (DRIFT)analysis

CO adsorption with on-line infra-red spectrometer was used in the present work to characterise the active sites present on the ruthenium nanoparticles with different supports (rutile, alumina, silica-alumina) and different synthesis methods.

The DRIFT spectra were recorded using a Bruker Vector 22 FT-IR spectrometer equipped with Spectra-Tech Diffuse Reflectance Accessory and a high-temperature in situ stainless steel cell (10 cm long) with ZnSe windows. In the experiment, 0.1g catalyst was first pre-reduced at 300 °C for 4 h under atmospheric pressure by a 30 ml / min^{-1} stream of 5 % H_2/ N_2. After switching to pure helium gas (99%) at the same flow rate, the sample was cooled down to room temperature. Subsequently, a stream of purified 5% CO / He was introduced into the cell until a steady state was reached (approximately 30-60 min). The CO adsorption at room temperature was recorded after helium was purged through the cell and until no further changes were observed.

3.2.4. Thermal analysis – Temperature Programmed Reduction (TPR)

In the TPR experiment, a defined mass (0.020g ± 0.005g) of catalyst powder was placed on a quartz-wool plug inside the quartz reactor tube. The sample was first pretreated by heating at 10 °C / min from 40 °C to 150 °C. Subsequently, the temperature was kept stable for 60 min, under a 10 ml /min flow of He to dry the sample before analysis. After

pretreatment was finished, the sample was cooled down to 40 °C and the TPR temperature ramp was started, heating at 6 °C / min up to 600 °C with a constant flow at 10ml/min of 5 wt % H_2 / Ar.

3.2.5. X-ray Powder Diffraction analysis (XRD)

For a typical X-ray powder diffraction experiment, about 0.15 g of powder catalyst sample was used. The samples were grinded using mortar to obtain the fine powder of less than 200-mesh size. Subsequently, the catalyst powder was placed on a glass slide and smothered with a glass slid to ensure a highly leveled sample. The prepared sample was loaded into a Philips DIFF 3, X-ray diffractometer with a Cu-anode source operating at 40KV and 30mA generating CuKα X-ray radiation at wavelengths $CuK\alpha_1$=1.5406 Å and $CuK\alpha_2$=1.54439 Å. The data was collected at 2 θ from 5° to 70° angles, with a step size of 0.02°, step speed of $0.5^{o}min^{-1}$ and at 1.25s per step. The obtained X-ray scans were compared to those of standard database and the phases were assigned using X'Pert HighScore software (version 1.0d).

3.2.6. X-ray Photoelectron Spectroscopy (XPS) analysis

For the XPS experiment, 0.05g of solid sample was grounded in a mortar and subsequently sprinkled on a copper plate with silver paste. The XPS spectra were measured with a Leybold LH 10 spectrometer equipped with a single-channel detector, employing Mg K_α radiation (1253.6 eV, anode operated at 10 kV × 23 mA). Ru (3d) with C (1s) superimposed, spectra were recorded with the analyzer in constant pass-energy mode (pass energy at 50 eV) of various ruthenium based catalytic systems. The XPS peaks were fitted using curve-fitting XPSPEAK41 software, by choosing the appropriate background shape and peak shapes.

3.2.7. Scanning Electron Microscopy (SEM) and Energy Dispersive X-Ray Spectroscopy (EDAX) analysis

For this technique, about 0.1g of the sample in the powder form was used and dispersed to cover the entire surface of a 25 mm diameter carbon disc mounted on an aluminium SEM specimen stubs (Agar Scientific) by a double sided adhesive tape. Then the sample stubs were arranged in the multiple stub sample holder for analysis using a High Vacuum Cambridge 360 Stereoscan Scanning Microscope fitted with an Oxford Instruments INCA for X-ray Analysis system. The samples were focused with a magnification of about 600k and four different areas of each of the samples were examined by EDX analysis with working distance set at 25 mm, dead time 50% and process time of 6 minutes.

3.2.8. Transmission Electron Microscopy (TEM) analysis

In the present work, the catalysts were characterised using a TEM CM 20 (the accelerating voltage 310 kV and 208 kV at nominal magnification) and a HRTEM JEOL 2010 (the accelerating voltage 600 kV, at nominal magnification 590 kV). The preparation of the samples for TEM examination required the dispersion of a few milligrams of the specimen in 5ml of acetone or ethanol using ultrasonic bath. Subsequently, a drop of this suspension was deposited on a 3 mm copper grid covered with perforated carbon film. Then, the solvent was dried out. The TEM observations were carried out with the solid particles across the holes. For determination of particle size distribution, not less than 100 particles from different areas of the sample were measured, using the Scandium software from Olympus Soft Imaging Solutions.

3.3. Hydrogen uptake measurements

The sorption of hydrogen by 9-ethylcarbazole was measured using a volumetric method (Sievert's method)

3.3.1. Sievert's method

In the present work, the hydrogen absorption of 9-ethylcarbazole was monitored using synthesized 5 wt % Ru on alumina catalyst. The reactant (0.2 g) mixed with catalyst (0.05g) was sealed in a 15 ml stainless steel sample chamber. In order to avoid the evaporation and condensation of the products outside the sample chamber, a cooling trap was used. Subsequently, the system was flushed several times with high purity hydrogen and tested for possible hydrogen leaks, using hydrogen detector. Then, the reaction chamber was heated up to required temperature using an oil bath. The temperature was monitored inside the sample chamber using a thermocouple. During the measurement, the reaction mixture was stirred with the aid of a PTFE encapsulated bar turned by a magnetic stirrer-heating mantle produced by Ika-Werke at the speed of 600 rpm/min. The pressure drop was monitored together with the temperature for a period of 20 hours. Based on the measurements, the logarithm of the obtained kinetic rate constants was plotted versus the reciprocal temperature to obtain the Arrhenius plot, from which the apparent activation energy was estimated.

3.4. Catalyst testing

This paragraph describes the typical experimental set-up and conditions used for molten and liquid phase hydrogenation of 9-ethylcarbazole and other heterocyclic compounds as well as gas phase dehydrogenation of 9-perhydroethylcarbazoles.

3.4.1. Materials

9-ethylcarbazole (97%), 1,4-Dioxane (ACS reagent ≥ 99 %), Dibenzothiophene (≥ 98%), 1,2,3,4-Tetrahydrocarbazole, Carbazole (≥ 95 %), 9H-Carbazole-9-ethanol (95%), Fluorene (98 %), Dibenzofuran (98%), Ru black, Pd black, Pt black, 5 wt % Ru /Al_2O_3, 5 wt % Ru /activated carbon (AC), 5 wt % Pd / AC, 65 wt % Ni / SiO_2-Al_2O_3, 5 wt % Rh /

Al_2O_3 and 5 wt % Rh / AC were purchased from Sigma- Aldrich. Hydrogen gas (99.9%) was supplied by Air-Products. Ethanol and cyclohexane, both HPLC-grade solvents were purchased from Fluka.

3.4.2. Hydrogenation of 9-ethylcarbazole in the molten form

The catalytic hydrogenation reactions in molten phase were performed in a 10 ml glass insert placed in a 300 ml stainless steel Parr batch reactor (showed in Figure 3.1) using magnetic stirring. In a typical experiment, 1g of 9-ethylcarbazole was placed in the glass container, followed by 0.2 grams of catalyst. The reactor was then sealed, flushed with hydrogen and heated to 130°C. When the desired temperature was reached, 70 bar of pure hydrogen was charged into the reactor and the reaction time was measured.. The reaction was stirred using a PTFE encapsulated bar and a magnetic stirrer produced by Ika-Werke at the speed of 600 rpm/min placed under the heating mantle of the autoclave. After the required reaction time, the autoclave was cooled down to room temperature using water bath, the pressure was released and the reaction mixture was analysed.

Figure 3.1. A Parr high pressure autoclave batch reactor used to carry out hydrogenation of 9-ethylcarbazole.

3.4.3. Hydrogenation of 9-ethylcarbazole in the liquid phase

The catalytic hydrogenation of 9-ethylcarbazole in solution was performed in a stainless steel 300ml Parr batch reactor (showed in Figure 3.1). In order to obtain the time versus concentration profiles for ruthenium based catalysts, 3 grams of 9-ethylcarbazole was

dissolved in 100 ml of cyclohexane followed by 0.15g of catalyst. However, to obtain the concentration versus time profiles for the catalytic systems based on other metals, milder conditions were used to allow comparison between different noble metals and nickel. Thus, 1 gram of 9-ethylcarbazole was dissolved in 100 ml of cyclohexane, followed by 0.2g of catalyst. The hydrogenation procedure followed was similar to the one described above (paragraph 3.4.2), apart from the fact that in case of the reaction in the solvent, small samples were removed periodically from the reactor for composition analysis. The control experiment was carried out in which the hydrogenation of 9-ethylcarbazole was repeated four times under standard reaction conditions and the results showed the variations of less than 5 % in the values of obtained conversions and selectivity in this series of experiments.

3.4.4. Hydrogenation of other heterocyclic compounds

The studied heterocyclic compounds for hydrogen storage, are gathered in Table 3.1. The hydrogenation reactions of these heterocyclic compounds were studied using previously described set-up and the autoclave shown in Figure 3.1. The hydrogenation procedure was the same as the one followed for hydrogenation of 9-ethylcarbazole but the solvent used was 1,4-dioxane. In short, 3 grams of the substrate was dissolved in 100 ml of 1,4-dioxane and subsequently 0.15 g of ruthenium black was added. Periodically, small samples were removed from the reactor for composition analysis using GC-MS.

Table 3.1. The characteristics of the possible heterocyclic candidates for hydrogen storage materials studied in the present work.

Molecule name	*Molecule structure*	*Molar mass [g/mol]*	*Maximum hydrogen uptake [%]*
Carbazole	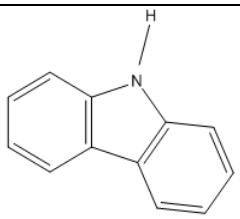	**167.2**	**6.7**
Carbazole-9-ethanol	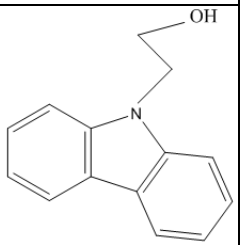	**211.3**	**5.4**
Tetrahydrocarbazole	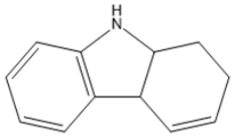	**171.2**	**4.4**
Acridine	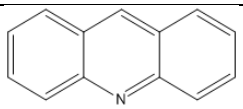	**179.2**	**7.2**
Fluorene	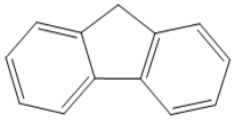	**166.2**	**6.7**
Dibenzofuran	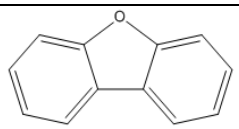	**168.2**	**6.7**

3.4.5. Dehydrogenation of 9-ethyl-perhydrocarbazole

9-perhydroethylcarbazole is not commercially available, thus it was synthesized using the previously described autoclave set up and the following conditions: 0.3 g of 5 % Ru / Al_2O_3, 6g of 9-ethylcarbazole at 130 °C, with 70 bar of H_2.

The dehydrogenation trials were performed using a 50 ml two neck round bottom flask equipped with two vacuum tight gauges and heated up using a hot-plate (Ika-Werke) and an oil bath equipped with a thermocouple. The reaction was performed in three atmospheres, namely: vacuum ($3.6 \cdot 10^{-3}$ mbar), hydrogen (1 bar) and nitrogen (1 bar) over Ru black, 5% Pt / Al_2O_3, 5 wt % Pd / AC, 5 wt % Pt / AC and 5 wt % Ru / AC catalysts. In a typical dehydrogenation experiment, 0.2 g of 9-ethyl-perhydrocarbazole was put in the flask followed by appropriate amount of the catalyst (10:1 molar ratio substrate / metal in the catalyst). Subsequently, the flask was flushed with nitrogen or hydrogen for 10 min to ensure oxygen free atmosphere. For some of the trials, vacuum was applied. Then, the flask was closed tightly using high vacuum silicone grease (Dow Corning, Sigma-Aldrich) and heated up to 200 °C. After reaching the temperature, the time of the reaction was measured. The temperature was kept stable for 4 hours. Finally, the flask was cooled down to room temperature using an ice-bath. Then, it was opened, washed with acetone and the reaction products were qualitatively analyzed using GC-MS.

3.5. Analysis of the reaction products

3.5.1. Conditions for GC-MS analysis

The intermediates and products of the reversible hydrogenation of 9-ethylcarbazole and other heteroaromatic compounds were detected and separated using a GC-MS system (Agilent 6890-5975E GC-MS) equipped with a non-polar capillary column (Agilent 19091s-433) and an auto-sampler. Helium at the pressure of 1.1 bar and the flow of 124 ml/min was used as a carrier gas. To minimize the injection error of the autosampler, 0.5 ml of 1,2,4-trimethylbenzene (TMS) solution (0.09 mol / dm^3) in cyclohexane or dioxane was used as an external standard. Before analysis, the separate calibration curves were prepared for each of the reactions analyzed, running at least five different concentrations

of the starting material with the time-temperature programme used later for the analysis of the specific experimental mixture. Response factor of 1 was assumed for all of the products. The temperature at the injection port was set at 250 °C and the injection volume was 1µl for all of the analyses performed. The detector used was an MSD- Triple Axis Detector HED-EM mass detector.

In typical GC-MS analysis, 1ml of the reaction mixture was put in the 1.5 ml sample vial, followed by 0.5 ml of TMB standard solution. The time-temperature programme was varied according to the structure of the molecules of interest. For the analysis of *9-ethylcarbazole hydrogenation and dehydrogenation*, the temperature was raised from room temperature up to 150 °C with a rate of 20 °C / min and held stable for 32 min. For the analysis of *carbazole-9-ethanol*, the temperature was raised from room temperature to 150 °C with a rate of 20°C/min and held stable for 5 min. Subsequently, the temperature was increased with the same rate up to 190 °C and held stable for 25 min. For the analysis of *fluorene*, the temperature was increased with the same rate from the room temperature up to 130 °C and held stable for 22 min. For the analysis of *dibenzofuran*, the temperature was increased from room temperature up to 100 °C and held stable for 5 min, subsequently the temperature was increased with the rate of 5° C / min up to 130 °C and held stable for 25 min. Finally, in the analysis of *carbazole*, *1,2,3,4-tetrahydrocarbazole* and *acridine*, the temperature was raised from room temperature up to 150 ºC and kept stable for 26 min.

To reliably compare the performance of the catalysts, the catalytic activity was computed per gram of metal present in the catalysts, according to the formula shown in **Error! eference source not found.** or per mole of the surface metal as shown in

Equation 3.2. The selectivity was calculated according to the formula shown in

Equation 3.3.

$$Catalytic\_Activity = \frac{9-ethylcarba\ zole\ converted\ [moles]}{total\ metal\ content\ [g] \times time\ [s]}$$ **Equation 3.1**

$$Catalytic\_Activity = \frac{9-ethylcarba\ zole\ converted\ [moles]}{surface\ metal\ [moles] \times time\ [s]}$$ **Equation 3.2**

$$Selectivity = \frac{product\ [moles]}{sum\ of\ products\ [moles]} \times 100$$ **Equation 3.3**

3.5.2. Sample preparation and conditions for NMR experiments

The NMR spectra were obtained from samples in solution and deuterated cyclohexane was used as a solvent. In a typical experiment, cyclohexane was firstly evaporated from the reaction mixture at ambient conditions during 12 hours. Subsequently, the reaction products were dissolved in 2 ml of deuterated cyclohexane (99.6 % atom supplied by Sigma-Aldrich). The catalyst was filtered out using a cotton wool fitted inside a Pasteur pipette. Then, the sample solution was transferred into the glass NMR tubes (Sigma-Aldrich). ^{1}H and ^{13}C NMR spectra were obtained at 400.13 (100.61) MHz on a Bruker Avance- 400 NMR spectrometer. The ^{1}H and ^{13}C NMR spectra, the ^{1}H, ^{1}H-DQF-COSY (double quantum coherence correlation spectroscopy), -JRES (J resolved) and –NOESY (nuclear overhauser effect spectroscopy), and the ^{1}H, ^{13}C-HSQC (heteronuclear single quantum coherence), -HMBC (heteronuclear multiple bond correlation) and –HSQC-TOCSY (total correlation spectroscopy) experiments were performed at 298 K using a 5 mm broadband inverse probe with z-gradient and 90° pulse lengths of 6.8 μs (^{1}H) and 14.9 μs (^{13}C). All spectra were recorded with the Bruker standard pulse programs and parameter sets. The $^{1}H/^{13}C$ chemical shifts were referenced internally using the resonance signals of cyclohexane-d_{12} at 1.38 /26.43 ppm.

3.6. Theoretical considerations

3.6.1. Development of the kinetic models

Kinetic models have been developed for the stepwise hydrogenation of 9-ethylcarbazole, fluorene, carbazole, 1,2,3,4-tetrahydrocarbazole, 9 H-carbazole-9-ethanol, dibenzofuran and acridine.

Firstly, for each of the reactions, the concentration-time profiles were obtained experimentally. In accordance with these profiles, the kinetic models were developed. The fitting of the obtained data to the modelled values for all of the hydrogenation reactions conducted was obtained following the step by step procedure, described in detail here for the example of hydrogenation of 9-ethylcarbazole and a minimum of 11 datapoints.

The developed model for the hydrogenation of 9-ethylcarbazole based on the experimentally obtained concentration changes in time of six species observed in the reaction is shown in Figure 3.2 together with the numbered rate constants for each of the reaction steps.

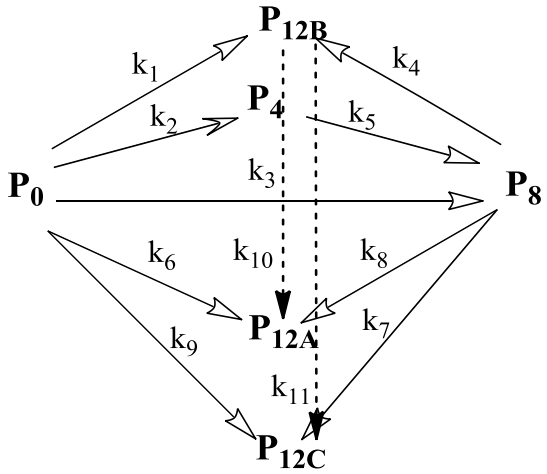

Figure 3.2. A simplified kinetic model of hydrogenation of 9-ethylcarbazole. Acronyms of the intermediates are explained in the text.

Subsequently, based on this model, the following differential equations were derived which are listed below (Equations 3.4 - 3.9);

$$\frac{dP_0}{dt} = -\left(k_1 + k_2 + k_3 + k_6 + k_9\right) P_0 \qquad \text{Equation 3.4.}$$

$$\frac{dP_4}{dt} = k_2 P_0 - k_5 P_4 \qquad \text{Equation 3.5}$$

$$\frac{dP_8}{dt} = k_3 P_0 + k_5 P_4 - (k_4 + k_8 + k_7) P_8 \qquad \text{Equation 3.6}$$

$$\frac{dP_{12A}}{dt} = k_6 P_0 + k_8 P_8 + k_{10}\ P_{12B} \qquad \text{Equation 3.7}$$

$$\frac{dP_{12B}}{dt} = k_1 P_0 + k_4 P_8 - (k_{10} + k_{11})\ P_{12B} \qquad \text{Equation 3.8}$$

$$\frac{dP_{12C}}{dt} = k_9 P_0 + k_7 P_8 + k_{11}\ P_{12B} \qquad \text{Equation 3.9}$$

where; P_0 is the concentration of 9-ethylcarbazole, P_4 is the concentration of 9-ethyl-tetrahydrocarbazole, P_8 is the concentration of 9-ethyl-octahydrocarbazole, P_{12A} is the concentration of 9-perhydrocarbazole stereoisomer A, P_{12B} is the concentration of 9-perhydrocarbazole stereoisomer B and P_{12C} is the concentration of 9-perhydrocarbazole stereoisomer C.

Equations 3.4 – 3.9 were readily solved to obtain the initial concentration-time profiles of the species by using the 4th and 5th order Runge-Kutta formulas (3) with the following boundary conditions imposed. At the starting point (time = 0 [s]) the concentration of the substrate was assumed to be 100% ($[P_0]$ = 100 (mole %)) and concentrations of all other species were assumed to be zero.

The first rate constant, k_0, was determined by a regression analysis of the P_0 concentration-time profile (derived from the conversion) against a first order integrated rate law as shown in Equation 3.10 below:

$$[P_0] = [P_0]_{t=0} \exp\left(-k_0\left(t+\delta\right)\right) \qquad \text{Equation 3.10}$$

where: $[P_0]_{t=0}$ represents the concentration of P_0 at the time zero (=100 mole%), whereas δ represents the correction factor for any lag time due to experimental error (determined from the regression analysis). Additionally, k_0 is the overall first order decomposition rate constant of the starting material, and is equal to the summation of k_1, k_2, k_3, k_6 and k_9.

The remaining rate constants were derived using a Nelder-Mead method (simplex method) Generally, the simplex method tests adjacent verticles of the feasible set (polytope) in sequence so that at each new vertex the objective function improves or stays unchanged (4). The initial parameters given in our work were: time, concentrations of the species and a set of starting values of the unknown rate constants. The mismatch between experimental and modelled values was calculated using root mean square (RMS). The distance of the experimental point from the modelled curve was defined as the difference between the observed value (y) and the predicted value ($\hat{y}$) and the number of data points was denoted n (5). Thus, for a set of n values of a discrete distribution the root mean square can be calculated as as showed in Equation 3.11.

$$d_{RMS} = \sqrt{\sum_{i=1}^{n}(y-\hat{y})^2} \qquad \text{Equation 3.11}$$

Thus, the unknown rate constants were solved iteratively to fulfil the conditions described by the reaction model and optimise a set of k values that would result in a minimum mismatch value by changing the k values. Due to the inherent limitations of the Nelder Mead Simplex method, the code developed forced the method to be restarted once the incremental improvement in the minimized function was achieved. This operation reset the

size of the simplex to its initial value, reducing the possibilities of convergence to non-stationary points or local minima. The effectiveness of this approach is depicted in Chapter 5. The calculations were continued until the convergence criteria were satisfied and the mismatch was not greater than the pre-set value. In case a local minimum was found by the software, the k values were changed accordingly to allow better optimisation of the fit. All calculations were performed using Matlab (version 7.5).

3.6.2. DFT calculations of the adsorption enthalpy

In this work, we employed the DFT calculations to investigate adsorption of 9-ethylcarbazole and the 9-ethyl-octahydrocarbazole stable intermediate on both terrace and step sites on Ru surface. The computing was done using Vienna ab initio simulation package (VASP). In the calculations, Ru (001) and Ru (109) were used to model flat terraces and surfaces containing low-coordinated step sites, respectively.

The adsorption enthalpies of the molecules can be calculated according to the Equation 3.12 (6):

$$\Delta \boldsymbol{E_{Ads}} = \boldsymbol{E_{Ads}} - \boldsymbol{E_{Met}} - \boldsymbol{E_{Mol}} \qquad \text{Equation 3.12}$$

where : E_{Ads} is the enthalpy of the catalyst with adsorbed molecule, E_{Met} is the energy of the metallic surface alone (cluster or slab) and E_{Mol} is the energy of the molecule in the gas phase.

3.6.3. DFT calculations of theoretical stability of intermediates and products of hydrogenation reaction

Quantum mechanics calculations were performed using Gaussian 03 software (7). All the calculations were performed with 6-311 + G(3df, 2p) basis set known as a large set, which provided the electronic energy for the geometry optimized molecules and a B3LYP hybrid functional for electron correlation method (8). The same basis set was used for estimation

the vibrational frequencies. Thermodynamic parameters of products and intermediates involving transitional, rotational and translational modes were taken into account. Subsequently, the calculated total enthalpy (the sum of electronic energies found from geometry calculations, and thermal, translational and vibrational energies) was compared to the sum of enthalpies for the starting material together with the total enthalpy of the moles of hydrogen added to create defined intermediate, according to the formula given below in Equation 3.13, where H is the sum of enthalpies and n is the number of moles of hydrogen added to the starting material.

$$H_{starting\ material} + n \cdot H_{H_2} = H_{intermediate\ product} \quad \text{Equation 3.13}$$

The energies contributions were corrected using a scale factor of 0.989, found to be optimal for this particular method and the basis set used (8). All the calculations have been done in a gas phase approximation. In order to introduce thermal effects, the total enthalpies for all of the hydrogenation reaction studied were calculated including thermal contributions to the free energies of the molecule at 403 K.

3.7. References

1. *Monodisperse FePt nanoparticles and ferromagnetic FePt superlattices.* **S. Sun, C. B. Murray, D. Weller, L. Folks, A. Moser,** Science, 2000, Vol. 287.
2. *Local structure around platinum in Pt/C catalysts employed for liquid-phase dehydrogenation of decalin in the liquid-film state under reactive distillation conditions.* **C. Shinohara, S. Kawakami, T. Moriga, H. Hayashi, S. Hodoshima, Y. Saito, S. Sugiyama,** Appl. Catal. A, 2004, Vol. 266.
3. *Numerical methods in chemistry,* **K. J. Johnson.** New York, Marcel Dekker, 1980.
4. *http://mathworld.wolfram.com/SimplexMethod.html.* [Online]
5. http://mathworld.wolfram.com/Root-Mean-Square.html
6. *Study of catalytic sites on ruthenium for hydrogenation of N-ethylcarbazole: Implications of hydrogen storage via reversible catalytic hydrogenation.* **K. A. Morawa Eblagon, K. Tam, K. M. Kerry Yu, S-L Zhao, X-Q Gong, H. He, L. Ye, L-C Wang, A. J Ramirez-Cuesta, S. C. Tsang,** J. Phys. Chem. C, 2010, Vol. 114.
7. Gaussian 03, revision B.05. Wallingford CT : Gaussian Inc, 2004.
8. *Exploring chemistry with electronic structure methods.* **J. B. Foresman, A. Frish,** Gaussian Inc, 1998.

4. Reversible hydrogenation of 9-ethylcarbazole in the molten form as a prototype material for hydrogen storage

4.1. Introduction

This chapter will be focused on the reversible hydrogenation of 9-ethylcarbazole in the molten form over noble metal catalysts to be used as a prototype of hydrogen storage system based on the liquid organic hydrides (LOH) concept. Several reports can be found in the literature concerning the dehydrogenation of 9-ethylcarbazole (1) (2) (3) (4) (5) (6) (7). However, since the hydrogenation step of 9-ethylcarbazole (hydrogen loading) is generally assumed to be taking place off-board, there is little interest in studying the regeneration of the storing material. Nevertheless, efficient hydrogenation of 9-ethylcarbazole in the molten state to 9-ethyl-perhydrocarbazole is undoubtedly a crucial step in developing a reversible hydrogen storage system based on 9-ethylcarbazole. Moreover, there are a few reports dealing with the mechanism of 9-ethylcarbazole hydrogenation in the presence of a solvent (1) (8) (9) (10) (11). Before our published work (12), there were no attempts reported to hydrogenate 9-ethylcarbazole in the molten state. Following our report, there was one study reporting hydrogenation of 9-ethylcarbazole in the molten state over Raney Nickel catalyst (8). Nevertheless, it is very important to demonstrate the direct applications of hydrogenation and dehydrogenation of the molten reactant without the unnecessary use of a solvent. It should be noted that the use of any solvent significantly decreases the theoretical hydrogen uptake capacity of the system, which is very often omitted in the literature. Additionally, it should be kept in mind that artifacts due to the solvent dilution could prohibit the practical validity of a reactant-solvent system.

The study of reversible catalytic hydrogenation of 9-ethylcarbazole in the molten state over noble metals catalysts as shown in Equation 4.1 is reported in the following chapter.

$$C_{14}H_{25}N \leftrightarrow C_{14}H_{13}N + 6\ H_2 \qquad \textbf{Equation 4.1}$$

The reaction conditions for the hydrogenation of molten 9-ethylcarbazole with ruthenium black as the catalyst have been optimised. The specific catalytic activities (per gram of metal) and the selectivities towards the fully hydrogenated product obtained by the catalysts were compared among the most active catalysts. The catalyst materials have been characterised by TEM, BET and EDAX techniques. The intermediates and products of the reaction were identified using combined GC-MS and NMR techniques. The rate constants and the apparent activation energy of 9-ethylcarbazole hydrogenation over 5 wt % Ru/Al_2O_3 catalyst were obtained. The reversibility of the system based on 9-ethylcarbazole in the molten state was demonstrated by some preliminary dehydrogenation trials of 9-ethyl-perhydrocarbazole.

It is noted that a part of the research described in this chapter has been published in (12) and the input of all the co-authors of the aforementioned article is greatly appreciated.

4.2. Materials and methods

Commercial catalysts were purchased from Sigma-Aldrich. Graphite, activated carbon, alumina, silica-alumina and zeolite were purchased from Johnson Matthey. Hydrogen gas of technical grade was supplied by Air-Products. The HPLC grade solvents were supplied by Fisher-Scientific. The supported catalysts were produced by mild chemical reduction method using $NaBH_4$ as a reducing agent. The details of the synthesis can be found in Chapter Three. The hydrogenation reactions were performed in a stainless steel Parr autoclave equipped with magnetic stirring and a temperature controller. The products and intermediates of the reaction were collected and subsequently analysed using off-line GC-

MS and NMR techniques. The hydrogen uptake of 9-ethylcarbazole was measured using Sievert's method. The details of the procedures are also described in Chapter Three.

4.3. Results and discussion

4.3.1. Characterisation of the catalysts

Physical properties such as metal particle size, metal loading obtained by EDAX analysis and total specific surface area of the selected catalysts are shown in Table 4.1.

Table 4.1. Physical properties of the catalytic systems investigated.CR stands for samples prepared by mild chemical reduction, COM are commercial samples, sd is standard deviation of the particle size measurements.

Catalyst (based on recipe value)	Synthesis method	Particle size [nm] (s.d)	BET specific surface area [m^2/g]	Average pore diameter [nm]	Metal loading [%] by EDAX
5 wt % Ru / Al_2O_3	CR	1.61(0.38)	152	11.7	4.8%
5 wt % Ru /TiO_2	CR	2.11 (0.55)	191	14.6	4.8%
5 wt % Ru / Al_2O_3	COM	9.08 (1.20)	83	12.0	-
5 wt % Ru / SiO_2-Al_2O_3	CR	2.37(0.61)	483	5.4	4.8%
5 wt % Ru / zeolite	CR	2.31(0.62)	343	3.2	4.7%
Ru / graphite	CR	2.30(0.58)	7	35.3	4.9%
5 wt % Ru /activated carbon	CR	2.99 (1.04)	538	5.2	4.8%
65 wt % Ni on SiO_2-Al_2O_3	COM	7.50 (1.54)	95	10.0	-
Ru black	COM	aggregated	22	24.4	-

As shown in Table 4.1, the BET surface measurements revealed that all the tested catalytic systems were mesoporous with a wide range of pore sizes. Furthermore, based on the results from the EDAX analysis depicted in the same table, the synthesis route of mild chemical reduction followed in this work, resulted in metal loadings close to the expected 5 wt % of metal. The representative EDAX spectrum of 5 wt % Ru on alumina (CR) is shown in Figure 4.1. The first and the highest peak in this EDAX spectrum belongs to the carbon disc mounted on the aluminium SEM specimen stub. The presence of the carbon from the sample holder was taken into account in the calculations of the sample composition.

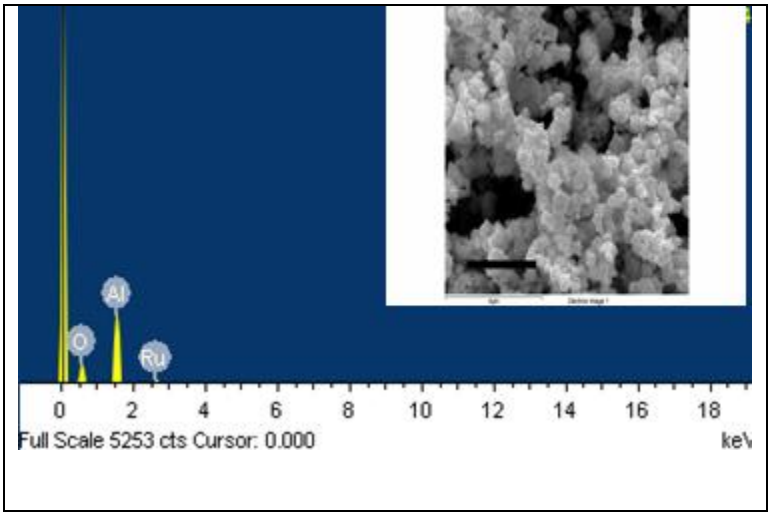

Figure 4.1 An EDAX spectrum showing the chemical composition of nominal 5 wt % Ru on alumina obtained using mild chemical reduction. The insert shows the topography of the surface of the same catalyst obtained using SEM. The scale bar in the SEM micrograph is 4 microns.

Figure 4.2 shows the XRD pattern of the same catalyst; 5 wt % Ru on alumina. The diffraction angle of 44.7° is consistent with the diffraction angle of 44.4° of the (101) plane and the angle of 58.3° which is consistent with the angle of 58.4° of the (102) plane of bulk hexagonal ruthenium (ICDD-JCPDS Card No. 06-0663). Nevertheless, it was noted that the peak at 44.7° is strongly overlapping with diffraction angle of 45.9° of the (400) plane of cubic aluminium oxide, which is a dominant phase in the sample. Because of this severe overlapping it was not possible to calculate the crystal size of ruthenium nanoparticles using the Scherrer equation. The XRD analysis confirmed that the synthesized catalyst contained ruthenium nanoparticles in zerovalent state. It should be underlined that the mild chemical reduction method used in the present work allowed to obtain very small metal nanoparticles, which were well dispersed on the support as it can be seen in the HRTEM images of the representative samples depicted in Figure 4.3. Images A, B and C show evenly dispersed ruthenium nanoparticles on various supports together with their particle size distributions. The image D of the best catalyst 5 wt % Ru/Al_2O_3 shows the spacing between lattice fringes. These spacing have been measured and the resulting distances of 2.1Å and 1.9Å agree well with hcp Ru as reported in ICSD 01-088-2333 XRD database.

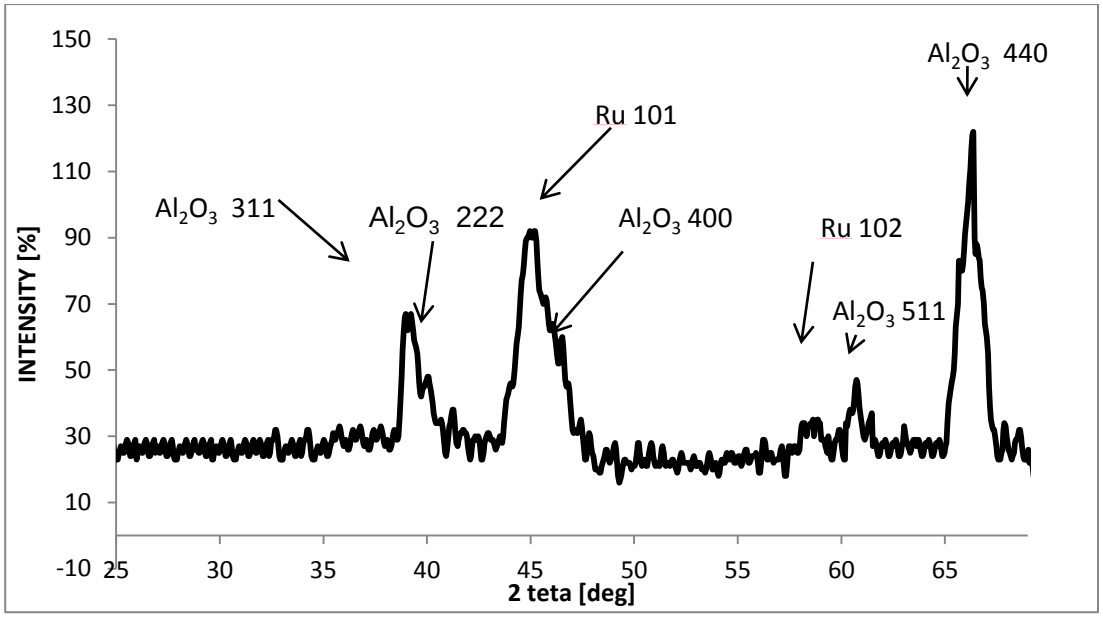

Figure 4.2 XRD pattern of nominal 5 wt % of rut on alumina

The average particle size of the catalysts was measured from the HRTEM images and the results are gathered in Table 4.1. As it can be seen from these results, the catalysts synthesized using chemical reduction at lower temperature results in much smaller particle size as depicted in Table 4.1 and thus much higher dispersion of ruthenium atoms for the catalytic reaction.

A)

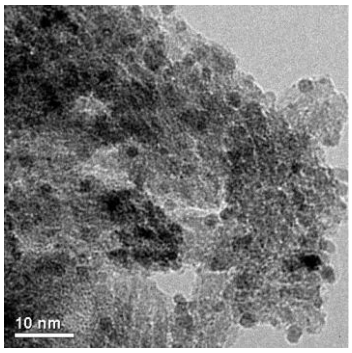

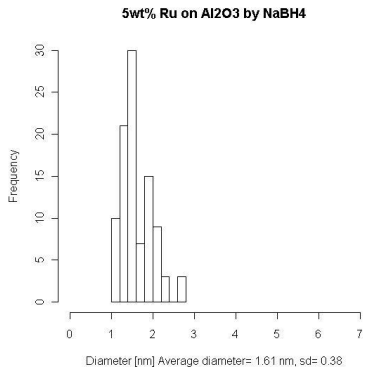

B)

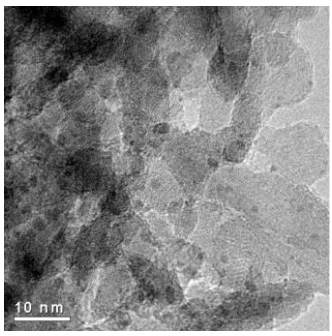

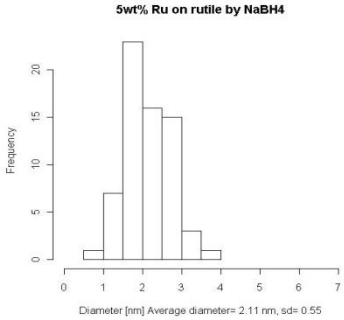

C)

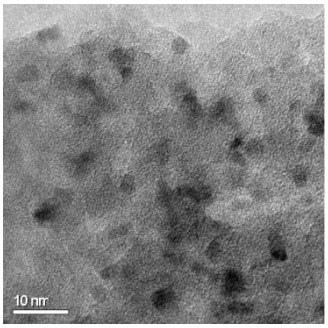

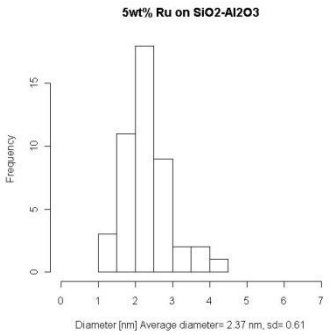

D)

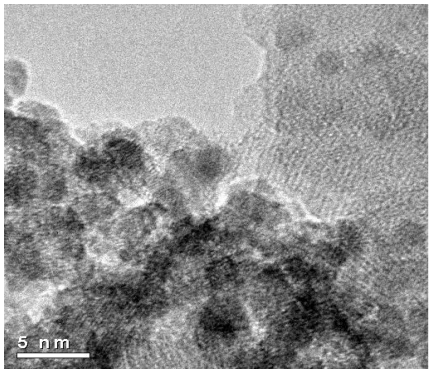

Figure 4.3. The HRTEM images showing A) 5 wt % Ru on Al_2O_3, B) 5 wt % Ru on TiO (rutile)$_2$, C) 5 wt % Ru on SiO_2-Al_2O_3 and D) 5 wt % Ru on Al_2O_3 at high magnification showing lattice fringes.

4.3.2. Preliminary studies of the reaction parameters

The ruthenium black catalyst was used in the preliminary study of 9-ethylcarbazole hydrogenation in the molten form. Ruthenium catalyst was chosen due to the fact that it was reported in the literature as a very active catalyst in the hydrogenation of aromatic compounds (13) (14), as well as because it is relatively cheap as compared to other precious metals such as Pd, Rh, Pt and Re. Additionally, we have selected the unsupported ruthenium to avoid a possible influence of the support on the activity and selectivity of the metal (15). The conversions obtained from batch reactions were determined by using ^{1}H-NMR technique. The results describing the influence of the reaction pressure are shown in Table 4.2. As expected, the conversion of 9-ethylcarbazole increases with the increasing pressure. The increase of hydrogen pressure, increases the solubility of hydrogen in the melted 9-etylcarbazole as well as facilitates the mass transfer of the hydrogen atoms towards the surface of the catalyst. Additionally, increasing the hydrogen concentration shifts the reaction equilibrium in the direction of the products. Due to the fact that it is not commercially feasible to use pressures as high as 100 bar (16), 70 bar of hydrogen pressure was selected as a standard condition for further research.

Table 4.2. Influence of the pressure on the conversion of 9-ethylcarbazole at 373K and 1:10 molar ratio of catalyst to substrate in 20 h reaction.

Pressure [bar]	***Conversion [%]***
50	42
70	65
100	80
125	83
150	90

The conversions obtained were also found to increase monotonically with temperature, from 80% at 373 K up to 95% at 393 K. The 9-ethylcarbazole was fully converted at 403 K. Thus, this temperature was chosen as a standard condition for further studies.

4.3.3. Influence of the reaction time

Once the standard reaction conditions were set to 403 K and 70 bar of hydrogen pressure, the influence of time on the reaction progress was studied. Because of the fact that the 9-ethylcarbazole in the molten form is very viscous, sampling of the mixture during ongoing reaction was not possible. Therefore, every time span was studied as a separate reaction. The analysis of the reaction mixtures obtained at different reaction times using GC-MS, have shown five major products, namely 9-ethyl-tetrahydrocarbazole (Pl 4 [H]), 9-ethyl-octahydrocarbazole (Pl 8 [H]) and three isomers of the fully hydrogenated product 9-ethyl-perhydrocarbazole (Pl 12 [H]). Besides the aforementioned main products, traces (≤ 0.1% selectivity) of 9-ethyl-hexahydrocarbazole (Pl 6 [H]) were also observed. All the intermediates and products of the reaction detected from GC-MS spectra are shown in the simplified scheme of 9-ethylcarbazole hydrogenation in Figure 4.4.

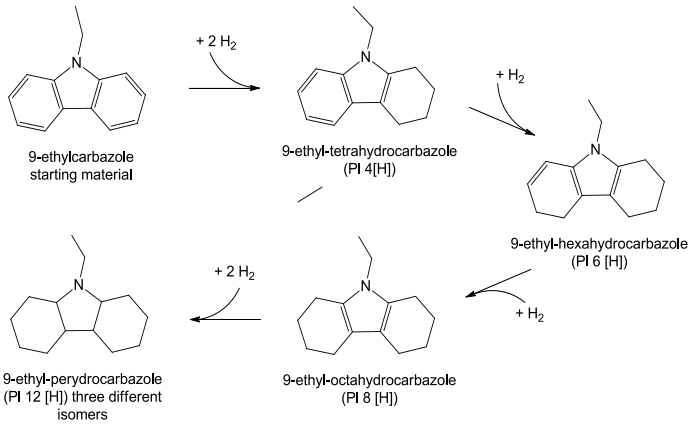

Figure 4.4. Simplified scheme containing intermediates and products of catalytic hydrogenation of 9-ethylcarbazole as seen on GC-MS spectra. Pl 4[H] and Pl 8[H] correspond to four and eight hydrogen atoms added to the starting material, respectively.

The product distribution over time obtained using Ru black catalyst in 20 hours reaction time is shown in Figure 4.5. As it can be seen from this profile, the Pl 4 [H] intermediate is the main initial product of the reaction and its concentration decreases in time.

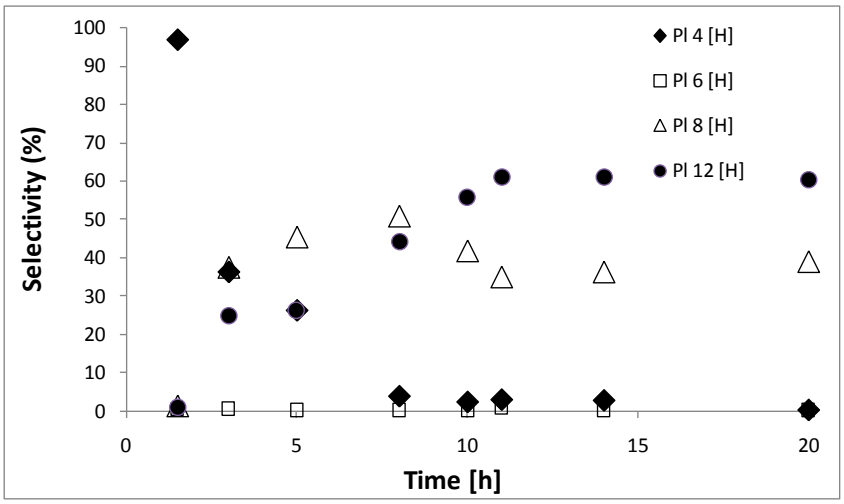

Figure 4.5. The products distribution versus time obtained after 20 hours of the reaction using Ru black catalyst. The names of the compounds are depicted in Figure 4.4.

Additionally, the rate of consumption of 9-ethyl-tetrahydrocarbazole is observed to be much faster than that of 9- ethyl-octahydrocarbazole. After prolonged times of reaction (up to 20 h), this intermediate still contained about 40% of the total products selectivity.

4.3.4. Influence of the catalytic system

The hydrogenation of 9-ethylcarbazole was investigated over a number of supported and unsupported nickel and noble metal catalysts in order to select the most active catalytic system for this reaction. Different catalysts were compared at 403 K, under 70 bar of hydrogen pressure, using 0.2 g of catalysts. This large quantity of catalyst was used to make the conditions milder for less active metals than ruthenium for comparison purposes. The details of the hydrogenation procedure can be found in Chapter Three.

For application in hydrogen storage it is essential to directly and efficiently hydrogenate the substrate without producing any side products. Thus, in order to optimise the relative hydrogen uptake, the catalytic activity and selectivity towards the sum of stereoisomers of fully the hydrogenated product (9-ethyl-perhydrocarbazole) for all of the catalytic systems studied were compared. The specific catalytic activity (Act) per gram of metal present and selectivities (Sel) were calculated as described in Chapter Three. The catalysts were compared based on the catalytic activity per gram of metal, since this value is important in

terms of metal utilization and the cost of the storage system. All screened catalytic systems are depicted in Table 4.3. Overall, the best combination of Sel and Act was clearly displayed by 5 wt % ruthenium on alumina prepared by mild chemical reduction (CR-actual loading 4.8 wt %). It is interesting to note that this catalyst showed much better performance in catalytic hydrogenation of molten 9-ethylcarbazole than its commercial counterpart with the same composition but synthesized at higher temperatures (see Table 4.3). The superior performance of the nominal 5 wt % Ru/Al_2O_3 (CR) can be ascribed to a better utilization of the metal atoms present in this catalyst as compared to the commercial counterpart.

Table 4.3. Catalytic activity and selectivity of screened catalytic systems for hydrogenation of molten 9-ethylcarbazole. COM stands for commercial catalyst, CR represents chemically reduced catalyst, using sodium borohydride solution. ETHC is 9-ethylcarbazole.

Sample (based on recipe value)	Catalytic activity x 10^{-3} (mM ETHC · gram of metal^{-1} · s^{-1})	Catalytic selectivity towards sum of PL 12 [H] stereoisomers (%)
5 wt % Ru/Al_2O_3 (CR)	8.2	98
5 wt % Ru/TiO_2 (CR)	7.9	96
5wt % Ru/Al_2O_3 (COM)	7.8	92
5 wt % $Ru/SiO_2Al_2O_3$ (CR)	7.5	96
5 wt % Ru on zeolite (CR)	7.2	78
5 wt % Ru on graphite (CR)	7.2	64
5 wt % Ru /AC (CR)	6.8	53
5 wt % Pd/ AC (CR)	1.5	2
Ru black (COM)	0.4	77
65wt % $Ni/SiO_2Al_2O_3$ (COM)	0.3	93
5 wt % Pt /AC (CR)	0.1	0.6
65 wt % Ni/ AC (CR)	0.05	33
5 wt % Ni/ AC (CR)	0	0

Table 4.3 reveals that the activity and selectivity critically depend on the type of metal. In general, the most active catalytic systems are ruthenium based supported catalysts, whereas unsupported ruthenium (ruthenium black) with expected low specific surface area

displays rather poor Act (see Table 4.1), mainly due to the poor metal utilization. The catalytic activity of the series of catalysts based on Ru, Pt, Pd and Ni supported on activated carbon (AC), prepared by the same chemical reduction method, decreased in the following order: Ru>Pd>Pt>Ni. The catalytic systems based on 5 wt % Ni did not show any activity under the selected reaction conditions and thus higher metal loadings of nickel were used to boost the conversions obtained by this system. Similarly, supported platinum did not display significant activity in 9-ethylcarbazole hydrogenation. Generally platinum is considered to be highly active in hydrogenation reactions of monoaromatic (17) and polyaromatic compounds (18). However, noble metals are known to be very sensitive to residual amounts of sulphur and nitrogen compounds present in the feedstock (19) (20). As early as in 1961, Freifelder et al (21) observed a rapid catalyst deactivation in the reduction of pyridine ring, and that the presence of acid was crucial to prevent the poisoning of the platinum catalyst. In addition, platinum metals were poisoned by basic nitrogen atoms of the hydrogenated products of pyrrole derivatives (pyrrolidines) in a non-acidic medium (22). It is clear that after the resonance of the 9-ethylcarbazole is broken in the hydrogenation reaction, the lone pair of electrons that was donated to the aromatic ring in 9-ethylcarbazole, becomes localized on the nitrogen atom in the products of this hydrogenation. Thus, the low activity of the platinum catalyst in this work might be attributed to the poisoning effect of the products of 9-ethylcarbazole hydrogenation.

The precise surface condition of metal nanoparticles, which determines the catalytic performance of the metal during catalytic test, is a function of the characteristics of the support (23). To evaluate the influence of the support, ruthenium was deposited onto various solid carriers *via* chemical reduction using sodium borohydride. The catalytic activity was found to be dependent on the type of support used and decreases in the following order: Al_2O_3> TiO_2> SiO_2-Al_2O_3 > zeolite ≥ graphite > activated carbon which

is shown in Table 4.3. It should be noted that this set of catalysts was prepared following the same procedure of mild chemical reduction using $NaBH_4$ solution, as described in Chapter Three.

From the results of TEM particle size measurements gathered in Table 4.1, the particle size of the catalysts in this method depends on the type of the support used in the preparation and decreases with more acidic supports. However, it should be noted that the variations in size are not significant. Moreover, the plain supports were found to be unreactive in the hydrogenation of 9-ethylcarbazole, thus it is clear that the metal was the only active phase in this reaction.

Several alternatives are offered in the literature for explaining the influence of the type of support on the activity of the metal. One possibility is that there is a metal-support interaction (SMSI) which changes the electronic properties of the metal nanoparticles (19). Another explanation could be that the improvement of the catalytic activity of the catalysts is the result of the creation of additional active sites at the metal-support interface which was observed in the hydrogenation of benzene over supported and unsupported Pd catalysts (24). In the present work, the higher activity of the catalysts dispersed on oxide supports would seem to be rather attributed to the additional adsorption sites, than to the SMSI, taking into consideration that the reduction of these catalysts took place at room temperature. However, to clarify this point, XPS analysis of the interaction of ruthenium metal with the support would be necessary and will be analysed in the next chapter.

The order of activity of supports agrees well with the results reported in (25) for 1-methylnaphthalene hydrogenation over sulfided molybdenum catalysts. Moreover, the pore size did not affect the activity of the catalyst. Additionally, comparing Table 4.1 and Table 4.3, no direct correlation has been found between the specific surface area of the support and activity and selectivity of the catalyst. Similar observations have been reported

by Shinohara in the dehydrogenation of decalin (26). With regards to selectivity in 9-ethylcarbazole hydrogenation towards a fully hydrogenated product, when comparing Ru on silica-alumina, zeolite and graphite, all having similar particle size and metal loading, the selectivity tends to decrease with decreasing acidity of the support.

4.3.5. Measurements of the hydrogen uptake

The hydrogen uptake capabilities of 9-ethylcarbazole were recorded in a series of hydrogen adsorption curves measured using a Sieverts' apparatus. The details about the measurement procedure can be found in Chapter Three. In this experiment, the percentage of hydrogen uptake was calculated from the changes of hydrogen pressure, assuming that the drop of pressure resulted only from the reaction of hydrogen with the substrate and taking 5.7 wt% as complete conversion of the starting material. The influence of the temperature on the hydrogen uptake over the most active catalyst 5 wt % Ru/Al_2O_3 (CR) was observed in a series of isotherms recorded at 120°C, 130°C, 140°C, 150°C and 170°C, respectively. An increment of the reaction rate was observed with increased temperature, as depicted in Figure 4.6.

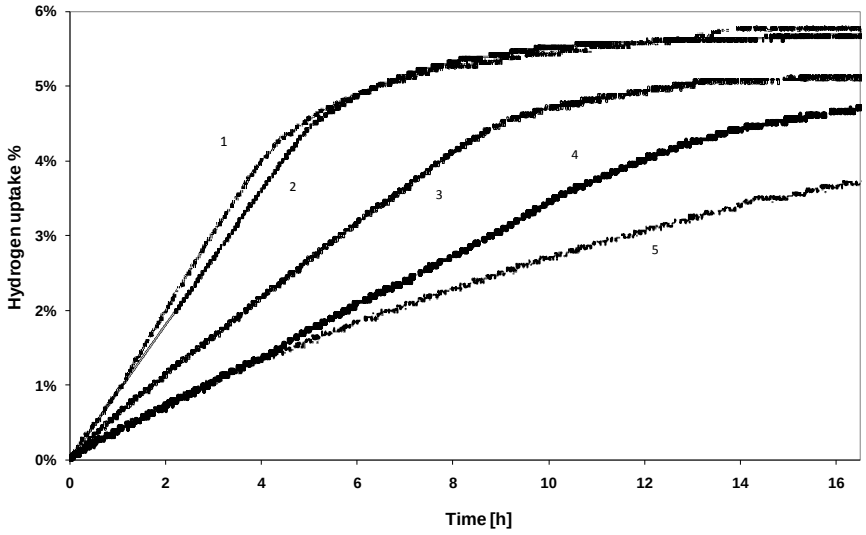

Figure 4.6. Hydrogen absorption curves in 9-ethylcarbazole hydrogenation over 5 wt % Ru/Al_2O_3 (CR) obtained at various temperatures 1- 170 °C, 2- 150°C , 3- 140°C , 4- 130 °C and 5- 120°C with an initial hydrogen pressure of 70 bar, recorded during 16.5 h.

From the isotherms depicted in Figure 4.6, it can be seen that the reaction rate accelerates with increasing temperatures in the range between 120°C to 170°C. Conversely, there is no significant difference between 150°C and 170°C at prolonged reaction times and under both conditions, the hydrogen uptake reaches the theoretical hydrogen uptake value for 9-ethylcarbazole (5.7 wt %). Generally, it should be expected that the increase in temperature would result in an increase in reaction rate, as commonly encountered in liquid phase hydrogenations (1) (9) (16). Nevertheless, the lack of further increase in reaction rate above 150°C encountered in our work could be attributed to the catalyst deactivation at such a high temperatures as it was also suggested in (8). Another explanation might be that the uptake rate at the highest temperature is limited by the mass transfer of the reactants.

The hydrogenation of 9-ethylcarbazole in the molten state has been assumed to be first order in the concentration of the heteroaromatic reagent and zero–order in the concentration of hydrogen, as suggested in the literature for similar reactions (1) (9). Based on the results of the initial hydrogen uptakes at various temperatures over 5wt % Ru/Al_2O_3 (CR), the first order rate constants were calculated. These rate constants together with the calculated initial catalytic activity per gram of metal are gathered in Table 4.4Table 4.4. As shown in this table, the initial catalytic activity of the 5wt % Ru /Al_2O_3 increased by 3 fold with an increase of temperature of 50°C. The increase of temperature also resulted in almost six-fold increase in the initial reaction rate. This implies that the conversion of 9-ethylcarbazole is higher at higher temperatures. The representative fit of the data obtained at 140°C into first order kinetics is shown in Figure 4.7.

Table 4.4. Rate constants and initial catalytic activity for 9-ethylcarbazole hydrogenation over 5 wt.% Ru/Al_2O_3 catalyst. These values were calculated based on rate constants derived from the isotherms showed in Figure 4.6

Temperature °C	*Rate constant, k $x10^{-2}$ (min^{-1})*	*Catalytic activity x 10^{-1} (mM ethc / gram of metal / s)*
120	0.14	0.40
130	0.16	0.47
140	0.26	0.67
150	0.63	1.12
170	0.81	1.23

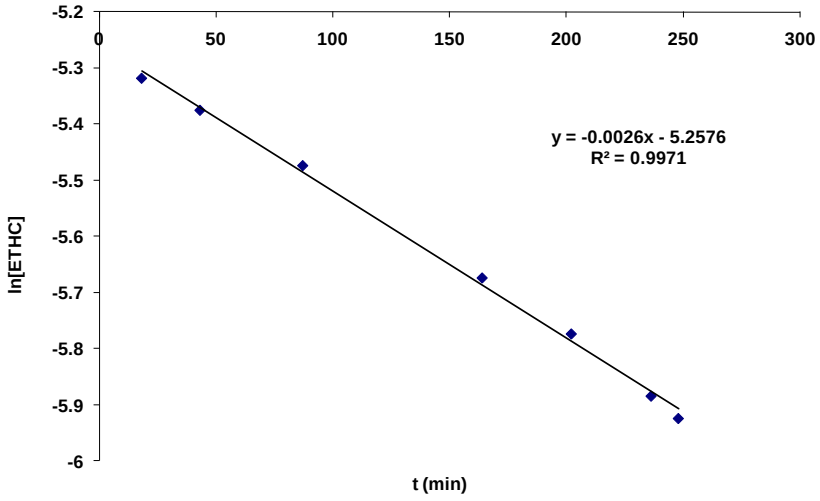

Figure 4.7. A fit of the experimental data into first order kinetics. Data collected at 140 °C, with an initial pressure of hydrogen of 70 bar, over 5 wt % Ru/Al_2O_3 catalyst.

The estimated first rate constants gathered in Table 4.4 were used to evaluate the apparent activation energy of hydrogenation of 9-ethylcarbazole in the molten state over 5 wt % Ru/Al_2O_3 (CR) catalyst. The activation energy was determined using linear regression according to the Arrhenius equation. The Arrhenius plot of the logarithm of the kinetic rate constants versus reciprocal temperature is shown in Figure 4.8.

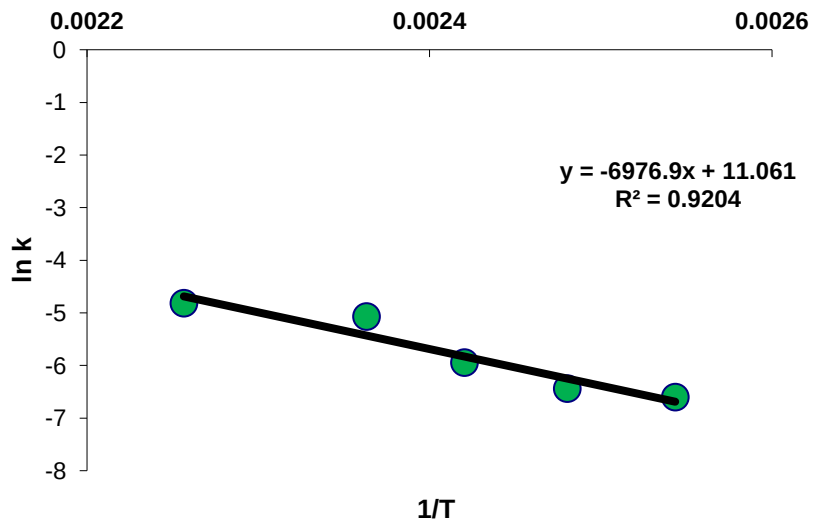

Figure 4.8. An Arrhenius plot using experimentally obtained rate constants.

The estimated activation energy of solvent-free 9-ethylcarbazole hydrogenation over 5 wt % Ru/Al_2O_3 was 58 kJ / mol based on the recorded consumption of hydrogen. This value is similar to the value of 65.17 kJ / mol obtained following our work by Ye et al (8) over Raney-nickel for the same reaction. However, it is lower than the apparent activation energy of 99.5 kJ / mol estimated by Sotodeh et al (9), who studied the hydrogenation of 9-ethylcarbazole in decalin over commercial 5 wt % Ru/Al_2O_3. It could be suspected that a certain degree of mass transfer could be present in the case of molten state reaction, due to the hydrogen solubility and diffusion being limited in this system as compared to the solvent based systems (12). However, no mass transfer resistance at the gas-liquid interface and from the bulk liquid phase to the surface of the catalyst was found recently in the studies of molten state hydrogenations of 9-ethylcarbazole over Raney-nickel (8). This implies that the difference in the apparent activation energies values can simply be the result of different experimental conditions (absence of solvent, smaller reactor, different stirring speed, different catalyst and different catalyst to reactant ratio, etc.). A more detailed kinetic study of 9-ethylcarbazole in the liquid phase over ruthenium based

catalysts using cyclohexane as a solvent was carried out and will be described in the following chapters..

4.3.6. The characterisation of the reaction products and intermediates using NMR techniques

In order to understand the reaction mechanism, the details of the structures of the products and intermediates were analysed and identified using NMR techniques. To our best knowledge, apart from our work (12), there is no report in the literature to address the formation of stereo-isomers of the products and intermediates during the hydrogenation of 9-ethylcarbazole hydrogenation. All reports concerning the hydrogenation reaction (1) (8) (9) are lacking in detailed identification of the reaction products, which is believed to be crucial in elucidating the reaction pathway and, subsequently, addressing the potential reversibility of the catalytic reaction.

The intermediates and final reaction products of the 9-ethylcarbazole hydrogenation identified by GC-MS analysis were: 9-ethyl-tetrahydrocarbazole (Pl 4 [H]), traces of 9-ethyl-hexahydrocarbazole (Pl 6 [H]), 9-ethyl-octahydrocarbazole (Pl 8 [H]) and a set of three different fractions of the fully hydrogenated 9-ethyl-perhydrocarbazoles (Pl 12 [H]). Figure 4.9 shows the high frequency part of the ^{13}C NMR spectra showing the progressing hydrogenation of 9-ethylcarbazole over ruthenium black as it can be seen from the appearance and disappearance of resonances in the aromatic part of the spectra. During NMR analysis of the fractions of the reaction mixtures run at varied times, similar products and intermediates were detected as the ones identified by means of GC-MS analysis (see Figure 4.4). However, the 9-ethyl-hexahydrocarbazole intermediate identified by means of GC-MS was not observed in the NMR spectra, most probably due to its concentration in solution being below the detection limit of the NMR technique. The products and

intermediates with the numbering of carbon atoms used for NMR chemical shift assignments are shown in Figure 4.10.

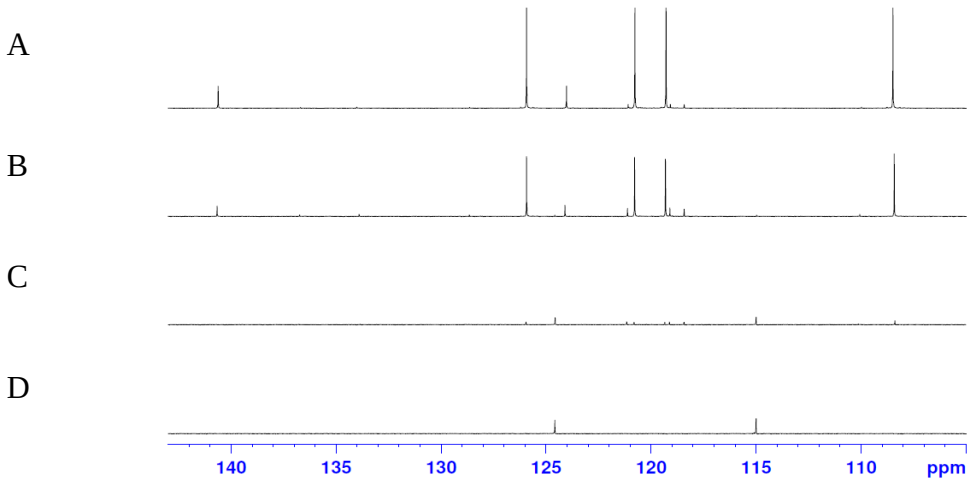

Figure 4.9. High frequency part of ^{13} C NMR spectra showing the appearance and disappearance of aromatic carbons with reaction progress using ruthenium black catalyst under 70 bar of hydrogen at 130° C. The times of the reactions varied as follows: A- 0.5h, B-2.5h, C-11.5 h and D- 23 h

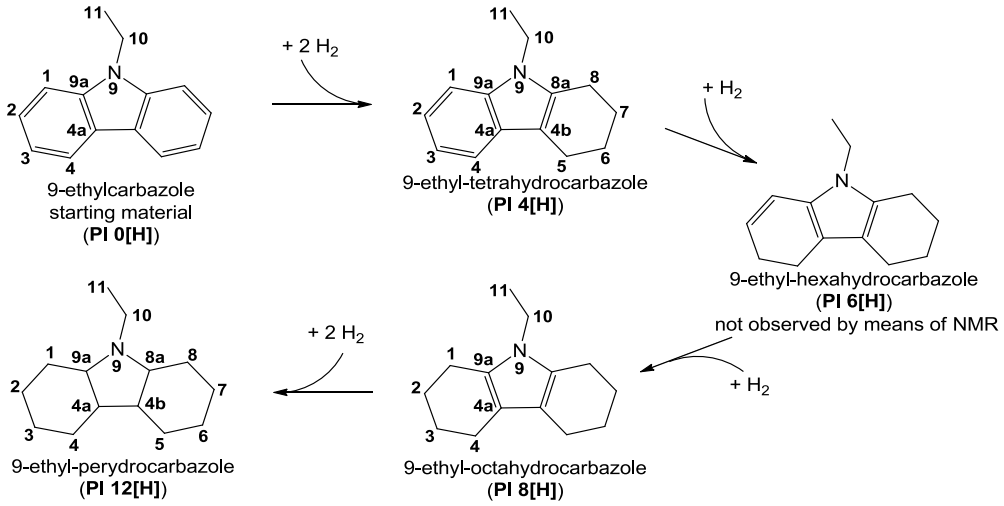

Figure 4.10 Chemical structures of intermediates and fully hydrogenated products of 9-ethylcarbazole hydrogenation together with the numbering of carbon atoms used for NMR signal assignments.

The structure of the first evolving intermediates of the reaction (9-ethyl-tetrahydrocarbazole) and (9-ethyl-octahydrocarbazole) were assigned using a procedure which consisted of the following steps; a) identification of protons and carbon atoms not

yet assigned to already known compounds over HSQC NMR experiments, b) identification of carbon atoms near these protons over the HMBC NMR spectra and c) additional assignments of the ^{1}H spin systems over $^{1}H,^{1}H$ DQF-COSY NMR experiments. In Figure 4.11, the 2D-correlated $^{1}H,^{13}C$ HSQC (correlations of H's to directly bound C's, bottom spectra) and HMBC (correlation of H's to C's 2-3 bonds apart, top spectrum) NMR spectra are shown. The red and blue coloured correlation signals belong to 9-ethylcarbazole (starting material) and to 9-ethyl-tetrahydrocarbazole (Pl 4 [H]), respectively. The chemical shifts and $^{1}H^{13}C$ HMBC and $^{1}H^{1}H$ DQF-COSY correlation results used for assigning of the structure of 9-ethyl-tetrahydrocarbazole are gathered in Table 4.5 and Table 4.6. The ^{1}H and ^{13}C chemical shifts of the 9-ethyl-octahydrocarbazole were easily assigned by the $^{1}H,^{13}C$ and $^{1}H,^{1}H$ correlated NMR spectra. All correlation signals found unambiguously verify the structure of the component shown in Figure 4.10 with the unsaturated pyrrole ring in the middle.

Figure 4.12 shows the aliphatic region of a 2D HSQC-TOCSY NMR experiment, which aided to identify the structure of 9-ethyl-octahydrocarbazole. This 2D NMR experiment consists of two main steps: firstly, the magnetization is transferred from each of the non-equivalent proton nuclei in the molecule to the directly bonded ^{13} C nuclei via proton-carbon scalar couplings (HSQC-step) and subsequently, the magnetisation is spread through the whole coupled homonuclear spin system via proton-proton coupling (TOCSY-step).

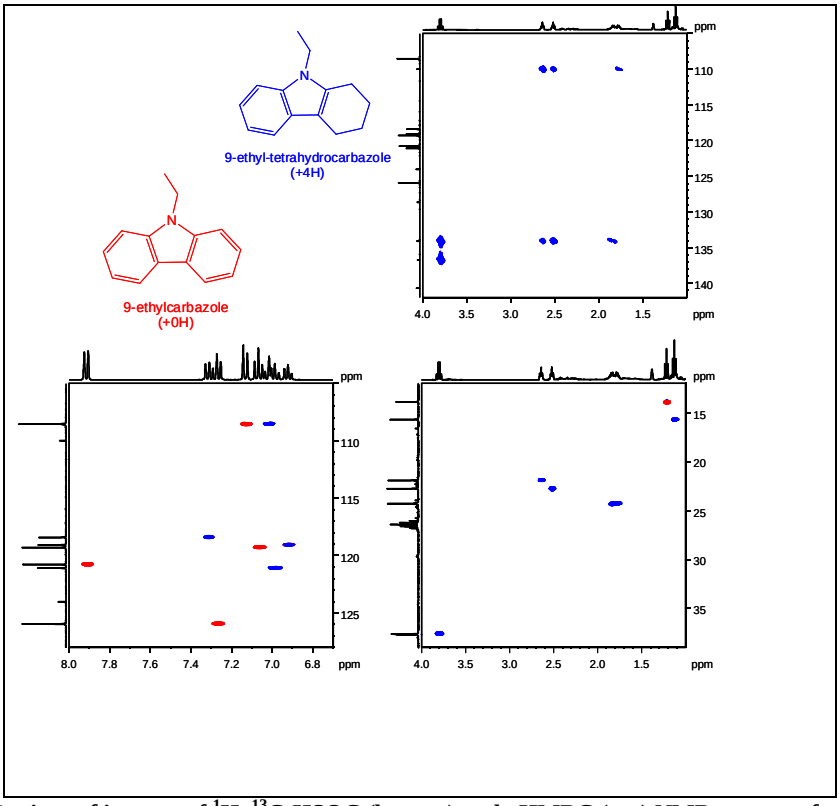

Figure 4.11. Regions of interest of ^{1}H, ^{13}C-HSQC (bottom) and –HMBC (top) NMR spectra of a mixture of 9-ethylcarbazole (starting material, in red) and 9-ethyl-tetrahydrocarbazole (+4H, in blue) quenched during an early stage (1h) of hydrogenation reaction.

Table 4.5 .^{1}H and ^{13}C chemical shifts of 9-tetrahydroethylcarbazole (Pl 4 [H])

Position	*$\delta(^{1}H)$ /[ppm]*	*$\delta(^{13}C)$ [ppm]*
1	7.04	108.4
2	6.98	121.1
3	6.92	119.1
4	7.32	118.4
4a	-	128.6
4b	-	110.0
5	2.65	21.9
6	1.79	24.3
7	1.86	24.3
8	2.54	22.8
8a	-	134.0
9a	-	136.7
10	3.85	37.6
11	1.16	15.7

Table 4.6 $^{1}H,^{13}C$-HMBC and $^{1}H,^{1}H$ DQF-COSY correlations used for NMR shift assignments of 9-ethyl-tetrahydrocarbazole.

HMBC correlations (w = weak)	*DQF-COSY correlations*
H-1→C-(3, 4a); H-2→C-(4, 9a); H-3→C-(1,4a); H-4 →C-(2, 4b, 9a); H-5→C-(4a, 4b, 7, 8a); H-6→C-(4b, 7, 8); H-7→C-(5, 6, 8a); H-8→C-(4aw, 4b, 6, 8a); H-10→C-(8a , 9a, 11), H-11→C-(10)	H-1→H-(2); H-2→H-(1, 3); H-3→H-(2, 4); H-4→H-(3); H-5→H-(6); H-6→H-(5); H-7→H-(8); H-8→H-(7); H-10→ H-(11); H-11→H-(10)

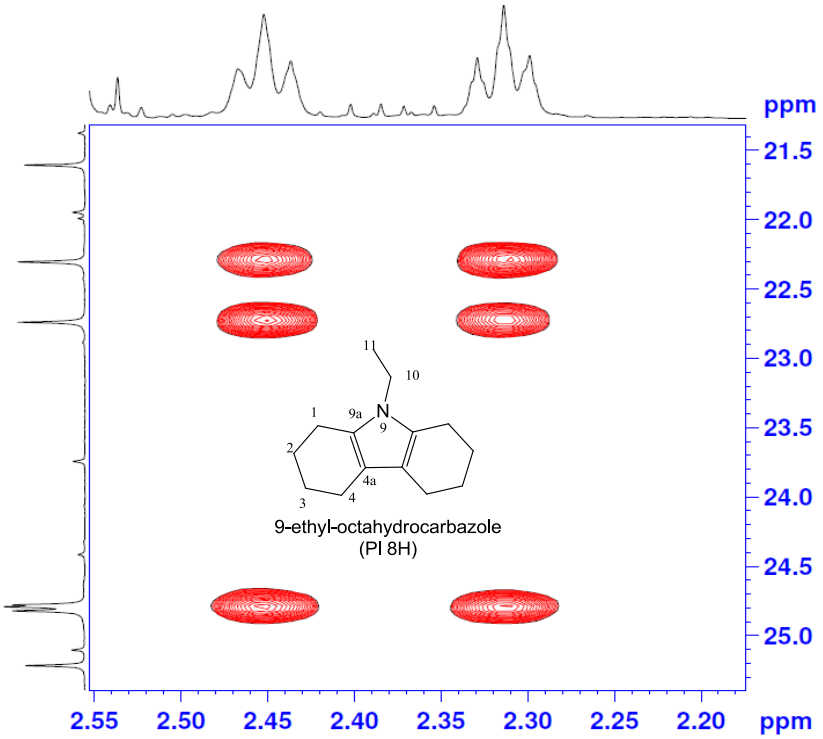

Figure 4.12. Region of interest of 2D ^{1}H, ^{13}C HSQC-TOCSY NMR spectra used for chemical shift assignment of the structure of 9-ethyl-octahydrocarbazole . Insert showing the structure of the compound together with the numbering used for chemical shift assignments. Numbering refers to the position of protons and carbons in the structure.

As a result, cross signals in the spin system between all the protons and carbons with at least one attached proton are obtained. Thus a HSQC-TOCSY NMR experiment aids in identifying coupled spin systems. A spin system is defined as a set of spins in a coupled system of spins in which no interruption of scalar coupling occurs. The horizontal axis in Figure 4.12 shows the chemical shifts of protons and the vertical axis shows the chemical

shifts of ^{13}C nuclei. The ^{1}H and ^{13}C chemical shifts of 9-ethyl-octahydrocarbazole are gathered in Table 4.7. The results from 2D correlated NMR experiments that were used to assign the structure of this intermediate are gathered in Table 4.8.

Table 4.7 ^{1}H and ^{13}C chemical shifts of 9-ethyl-octahydrocarbazole (Pl 8 [H])

Position	***δ(^{1}H) /ppm***	***δ(^{13}C) [ppm]***
1	2.42	22.7
2	1.75	24.8
3	1.67	24.8
4	2.32	22.3
4a		114.9
9a		124.6
10	3.53	37.6
11	1.07	17.0

Table 4.8. $^{1}H,^{13}C$-HMBC and $^{1}H,^{1}H$ DQF-COSY correlations used for NMR shift assignments of 9-ethyl-octahydrocarbazole (Pl 8 [H]).

HMBC correlations (w=weak)	***DQF-COSY correlations***
H-1→C-(3, 4a, 9a); H-2→C-(4, 9a); H-3→C-(1, 4a); H-4→C-(2, 4a, 9a); H-10→C-(9a, 11); H-11→C-(10)	H-1→H-(2); H-2→H-(1, 3); H-3→H-(2, 4); H-4→H-(3); H-10→H-(11); H-11→H-(10)

During the analysis of the NMR spectra of 9-ethyl-perhydrocarbazoles four different sets of resonances belonging to fully hydrogenated products were identified, whereas only three isomers of Pl 12 [H] were identified based on the previous GC-MS analysis. Since fully hydrogenated (Pl 12 [H]) products of 9-ethylcarbazole possess 4 stereo centres at positions 4a, 4b, 8a and 9a of the molecule (see Figure 4.10), therefore a maximum number of 2^4 = 16 stereoisomers are theoretically possible. This number can be considerably reduced in case of the molecules that posses the elements of symmetry (27). Owing to mirror planes and / or C2 axes transforming one structure into another, the maximum number in case of 9-ethylcarbazole is reduced to 6 molecules distinguishable by means of NMR(see Figure 4.13). As a result of the presence of mirror planes and/or C2

axes within the individual structures, only 8 carbon resonances are expected for the 4 symmetric products (structures A-D in Figure 4.13), whereas a total of 14 carbon resonances are expected in the ^{13}C NMR spectra for the asymmetric products (structures E and F in Figure 4.13).

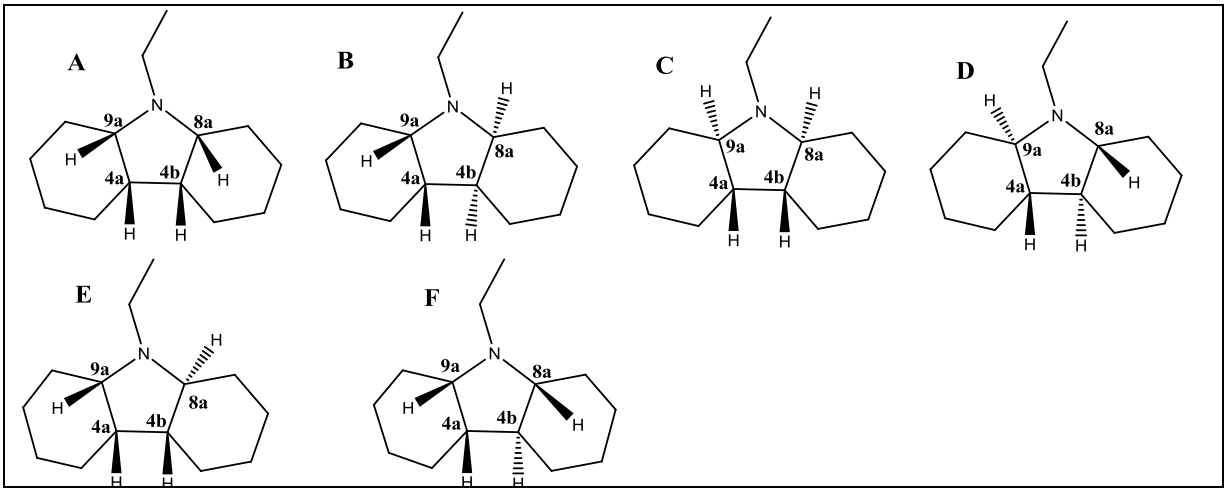

Figure 4.13 Chemical structures of all six 9-ethyl-perhydrocarbazole stereoisomers distinguishable by means of NMR (absolute configuration shown arbitrarily) with partial numbering of carbon atoms used for stereochemical assignments. Upper row shows symmetric compounds (8 different carbon resonances are expected for each of them). Bottom row shows two asymmetric compounds (14 different carbon resonances are expected for each of them)

Four different sets of NMR resonances belonging to fully hydrogenated products were found in the NMR spectra of reaction mixtures obtained using 5 wt % Ru/TiO_2 (CR). The reaction mixture resulting from the prolonged time of the reaction (20h), showed a selective increase of 14 carbon resonances (see Figure 4.14) with similar signal intensities in the aliphatic region of the ^{13}C NMR spectrum. When the hydrogenation reaction was quenched much earlier, the ^{13}C NMR resonances of this species continuously showed equal chemical shifts but with considerably lower relative signal intensities compared to the spectrum shown in Figure 4.14. With the aid of a ^{13}C-HSQC-TOCSY experiment which allows to obtain a magnetization transfer over the whole conjunct spin system of each component, it was possible to evaluate the number of carbons and their chemical shifts from cross peaks in the F1 (^{13} C) dimension, starting from the "outstanding" ^{1}H NMR resonances at 0.88 ppm. Similarly, starting from individual ^{13}C resonances it was

possible to evaluate the corresponding ^{1}H NMR data in the F2 (^{1}H) dimension. It is clear that from the analysis of a HSQC-TOCSY spectrum the attached N-ethyl groups are not detectable, but they could be assigned over the $^{1}H,^{13}C$-HMBC experiments which show longer distance correlations over 2-3 bonds.

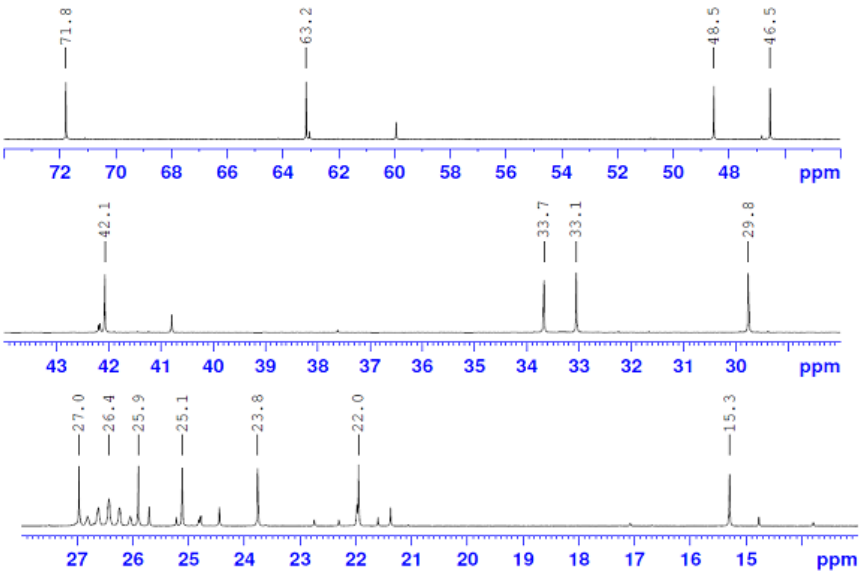

Figure 4.14.1D ^{13}C NMR spectra of the reaction mixture prepared using 5 wt % Ru on rutile at 130 °C, 20 hours and 70 bar of hydrogen. The ^{13}C chemical shifts of the signals belonging to structure E are indicated and the set of signals around 26.4 ppm belongs to deuterated cyclohexane

Thus, the $^{1}H,^{13}C$ HSQC-TOCSY NMR experiment showed that the magnetization of the 'outstanding' proton at 0.889 ppm is transferred over the conjunct system of six closely attached carbons (C-(1-4,4a,9a), Figure 4.15 a) and to all 12 carbons in the spin system of stereo isomer E (see Figure 4.15 b). These results have led to the conclusion that the main product of the reaction over this catalytic system must be asymmetric. All chemical shifts were fully assigned over the $^{1}H,^{1}H$ -DQF-COSY and $^{1}H,^{13}C$ HSQC and HMBC NMR experiments. Owing to the observation of a large vicinal coupling constant ^{3}J (H8aH4b) ≈ 10 Hz a *trans diaxial* configuration of these two protons can be envisioned, whereas ^{3}J (H4a H9a) is rather small. From chemical shift arguments with $\Delta\delta^{13}C$ of 8.6 ppm for the carbon pair C8a / C9a and of only 2.1 ppm for C4a / C4b, further evidence was found for the structure of the main asymmetrical product to have configuration E (Figure 4.13) with

H-8a and H9a in *trans* positions. For the minor asymmetric product F present in low amounts in the mixture of the stereoisomers of 9-ethyl-perhydrocarbazole, values of $\Delta\delta^{13}C$ of 2.1 (for C8a / C9a) and 9.5 ppm (for C4a / C4b) were observed. This observation supports the presumption that H4a and H4b are in *trans* position in this isomer, which strongly indicates structure F (Figure 4.13).

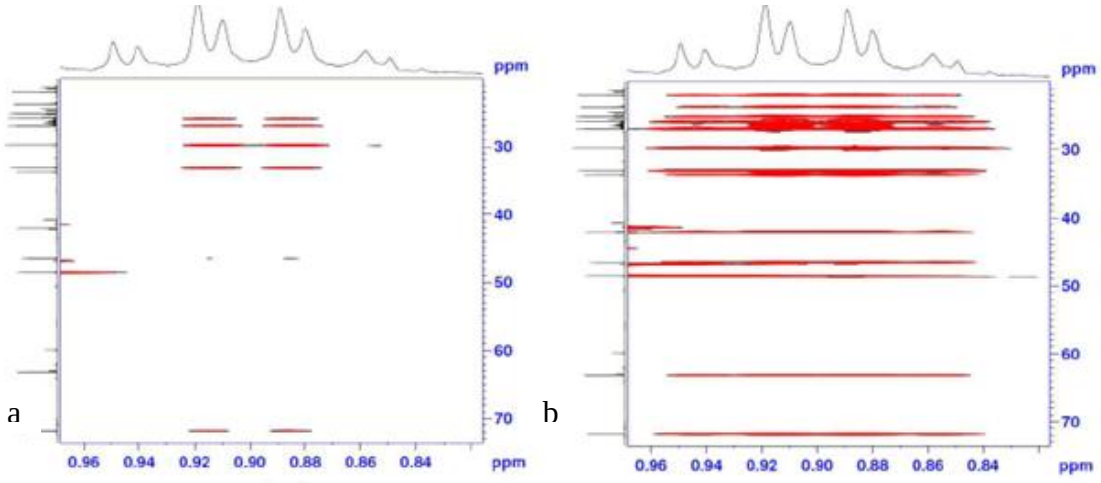

Figure 4.15. Regions of interest of ^{1}H ^{13}C-HSQ-TOCSY NMR spectra showing the correlations of H-1 in stereoisomer E of 9-ethyl-perhydrocarbazole (numbering of carbons shown in Figure 4.10. Spectrum a) correlations to 6 carbons C(1-4,4a,9a) in a closely attached spin system (spectrum shown using a high threshold value) and b) correlations to all 12 carbons (C-(1-8,4a,4b,8a,9a) in the spin system (spectrum shown using a low threshold value).

The reaction mixture obtained using unsupported ruthenium black catalyst in prolonged reaction time (20 h) was also analysed. It was found that the main reaction product consisted of a mixture of two stereoisomers with different structures than the asymmetric stereoisomers E and F in Figure 4.13. Two sets of six distinct carbon resonances were found in the HSQC-TOCSY NMR spectrum, which led to the assumption that the two additional species must be symmetric and that their chemical structures belong to the four structures A-D shown in Figure 4.13. Even though the 1D ^{13}C NMR spectra were not recorded using sufficiently long relaxation delays for full relaxation of the carbon nuclei, almost identical relative signal intensities were observed for each of two sets of resonances for the new species. Notably, C10 and C11 (ethyl group) of these obviously symmetric products exhibited half the intensity as compared to the resonances of all other carbons.

Moreover, it was found that in the mixture of symmetrical products obtained in the reaction over ruthenium black catalyst, one of the products exists in much higher concentration (the ratio of concentrations ≈4/1). The assignments of chemical shifts to individual positions of the core structure in the molecule were achieved with the aid of the DQF-COSY, HSQC and HMBC correlations and chemical shift arguments. However, the evaluation of the relative stereochemistry of the symmetrical products proved to be a challenging part. The normally applied NMR technique to assign relative conformations of structures is the Nuclear Overhouser Effect (NOE) enhancement. Additionally, NOE experiments are widely used for the evaluation of complex structures, since protons "close in space" give rise to structural information (28). Since the 9-ethyl-perhydrocarbazoles of interest are both symmetric, each proton and carbon resonance detected originates from two homotopic carbons or hydrogen atoms, which are not distinguishable by means of NMR with the consequence that the NOE experiment fails. It must be noted that interactions through space for symmetric compounds could be also observed in HSQC-NOESY type of experiments, but this experiment could not be performed since it requires reasonable concentrated samples of high purity. In principle, structural information could also be gained over ^{1}H-^{1}H homonuclear or ^{1}H -^{13}C heteronuclear coupling constants. Unfortunately, the reaction mixtures did not consist of pure compounds and in the obtained mixtures of products at least partial overlap of resonances even in 2D correlated NMR spectra was always observed. Several trials were made to purify the mixtures using techniques such as column chromatography, flash chromatography and thin layer chromatography with a variety of mobile phases and solvent compositions. These were not successful, presumably due to very similar adsorption properties of the different isomers of 9-ethyl-perhydrocarbazole. It can be envisaged, that the mixture of 9-ethyl-

perhydrocarbazoles could be separated on a preparatory GC-MS machine equipped with a non-polar column, however the access to this equipment was not found.

It is well known that the hydrogenation mechanism of carbon-carbon double bonds over metal catalysts is intrinsically *cis* in character and consists of the concerted attack of hydrogen on the side of the adsorbed molecule that faces the surface. This mechanism has been observed in a wide variety of experiments, including hydrogenation, deuteration and isotopic exchange experiments as described in (29). Additionally, it is known that most of the aromatic molecules adsorb preferentially with their plane parallel to the surface of group VIII metal catalysts via interaction of its π electrons (30). Thus, taking into account the aforementioned reaction mechanism and the mode of adsorption of the reagent on the catalyst as well as the structures of the intermediate compounds (see below), the formation of species C and D from Figure 4.13 is fairly unlikely. As a result, the symmetrical products of 9-ethylcarbazole hydrogenation would be expected to have the stereochemistry of structures A and B in Figure 4.13. Moreover, due to the adsorption of 9-ethylcarbazole on the catalysts surface, it is envisaged that the main product of the 9-ethylcarbazole hydrogenation over ruthenium black could have structure A. However this argumentation does not explain the possible creation mechanism of structures B, E and F. Assuming that there is no stable 9-ethyl-decahydrocarbazole (Pl 10 [H]) formed, since no traces of this compound were observed in the reaction mixtures using any of the analytical methods, it can be expected that 9-ethyl-perhydrocarbazoles could be directly made from 9-ethyl-octahydrocarbazoles. Thus, the structure of the resulting isomer of 9-ethyl-perhydrocarbazole would depend strongly on the mesomeric structure of 9-ethyl-octahydrocarbazole and on the strength and geometry of its adsorbed form on the catalyst surface. Figure 4.16 is showing the possible reaction mechanisms of production of 9-ethyl-perhydrocarbazole isomers from different mesomeric

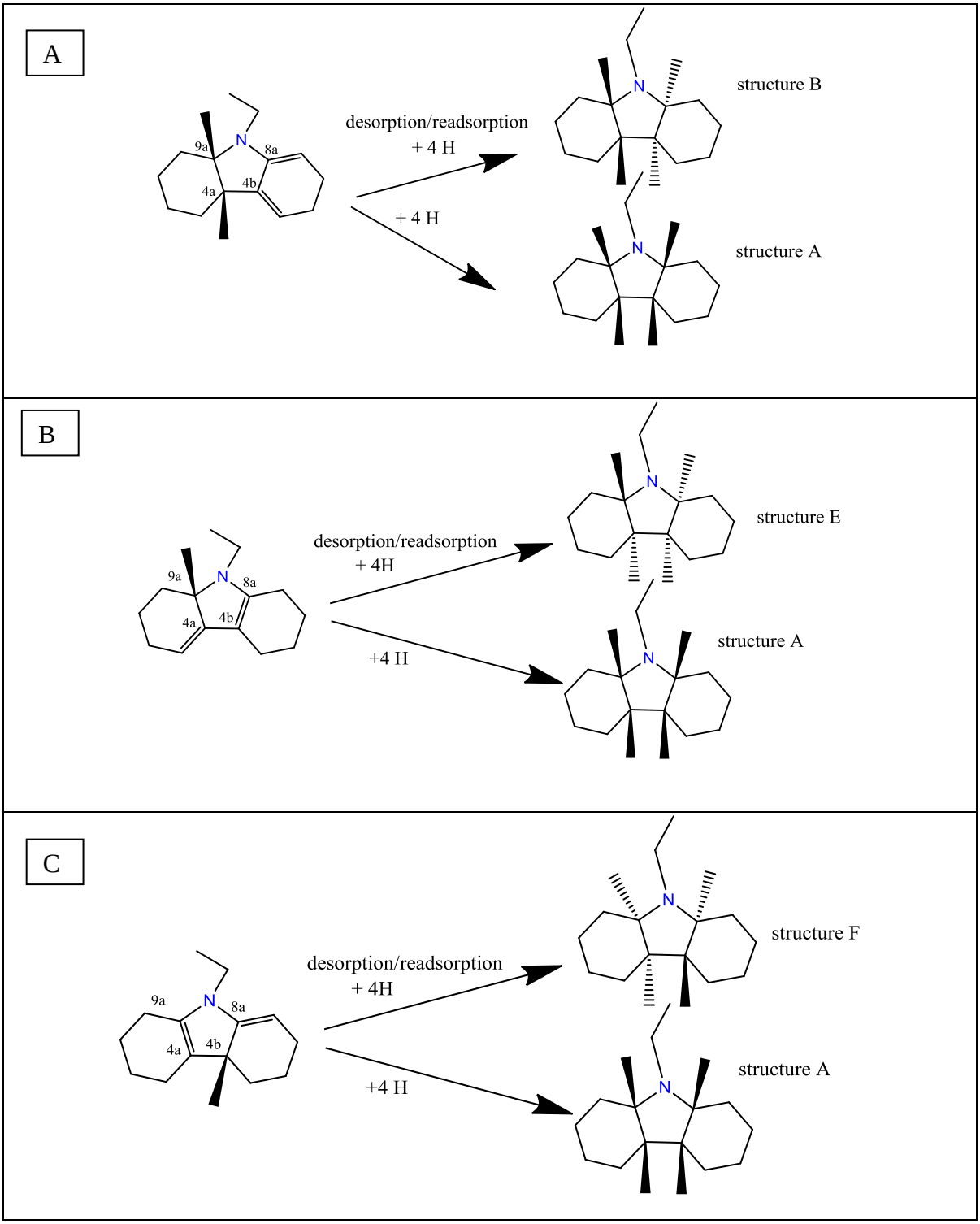

Figure 4.16 Possible mechanisms of formation of 9-perhydroethylcarbazole's isomers A,B,E and F. For clarity purposes, only hydrogen atoms attached to carbons numbered 4a, 4b, 8a, 9a are shown.

structures of 9-ethyl-octahydrocarbazoles. As it is shown in Figure 4.16A, if the 9-ethyl-octahydrocarbazole is originally formed with the hydrogen atoms at positions 9a and 4a directed towards the surface of the catalyst, than 9-ethyl-perhydrocarbazole structure A can be produced by cis-hydrogenation of the remaining double bonds in the molecule.

However, from the same mesomeric structure of 9-ethyl-octahydrocarbazole, structure B of 9-ethyl-perhydrocarbazole can also be produced if the intermediate desorbs and subsequently readsorbes with hydrogen atoms in positions 9a and 4a facing away from the surface. Similarly, as shown in Figure 4.16.B, assuming that 9-ethyl-octahydrocarbazole has a structure with the hydrogen at position 9a oriented towards the surface of the metal, it can be expected that if this intermediate desorbes and subsequently readsorbes with the hydrogen at position 9a facing away from the catalyst surface that 9-ethyl-perhydrocarbazole structure E will be produced by cis addition of the remaining four hydrogen atoms. In case if the reaction takes places in a direct manner on the surface of the catalyst and no desorption of the intermediate takes place, than 9-ethyl-perhydrocarbazole structure A will be expected to be produced by cis addition of hydrogen atoms. Figure 4.16 C shows very similar mechanism of possible creation of 9-ethyl-perhydrocarbazole structure F incorporating the desorption step of the 9-ethyl-octahydrocarbazole intermediate as well as the production mechanism of 9-ethyl-perhydrocarbazole structure A. Therefore, it can be concluded that the catalytic systems, which decrease the strength of the interaction between 9-ethyl-octahydrocarbazole and metal surface, will result in higher selectivities towards 9-ethyl-perhydrocarbazoles structures B, E, and F.

The HMBC and DQF-COSY correlations that were used to assign the chemical shifts of the individual positions of the symmetric A and B and asymmetric compounds E and F are summarized in Table 4.9.

It should be noted that the composition of the final product varied with the type of catalyst used as well as with the time of the reaction. The different compositions of 9-ethyl-perhydrocarbazole product as a function of reaction time and the structure of the catalysts will be discussed in Chapter Five.

Table 4.9 $^{1}H,^{13}C$-HMBC and $^{1}H,^{1}H$ DQF-COSY correlations used for NMR shift assignments of stereoisomers E, F, A and B

Compound	HMBC correlations (w = weak)	DQF-COSY correlations
E	H-1→C-(2, 3, 9a); H-2→C-(4); H-3→C-(1,2, 4a); H-4→C-(3, 9a); H-4b→C-(6,8); H-5→C-(4^a, 4b, 8a); H-6→C-(4b, 5, 8); H-8a→C-(4a, 4bw,7,8w, 10); H-9a→C-(1, 2, 4^a,4b,10); H-10→C-(8a, 9a, 11) H-11→C-(10)	H-1→H-(2); H-2→H-(1); H-4a→H-(9a); H-4b→H-(8a); H-8→H-(8a); H-8a→H-(4b,8); H-9a→H-(4a); H-10→H-(11); H-11→H-(10)
F	H-4b→C-(9a); H-7→C-(8a); H-8a→C-(4aw,4b,5,7,9a,10); H-9a→C-(2,4.4aw,10); H-10→C-(8a, 9a, 11); H-11→C-(10)	H-1→H-(9a); H-4a→H-(9a); H-4b→H-(8a); H-8a→H-(4b); H-9a→H-(4a,1); H-10→H-(11); H-11→H-(10)
A	H-4→C-(9a); H-4a→C-(4a,9aw); H-9a→C-(1,2,4,4a,9a); H-10→C-(9a,11); H-11→C-(10)	-
B	H-2→C-(9a); H-3→C-(1); H-4a→C-(1w,4, 4a, 9a); H-9a→C-(4a); H-10→C-(9a, 11); H-11→C-(10)	–

4.3.7. The trials of dehydrogenation of 9-ethyl-perhydrocarbazoles

Despite the fact that the present work was focussed mainly on the hydrogenation part (hydrogen loading) of the 9-ethylcarbazole based hydrogen storage system, some trials of the reverse reaction were performed in batch mode. The experimental details can be found in Chapter three, paragraph 3.4.5. The aim of these trials was simply to verify the reversibility of the system based on 9-ethylcarbazole hydrogenation-dehydrogenation cycle. Thus, only one set of conditions was tested. The temperature was set at the boiling point T= 200 °C of the 9-ethylcarbazole substrate. This temperature was tested before by Pez et all in (31) for the dehydrogenation of this molecule over Pd supported on carbon catalysts. The ratio of starting material to the catalysts was set at 10:1 molar ratio in order to obtain the so-called superheated liquid film state –type catalysis (32) under reactive distillation conditions. The concept of superheated liquid film state conditions was first developed by Hodoshima et al. (33). Thus, it was reported that when the catalyst surface was covered with a thin film of liquid substrate, the highest catalytic activities were observed. This result was explained by the fact that in the liquid-film state the temperature

of the catalyst surface is higher than the boiling point of the reactant solution. The temperature gradients arising at liquid-film conditions and suspension state are shown in Figure 4.17. Additionally, the catalyst is only wetted by the reagents. Moreover, further increase the conversions due to shifting the reaction equilibrium towards the side of the products can be obtained by continuous removal of the hydrogen from the reaction mixture. However, the on-line removal of the hydrogen produced was not possible in our set-up.

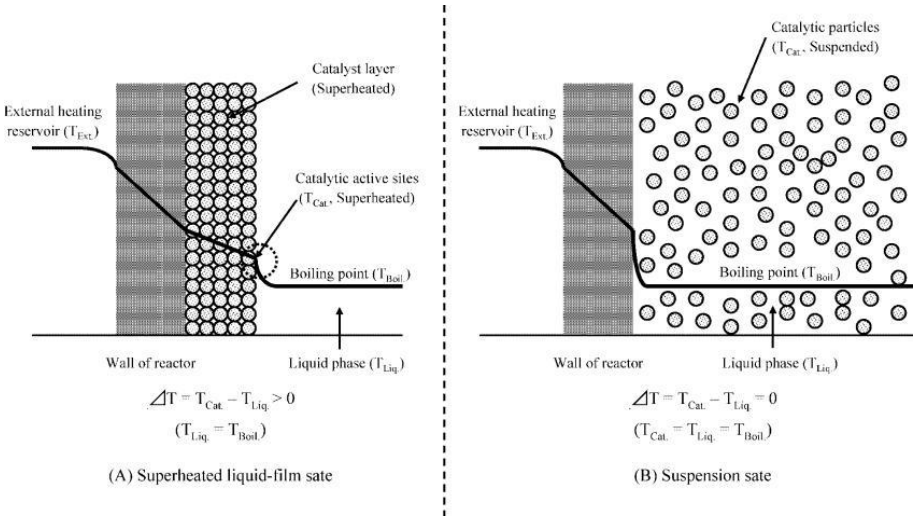

Figure 4.17. Temperature gradients arising from external heating of the reactor with A) the catalyst wetted by the thin layer of substrate B) catalyst suspended in the liquid substrate (34).

In addition to our preliminary study, it was observed that if the catalyst to substrate ratio was lower than 1:10, the surface of the catalyst was getting dry during the first 10 minutes of the reaction and no significant conversions were observed in the reaction mixture under boiling conditions. Similar observation was made by Saito et al. in (35) during 2-propanol dehydrogenation, who called this state the 'sand-bath state'.

Pez et all (2) have screened over 40 catalyst in dehydrogenation of 9-ethylcarbazole and found that the highest reaction rate was given by Pd/Al_2O_3 catalyst. In the present work, it was decided to test the following catalysts: Ru black, 5% Pt/Al_2O_3, 5 wt % Pd/AC

(activated carbon), 5 wt % Pt/AC and 5 wt % Ru /AC in dehydrogenation of the mixture of the isomers of 9-ethyl-perhydrocarbazole.

The dehydrogenation reactions were performed in the period of 4 hours at 200 °C and then the reaction mixture was analysed using GC-MS. The set-up used for the reaction (see Figure 4.18) was equipped with two vacuum tight gauges to allow the change of the atmosphere inside the flask.

Figure 4.18. The set-up used for the dehydrogenation of the mixture of stereoisomers of 9-perhydroethylcarbazole over selected commercial catalysts.

The results from the GC-MS analysis of the reaction mixtures showed a fully dehydrogenated product (9-ethylcarbazole) in case of platinum catalysts under vacuum, hydrogen and nitrogen atmospheres. The resulting original mass spectrum of the product is shown in Figure 4.19. Based on the retention time and fragmentation pattern showed in this spectrum, the product was unquestionably recognised as 9-ethylcarbazole. The base peak with a molecular mass of 180 is created by removing the ethyl group from the 9-ethylcarbazole molecule.

During the reaction taking place in vacuum, the reaction atmosphere was probed using off-line gas chromatograph (Agilent 7890 A) with TCD (thermal conductivity) detector which showed the presence of hydrogen along with traces of nitrogen and oxygen. The hydrogen

unquestionably originated from the sample, but oxygen and nitrogen came from air that entered the chromatograph during manual injection.

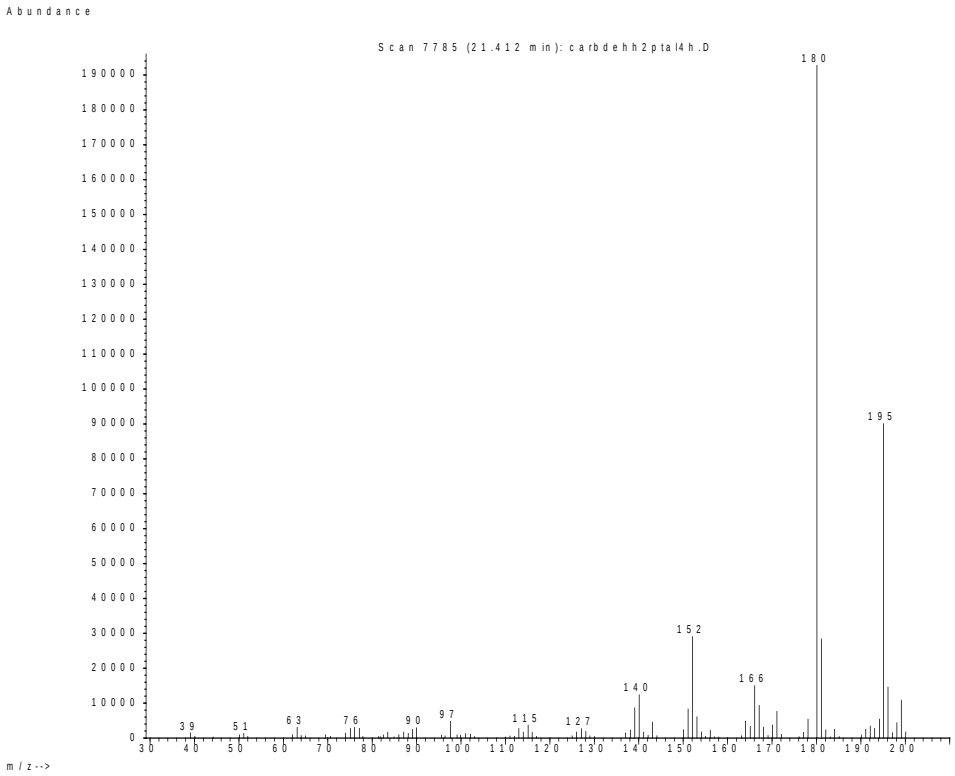

Figure 4.19. Mass spectrum of the product of 9-perhydroethylcarbazole dehydrogenation over 5 wt % Pt/Al_2O_3.

The analysis of the resulting mixtures from dehydrogenation reactions performed over supported palladium and supported ruthenium catalysts under the same reaction conditions in three tested atmospheres did not show complete conversion of the starting material. In the mixtures obtained using Pd catalyst, additionally 10% of 9-ethyl-octahydrocarbazole was observed and in the mixtures obtained over ruthenium catalyst, we have observed 20% of 9-ethyl-octahydrocarbazole and 12% of 9-ethyl-tetrahydrocarbazole, respectively. The presence of these intermediates can be associated with their adsorption geometries and the electronic structures of Pd and Ru metals. When the dehydrogenation was performed over ruthenium black catalyst, no significant conversions of starting material were obtained in all three atmospheres tested. This is probably the consequence of the small surface area of unsupported ruthenium catalysts, which made the adsorption of the substrate from the gas

phase difficult. Additionally, due to the absence of support, the catalyst could have been deactivated by sintering at the reaction temperature (200 °C).

Summarising, the hydrogen system based on 9-ethylcarbazole was proved reversible under reasonably mild reaction conditions. The complete dehydrogenation of the mixture of 9-ethyl-perhydrocarbazole stereoisomers was obtained in 4 hours at 200°C under three different atmospheres using Pt based catalysts. The reaction mixtures obtained over supported palladium and ruthenium catalysts showed the presence of intermediate products after 4 hours of reaction in three atmospheres studied. Ruthenium black catalysts proved to be not active in the dehydrogenation reaction under liquid-film conditions. Thus, the presence of the support was found to be essential for the reaction to take place. However, no influence of the type of the support (alumina or activated carbon) was noted. The reaction atmosphere (vacuum, hydrogen or nitrogen) also did not significantly affect the dehydrogenation reaction. It should be taken into consideration; however that only one set of conditions was studied for this reaction. Moreover, it is difficult to perform any quantitative analysis based on the assumption that the concentration of the species is proportional to the peak area on GC spectra. The calibration curve could not be prepared because of the lack of standard materials. Therefore, further work would be necessary to verify the results obtained. However, the goal of obtaining the general overview of the dehydrogenation of 9-ethyl-perhydrocarbazoles was achieved.

4.4. Conclusions

It was demonstrated that the reversible hydrogenation and dehydrogenation of 9-ethylcarbazole in the molten state is feasible under reasonably mild conditions. The trials of dehydrogenation reaction were found successful over various catalysts. Thus, this system has a potential for hydrogen storage. Several catalytic systems based on noble metals and nickel were screened for the 9-ethylcarbazole hydrogenation in molten state.

The conversion and selectivity was found to be critically dependant on the type of metal and support used. Additionally, a very active hydrogenation catalyst, nominal 5 wt % Ru on alumina, was synthesized by means of mild chemical reduction and has shown better performance than its commercially available counterpart with the same composition. Two symmetric and two asymmetric fully hydrogenated products and two other intermediates were identified and their structures were assigned with the aim of NMR spectroscopy experiments. In addition, the stereochemistry of the intermediates and products suggests that the catalytic reaction is not taking place only as a simple concerted hydrogenation. The observation of the asymmetrically hydrogenated compounds E and F from Figure 4.13 as products under the chosen reaction conditions is rather surprising with regard to the expected concerted attack of two protons on the same side of a molecule on a double bond. Their possible formation mechanisms were therefore proposed, which involve desorption and readsorption steps of the weakly adsorbed intermediates on different metal surface sites, giving different intermediates and products from the surface of the catalyst. Since different molecular structures may interact with the surface in a different manner, it is thus believed that the possible variety of stereoisomers of products and intermediates can give implications on the extent and duration of the recyclability of the spent fuel. It should be noted that the geometry of the intermediates have also an influence on their adsorption mode on the metal's catalytically active sites. Therefore, it is important to quantify their concentration and subsequently derive the reaction pathway under the conditions studied. Due to the fact that the most active catalytic systems in the hydrogenation of 9-ethylcarbazole were found to have ruthenium as an active phase, the subsequent study will be focused on developing the reaction model over ruthenium. The detailed study of the reaction pathway, together with the analysis of the active sites on ruthenium based catalytic systems will be presented in the following chapter.

4.5. References

1. *Kinetics of H_2 recovery from dodecahydro-N-ethylcarbazole over a supported Pd catalyst.* **F. Sotoodeh, L. Zhao, K. J. Smith.** Appl.Catal.A, 2009, Vol. 362.
2. *US patent 7101530.* **G. P. Pez, A. R. Scott, A. C. Cooper, H. Cheng.** 2006.
3. *US patent 7351395.* **G. P. Pez, A. R. Scott, A. C. Cooper, H. Cheng, F. C. Wilhel, A. Abdourazak.** 2008.
4. http://www.iphe.net/docs/Meetings/Lucca_Italy_05/Cooper.pdf. [Online]
5. http://www.hydrogen.energy.gov.[Online].
6. *An integrated hydrogen storage and delivery approach using organic liquid -phase carriers.* **A. C. Cooper, K. M. Campbell, G. P. Pez,** 2006.
7. *Dehydrogenation of N-ethylperhydrocarbazole catalyzed by PCP pincer iridium complexes: Evaluation of a homogenous hydrogen storage system.* **A. Zhaohui, I. Tonks, J. Belli, C. M. Jensen,** J. Organomet. Chem., 2009, Vol. 694.
8. *Kinetics of 9-ethylcarbazole hydrogenation over Raney-Ni catalyst for hydrogen storage.* **X. Ye, Y. An, G. Xu,** J. Alloys Compd., 2010, Vol. 509.
9. *Kinetics of hydrogen uptake and release from heteroaromatic compounds for hydrogen storage.* **F. Sootodeh, L. Zhao, K. J. Smith,** Ind. Eng. Chem. Res., 2010, Vol. 49.
10. Structure sensitivity of dodecahydro-N-ethylcarbazole dehydrogenation over Pd catalysts. F.Sootodeh, K. J. Smith, J. Catal., 2011, Vol.49.
11. *Study of catalytic sites on ruthenium for hydrogenation of N-ethylcarbazole: implications of hydrogen storage via reversible catalytic hydrogenation.* **K. Morawa Eblagon, K. Tam, K. M. Kerry Yu, S-L. Zhao, X-Q Gong, H. He, L. Ye, L-C Wang, A. J. Ramirez-Cuesta, S.C.Tsang,** J. Phys. Chem. C, 2010, Vol. 114.
12. *Hydrogenation of 9-ethylcarbazole as a prototype of a liquid hydrogen carrier.* **K. Morawa Eblagon, D. Rentsh, O. Friedrichs, A. Remhof, A. Zuettel, A .J . Ramirez-Cuesta, S. C. Tsang,** Int. J. Hydrogen Energy, 2010, Vol. 35.
13. *Thermally reduced ruthenium nanoparticles as a highly active heterogenous catalyst for hydrogenation of monoaromatics.* **F. Su, L. Lv, F. Y. Lee, T. Liu, A. I. Cooper, X. S. Zhao.** J. Am. Chem. Soc, 2007, Vol. 129.
14. *Efficient and practical arene hydrogenation by heterogenous catalysts under mild conditions.* **T. Maegawa, A. Akashi, K. Yagucchi, M. Shigetsura, Y. Mangucchi, H.Sajiki,** Chem.Eur.J, 2009, Vol. 28.
15. *Factors governing the catalytic reactivity of metallic nanoparticles.* **D.Uzio, G.Berhault,** Catal.Rev., 2010, Vol. 52.
16. **R. L. Augustine.** *Heterogenous catalysis for synthetic chemist.* New York: Marcel Dekker, 1996.
17. *Competitive hydrogenation of benzene and toluene on palladium and platinum catalysts.* **D. Poondi, M. A. Vannice,** J. Catal, 1996, Vol. 161.
18. *Slurry-phase hydrogenation of aromatic compounds over supported noble metal catalysts.* **M. Koussathana, D. Vamvouka, H. Economou, X. Verykios.** Appl. Catal., 1991, Vol. 77.
19. *Hydrogenation of tetralin on silica-alumina Pt catalysts. II. Influence of the support on catalytic activity.* **M. F. Wiliams, B. Fonte, C. Woltz, A. Jentys, J. A. R. van Veen, J. A. Lercher,** J. Catal., 2007, Vol. 251.

20. *Effect of sulfur or nitrogen poisoning on the activity and selectivity of y-zeolite-supported Pt-Pd catalysts in the hydrogenation of tetralin.* **C. C. Costa Augusto, J. L.Zotin, A.da Costa Jr.** Catal.Lett, 2001, Vol. 75.
21. *Reductions with ruthenium. II Its use in hydrogenation of pyridines.* **M. Freifelder, G. R. Stone,** J. Org. Chem, 1961, Vol. 26.
22. *Hydrogenation of pyrrole derivatives. Prt v. Poisoning effect of nitrogen on precious metal on carbon catalysts.* **L. Hegedus, T. Mathe,** Appl. Catal. A, 2002 Vol. 226.
23. *Studies on ruthenium catalysts.Part 3.Effects of type of support, method of preparation and conditions of use of Ru/TiO2 catalysts on their behaviour in n-butane hydrogenolysis.* **G.C.Bond, R.R.Rajaram, R.Yahya, J. Mol. Catal.,** 1991, Vol. 69.
24. *Benzene hydrogenation over supported and unsupported palladium I Kinetic behaviour.* **P.Chou, M.A.Vannice.**, J.Catal., 1987, Vol. 107.
25. *Support effect on the catalytic activity and properties of sulfided molybdenum catalysts.* **H.Shimada, T.Sato, Y.Yoshimura, J.Hirashi, A.Nishijima.,** J.Catal, 2004, Vol. 110.
26. *Local structure around platinum in Pt/C catalysts emplayed for liquid-phase dehydrogenation of decalin in the liquid-film state under reactive disilation conditions.* **C. Shinohara, S. Kawakami, T. Moriga, H. Hayashi, S. Hodoshima, Y. Saito, S. Sugiyama,** Appl. Catal. A, 2004, Vol. 226.
27. *Stereoisomerism and local chirality.* **K. Mislow, J. Siegel.**, J. Am. Chem. Soc, 1984, Vol. 106.
28. *http://www.chem.ox.ac.uk/spectroscopy/nmr/nmrfacility.htm.* [Online] 2010.
29. *Deuteriation and deuterogenation of naphtalene and two octalins.* **A. W. Weitkamp**, J. Catal., 1966, Vol. 6.
30. *The adsorption and hydrogenation of benzene and toluene on alumina and silica-alumina supported palladium and platinum catalysts.* **J. M. Orozco, G. Webb.**, Appl. Catal., 1983, Vol. 6.
31. *Hydrogen storage and delivery in a liquid carrier infrastructure- presentation.* **G. Pez, A. C. Cooper, H. Cheng, B. A. Toseland, K. Cambell.,** Allentown, 2006.
32. *Hydrogen storage by decalin/naphthalene pair and hydrogen supply to fuel cells by use of superheated liquid-film-type catalysis.* **S. Hodoshima, S. Takaiwa, A. Shono, K. Satoh, Y. Saito**, Appl. Catal., 2004, Vol. 283.
33. *Liquid-film-type catalytic decalin dehydrogeno-aromatization for long-term storage and long distance transportation of hydrogen.* **S. Hodoshima, H. Arai, Y. Saito,** Int. J. Hydrogen Energy, 2003, Vol. 28.
34. *Chemical recuperation of low-quality waste heats by catalytic dehydrogenation of organic chemical hydrides and its energy analysis.* **S. Hodoshima, A. Shono, Y. Saito,** Energy Fuels, 2008, Vol. 22.
35. *Hydrogen storage in organic hydrides at low energy consumption-conference proceedings.* **Y. Saito, S. Hodoshima, A. Shono.** Lyon France, 2006.

5. Study of catalytic sites on ruthenium in liquid-phase hydrogenation of 9-ethylcarbazole - Development of the reaction model and implications of the reversible hydrogen storage in this system.

5.1. Introduction

Many of the heterocyclic compounds were reported to be difficult to hydrogenate or their hydrogenation reactions were complicated due to side reactions (1). Pyrrole and its derivatives are among the most difficult heterocycles to be hydrogenated, probably due to the relative rigidity of the five member ring (2). The liquid phase hydrogenation of 9-ethylcarbazole was first reported by Adkins and Coonradt (3) who hydrogenated 9-ethylcarbazole over nickel and obtained 10 % selectivity for 9-ethyl-tetrahydrocarbazole and 33 % towards fully hydrogenated 9-ethyl-perhydrocarbazole with 89 % conversion in 15 minutes at 200 °C. The same authors also reported similar results for hydrogenation of 9-ethylcarbazole over copper chromite catalyst at 240°C during 1.5 hours of reaction. The 9-ethyl-hexahydrocarbazole intermediate was not observed over this catalyst. In addition, the carbazoles were found to be more resistant towards hydrogenation than indoles and phenylpyrroles. The reason for this is that the benzenoid ring in the latter decreases the resonance in the pyrroloid ring (3). More recently, the reversible hydrogenation of 9-ethylcarbazole was studied by Sotoodeh and co-workers in a series of publications(4) and (5). During hydrogenations of 9-ethylcarbazole in decalin at 150 °C in 1 hour over a commercial 5 wt % Ru/Al_2O_3 catalyst under 7MPa of hydrogen, the authors obtained nearly 100 % conversion. The analysis of the liquid samples confirmed the production of 9-ethyl-tetrahydrocarbazole, 9-ethyl-hexahydrocarbazole, 9-ethyl-octahydrocarbazole, 9-ethyl-decahydrocarbazole and the fully hydrogenated product. However, the analysis of the stereochemistry of the products and intermediates of this reaction was not conducted and additionally no stereoisomers of the fully hydrogenated products were reported. The

kinetics of hydrogenation of 9-ethylcarbazole over Raney-Ni was also studied in the temperature range of 120-240 °C (6). In accordance with the calculations performed in this work (6), the hydrogenation reaction was reported to be controlled solely by surface chemical reaction on the catalyst and mass transfer resistance at the gas-liquid interface was found to be marginal.

In the previous chapter, the results from the hydrogenation of 9-ethylcarbazole in the molten state were reported. The stereochemistry of the reaction products and intermediates with the aid of NMR techniques was analysed and it was possible to assign four different stereoisomers of the fully hydrogenated product. It is believed that only the detailed analysis of the reaction products can allow developing the link between the structure and the adsorption geometry of the intermediate on the metal surface. This in turn lies in the heart of understanding the catalytic process. It should be noted that the success of developing a catalytic hydrogen storage concept based on reversible hydrogenation of 9-ethylcarbazole is highly dependent on finding an efficient catalyst. In the previous chapter, we reported that ruthenium, out of all the noble metals studied, showed the best performance in hydrogenation of 9-ethylcarbazole in the molten state. The present chapter will be focussed on finding a correlation between the active sites present on the catalyst surface and the observed differences in catalytic performance between various tested catalysts. It is known that the ratio between saturated and unsaturated sites on the surface of the catalyst is strongly influenced by the size of the particles as shown in Figure 5.1. As it can be seen, the proportion of different active sites changes drastically in the region of diameters from 1 to 5 nm, and the density of unsaturated sites such as corners and edges decrease with increase in the size of the nanoparticle.

The direct influence of the type of active sites on the reaction selectivity and catalyst performance is unknown at present. Thus, in this chapter a detailed structure-catalysis

relationship in hydrogenation of 9-ethylcarbazole over ruthenium based catalytic systems will be elucidated from the combined experimental and theoretical study. The working model for hydrogenation of 9-ethylcarbazole over two types of active sites will be developed.

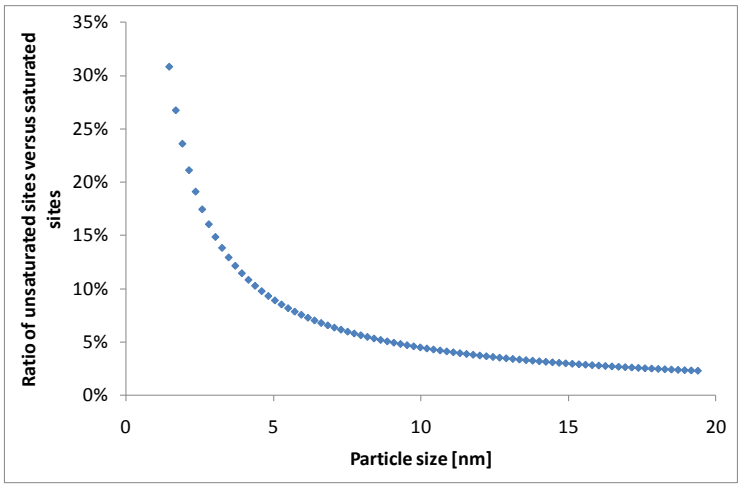

Figure 5.1. Theoretical ratio of unstaturated to saturated site on a nanoparticle surface versus particle size. Based on model and assumptions from (7).

It is noted that a large part of the work described in this chapter has been published (8).

5.2. Materials and methods

The catalysts used in this chapter were synthesized following the mild chemical reduction synthesis route as described in Chapter Three. These catalysts are marked (CR) for chemically reduced. The commercial catalysts 5 wt % Ru/Al_2O_3 and ruthenium black are marked (COM). The commercial catalysts and 9-ethylcarbazole (95%) were purchased from Sigma-Aldrich. It should be underlined that all the catalysts used in this chapter were previously tested in 9-ethylcarbazole hydrogenation in the molten state in Chapter Four.

It is noted that the hydrogen storage system based on reversible hydrogenation of 9-ethylcarbazole studied in the present work is intended to be solvent free. As a result, the kinetics of the 9-ethylcarbazole hydrogenation should be studied in the solvent-free molten form. However, due to the fact that the melt is very viscous, it is impossible to be sampled

at regular intervals. Thus, cyclohexane was used as a solvent in the study of 9-ethylcarbazole hydrogenation. The choice of the solvent was governed primarily by the solubility of the starting material. Additionally, the series of control experiments proved that the presence of cyclohexane did not affect significantly the selectivity (data not shown) and conversion of the reaction. However, slightly faster rates were observed using the solvent as shown in Figure 5.2 in the reactions using ruthenium black catalyst. This result was attributed to the lower solubility and mobility of hydrogen in the melt.

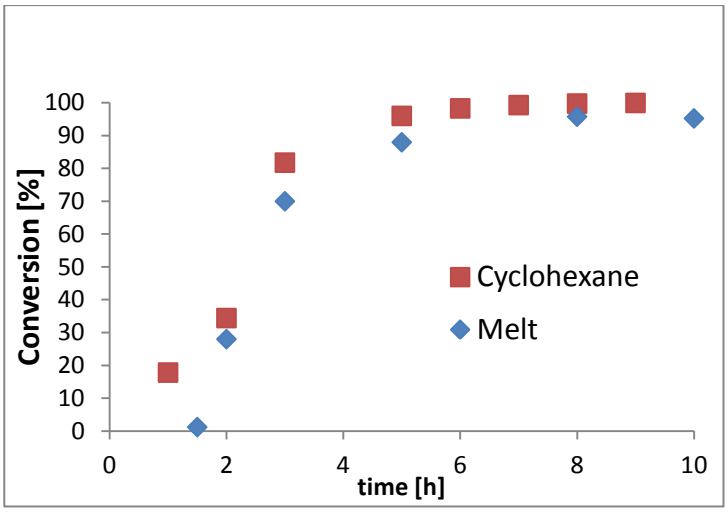

Figure 5.2. Comparison of the conversion of 9-ethylcarbazole in the hydrogenation over ruthenium black catalyst in cyclohexane and in molten state obtained at standard conditions.

5.3. Results and discussion

5.3.1. Catalyst characterisation

One unsupported and four supported ruthenium based catalyst were studied in liquid phase hydrogenation of 9-ethylcarbazole, namely: 5 wt % Ru/alumina (CR), 5 wt % Ru/alumina (COM), 5 wt % Ru/rutile (CR), 5 wt % Ru/silica-alumina (CR) and ruthenium black. The metal content used in the names of the catalysts in the present chapter is based on the recipe value. The correct metal content was obtained using EDAX analysis. The used catalysts were also previously characterised with the aid of TEM, BET and XRD experiments. All these results were presented in Chapter Four, paragraph 4.3.1 Further

characterisation of the factors influencing the catalysts activity and selectivity was carried out to get a closer insight into the relationship between catalyst structure and its performance in liquid phase hydrogenation of 9-ethylcarbazole. The reduction behaviour of the ruthenium on the surface of the catalyst was studied using temperature programmed reduction (TPR) experiments. The composition of the surface of ruthenium black and supported ruthenium catalysts as well as the possible electronic interaction between ruthenium and different types of supports was studied using X-ray photoelectron spectroscopy (XPS) experiments.

CO-chemisorption

The metal dispersion is likely to be one of the most critical factors affecting the catalyst performance. Therefore, CO chemisorption was employed for the evaluation of the active metal dispersions and metal surface areas of the samples of catalysts and the results are listed in Table 5.1 It is worth noting that the catalyst obtained via mild chemical reduction displayed much larger metal areas and dispersions than commercially available catalyst with the same composition. This can be the consequence of the reduction temperature used during synthesis of these catalysts. The higher the reduction temperature, the higher is the possibility of sintering of metal particles.

Table 5.1. Metal areas and dispersions of the catalysts were obtained with the aid of CO chemisorption measurements. (CR) are catalysts produced via mild chemical reduction, (COM) are commercially available catalysts.

Catalyst (based on recipe value)	*Metal area [m^2/g]*	*Dispersion [%]*
5 wt % Ru/Al_2O_3 (CR)	10.96	46.75
5 wt % Ru/Al_2O_3 (COM)	3.91	16.69
5 wt % Ru/TiO_2 (CR)	11.30	48.21
5 wt % $Ru/ SiO_2/Al_2O_3$ (CR)	9.82	41.89
Ru black (COM)	4.78	1.01

Temperature programmed reduction (TPR)

The freshly reduced surface of ruthenium is covered with a thin film of oxide when it is exposed to oxygen at room temperature, which becomes thicker at higher temperatures (8). In addition, it was reported previously (9), that even small amounts of oxygen on the surface of supported ruthenium particles can drastically influence the activity of the catalyst. Thus, with respect to the present work, it would seem of importance to study the reduction behaviour of the surface layer of ruthenium oxide on the selected catalysts. Additionally, TPR experiments can also shed a light on the interaction of metal nanoparticles with the supports. Therefore, TPR profiles of the studied catalysts were obtained following the method described in Chapter Three, paragraph 3.2.4 and the resulting patterns are shown in Figure 5.3.

The experiments showed that supported ruthenium catalyst is oxidised to a greater extent than unsupported ruthenium black catalysts. It was found previously that the enthalpy of chemisorption of oxygen on ruthenium is increased by the presence of oxide support (8). Therefore, there is more different ruthenium oxide species expected to be detected on the supported samples. This is indicated by the presence of more than one peak on TPR profiles of these catalysts. Unsupported catalyst (ruthenium black) shows a single reduction peak at 380 K, which can be attributed to the reduction of surface RuO_2 (10) (11). It should be noted that for supported catalyst, the reduction of surface ruthenium (II) oxide takes place at lower temperatures (339 K for 5 wt % Ru/Al_2O_3 (CR) as compared to 375 K for 5 wt % Ru/Al_2O_3 (COM), 369 K for 5 wt % $Ru/SiO_2Al_2O_3$ (CR), 340 K for 5 wt % Ru/TiO_2 (CR)). This can be a result of smaller particle size and better dispersion of metal nanoparticles on the surface of the carrier as compared to unsupported ruthenium black. A similar observation was reported (12), for RuO_2 nanoparticles supported on carbon nanotubes.

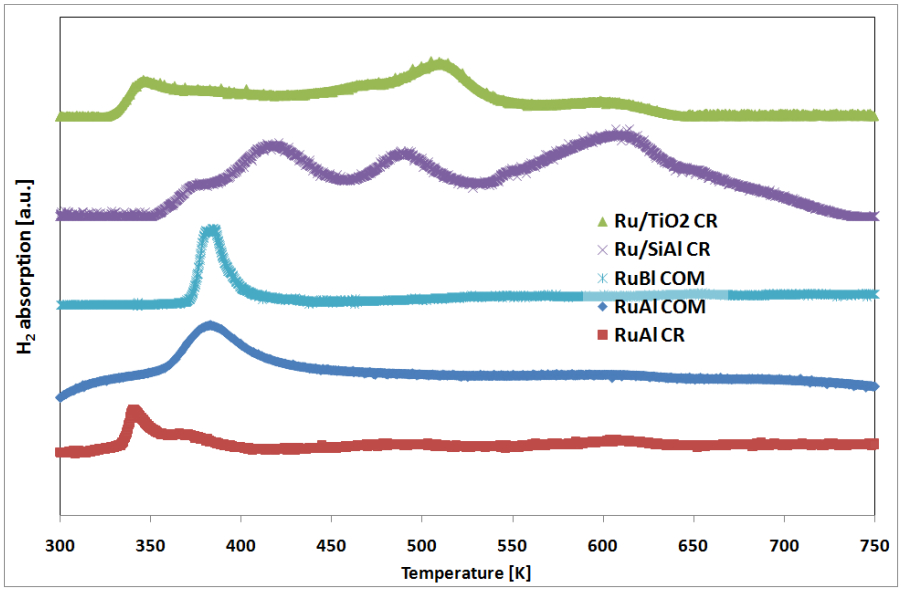

Figure 5.3. TPR profiles of ruthenium catalysts. Ru/SiAL- 5 wt % Ru/SiO_2-Al_2O_3, RuAl- 5 wt % Ru/Al_2O_3, RuBl –ruthenium black, CR-chemically reduced, COM-commercial sample.

The most active 5 wt % Ru/Al_2O_3 (CR) catalyst showed a strong peak with relatively high intensity at low temperatures. This can be attributed to an easier reduction and on the other hand it may also suggest weak interaction between ruthenium and support. Similar findings were previously reported (13) in the case of ruthenium nanoparticles supported on $BaCeO_3$. Additionally, the low temperature peak in 5 wt % Ru /Al_2O_3 (CR) profile is asymmetrical, which can be the evidence of two different types of RuO_2 present on the catalyst surface. These ruthenium oxides differ slightly between each other in interaction with the support. On the other hand, the reduction peak of the commercial 5 wt % Ru/Al_2O_3 (COM) catalyst appears at higher temperature and is much wider. This can point towards aggregation of RuO_2 clusters which may cause decreased activity of this catalyst. Based only on the analysis of the TPR spectra it is very difficult to identify the higher temperature peaks present on the profiles of 5 wt % Ru/TiO_2 (CR) and 5 wt % Ru/SiO_2-Al_2O_3 (CR) catalysts. This high temperature peaks could be attributed to the ruthenium (II) oxide species strongly interacting with the support as suggested in the literature (14). It should be noted that the peak positions obtained in our work may differ slightly from the

values reported in the literature, due to the different metal loading, catalyst synthesis and pre-treatment as well as parameters of the TPR experiments.

To sum up, TPR experiments showed the presence of different types of ruthenium oxides on the surface of supported catalyst and one type of oxide over ruthenium black. Furthermore, the TPR experiments showed that the catalyst synthesized at higher temperatures has aggregated oxide clusters. It is clear that aggregation of ruthenium nanoparticles leads to the formation of higher number of terraced sites.

XPS studies of ruthenium catalysts.

All of the ruthenium based catalysts used were characterised by XPS in order to confirm the oxidation state of ruthenium on the surface of the catalyst as well as to determine the possible influence of the presence of the support on the oxidation state of the ruthenium metal. The XPS experiments showed the existence of two different ruthenium species in each of the catalysts. The details of the XPS measurement can be found in Chapter Three, paragraph 3.2.6. The XPS experiments were performed studying the 3d level which is known to present a high cross-section and therefore shows high intensity (30). Range of about 15 eV (275 -290 eV) was examined for each of the samples. All the spectra contained the Ru $3d_{5/2}$ and Ru $3d_{3/2}$ peaks which resulted from the spin-orbital splitting. The distance between the doublet peaks was fixed at around 4.2 eV. It is well known that Ru $3d_{3/2}$ overlaps with C1s peak (around 285.5 eV). This carbon peak originates from the traces of carbonaceous impurities that are normally present on the surface of the catalyst or inside the sample chamber of the spectrometer (15). Thus, the main peaks observed in XPS spectra of all of the samples originate from Ru 3d centred at 279-284 eV and C 1s peak at about 284 eV. Careful deconvolution was performed for all of the profiles. Data processing consisted of the calibration of peak positions against the C 1s line, Shirley background and

step-by-step spectra analysis. All of the XPS spectra were deconvoluted into symmetric Gaussian 80 %- Lorentzian peaks following the guidelines in the literature (16).

The representative XPS spectra obtained for Ru black and 5 wt % Ru/Al_2O_3 (CR) are shown in Figure 5.4. The XPS spectra of Ru black (Figure 5.4 A) showed peaks at 279.6 eV and 284.8 eV that can be attributed to ruthenium in metallic state (Ru^0) (16) (17) (18). In addition, the C 1s peak was present at 283.6 eV. Another peak was found at 280.7 eV which can be assigned to oxidized ruthenium (RuO_2) as reported in (19) and (20). It is clear that the presence of oxidized ruthenium on the surface of the catalysts cannot be avoided, due to the fact that ruthenium metal can be oxidised very easily in open air. Additional contribution at the binding energy of 287.5 eV assigned to carbonacous species associated with hydrogen or/oxygen (21) or C=O structures (22) was necessary to fit correctly the experimental Ru $3d_{3/2}$ peak. Similarly, on the XPS spectra of 5 wt % Ru/Al_2O_3 (CR) in Figure 5.4 B, five peaks are observed; two due to the metal species, one of oxidized ruthenium and two from carbonaceous contaminants. The signals at 280.0 eV and 284.4 eV can be attributed to finely dispersed ruthenium metal (23) (17), the signal at 280.8 eV is in agreement with the reported value of 281.0 eV for RuO_2 (19). In addition, the peak at 284.5 eV is identified as a C 1s line. Carbonaceous species and their oxidation products were also present on the surface of 5 wt % Ru/Al_2O_3 (CR) catalysts and resulted in a peak with binding energy of 288.5 eV (see Figure 5.4 bottom). From the XPS spectra of ruthenium black and 5 wt % Ru/Al_2O_3 (CR) it can be seen that the binding energy of Ru $3d_{5/2}$ is different for these two catalysts. The higher binding energy of 280.0 eV in case of 5 wt % Ru/Al_2O_3 (CR) as compared to 279.6 eV was expected based on the literature review (15).

A

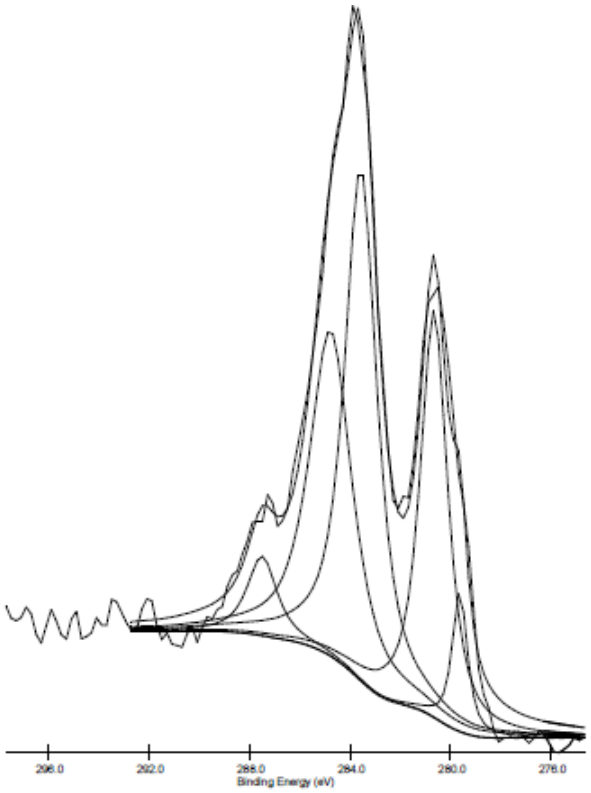

B

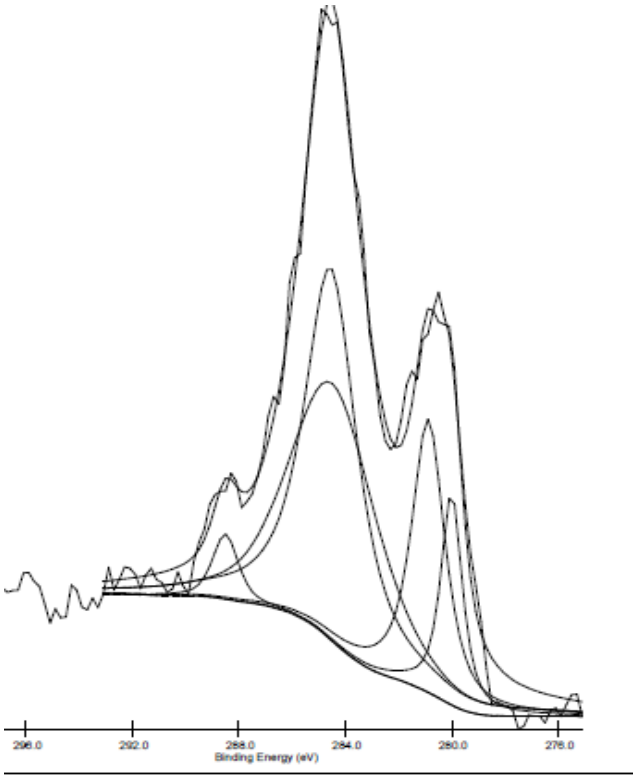

Figure 5.4. The representative C 1s, Ru 3d $_{3/2}$ and Ru 3d $_{5/2}$ XPS spectrum of ruthenium black catalyst (top - A) and 5 wt % Ru/Al_2O_3 (CR) bottom - B.

In addition, the binding energy of Ru^0 $3d_{5/2}$ obtained for ruthenium black in our work of 279.6 eV is in a reasonable agreement with the value of 280.2 eV reported for ruthenium black catalyst by Larichev (15). Generally, 0.4-0.5 eV (27) lower values of binding energy are reported in the literature for bulk ruthenium metal with respect to supported ruthenium nanoparticles (17)(23)(11) (25). In addition, alumina is known to be an electron-withdrawing support (24). The presence of electron-withdrawing supports was previously reported to result in higher binding energies of ruthenium metal as compared to ruthenium metal supported on MgO or CaO catalysts (24). These supports enhance the hydrogenation activity, due to making ruthenium metal electron- poor. This in turn facilitates the adsorption and activation of the substrates and intermediates of the reaction. In addition, the lower intensity of Ru^0 $3d_{5/2}$ on the spectra of ruthenium black is attributed to the much smaller dispersion of this catalyst as compared to supported 5 wt % Ru/Al_2O_3 (CR). Therefore, much less ruthenium metal can be detected on the surface of the unsupported catalyst.

The XPS spectra of the remaining samples, namely 5 wt % Ru/Al_2O_3 (COM), 5 wt % Ru/TiO_2 (CR) and 5 wt % Ru/SiO_2-Al_2O_3 (CR) (data not shown), displayed mainly similar features to the spectra discussed above. However, in order to fit the XPS spectra of 5 wt % Ru/TiO_2 (CR) and 5 wt % Ru/SiO_2-Al_2O_3 (CR) catalysts correctly, additional low intensity peaks at around 182.0 eV had to be placed. These peaks can be assigned to ruthenium chlorine species (25). These results explain the origin of the high temperature reduction peaks observed previously in the TPR experiments. These chlorine species must have originated from the ruthenium chloride precursor used in the synthesis of the catalysts. The binding energies of ruthenium 3 $d_{5/2}$ clusters with different supports are listed in Table 5.2. There is a significant shift in binding energy of ruthenium metal in all of the samples with respect to pure ruthenium (ruthenium black). These results confirm that the binding

energy of ruthenium strongly depends on the nature of the oxide support. The lowest binding energy of Ru 3d $_{5/2}$ out of the supported samples is displayed by both ruthenium catalysts supported on alumina. The shift in binding energy is probably the result of the charge transfer in the catalytic system. It was reported before that electronic metal-support interaction becomes influential for small particles (below 5 nm) (24). From the results gathered in Table 5.2, it is clear that the moderate electronic interaction between metal and support is taking place in the present work. In general, the electronic interaction of metal and the support affects the electron density of metal which results in the binding energy shift in XPS spectra. Thus, the electron affinity of the support can indirectly control the activity and selectivity of the catalysts (24). The higher binding energy of ruthenium in the ruthenium supported on alumina (CR) can be the result of its smaller particle size as compared to the commercial counterpart. It has been reported elsewhere, that 4d binding energy of Pt catalysts decreased with increasing particle size (26).

Table 5.2. Values of binding energies of Ru 3d species obtained on different catalysts.

Catalyst	***Ru 3 d $_{5/2}$***	***Ru 3d $_{3/2}$***
Ru black	279.6	284.8
5 wt % Ru/Al_2O_3 (CR)	280.0	284.4
5 wt % Ru/TiO_2 (CR)	280.5	284.6
5 wt % Ru/SiO_2-Al_2O_3 (CR)	280.1	284.4
5 wt % Ru/Al_2O_3 (COM)	279.8	284.5

In addition, the binding energy of ruthenium supported on rutile is higher than the binding energy of ruthenium on alumina (see Table 5.2), which agrees well with the previously reported XPS results for Pt catalysts (26). This difference in binding energies was explained by rutile being more electron withdrawing support than alumina (24).

To sum up, the XPS studies showed electronic interaction of ruthenium metal with the support, which resulted in the observed shifts in binding energies of Ru 3d $_{5/2}$ in supported samples with respect to the binding energy recorded for ruthenium black sample. The ruthenium supported on alumina was found to be the most electron rich out of the

supported catalysts studied, because of the relatively low binding energy displayed by this catalyst. It appears that the properties of the supported catalysts can be influenced by the chemical interaction between ruthenium metal and the support. It is clear from obtained XPS results that appropriate selection of the support is very important factor, because the type of the support affects the electron density of the metal which in turn can strongly influence the adsorption of the substrates on the surface of the catalyst. Generally, the composition of the catalysts obtained over XPS experiments agreed well with the compositions expected based on TPR measurements results. Additionally, high temperature reduction peaks observed in TPR results were identified as originating from chlorine species, from the catalyst precursor.

5.3.2. Results from catalysts testing

The comparison of the catalytic activity in liquid phase hydrogenation of 9-ethylcarbazole obtained in first hour of 20h testing period at 130 °C and 70 bar hydrogen pressure are gathered in Table 5.3. The catalytic activity was computed based on the metal loadings (obtained from EDAX analysis) and with respect to the moles of 9-ethylcarbazole converted over a mole of surface metal according to the equation listed in Chapter Three, paragraph 3.5.1.

Table 5.3.Comparison of catalytic activities obtained in liquid phase hydrogenation of 9-ethylcarbazole by various ruthenium based catalysts.

Catalyst (based on recipe value)	*Catalytic activity* $[mol\ ETH \cdot mol_{met}^{-1} \cdot s^{-1}]$
5 wt % Ru/Al_2O_3 (CR)	1.47
5 wt % Ru/Al_2O_3 (COM)	0.13
5 wt % Ru/TiO_2 (CR)	0.53
5 wt % $Ru/SiO_2/Al_2O_3$	0.27
Ru black (COM)	0.25

It is interesting to note that under the conditions studied here, the ruthenium catalyst produced by mild chemical reduction was found to show much higher activity for the

hydrogenation of 9-ethylcarbazole to 9-ethyl-perhydrocarbazoles (Pl 12 [H]) than its commercial counterpart with the same composition. The comparison of the conversion and selectivity obtained using different ruthenium based catalytic systems is shown in Figure 5.5. As it can be seen from Table 5.3 and Figure 5.5, the commercial 5 wt % Ru/Al_2O_3 synthesized under elevated temperatures displayed poor activity and selectivity towards Pl 12 [H], while the same catalyst formulation but synthesized using milder chemical reduction at 90 °C gives excellent activity and selectivity towards fully loaded products. This could be the consequence of the better metal utilization in the chemically reduced catalysts, which contains higher density of more efficient active sites on the surface for this reaction. Higher activity of supported catalyst, versus unsupported ruthenium black might be the result of the properties of supports found previously in XPS experiments. XPS results showed that the studied supports are electron-withdrawing supports, making the ruthenium particles electron deficient. As it was previously reported (27) by Sun et al, donating electrons from non-basic compounds such as 9-ethylcarbazole is favourable over electron transferring from the catalyst surface to LUMO (lowest unoccupied molecular orbital) of the organic substrate. The ruthenium supported on rutile (5 wt % Ru/TiO_2) and on silica alumina (5 wt % Ru /SiO_2-Al_2O_3) obtained moderate conversions, but much lower selectivities than 5 wt % Ru/Al_2O_3 (CR) (see Figure 5.5 and Table 5.3). Nevertheless, the worst performance was displayed by commercial 5 wt % Ru/Al_2O_3 catalyst.

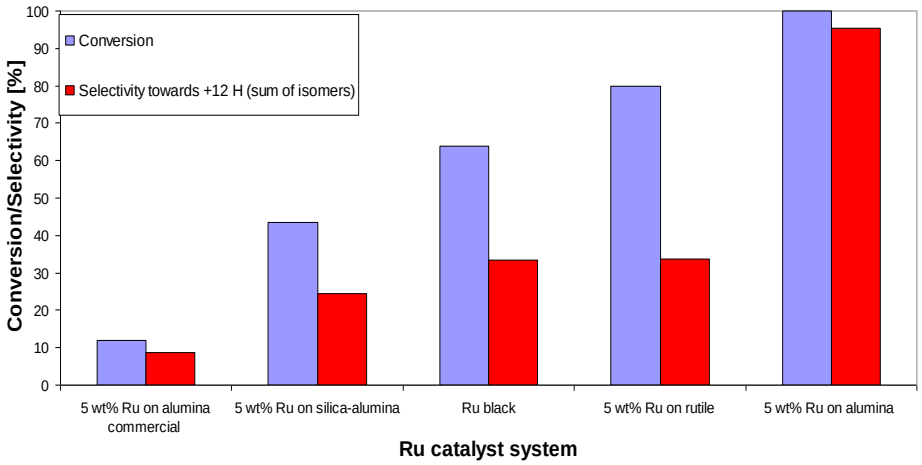

Figure 5.5. Comparison of catalytic performance (conversion and selectivity) for hydrogenation of 9-ethylcarbazole to 9-ethyl-perhydrocarbazole over different Ru catalysts quenched at 3 hours at 130 °C and 70 bar H_2. 5 wt % Ru/Al_2O_3 and ruthenium are commercial catalysts.

However, careful inspection of the obtained data revealed that the activity and selectivity of the supported samples was in general also inversely related to the metal particle size (for particle sizes see Chapter Four, paragraph 4.3.1).

5.3.3. Analysis of the reaction products and intermediates

From the GC-MS analysis of the reaction mixtures sampled in the different time spans, the hydrogenation of 9-ethylcarbazole appeared to be stepwise. The intermediate species and products of this reaction in cyclohexane were the same as the previously described products of this reaction in the molten state (Chapter Four, paragraph 4.3.6). Therefore, it is likely that the presence of the solvent did not have any significant influence on the reaction pathway. Additionally, under the reaction conditions studied, no secondary processes (such as ring opening or denitrogenation) were observed with an exception of isomerization of the final products. Lack of any side reactions can be attributed to the relatively mild reaction conditions in the liquid state (130°C, 70 bar). However, during prolonged reaction times (t > 22 h), when the full conversion was reached, some hydrogenolysis of the C-N bond in 9-ethyl-perhydrocarbazoles was observed, leading to the production of 9-perhydrocarbazole.

Similar products of 9-ethylcarbazole hydrogenation were previously observed by Sotodeh et al who studied a similar reaction using decalin as a solvent at 150 °C (28). In the present work, among the reaction products obtained in cyclohexane, high quantities of 9-ethyl-tetrahydrocarbazole (Pl 4 [H]), 9-ethyl-octahydrocarbazole (Pl 8 [H]) and only a trace level of 9-ethyl-hexahydrocarbazole (PL 6 [H]) were obtained. Because of the observed concentrations of the latter intermediate being extremely low, it was not accounted for in further analysis, in order to simplify the modelling of the reaction pathway.

5.3.4. Modelling of the reaction pathway

The product distributions versus time were obtained for all of the systems studied in the period of 24 hours reaction by sampling the reaction solution and subsequent composition analysis using GC-MS. The representative plots of concentrations of substrate and products versus time of the reactions are shown in Figure 5.6, for the most active catalysts: 5 wt % ruthenium supported on: Al_2O_3 (CR) – profile a, TiO_2 –profile b, SiO_2 –Al_2O_3-profile c and for unsupported ruthenium black – profile d. The experimentally obtained product distributions versus time over these four ruthenium based catalyst were used to model the reaction kinetics. Considering the differences between the product distributions over ruthenium black catalyst with large particle size and the small particles of supported catalysts, two types of active sites were analysed; flat face (terrace) sites which are typical for large particle catalysts, and highly unsaturated sites (steps and corners) that are typical for small defected metal particles as it was mentioned in the introduction to this chapter (see Figure 5.1). The proposed kinetic model was developed accounting for the structures of the intermediates and final products obtained from the series of NMR experiments in Chapter Four, paragraph 4.3.6.

The proposed reaction model is based on the following assumptions and standpoints:

1) The reaction is first order in the concentration of 9-ethylcarbazole and zero-order in hydrogen. This is in agreement with the literature findings (28)
2) The presence of 9-ethyl-hexahydrocarbazole is discarded, due to only trace levels of this intermediate found in the reaction solution
3) The only active sites on ruthenium are considered to be responsible for activation of both, heterocyclic substrate and hydrogen gas
4) The active sites on the metal that are used for adsorption of hydrogen gas are different than the sites used for activation of 9-ethylcarbazole and the reaction intermediates, therefore no site competition occurs between gas molecules and the substrate
5) No other side reactions, apart from isomerisation of the final product occur
6) All of the intermediate reactions are parallel routes and can take place simultaneously

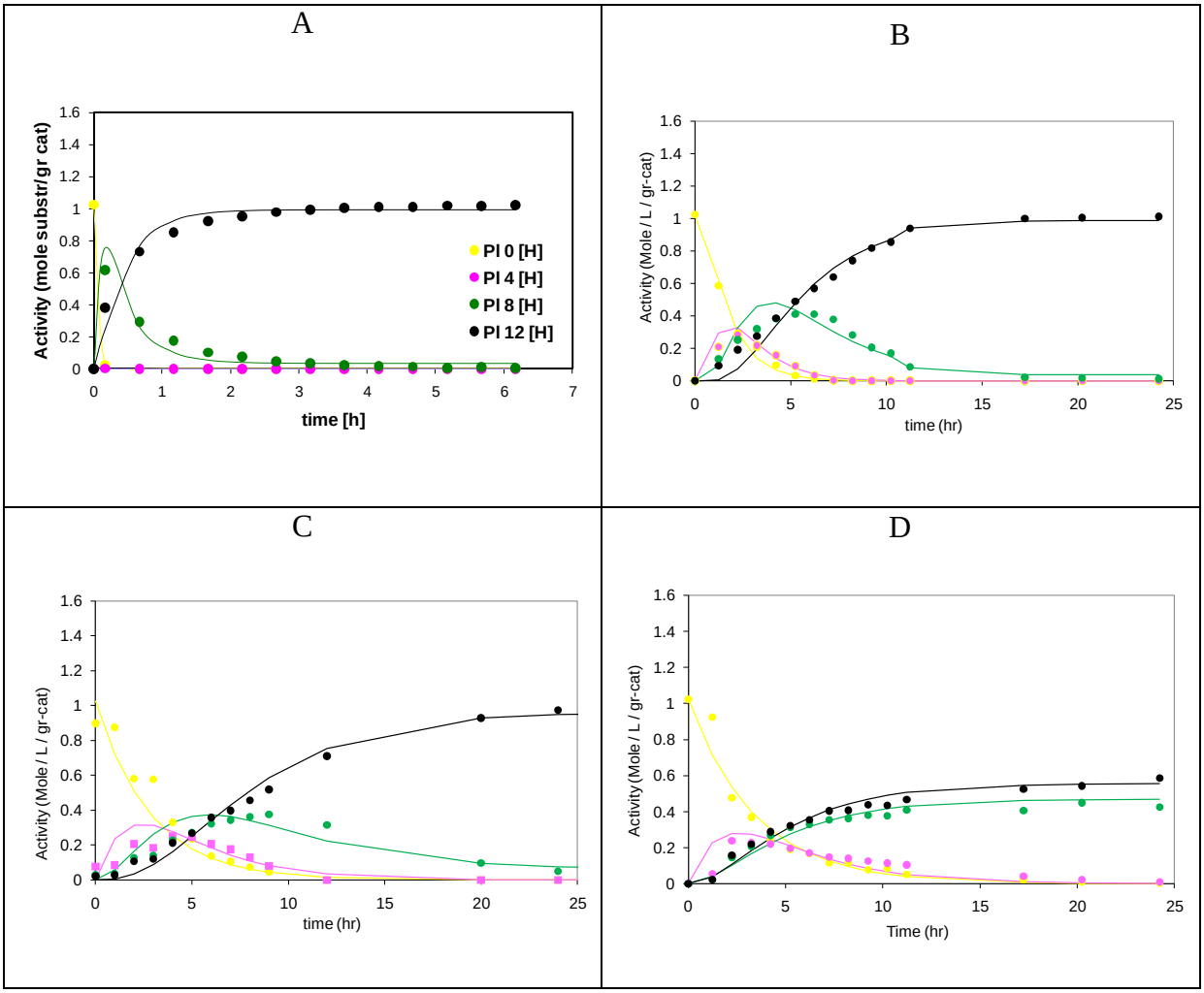

Figure 5.6 Substrate and product concentration changes in time during hydrogenation of 9-ethylcarbazole over a) 0.1g 5 wt % Ru/Al_2O_3 (CR), b) 0.15g Ru/TiO_2 (CR), c) 0.15g Ru/SiO_2-Al_2O_3 (CR) and d) 0.15 g Ru black (COM).

The proposed reaction network for 9-ethylcarbazole hydrogenation over ruthenium based catalysts is shown in Figure 5.7. Based on this network, the reaction kinetics was modelled as described in Chapter Three, paragraph 3.6.1.

It should be noted that during NMR analysis described in Chapter Four (paragraph 4.3.6), it was found that the main product of hydrogenation of 9-ethylcarbazole, contains four different isomers, two symmetrical and two asymmetrical. Unfortunately, due to their very close physical properties, the two symmetrical isomers of Pl 12 [H] elute from the column at the same retention time. Thus, a GC-MS equipped with a non-polar column is not able

to distinguish between the two symmetrical stereoisomers of Pl 12 [H]. Therefore, for quantitative analysis, these symmetrical isomers had to be considered as a mixture of two compounds.

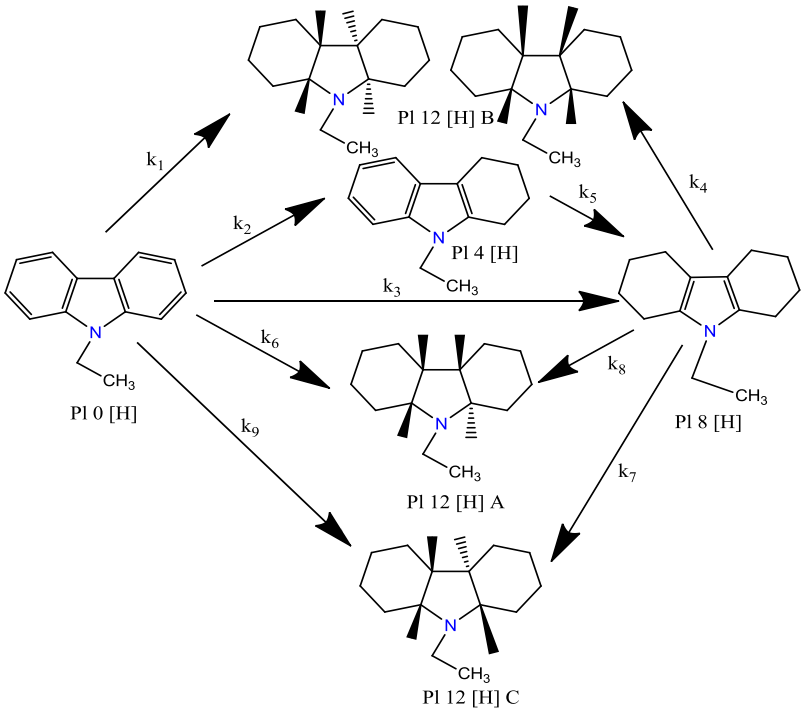

Figure 5.7. The modelled pathway of hydrogenation of 9-ethylcarbazole over ruthenium based catalysts. The acronyms of the intermediates and products are explained in the text .The numbers of the rate constants were used in the modelling.

For clarity purpose, the fractions of the fully loaded material identified using GC-MS are shown again in Figure 5.8, with the name abbreviations used in quantitative analysis of the relative concentrations of these species in the mixture of products in the present chapter. The reaction network is more complicated by the existence of these four stereoisomers of the fully hydrogenated product. As it was mentioned before, the presence of the different isomers of Pl 12 [H] was never accounted for and all the previous works reported in the literature (5)(28)(6) reported only single stereoisomer of the fully loaded product.

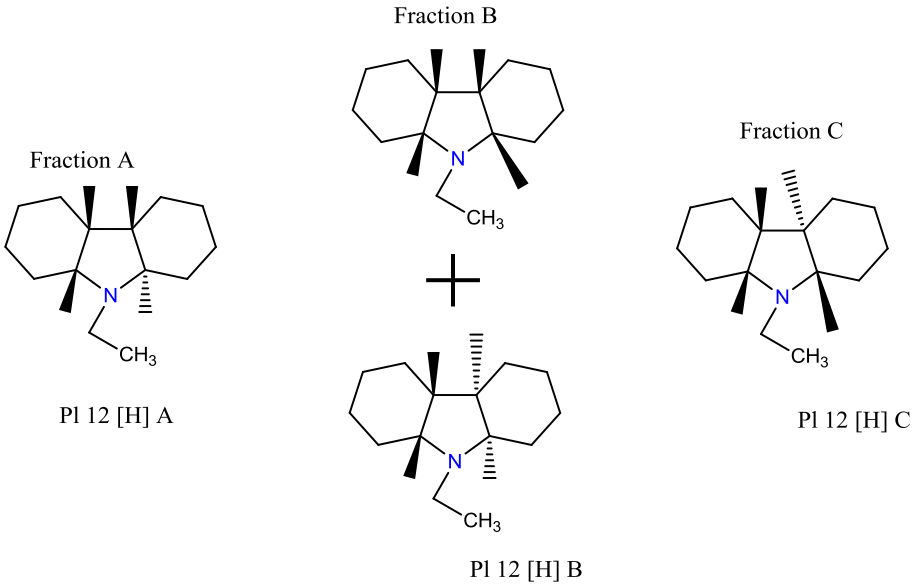

Figure 5.8. Four fractions of the fully hydrogenated product (9-ethyl-perhydrocarbazole) identified over NMR experiments and observed in GC-MS analysis as separate peaks with different retention times. Fraction A contains one hydrogen atom on the other side of the molecule, fraction B contains two isomers, one with all four hydrogen atoms on the same side of the molecule and second with two hydrogen atoms on the same side and two on the opposite side of the molecule, fraction C contains one isomer with one hydrogen atom on the opposite site of the molecule. It should be noted that the isomers in fraction B were not separable on the GC-MS column and are quantified together as a mixture.

In the product concentration change showed in Figure 5.6, it can be noticed that the distributions of intermediates display "volcano" profiles of 9-ethyl- tetrahydrocarbazole (Pl 4 [H]) and 9-ethyl-octahydrocarbazole (Pl 8 [H]) over all the catalyst systems. In addition, Pl 4 [H] seems to be converted in a stepwise manner into Pl 8 [H], which is especially significant reaction over ruthenium black catalyst. On the contrary, over supported catalysts, the increase of the concentration of Pl 8 [H] is almost parallel to the increase of the concentration of Pl 4 [H]. This may suggest that Pl 8 [H] intermediate is created via two different mechanisms. To account for this observation, in our reaction model (Figure 5.7), it was proposed that Pl 8 [H] can be produced following stepwise addition of hydrogen atoms to Pl 4 [H] as well as it can be formed directly from the substrate, without desorption of any intermediates from the surface of the catalyst. Subsequently, it is clear that the Pl 8 [H] is consumed to form the isomers of 9-ethyl-perhydrocarbazoles (see Figure 5.7). It is apparent that it takes much more time for the less active 5 wt % Ru /TiO_2 or 5 wt % Ru/$SiO_2Al_2O_3$ to further convert Pl 8 [H] as compared to

5 wt % Ru/Al_2O_3 (CR) (Figure 5.6). Furthermore, over 5 wt % Ru/Al_2O_3 (CR) catalyst, only a trace level of Pl 4 [H] was obtained. On the other hand, over unsupported catalysts, ruthenium black, the Pl 8 [H] intermediate accumulated up to 44 % of the reaction products and subsequently its concentration remained unaltered throughout the 24 h of a testing period. Furthermore, over ruthenium black, the rate of consumption of Pl 4 [H] was observed to be much slower than over supported catalysts. In addition, it has been noted in Figure 5.6 that the rate of increase in the concentration of the fully hydrogenated product is greater than the rate of further conversion of Pl 8 [H], which suggests that the Pl 12 [H] can be also formed via another reaction pathway. Taking this observation into consideration, in our reaction model shown in Figure 5.7, all fully hydrogenated products can be produced via indirect way, through further hydrogenation of Pl 8 [H] as well as via direct pathway from the substrate.

The modelled results fitted as lines in Figure 5.6 confirmed that hydrogenation of 9-ethylcarbazole under our reaction conditions is well described by the developed simplified first order model. The fit of experimentally measured concentration values with the calculated data is good. The calculated rate constants for individual reactions depicted in Figure 5.7, are gathered in Table 5.4. As it can be seen from the calculated rate constants, the reaction takes mainly indirect pathway over all of the catalysts studied. The indirect pathway involves the formation of Pl 4 [H] and then subsequent additions of hydrogen atoms to form Pl 8 [H]. It is interesting to find that significant rate constant values for the direct formation of Pl 8 [H] were only noted over supported catalysts (see Table 5.4). In addition, the rate constant of formation of Pl 8 [H] from Pl 4 [H] over all of the ruthenium catalysts studied was higher than the rate constant of further conversion of Pl 8 [H] into Pl 12 [H] isomers. This inevitably resulted in the accumulation of Pl 8 [H] in the solution, regardless of the catalyst.

Table 5.4. First –order calculated rate constants for the hydrogenation of 9-ethylcarbazole over ruthenium based catalysts. The unit of the rate constant is [h^{-1}]

Catalyst based on the recipe basis	k_0	k_1	k_2	k_3	k_4	k_5	k_6	k_7	k_8	k_9
5 wt % Ru/Al_2O_3	2.0	0.01	1.8	0.12	0.41	2.0	0.02	0.06	0.03	0.06
5 wt % Ru/TiO_2	1.0	0.13	0.57	0.18	0.11	0.48	0.08	0.07	0.00	0.03
5 wt % Ru/Al_2O_3-SiO_2	0.90	0.02	0.70	0.15	0.08	0.34	0.00	0.06	0.02	0.02
Ru black	0.88	0.25	0.61	0.00	0.08	0.53	0.01	0.02	0.01	0.01

In order to circumvent the known limitations of the Nelder Mead Simplex method, the optimization code was re-run iteratively by using the last best known array of k values and forcing a restart and resetting the simplex. This solution was reported to have been used widely in the literature to avoid this known limitation of the Neldear-Mead method (29). This is better depicted by solving a sample (5 wt % Ru/Al_2O_3-SiO_2) and using values well over and well under the expected optimum and observing the value of the optimised work function (mean square error, MSE). The results for each consecutive iteration are summarised in Table 5.5.

The development of the two approaches with consecutive cycles is depicted in Figure 5.9. The plateaus are associated with local minima or saddle points. These are overcome by resetting the simplex and are followed by sudden drops in the optimised function.

The obtained k-values with values close to zero point towards certain reactions not taking place.

Table 5.5. Evolution of the ks and the mean square error of the fitting (MSE) with consecutive iterations of the Mead Nelder method. Each Iteration was started after 1500 calculations or after the convergence criteria was reached. The top table represents a regression from initial low values and the bottom table is a regression from high values.

	k1	k2	k3	k4	k5	k6	k7	k8	k9	k10	k11	MSE
Initial value	0	0	0	0	0	0	0	0	0	0	0	17.53
Iteration 1	6.18E-02	3.43E-11	2.08E-01	2.48E-02	5.09E-02	2.47E-01	3.43E-02	2.50E-02	1.48E-10	2.46E-02	1.67E-02	10.77
Iteration 2	2.48E-01	4.96E-11	5.12E-01	6.96E-02	4.33E-07	7.59E-02	1.92E-02	1.33E-05	1.15E-11	1.28E-02	2.33E-02	5.36
Iteration 3	2.15E-01	9.74E-11	5.69E-01	7.88E-02	1.22E-07	9.42E-02	3.11E-02	1.71E-10	2.71E-11	8.21E-03	2.81E-02	5.29
Iteration 4	1.14E-01	2.87E-02	5.69E-01	7.89E-02	3.81E-02	9.42E-02	3.09E-02	2.26E-10	5.89E-17	8.21E-03	2.81E-02	5.16
Iteration 5	2.93E-03	2.02E-01	5.13E-01	1.53E-01	1.70E-01	1.23E-01	2.56E-07	5.28E-10	1.47E-16	4.05E-08	5.28E-02	3.51
Iteration 6	8.32E-02	5.43E-01	1.32E-01	1.57E-01	4.79E-01	1.13E-01	1.57E-05	1.16E-08	1.75E-14	7.23E-07	5.13E-02	2.21
Iteration 7	1.34E-01	5.64E-01	1.74E-01	1.03E-01	4.86E-01	1.08E-01	8.11E-02	4.52E-05	4.92E-12	1.72E-03	2.32E-02	1.85
Iteration 8	1.32E-01	5.72E-01	1.80E-01	1.11E-01	4.84E-01	7.84E-02	7.35E-02	6.01E-04	1.42E-12	1.15E-02	2.21E-02	1.63
Iteration 9	8.49E-02	5.90E-01	1.72E-01	1.06E-01	4.41E-01	5.33E-03	7.04E-02	7.98E-03	4.77E-02	1.15E-02	2.21E-02	1.62
Iteration 10	3.39E-02	6.09E-01	1.58E-01	8.48E-02	4.06E-01	4.04E-03	6.74E-02	2.00E-02	9.48E-02	1.15E-02	2.21E-02	1.61
Iteration 11	1.88E-02	6.98E-01	1.54E-01	8.42E-02	3.44E-01	5.51E-04	6.35E-02	2.31E-02	2.84E-02	1.15E-02	2.21E-02	1.60
Final iteration	1.88E-02	6.98E-01	1.54E-01	8.42E-02	3.44E-01	5.51E-04	6.35E-02	2.31E-02	2.84E-02	1.15E-02	2.21E-02	1.60

	k1	k2	k3	k4	k5	k6	k7	k8	k9	k10	k11	MSE
Initial value	5	5	5	5	5	5	5	5	5	5	5	19442.7
Iteration 1	3.48E-01	3.89E-01	6.15E-03	1.14E+01	8.25E+00	2.03E-03	2.08E+00	7.25E+00	6.13E+00	4.41E+00	1.22E+01	13.97
Iteration 2	3.58E-01	5.89E-01	1.16E-02	2.55E+01	2.14E-01	4.38E-03	3.38E-03	4.49E+00	1.95E-02	7.27E-02	1.53E-01	9.43
Iteration 3	1.61E-01	6.81E-01	9.19E-03	1.21E-01	5.60E-01	4.86E-03	7.65E-03	3.93E-02	5.84E-03	2.26E-03	4.04E-02	2.17
Iteration 4	1.14E-01	5.78E-01	1.56E-01	1.38E-01	4.95E-01	2.23E-04	6.28E-03	3.60E-02	5.12E-02	5.59E-11	4.65E-02	1.92
Iteration 5	4.55E-02	6.64E-01	1.55E-01	9.74E-02	4.84E-01	5.44E-04	6.31E-02	2.41E-02	3.48E-02	1.11E-12	2.73E-02	1.69
Iteration 6	1.32E-02	6.72E-01	1.55E-01	7.38E-02	4.84E-01	7.84E-04	6.35E-02	2.41E-02	5.93E-02	1.15E-02	2.21E-02	1.60
Iteration 7	1.88E-02	6.97E-01	1.55E-01	8.03E-02	3.44E-01	7.84E-04	6.35E-02	2.41E-02	2.81E-02	1.15E-02	2.21E-02	1.60
Final iteration	1.88E-02	6.97E-01	1.55E-01	8.03E-02	3.44E-01	7.84E-04	6.35E-02	2.41E-02	2.81E-02	1.15E-02	2.21E-02	1.60

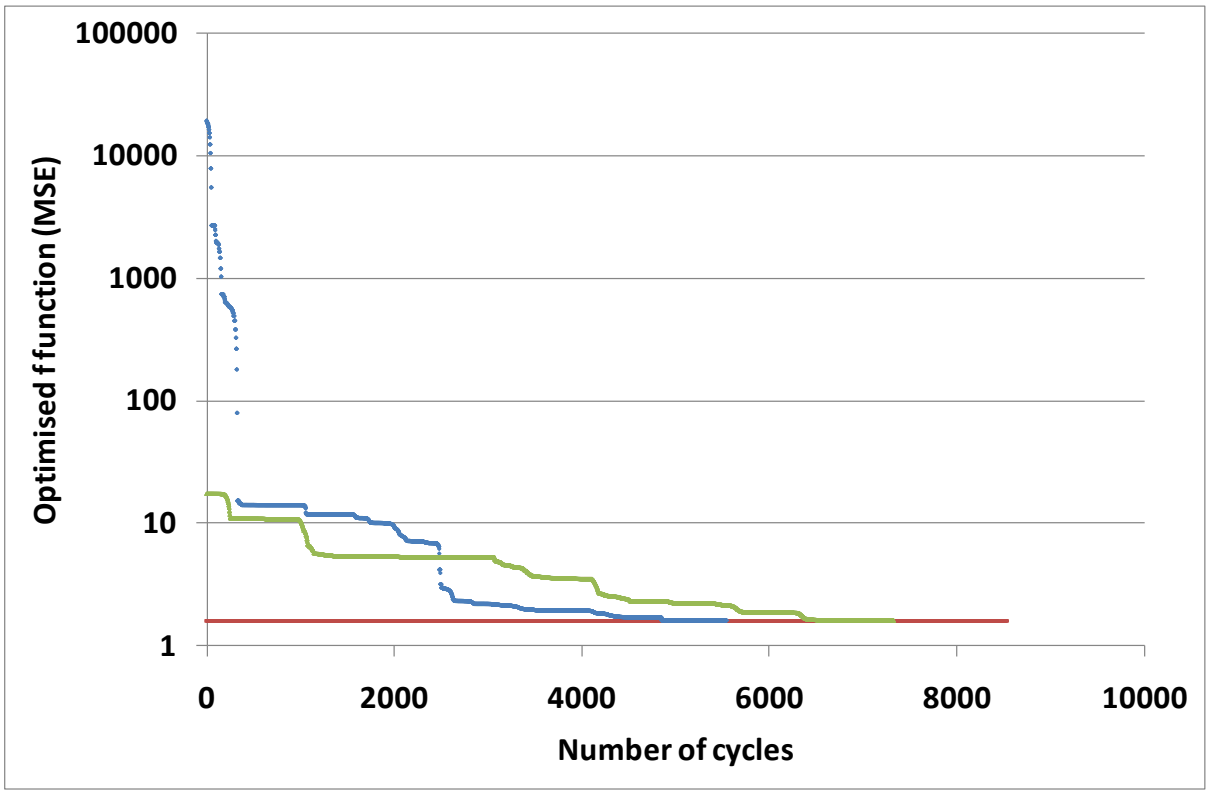

Figure 5.9. Evolution of the optimised function versus number of cycles. The red line represents the final mean squared error (MSE). The green line represents the optimisation from a minimum and the blue line represents the optimisation from a maximum.

In order to verify the proposed reaction mechanism, the distribution of the fully hydrogenated isomers of 9-ethyl-perhydrocarbazole over unsupported ruthenium black catalyst and supported catalysts was studied. Figure 5.10 shows representative distribution profiles of the isomers of Pl 12 [H] (see Figure 5.8 for structures) versus time obtained over 5 wt % Ru/TiO_2 (rutile) (CR) and ruthenium black catalysts together with the ratio of concentrations of the symmetrical product Pl 12 [H] B versus the sum of all the Pl 12 [H] products. It should be underlined however, that profiles with very similar trends to the one shown here for 5 wt % Ru/rutile (CR) were obtained for all of the other supported catalysts tested. It can be observed in profiles shown in Figure 5.10 that over unsupported ruthenium black catalyst with relatively bigger size (synthesis at higher temperatures), the primary main product of the reaction is symmetrical Pl 12 [H] B, which at the beginning of the reaction contains over 90 % of the sum of products. In addition, the high selectivity towards this product was stable in the testing period. Similarly, over supported small ruthenium nanoparticles, the main reaction product appears to be also Pl 12 [H] B, however the selectivity towards this product is significantly lower and approximately equal to the selectivity towards Pl 12 [H] A.

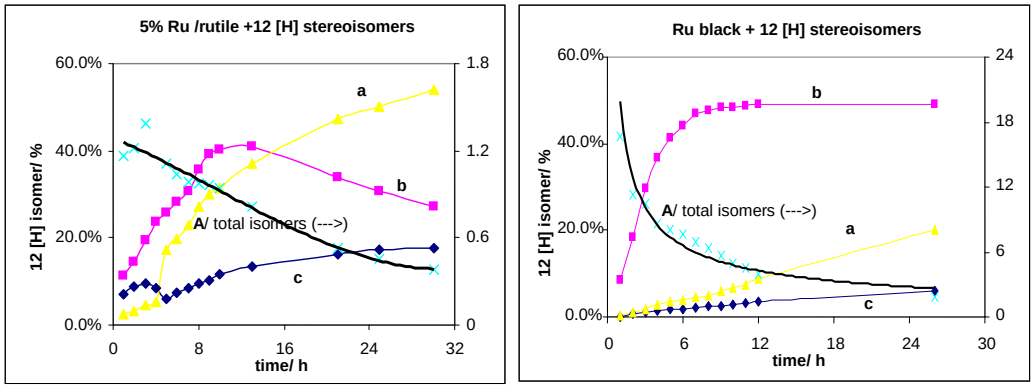

Figure 5.10. The concentration versus time for the three phases of 9-ethyl-perhydrocarbazole (+ 12 [H]) observed in the GC-MS analysis of the reaction mixture of 9-ethylcarbazole hydrogenation over 5 wt % Ru/rutile (CR) on the left, and ruthenium black on the right .The reaction conditions; 130 °C, 70 bar hydrogen, 3 g of substrate and 0.15 g of catalyst.

It should be noted that unsymmetrical isomer Pl 12 [H] A was experimentally found to be the most stable product of this reaction. The trans products were reported previously to be the most stable in hydrogenation of o-xylene (30) and naphthalene (31). In addition, while the reaction progresses over supported catalyst, the isomer Pl 12 [H] B is converted into isomer Pl 12 [H] A and Pl 12 [H] C. Accordingly with these findings, a model of the isomerisation reaction was proposed which is shown in Figure 5.11**.** It is important to note that the isomerisation reaction was observed only when the starting material was fully converted, which may suggest that there could be some site competition taking place between Pl 12 [H] products and other reaction intermediates. This site competition could be taking place for highly unsaturated sites over which the adsorption of these intermediates and products is expected to be facilitated. The calculated rate constants of the isomerisation for the catalysts studied are gathered in Table 5.6. It is clear that this reaction must be taking place on the highly unsaturated sites, because of the fact that it was not observed over ruthenium black catalyst containing mainly terraced (flat) surfaces.

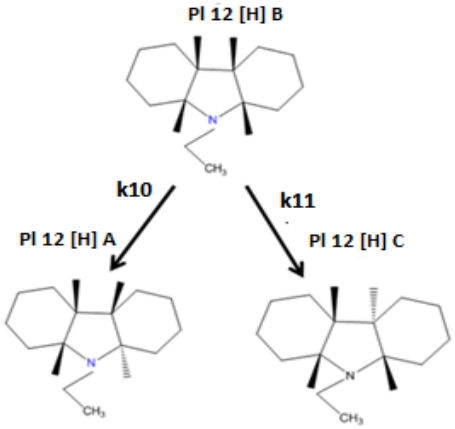

Figure 5.11. The proposed mechanism of isomerisation of 9-ethyl-perhydrocarbazole over ruthenium catalysts.

As it can be seen from Table 5.6, the isomerisation of Pl 12 [H] B into Pl 12 [H] A is more favourable than the isomerisation of Pl 12 [H] B into Pl 12 [H] C which only shows

significant rate constant over 5 wt % Ru/TiO_2 (CR). It should be noted that Pl 12 [H] C product is in minority over all of the catalysts studied. In addition, it was found that the ratio of symmetrical product Pl 12 [H] B versus the sum of isomers observed over 5 wt % Ru/TiO_2 at the beginning of the reaction is around 1.2 and subsequently decreases to 0.5 (see Figure 5.10).

Table 5.6. Calculated rate constants of the proposed isomerisation reaction of 9-ethyl-perhydrocarbazole isomer B.

Catalyst	k_{10}	k_{11}
5 wt % Ru/Al_2O_3 (CR)	0.083	0.000
5 wt % Ru/TiO2 (CR)	0.011	0.022
5 wt % Ru/SiO_2- Al_2O_3	0.052	0.000
Ru black	0.000	0.000

The gradual decrease in the ratio of isomers clearly implies that isomerisation reaction of Pl 12 [H] B into the more thermodynamically stable asymmetrical structures Pl 12 [H] A and/or Pl 12 [H] C is taking place. On the other hand, over unsupported ruthenium black catalyst, extremely high ratio greater than 18 was obtained at the beginning of the reaction and did not display any significant drop during the testing period as it can be seen in Figure 5.10.

Considering the differences in stability of Pl 8 [H] as well as the differences in the selectivity pattern in the composition of the final product over supported and unsupported catalysts it can be implied that the selectivity of liquid phase hydrogenation of 9-ethylcarbazole is governed by the type of active sites available on the catalysts surface. During subsequent hydrogenation of Pl 8 [H] to form isomers of Pl 12 [H], two molar equivalents of H_2 have to be added to the 'pyrrole' ring, situated in the middle of the molecule. Owing to the hydrogenation being intrinsically cis in character (32), it could be expected that mainly in the presence of flat terrace sites, the adsorption of the substrate and intermediates would be flat, parallel to the metal surface. Thus, the hydrogen atoms would

be added on the same side of the molecule to produce a symmetrical product Pl 12 [H] B. This could explain the high concentration of this isomer in the reaction mixtures obtained over unsupported ruthenium (see Figure 5.10) which contains high ratio of flat surfaces. However, based on the geometrical considerations of the structure of Pl 8 [H] intermediate, once it desorbs from the surface of the metal, it would prefer to re-adsorb on the low coordination sites (step, or corner sites) to undergo further hydrogenation. This is due to the fact that on the low coordination sites, the steric constrains are normally more relaxed, which will be shown in the calculations later on in this chapter. Owing to the fact that most sites over ruthenium black catalyst are flat, terrace sites, the re-adsorption of Pl 8 [H] intermediate must be greatly impeded resulting in the accumulation of this intermediate in the solution. However, over supported catalysts, the re-adsorption of this intermediate is much easier due to the presence of higher density of low coordination sites, where this intermediate is able to adsorb via unsaturated carbon-carbon bonds with d-electrons of the metal or less likely via δ- δ interaction with the lone pair of electrons on the nitrogen. This mode of adsorption of Pl 8 [H] displays tilted geometry, where the molecule is perpendicular to the surface of the metal catalyst. As a result, in the presence of high density of unsaturated sites on small supported catalysts, Pl 8 [H] does not accumulate for longer period of time in the solution.

The ratio of the concentration of the asymmetric products depends on the structure of Pl 8 [H] intermediate which may vary due to the double bond migration during hydrogenation. The double bond migration was previously observed in hydrogenation of dimethylocyclohexanes in ethanol over noble metal catalysts (33). The proposed mechanisms of formation of asymmetrical products were discussed in Chapter Four, paragraph 4.3.6. This mechanisms are very likely to involve desorption and re-adsorption

of Pl 8 [H] intermediate observed previously in formation of cis or trans decalin (31), or the roll over mechanism described in hydrogenation of o-xylene (30).

5.3.5. Implications of hydrogen storage via reversible hydrogenation of 9-ethylcarbazole

As far as the catalytic hydrogen storage for practical use is concerned, an efficient catalyst must be capable of promoting both hydrogenation and dehydrogenation reactions. The rapid interconversion of various intermediate substances between the unsaturated and fully loaded forms will lead to a maximum storage capacity of hydrogen and its delivery at acceptable rates. The formation of kinetically stable intermediates may cause problems with the reversibility of the process. It is believed that the rate of desorption of the intermediates from the surface of the catalyst to the solution and their subsequent conversion are related to the kinetic stability and the preferable adsorption geometry of these intermediates on the surface of the catalysts. The adsorption enthalpy of the substrates and partially hydrogenated products is expected to vary with the type of active sites present on the surface of the catalyst. Therefore, the detailed understanding of the hydrogenation mechanism with regards to the location and direct function of the active sites on the metal surface is crucial in order to improve the efficiency of the catalytic systems.

5.3.6. Characterisation of the active sites on the surface of the catalyst

In order to verify the developed reaction model, it is important to characterise the types of active sites present on the surface of ruthenium catalyst. Thus, CO chemisorption was employed to examine surface sites of the pre-reduced catalysts. The details of the experimental set-up and the conditions of the analysis can be found in Chapter Three, paragraph 3.2.3. CO adsorption spectra were collected for all the supported ruthenium catalysts studied in this chapter. Unfortunately, no significant CO adsorption was observed

over ruthenium black catalyst, probably due to the low dispersion and/or specific surface area of this catalyst. Additionally, it is probable that the catalyst pre-treatment at 300°C prior to CO chemisorption experiments led to sintering of ruthenium black catalysts and resulting in a decrease in its activity. Spectra collected following adsorption of CO at room temperature on supported catalysts pre-treated in H_2 are shown in Figure 5.12. The relative peak areas were calculated from IR spectra and the results are presented in Table 5.6.

At room temperature, CO remained strongly bonded on the catalysts surface and three main features were clearly visible in the spectrum: a relatively weak and broad band centred at (1975-2025 cm-1) in low frequency (LF) region, a strong band with high intensity at (2040-2100 cm-1) in high frequency (HF1) region and another strong band with lower intensity centred at (2110-2130 cm-1) in a high frequency (HF2) region. It should be clear that the variety of carbonyls and their relative wavenumber is dependent on the type of support, catalyst precursor, reduction temperature and metal dispersion (33).

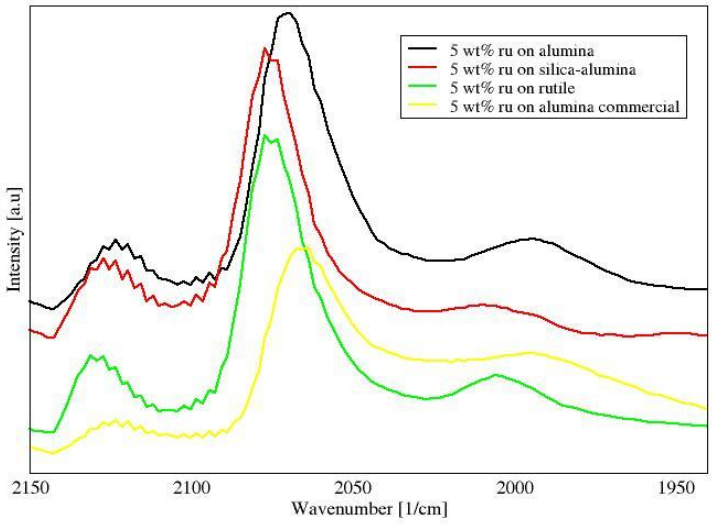

Figure 5.12. Comparison of different CO adsorption modes on supported Ru catalysts: three different adsorption species, namely linear (terminal) carbonyl (2110-2130cm^{-1}) multicarbonyl (2040-2100 cm^{-1}); and bridging carbonyl (1975-2025 cm^{-1}) are clearly visible.

Table 5.7. Relative peak areas of the chemisorbed CO and corresponding ratios of different adsorption modes.

Catalyst (based on the recipe)	CO adsorption modes			Multi-carbonyl /Bridging
	Linear (2110-2130 cm^{1})	Multi- (2040-2100 cm^{-1})	Bridging (1975-2025 cm^{-1})	
5wt % Ru on alumina (COM)	0.09	0.55	0.22	2.51
5 wt % Ru on silica alumina (CR)	0.29	0.86	0.15	5.58
5 wt % Ru on rutile (CR)	0.27	0.76	0.14	5.47
5 wt % Ru on alumina (CR)	0.23	1.28	0.20	6.37

The recorded CO absorption bands can be assigned as follows; linear (terminal) carbonyl (2110-2130 cm^{-1}), multicarbonyl (2040-2100 cm^{-1}), and bridging carbonyl (1975-2025 cm^{-1}). It is known from the literature (34) (35) (36) (37) that the linear and multicarbonyl CO adsorbed species favourably occur at low coordination metal sites (corner, edge, etc), while the bridging CO species prefer flat and highly coordinated metal sites. The observed low ratio of multicarbonyl to bridging CO species over commercial 5 wt % Ru /Al_2O_3 (COM) is in a good agreement with the fact that large metal particles (synthesized at high temperature) contain large proportion of terrace sites as it was suggested previously. Similarly, the 5 wt % Ru /Al_2O_3 (CR) catalyst prepared under mild chemical reduction contains smaller metal particles having large number of low coordination metal sites, which leads to high ratio of multicarbonyl to bridging CO modes (see Table 5.6). The results from CO adsorption agree well with the previously presented TPR results, which also identified that commercial 5 wt % Ru /Al_2O_3 (COM) may contain sintered metal clusters which are likely to have higher density of flat surfaces. These sites were found to be less efficient in hydrogenation of 9-ethylcarbazole.

5.3.7. Reaction mechanism -theoretical considerations

The high activity and selectivity of 5 wt % Ru/Al_2O_3 (CR) can be attributed to the existence of small metal particles with high density of unsaturated sites. The activity of this catalyst can be further improved by the interaction of ruthenium metal with the support, which renders ruthenium metal electron deficient as shown in XPS experiments. In addition, the unsaturated sites on this catalyst are thought to be very efficient in converting the intermediates of the reaction to the final product. The presence of these sites was confirmed by the high ratio of multicarbonyl to linear CO adsorption modes and lower reduction temperatures in the TPR experiments. The presence of small well dispersed particles in this catalyst was also confirmed by TEM images of this sample (Chapter Four, paragraph 4.3.1). On the other hand, the accumulation of Pl 8 [H] intermediate in the solution, when the reaction is performed over ruthenium black catalyst is attributed to the presence of faceted particles as it can be seen in TEM images of ruthenium black catalyst shown in Figure 5.13.

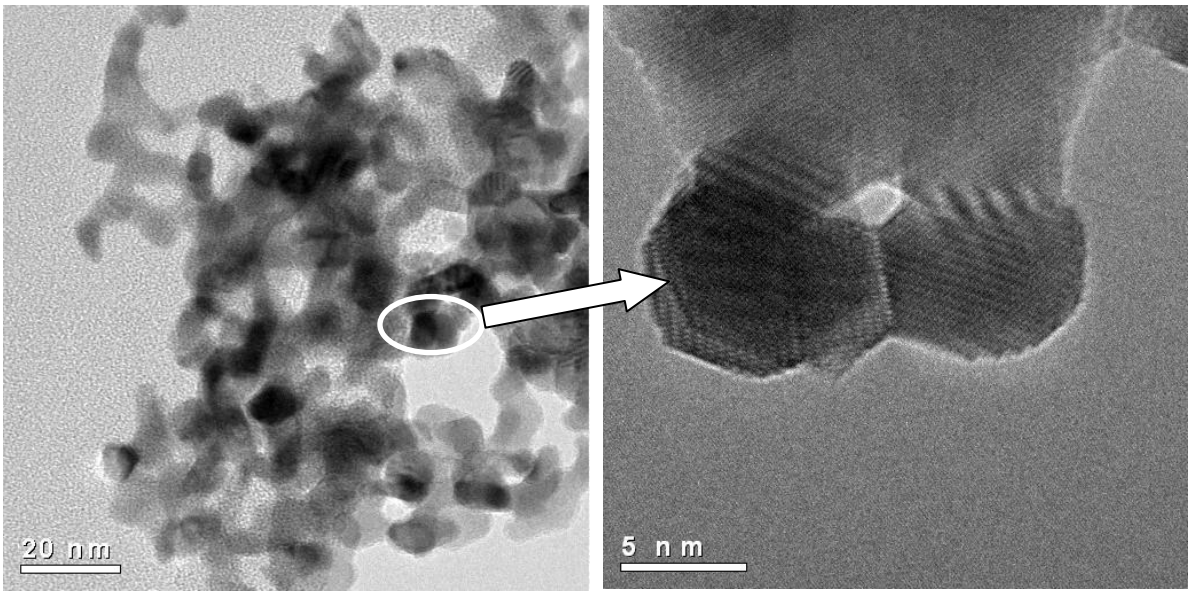

Figure 5.13. HRTEM images of strongly sintered large faceted particles of commercial ruthenium black catalyst.

These saturated sites are clearly not able to further hydrogenate the 9-ethyl-octahydrocarbazole intermediate, even in the presence of an excess of hydrogen. This is in

line with what was proposed before, that catalysts with large proportion of terrace sites relative to low coordination sites display poor ability to re-adsorb Pl 8 [H] intermediate as well as displaying lower overall activity (compare Figure 5.2 and Table 5.6) in the hydrogenation of 9-ethylcarbazole. Furthermore, it is clear that the geometry of the molecule can strongly influence its ability and mode of adsorption on the catalyst surface. It was thus decided to use DFT calculations to model the adsorption energy of the substrate (9-ethylcarbazole) and the stable intermediate (9-ethyl-octahydrocarbazole) on both; step sites (low coordination sites) and flat terraced sites (saturated sites).

It is also important to obtain information about the relative stability of the different intermediate structures in 9-ethylcarbazole hydrogenation. The total energies of over 96 different possible configurations of all intermediates of the reaction were calculated using DFT methods. All the experimental details about the modelling methods used can be found in Chapter Three.

5.3.7.1. Estimation of the adsorption enthalpy using DFT methods

DFT methods were employed for estimation of adsorption energies of different molecules on the surface of transition metals, as shown in references (38), (39) and (40). In this work, the energetics of adsorption of the substrate and the Pl 8 [H] stable intermediate were investigated. The calculated structures of 9-ethylcarbazole adsorbed on the flat Ru (001) and on step Ru (109) are shown in Figure 5.14. The calculated values of adsorption energy of the substrate on the flat sites is E_a = 2.56 eV and on the step sites E_a = 1.61 eV. These results confirm that 9-ethylcarbazole adsorbs stronger on the flat sites than on the typical unsaturated sites. The high adsorption energy of parallel adsorption of the substrate on the surface of the catalyst can be the result of more favoured interaction between the planar polyaromatic rings and the surface atoms of ruthenium. The effect of co-adsorbed hydrogen atoms on the adsorption of 9-ethylcarbazole was also taken into account by

filling the neighbour surface hollow sites around the adsorbed rings with hydrogen atoms. It was found that the presence of hydrogen does not affect the adsorption of the substrate and the resulting adsorption energy had almost identical value (~2.6 eV). This result supports our previously made assumption that no competitive adsorption between 9-ethylcarbazole and hydrogen is taking place in this reaction. Adsorption energy of the stable intermediate (Pl 8 [H]) was then studied over the ruthenium metal. The calculated adsorption energy of Pl 8 [H] intermediate on the flat surface was as low as 0.32 eV with the ethyl group facing up and almost zero with ethyl group facing down. The kinetically favoured desorption of this intermediate from the terraced sites in shown in Figure 5.15. As it can be seen from this figure, the geometry of the stable intermediate Pl 8 [H] was greatly altered from planar geometry of 9-ethylcarbazole, by the newly introduced hydrogen atoms. This tilted geometry of Pl 8 [H] molecule most probably prevents it from close interaction with the surface of the catalyst as well as it is successfully blocking nitrogen species of the 'pyrrole' ring from participating in the adsorption. In addition, another geometric constrain is introduced by the rotating ethyl group, which further decreases the strength of adsorption.

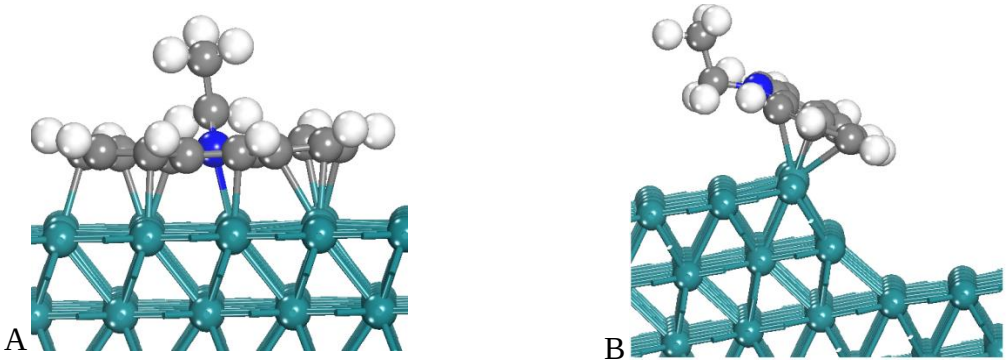

Figure 5.14. Calculated structure of 9-ethylcarbazole adsorbed on A) flat, terraced site Ru(001), B)stepped site with two atomic height Ru(109).

The extremely weak interaction of Pl 8 [H] with the surface of the catalyst hinders its further conversion into the fully hydrogenated products. As a result, a large proportion of

the Pl 8 [H] intermediate can be expected to desorb from the surface of the catalyst. Additionally, the re-adsorption of this intermediate on the same type of the flat sites is very unlikely, which can lead to high accumulation of this intermediate in the reaction mixture obtained experimentally over ruthenium black catalyst.

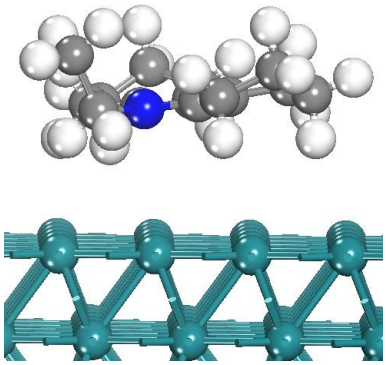

Figure 5.15. Energetically favourable desorption of 9-ethyl-octahydrocarbazole from Ru (001) sites.

On the other hand, much higher adsorption energies were found for Pl 8 [H] intermediate on the edges of the ruthenium catalyst. The extensive calculations of adsorption at one-atomic-height to two atomic height steps were performed and the resulting modelled structures of 9-ethyl-octahydrocarbazole are shown in Figure 5.16. The adsorbed Pl 8 [H] intermediate can be seen to form one N-Ru bond with the surface of one-atom height step of Ru (109) (Figure 5.16 B), and the adsorption energy is estimated to be 0.89 eV, much higher than that at the flat terrace (~0.3 eV). In Figure 5.16, different two-atomic-height steps on Ru (109) and the calculated structures of corresponding adsorbed Pl 8 [H] intermediate are also illustrated. The estimated adsorption energies at these different step sites are similar to each other. The results for the structures shown in Figure 5.16 are as follows; $E_{a\,(D)}$ =1.02 eV, $E_{a\,(F)}$ =1.09 eV and $E_{a\,(H)}$ =0.92 eV. The above DFT adsorption energy calculations shows clearly that the Pl 8 [H] intermediate at various edge site configurations exhibits much higher stability as compared to its stability on the flat terraces. This is the result of the changed geometry of this intermediate that prevents it from getting close to the terrace surface.

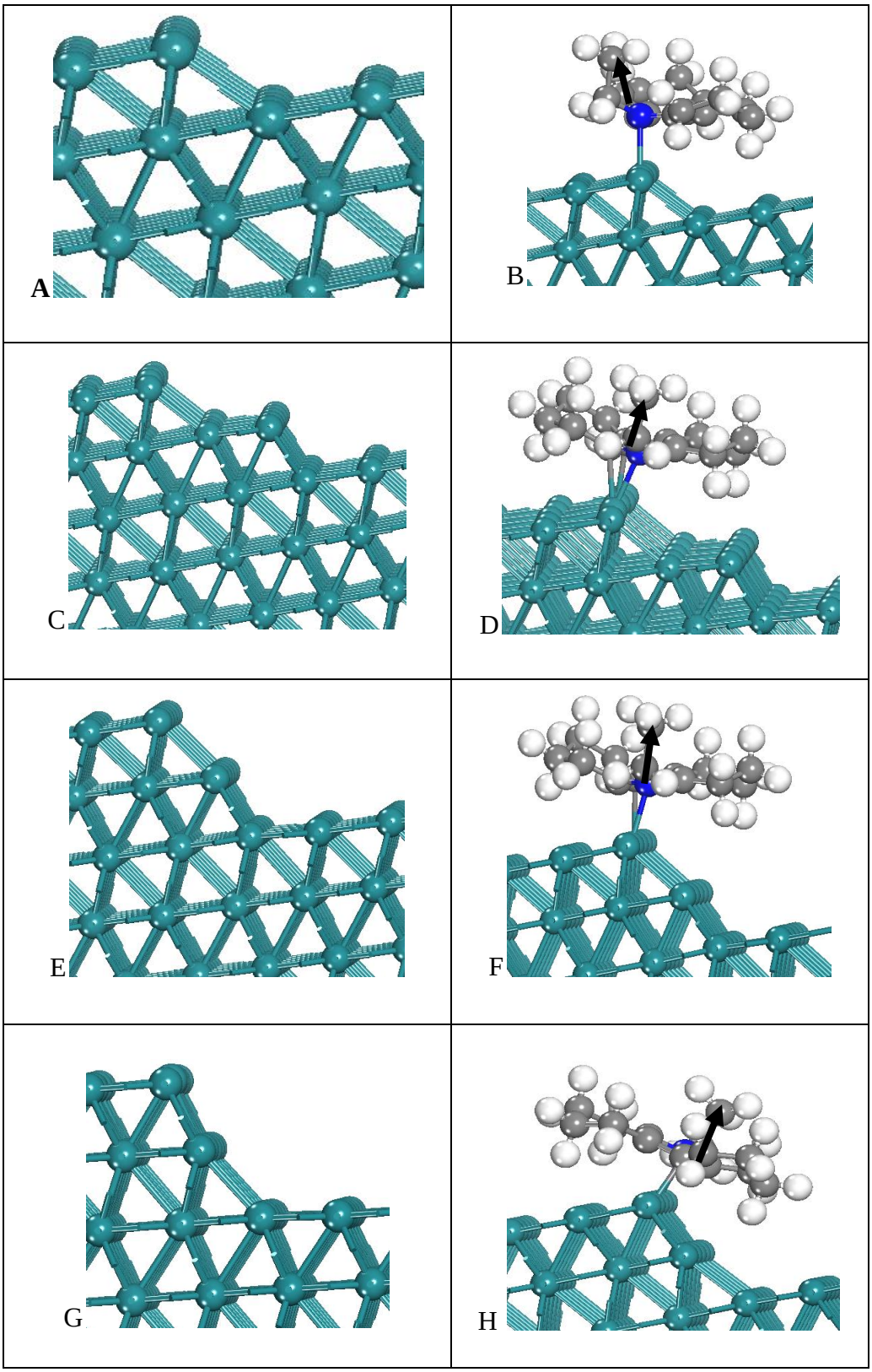

Figure 5.16. Calculated structures of one –atom-height (A) and two-atom-height (C,E,G) steps of Ru (109) and corresponding adsorption structures of Pl 8 [H] intermediate on these surfaces (B,D,F,H). The black arrow specifies the position of ethyl group.

It was found that those repulsive interactions no longer exist on the step or edge sites of the metal. In the absence of these repulsive interactions, the active species in the molecule, such as N and unsaturated C, are able to bind with the Ru atoms along the edge. As a result it could be expected that the Pl 8 [H] intermediate desorbed from the active flat sites should be able to re-adsorb favourably only on the edges of Ru (109) for subsequent reaction. This can only take place if the sufficient defective step sites are present. These findings explain well the accumulation of Pl 8 [H] intermediate in the reaction mixtures obtained over ruthenium black catalyst containing mainly terrace sites. It should also be noted that the described migration mechanism of the intermediates during catalytic hydrogenation of 9-ethylcarbazole over ruthenium catalysts accounts well for the reported product compositions.

5.3.7.2. DFT quantum mechanics calculations of the theoretical stability of the reaction species.

The relative stabilities of different candidate intermediate compounds and products of 9-ethylcarbazole hydrogenation were calculated using DFT methods. The theoretical enthalpies of the reaction in the gas phase were computed at 403 K. The details concerning the calculation method were described in Chapter Three, paragraph 3.6.3.The differences of enthalpies at a finite temperature of 403 K (reaction temperature at standard conditions and atmospheric pressure) for different intermediates and products of the reaction are shown in Figure 5.17 together with the optimised geometrical structures of the theoretically most stable species. It should be clarified that the calculated more negative differences result in greater relative stability of the species.

As it can be seen from Figure 5.17, the favourably produced intermediates are; Pl 4 [H], Pl 6 [H], Pl 8 [H] and Pl 12 [H]. In addition, there are five theoretically possible

stereoisomers of the fully hydrogenated 9-ethyl-perhydrocarbazoles, whose energies do not differ significantly from each other.

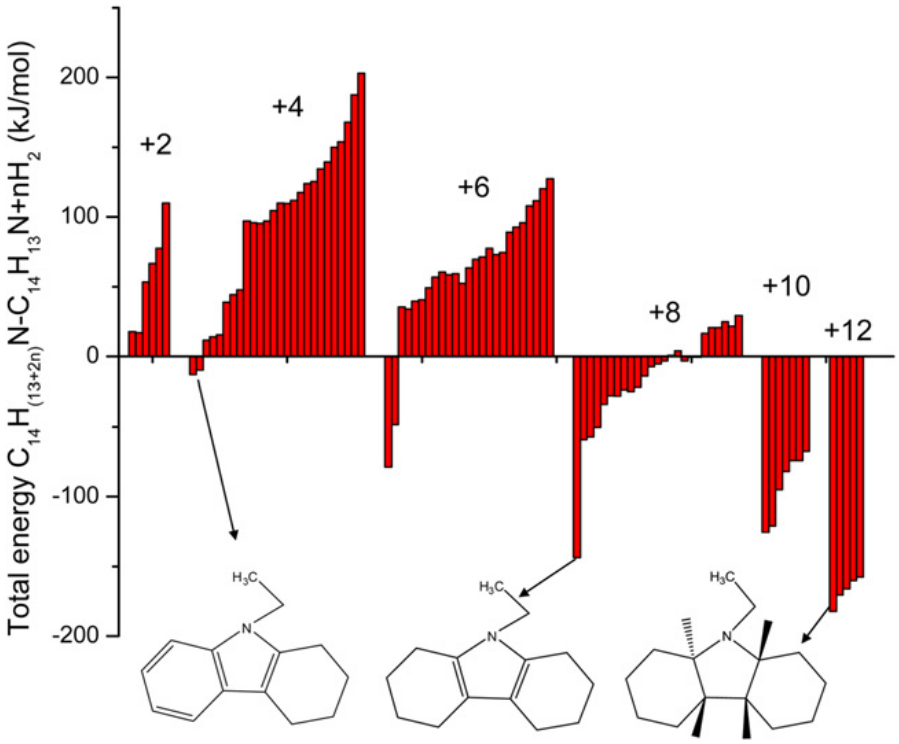

Figure 5.17. Calculated DFT enthalpy differences between the reaction substrate (9-ethylcarbazole) and its partially hydrogenated intermediates in the gas phase.

From these calculations, it is clear that there is an energy penalty for most of the isomers of the intermediates and only some of the configurations of the intermediates are energetically favourable to be produced. For example, there is no possible products with only one mole of hydrogen added (9-ethyl-dihydrocarbazole (Pl 2 [H]) that would be more stable than the reactant. Similarly, only a few structures of Pl 4 [H] and Pl 6 [H] are stable. In general, as it is shown in Figure 5.17, the energy of the system (without consideration of the activation energies barriers) can suggest that the direct formation of isomers of Pl 12 [H] should be favoured. Additionally, based solely on the theoretical calculations, the formation of Pl 10 [H] intermediate could be expected along with the production of Pl 8 [H] intermediates. However, under our reaction conditions, no production of Pl 10 [H] was recorded. In addition, only traces of this intermediate were observed by Sotoodeh et al. (5)

Moreover, there are two energetically favourable structures of Pl 6 [H] (9-ethyl-hexahydrocarbazole). Pl 6 [H] was observed in trace levels only in GC-MS analyses. Nevertheless, high concentrations of Pl 8 [H] over all ruthenium catalysts were observed. The optimised geometry in the DFT calculations of this compound compared to the flat geometry of the substrate is shown in Figure 5.18. It is clear that the addition of hydrogen results in the molecule bending and tilting. The selectivity towards this intermediate was around 35 - 40 % when ruthenium black catalyst was used, which is clearly the result of the steric hindrance imposed by terraced sites, which are in majority on the surface of this catalyst. From the result shown in Figure 5.17, it is clear that Pl 8 [H] intermediate is extremely favourable to be produced due to a very large negative enthalpy difference that is almost as low as the enthalpy difference of the fully hydrogenated products of the reaction (Pl 12 [H]). The enthalpies of hydrogenation of the most stable reaction intermediates together with their modelled structures are gathered in Table 5.8.

It is interesting to note that the modelled structures of the species with the lowest enthalpy difference shown in this table agree well with the structures of the intermediates assigned over NMR experiments in Chapter Four. Thus, the theoretically expected species were indeed observed experimentally.

To sum up, the results from DFT calculations showed reasonable agreement with the experimental results. It was observed that theoretically different isomers can be produced in hydrogenation of 9-ethylcarbazole, thus it is likely that the reaction is able to take different parallel routes. In turn, these pathways can influence the final stereochemistry of the fully loaded product. Nevertheless, it should be underlined that the results from these DFT calculations should be viewed only as a general guideline, since they were performed

for the reactants in the gas phase without taking into consideration the influence of the catalyst, nor that of the solvent.

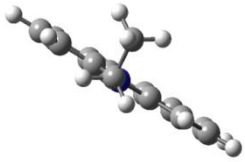

A B

Figure 5.18. The optimised geometry of A) 9-ethylcarbazole and B) 9-ethyl-octahydrocarbazole as the result of quantum mechanics calculations.

Table 5.8. Enthalpies of hydrogenation in [kJ/mol] (including thermal, rotational, translational and zero-point energies contributions) for the most stable intermediates and products as a function of hydrogen loading at finite temperature of 403 K. The structures of the modelled species are provided as follows; numbers in the square brackets refer to the carbon positions at which hydrogen atoms were added (see provided figure for numbering). The calculated structures of the fully hydrogenated products are provided directly.

	(Pl 4 [H])	(Pl 8 [H])	(Pl 12 [H])
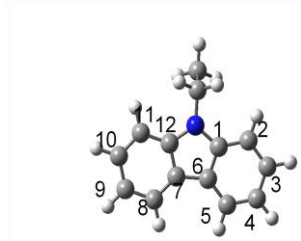	[3456] -12.1	[2345891011] -157.7	Stereoisomer **E** -210.7
	[1234] -9.8	[345678910] -73.4	Stereoisomer **F** -199.2
		[3456891011] -71.3	Stereoisomer **B** -191.2
		[56789101112] -65.6	Stereoisomer **A** -188.7
		[34569101112] -46.8	
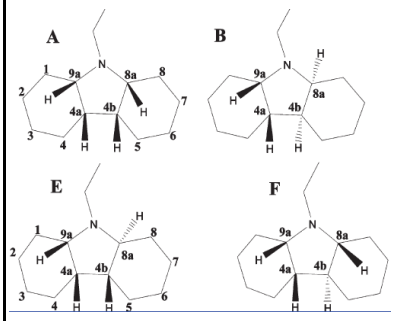		[123689101112] -41.9	
		[1456891011] -42.1	
		[12349101112] -37.9	
		[1256891011] -38.3	
		[3456781112] -35.5	

5.3.8. Site dependent catalysis

Based on the gathered results, the reaction model was proposed showing the consecutive hydrogenation of 9-ethylcarbazole over terrace and low coordination sites which is presented in Figure 5.19. According to this model, the addition of the hydrogen atoms on the planar (flat) surfaces takes place in a symmetrical fashion, simultaneously to both of the aromatic rings. This is the result of the more favourable planar adsorption of the substrate on the surface of this catalyst as shown by the DFT calculations. If the desorption of Pl 8 [H] intermediate takes place before the fully loaded product is formed, then due to the geometrical constraints (Pl 8 [H] geometry is shown in Figure 5.18) this intermediate is expected to "encounter difficulties" in re-adsorption on the flat active sites. As a result, in accordance with the DFT calculation of adsorption energy, this intermediate is very likely to adsorb successfully for further conversion only on step/corner sites. Thus, the Pl 8 [H] intermediate is believed to migrate to these sites. Because of the fact that ruthenium black catalyst has a very low availability of the unsaturated sites with respect to that of flat sites as it was shown in TPR and TEM results, the accumulation of Pl 8 [H] intermediate in the solution is unavoidable in this catalytic system. However, the part of the Pl 8 [H] intermediate which does not desorb from the surface is most likely forming symmetrical product Pl 12 [H] B through surface concerted hydrogenation (as shown in Figure 5.19.). On the contrary, when the hydrogenation of 9-ethylcarbazole is taking place over small, defected catalysts such as 5 wt % Ru/Al_2O_3 (CR), the adsorption of the starting material is expected to take place in the tilted fashion (through δ-Π interaction) on the low saturated sites of the catalyst. Thus, the hydrogenation is bound to take place more favourably asymmetrically and the hydrogen atoms are added by turns to both of the rings.

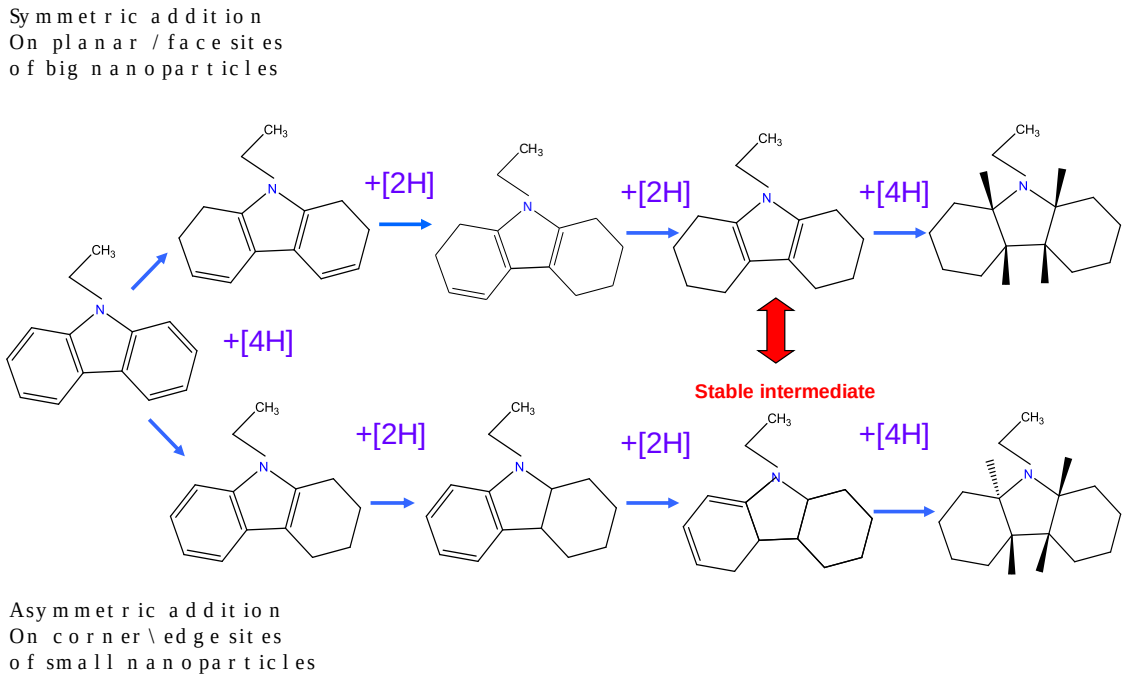

Figure 5.19. Two- site kinetic model of 9-ethylcarbazole hydrogenation over ruthenium catalysts.

The accumulation of Pl 8 [H] for long periods of time was not observed over this catalyst, because of the high concentration of step/edge sites. It was shown in DFT calculations that these sites are favourable for adsorption of Pl 8 [H]. Therefore, in case of the small supported catalyst, the stable intermediate (Pl 8 [H]) does not have to 'queue' in the solution for further conversion, because there is high availability of sites for its re-adsorption. As a result, the Pl 8 [H] is re-adsorbed on the low-coordination sites and it is expected to form asymmetrical fully loaded products such as the most thermodynamically stable Pl 12 [H] A (see Figure 5.19). In addition, the expected adsorption modes on terraced sites of ruthenium black and step sites of 5 wt % Ru /Al_2O_3 (CR) are shown in Figure 5.20.

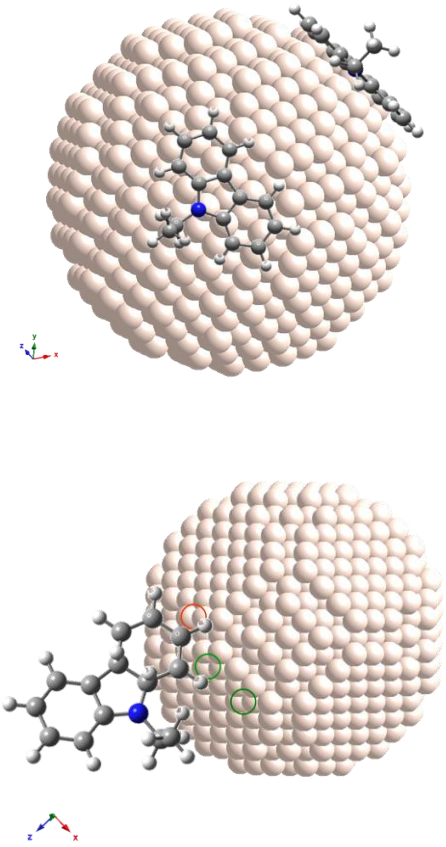

Figure 5.20. The modes of adsorption of the substrate on top; terraced sites on unsupported ruthenium black, bottom; step /edge sites on small defected nanoparticles. The unsaturated corner/edge sites are circled.

The adsorption is preferentially flat on the terraced sites which are in majority on unsupported ruthenium black. On the other hand, the adsorption of 9-ethylcarbazole on step-terraced sites is tilted with respect to the metal surface and can take place via sigma-sigma interaction of the unsaturated double bonds between carbon atoms in the aromatic ring or less probably via interaction of the less sterically accessible lone pair of electrons on nitrogen atom. It should be underlined that the proposed two-site model agrees well with the previously presented differences in composition of the fully loaded Pl 12 [H] product over supported and unsupported catalysts (see Figure 5.10).

5.4. Conclusions

In optimisation of hydrogen storage using LOH approach, a catalyst development is a primary step for further progress (41). In this chapter, supported and unsupported ruthenium based catalysts were tested in liquid phase hydrogenation of 9-ethylcarbazole. The kinetic model of the hydrogenation reaction was developed that described well the experimental data. The model accounted for different active sites present on the catalyst surface and included complex reaction network involving simultaneous reactions as well as isomerisation reactions of the fully loaded product. The developed reaction model provides a tool for optimisation of highly active and selective catalyst for reversible storage of hydrogen, using 9-ethylcarbazole system. In addition, most of the structures of the compounds found experimentally in the reaction solution, agreed well with the most stable structures predicted in DFT calculations. The most active and selective catalyst in the hydrogenation of 9-ethylcarbazole was found to be 5 wt % Ru/Al_2O_3 synthesized by chemical reduction. This catalyst under the studied reaction conditions turned out to be superior to ruthenium black. This is due to the fact that it contained small distorted and defected particles which provided much better active sites for consecutive addition of hydrogen atoms without accumulation of any reaction intermediates. On the contrary, unsupported ruthenium black containing large proportion of flat surface, had low overall activity in this reaction as well as it was leading to the formation of a stable intermediate (Pl 8 [H]). Furthermore, it was shown both experimentally and theoretically that the steric constraints imposed on Pl 8 [H] intermediate by the terraced sites on the surface of ruthenium black, make this catalyst ineffective in hydrogenation of 9-ethylcarbazole. Therefore, unsupported catalyst synthesized at higher temperatures can create recyclability problems, thus it's use should be avoided. High temperature sintering of catalyst can lead to the formation of faceted islands of metal on the catalyst surface which disrupt the

balance of active sites and as a result can create problems in repeated loading and unloading of the storage material. In addition, the theoretical calculations showed that isolated metal sites, as opposed to terrace sites, do not show high adsorption energy of the polyaromatic substrate. Thus, it seems that the optimisation of an active catalyst based on ruthenium metal for this storage system should focus on the development of proper balance of terraced and low coordination active sites on the small metal particles. This balance can be achieved by alloying ruthenium nanoparticles with different metals or by decorating high indexed planes of ruthenium with promoter atoms. The adsorption energy of the substrate and intermediates on the surface of the catalyst can also be influenced by changing the type of the support and thus tailoring the electron density on the metal as shown in our XPS studies. The obtained results also offer a way of designing new organic carriers by focussing on the energies of adsorption so as to favour concerted hydrogenation of the polyaromatic substrate without desorption of the intermediates from the catalyst surface. This can be achieved by changing the type of heteroatom in the structure, addition of the electron donating/withdrawing substituent outside the ring, or by designing unstable, multicyclic structures.

To sum up, it was shown that successive hydrogenation or dehydrogenation processes can impose subtle changes in the structures and adsorption geometries of the partially hydrogenated intermediates. In the case of 9-ethylcarbazole, the Pl 8 [H] "pyrrole" intermediate, once it desorbs from the catalysts surface, it accumulates in the solution. This intermediate compound is unable to be further hydrogenated on the flat surface and has to 'search' for any available lower coordination sites, such as steps, for subsequent hydrogenation. The low coordination sites impose less steric hindrance to subsequent hydrogen additions to Pl 8 [H], leading to hydrogen scrambling on the either sides of the molecule, and as a result, formation of asymmetrical Pl 12 [H] products. In addition, the

asymmetric products are expected to cause problems in the dehydrogenation reaction, due to possible creation of steric hindrance effects during adsorption on the surface of the catalyst.

5.5. References

1. *Liquid hydrogenation of some heterocyclic nitrogen compounds over ruthenium catalysts.* **A. A. Ponomarev, A. S. Chegolya, V. N. Dyukareva,** Chem. Heterocycl, 1966, Vol. 2.
2. *Hydrogenation of pyrrole derivatives I.Hydrogenations over palladium.* **L. Hegedus, T. Mathe, A. Tungler.** Appl. Catal, 1996, Vol. 143.
3. *The selective hydrogenation of derivatives of pyrrole, indole, carbazole and acridine.* **H. Adkins, H. L. Coonradt,** J. Am. Chem. Soc, 1941, Vol. 63.
4. *Kinetics of H_2 recovery from dodecahydro-N-ethylcarbazole over supported Pd catalyst.* **F. Sootodeh, L. Zhao, K. J. Smith,** Appl. Catal. A, 2009, Vol. 362.
5. *Kinetics of hydrogen uptake and release from heteroaromatic compounds for hydrogen storage.* **F. Sotoodeh, K. J. Smith,** Ind. Eng. Chem. Res., 2010, Vol. 49.
6. *Kinetics of 9-ethylcarbazole hydrogenation over Raney-Ni catalyst for hydrogen storage.* **X. Ye, Y. An, G. Xu,** J. Alloys Compd., 2010, Vol. 509.
7. *The statistics of surface atoms and surface sites on metal crystals*. **R. van Hardeveld, F. Hartog,** Surf. Sci., 1969, Vol. 15.
8. *Ruthenium hydrogenation catalysts activation characterisation application -doctoral dissertation.* **P. G. J. Koopman,** Delft University Press, 1981.
9. *Influence of the trace oxygen on the hydrogenation activity of Ru/Al_2O_3 catalyst.* **H. Seki, M. Ohshima, H. Kurokawa, H. Miura,** Reac. Kinet. Mech. Cat., 2010, Vol. 101.
10. *Characterisation of alumina supported nickel-ruthenium systems.* **J.M. Rynkowski, T. Paryjczak, M. Lenik,** Appl. Catal. A, 1995, Vol. 126.
11. *Metallic osmium and ruthenium nanoparticles for CO oxidation.* **C. Li, W. K. Leong, Z. Zhong,** J. Organomet. Chem, 2009, Vol. 694.
12. *Facile preparation of RuO_2/CNT catalyst by homogenous oxidation precipitation method and its catalytic performance.* **X. Fu, H. Yu, F. Peng, H. Wang, Y. Quian,** Appl. Catal., 2007, Vol. 321.
13. *Low temperature ruthenium catalyst for ammonia synthesis supported on $BeCeO_3$.* **X-L. Yang, W-Q Zhang, C-Gu. Xia, X-M. Xiong, X-Y Mu, B. Hu,** Catal. Commun., 2010, Vol. 11.
14. *Hydrogenation of oleic acid over ruthenium catalysts.* **M. J. Mendes, O. A. A. Santos, E. Jordao, A. M. Silva,** Appl. Catal, 2001, Vol. 217.
15. *Valence state study of supported ruthenium Ru/MgO catalysts.* **Y. V. Larichev,** J. Phys. Chem. C, 2008, Vol. 112.
16. *XPS study of Ru/Fe_2O_3 catalysts for water-gas shift reaction.* **A. Basinska, J. Stoch, F. Domka,** J. Environ. Sci., 2003, Vol. 12.
17. *An XPS study on ruthenium compounds and catalysts.* **C. L. Biachi, V. Ragaini,** Mater. Chem. Phys., 1991, Vol. 29.
18. *A study of ruthenium catalysts on oxide supports.* **M. G. Cattania,** Surf. Sci., 1989, Vol. 211/212.
19. *NH_3-TPD and XPS studies of Ru/Al_2O_3 catalyst and HDS activity.* **M. Nagai, K. Koizumi, S. Omi,** Catal. Today, 1997, Vol. 35.
20. *A study of ruthenium in zeolite-Y by X-ray photoelectron spectroscopy.* **L. A. Pedersen, J. H. Lunsford,** J. Catal., 1980, Vol. 61.
21. *Surface properties and catalytic behaviour of Ru supported on composite La_2O_3-SiO_2 oxides.* **B. M. Faroldi, E. A. Lombardo, L. M. Cornaglia,** Appl. Catal. General, 2009, Vol. 369.

22. *Ru nanoparticles stabilized by poly(n-vinyl-2-pyrrolidone) grafted onto silica: very active and stable catalysts for hydrogenation of aromatics.* **X. Zhou, T. Wu, B. Hu, T. Jiang, B. Han,** J. Mol. Catal., 2009, Vol. 306.
23. *XPS and FTIR study of Ru/Al_2O_3 and Ru/TiO_2 catalysts: Reduction characteristics and interaction with methane-oxygen mixture.* **C. Elmasides, D. I. Kondarides, W. Gruenert, X.E. Verykios,** J. Phys. Chem. B, 2009, Vol. 103.
24. *Electronic interaction between supports and ruthenium catalysts for the hydrogention of carbon monoxide.* **T. Ishihara, K. Harada, K. Egucchi, H. Arai,** J. Catal., 1992, Vol. 136.
25. *Study on the electro-activity and non-stochiometry of a Ru-based mixed oxide electrode.* **K. W. Kim, E-H. Lee, J-S. Kim, K-H.Shin, K-Ho Kim,** Electrochim. Acta, 2001, Vol. 46.
26. *XPS investigations of Pt and Rh supported on Al_2O_3 and TiO_2.* **T. Huzinga, H. F. J. Van't Blik, J. C. Vis, R. Prins,** Surf. Sci., 1983, Vol. 135.
27. *Correlating the electronic properties and HDN reactivities of organonitrogen compounds:an ab initio DFT study.* **M. Sun, A. E. Nelson, J. Adjaye,** J. Mol. Catal. A, 2004, Vol. 222.
28. *Kinetics of H_2 recovery from dodecahydro-N-ethylcarbazole over a supported Pd catalyst.* **F. Sotoodeh, L. Zhao, K. J. Smith,** Appl. Catal. A, 2009, Vol. 362.
29. *Optimization by Direct Search: New Perspectives on Some Classical and Modern Methods.* **T. G. Kolda, R. M. Lewis, V. Torczon,** SIAM Review, 2003, Vol. 45.
30. *Gas phase hydrogenation of o-xylene over palladium catalysts.* **M. Viniegra, G. Cordoba, R. Gomez,** J. Mol. Catal, 1990, Vol. 58.
31. *Hydrogenation of benzothiophene-free naphtalene over charcoal-supported metal catalysts in supercritical carbon dioxide solvent.* **N. Hiyoshi, M. Osada, Ch. V. Rode, O. Sato, M. Shirai,** Appl. Catal. A, 2007, Vol. 331.
32. *Effect of sulfur or nitrogen poisoning on the activity and selectivity of y-zeolite-supported Pt-Pd catalysts in the hydrogenation of tetralin.* **C. C. Costa Augusto, J. L. Zotin, A. da Costa Faro Jr,** Catal. Lett., 2001, Vol. 75.
33. *Stereochemistry and mechanism of catalytic hydrogenation of dimethylcyclohexane.* **S. Mitsui, S. Imaizumi, A. Nanbu, Y. Senda,** J. Catal., 1975, Vol. 36.
34. *On the mechanism of CO adsorption on silica-supported ruthenium catalyst.* **M. Kantcheva, S. Sayan,** Catal. Lett., 1999, Vol. 60.
35. *FTIR studies of CO adsorption on Al_2O_3 and SiO_2-supported catalysts.* **S. Y. Chin, C. T. Wiliams, M. D. Amiridis,** J. Phys. Chem B, 2006, Vol. 110.
36. *FTIR study of CO interaction with Ru/TiO_2 catalysts.* **K. Hadjiivanov, J. C. Lavalley, J. Lamote, F. Mauge, J. Saint-Just, M. Che,** J. Catal., 1998, Vol. 176.
37.*Engineering performed cobalt doped platinum nanocrystals for ultraselective hydrogenation.* **S. C. Tsang, N. Cailuo, W. Oduro, A. T. S. Kong, L. Clifton, K. M. K. Yu, B. Thiebaut, J. Cookson, P. Bishop,** ACS Nano, 2008, Vol. 2.
38. *Adsorption of tetralin and hydrogented intermediates and products on the (100) surfaces of Ir, Pt, and Pd: A DFT study.* **X. Li, M. S. M. Wong, K. H. Lim,** Theor. Chem. Acc., 2009, Vol. 127.
39. *Adsorption site preference of CO_2 on Pt(100) surface by ab initio calculations.* **Y. Pan, J. M. Zhang, W. M. Guan, K. H. Zhang, S. Chen,** J. Phys. Chem. Solids, 2010, Vol. 72.
40. *A DFT study on benzene adsorption over a corner site of tungsten sulfides.* **R. Koide, E. J. M. Hensen, J. F. Poul, S. Cristol, E. Payen, H. Nakamura, R. A. van Santen,** Catal. Today, 2008, Vol. 130.
41. *Hydrogen storage in liquid organic hydrides.* **R. H. Crabtree,** Energy Environ. Sci., 2008, Vol. 1.

6. Kinetics of liquid phase hydrogenation of 9-ethylcarbazole over ruthenium based catalysts

6.1. Introduction

The main interest of chemical kinetics is the study of rates of reaction and the factors that can affect them (1). In this chapter, the influence of some thermodynamic parameters on the catalytic liquid phase hydrogenation of 9-ethylcarbazole using ruthenium black (commercial) and 5 wt % Ru on alumina (chemically reduced) catalysts were investigated. The influence of the reaction time, temperature, pressure and the type of solvent on the conversion and selectivity of the catalysts were studied. The rate constants and the activation energies were determined and compared for these two catalytic systems.

6.1.1. Reaction order

The manner at which the rate of the reaction is influenced by the concentration of the reacting substances can be indicated by the order of reaction (1). The functional relationship describing this dependence is called rate equation. The interpretation of the kinetic data is based on the Law of Mass Action, which says that in the diluted solution the rate of elementary reaction is proportional to the concentration of the reactants raised to the power of their stochiometric coefficients and it is independent of other concentrations and reactions (2).

Therefore, for the simple reaction of

$$A+B \longrightarrow C + D \qquad \text{Equation 6.1}$$

The equation can be described as:

$$R= k [A]^{\alpha} [B]^{\beta} \qquad \text{Equation 6.2}$$

Where; R is a rate of the reaction, and α and β are the orders of the reaction with respect to reactants A and B. The overall reaction order is a sum of α and β, respectively (1). The constant of proportionality k is the rate coefficient, and it can vary with temperature, concentration of the reactant, pressure, type and a physical state of the catalyst (3). The most common orders of reaction are zero, first, and second order. The third order reactions are rare and unlikely to occur (1). For the first order reactions, the rate depends only on the concentration of one of the reactants and in the second order reactions, the rate depends on the concentration of one second order reactant or two first order reactants. There are several methods to deduct the reaction order; tabular method, half-life method, guggenheim's method for first-order reactions, differential method, or isolation method (1). In the present study, the graphical method to determine the rate constant k and the reaction order was used. It should be noted that the order of the reaction does not have to be an integral (4). In the heterogeneously catalyzed liquid-phase reactions, such as hydrogenation of 9-ethylcarbazole, parameters such as quantity of catalyst, its type and characteristics, the pressure of the gas reactant, agitation and finally temperature, are important variables affecting the rate of the reaction.

6.1.2. Influence of temperature

In the sequence of steps in heterogenous catalysis, the reactant adsorption, interaction of adsorbed species and product desorption are mostly affected by changes in the reaction temperature. Moreover, temperature also affects the mass transport but to the smaller degree (5). The rate of the reaction and hence the rate coefficient strongly depend on temperature. A general rule is that the rate of reaction doubles with the rise in temperature of 10 °C (6). However, it is important to note that high temperatures can shorten the catalyst life and influence the selectivity of the catalyst. The basis of the effect of temperature on equilibrium constants were created by Hood (1885) and van't Hoff (1884),

and were later extended by Arrhenius (1889) to the final relationship known as Arrhenius law or Arrhenius equation (6) depicted in Equation 6.3:

$$k = Ae^{-\frac{E}{RT}}$$ Equation 6.3

where: k-is a rate constant, factor $e^{-\frac{E}{RT}}$ is a Boltzman expression, R- is a gas constant, T is an absolute temperature, A is a frequency factor (2) and E is the activation energy. From plotting log k against reciprocal of temperature, the activation energy can be determined from the slope of the straight line.

In order for the two molecules to react with each other, they have to collide with each other (7). The main point of the Arrhenius law is that a molecule in order to react has to posses some threshold energy **ε**, and the fraction of the molecules that posses this minimum amount of energy is given by the expression exp(–**ε/kt).** This threshold energy that allows the molecule to pass from initial state to activated state is known as activation energy (8).

6.1.3. Influence of pressure

Generally, at the lower pressure values, the increase in pressure of the gas reactant brings about the increase in reaction rate, but above a certain value further increase in pressure has limited or no influence on the reaction rate (5). Moreover, the pressure can influence the reaction selectivity, especially in consecutive hydrogenation reactions (9). Generally, the selectivity towards the intermediate product is proportional to the decrease in pressure with increasing degree of conversion (10) (11). With the assumption that one reaction step

was rate limiting, Siegel (12) ruled out that different active sites are activated at different pressures, which can result in the changes in selectivity.

6.1.4. Influence of solvent

The effect of the solvent on heterogeneously catalyzed reactions is very complex combination of physical and chemical phenomena, and depends on many variables such as nature of active sites present, the catalyst support and also on the substrate of the reaction (5) Type of the solvent influences which functional group will be selectively hydrogenated from a mixture of substrates (13). Furthermore, the solvent can affect the stereochemistry as well as amount and extent of isomerisation of intermediates and products (14). Some solvents having unshared electron pairs are able to absorb on the catalyst surface and therefore modify the extent to which the other reactants are adsorbed, which in turn can alter the selectivity, activity and stereo selectivity of the reaction. It was found that non polar substrates are more favourably adsorbed on the catalyst surface in polar solvents, whereas non-polar solvents tend to increase the adsorption of polar reactants (5).

6.1.5. Mass transport limitations

All the physical processes of mass transport can have big impact on the reaction rate and also on selectivity of the reaction. The reaction variables (15) that can affect the mass transport processes in the three phase batch reactor are: agitation, pressure, amount of catalyst, size of the nanoparticles, temperature and the concentration of the reagent. Reactions heavily influenced by mass transport limitations show no significant change in reaction rate as temperature increases (7).

6.2. Results and discussion

The influence of the thermodynamic parameters such as temperature and pressure on the rate and selectivity of hydrogenation of 9-ethylcarbazole was studied over ruthenium based catalysts. The reason for selecting these two catalysts was that they were found to show significant differences in selectivity as well as in activity in hydrogenation of 9-ethylcarbazole. The results of these hydrogenations were described in the previous chapter. For catalytic testing and the study of kinetics, smaller quantities of 5 wt % Ru/Al_2O_3 catalyst were used (0.1 g as opposed to 0.15 g of ruthenium black catalyst) under the same testing conditions (3g of 9-ethylcarbazole in 100 ml of cyclohexane) due to the differences found in activity between these two catalysts as described in Chapter Five.

6.2.1. Reaction order, rate parameters and activation energies

Considering the hydrogenation of *9-ethylcarbazole* (ETHC) to its products, the reaction is represented by the equation 6.4;

$$ETHC + 6H_2 \xrightarrow{k} products \qquad \text{Equation 6.4}$$

The rate of the reaction is proportional to the concentration of 9-ethylcarbazole, which can be represented in Equation 6.5

$$R = k[ETHC]^{\alpha}[H_2]^{\beta} \qquad \text{Equation 6.5}$$

The decrease in concentration of 9-ethylcarbazole was faster with increasing temperature as shown in Figure 6.1. This profile is representative for the reactions run using 5 wt % Ru/Al_2O_3 catalyst, however similar profile was also obtained for reactions run using ruthenium black commercial catalyst. For a first order reaction (unimolecular

reaction), the rate of the reaction depends on the concentration of the species to the first power.

$$R = -\frac{d[ETHC]}{dt} = k[ETHC] \Rightarrow \frac{d[ETHC]}{[ETHC]} = -kdt$$
$$\int_{t=0}^{t=t} \frac{d[ETHC]}{[ETHC]} = -k\int_{t=0}^{t=t} dt$$
$$\ln \frac{[ETHC]}{[ETHC]_0} = -kt$$

Equation 6.6

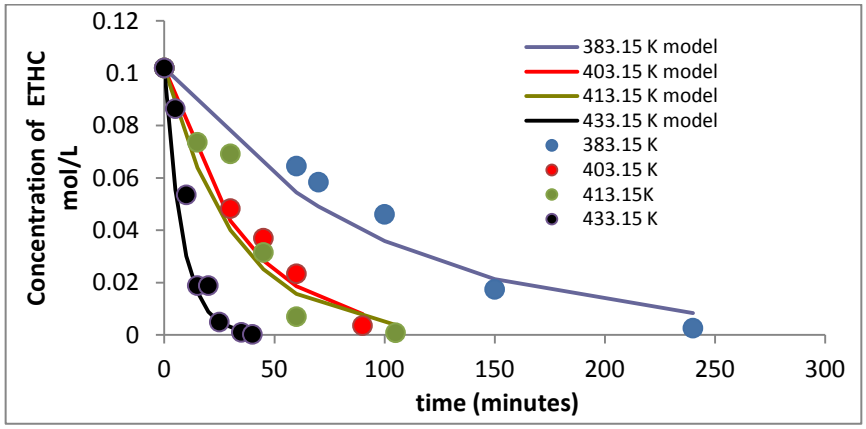

Figure 6.1. A representative profile of change in 9-ethylcarbazole concentration with time at various temperatures over 5 wt % Ru/Al_2O_3 catalyst.

From Equation 6.6, plotting ln [ETHC] against time (t) results in a straight line with slope of –k. The plot should be linear in case of the first order reaction (1). The experimental data obtained using 0.1g of 5 wt % Ru/Al_2O_3 at 403.15 K is shown in Figure 6.2 fits to a first order reaction up to almost 100% conversion since the curve is linear. Hence, 9-ethylcarbazole hydrogenation is a first order reaction with respect to 9-ethylcarbazole concentration with the rate constant of 0.044 min^{-1} (7.33 x 10^{-4} s^{-1}), which agrees well with literature (16). Additionally, when the reaction progresses, only a small amount of the gas is consumed and thus its concentration can be assumed constant. The reaction is zero order in concentration of hydrogen gas.

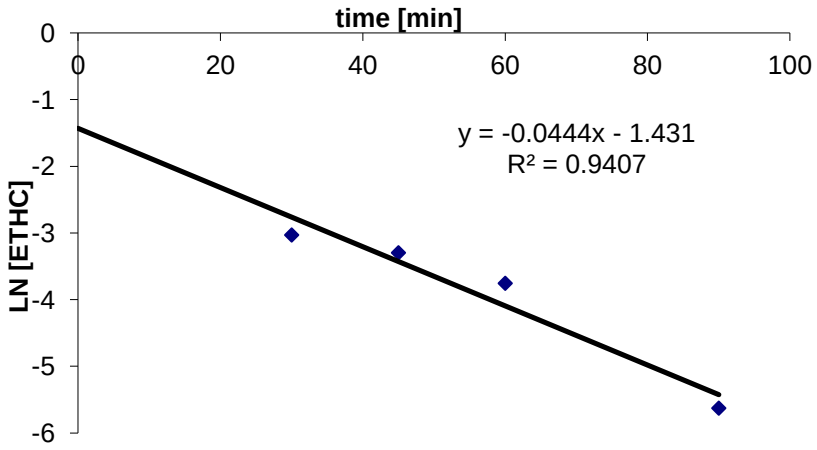

Figure 6.2. A representative fit of the experimental data into 1 st order kinetics. Data collected at 403.15 K, using 5 wt % Ru/Al_2O_3 catalyst.

Taking into consideration the Arrhenius equation (17) explained before:

$$k = A\, e^{-E_a/RT} \qquad \text{Equation 6.7}$$

If logarithms (ln) are taken of Equation 6.7, then:

$$lnk = lnA - \frac{E_a}{RT} \qquad \text{Equation 6.8}$$

Thus, a plot of the logarithm of the experimental rate constant against the inverse of the absolute temperature is a straight line, as shown in Figure 6.3 where the intercept represents ln A and the slope is $-E_a/R$.

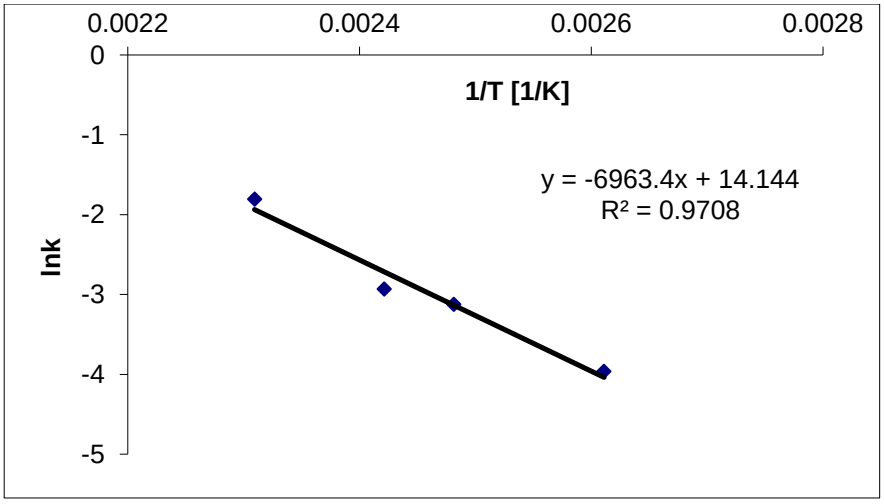

Figure 6.3. Arrhenius plot of 9-ethylcarbazole hydrogenation using 5 wt % Ru/Al_2O_3 catalyst.

The activation energy of the reaction can be easily calculated using the slope of the graph as follows;

$$slope = -\frac{E_a}{R} \qquad \text{Equation 6.9}$$

using R = 8.314510 $JK^{-1}mol^{-1}$

The apparent activation energy (E_a) for 9-ethylcarbazole consumption of 57.9 kJ/mol was computed for reaction catalysed with 5 wt % Ru/Al_2O_3 catalyst. Similar procedure for the 9-ethylcarbazole hydrogenation catalysed by ruthenium black (Arrhenius plot shown in Figure 6.4) leads to calculated activation energy of 64.7 kJ/mol.

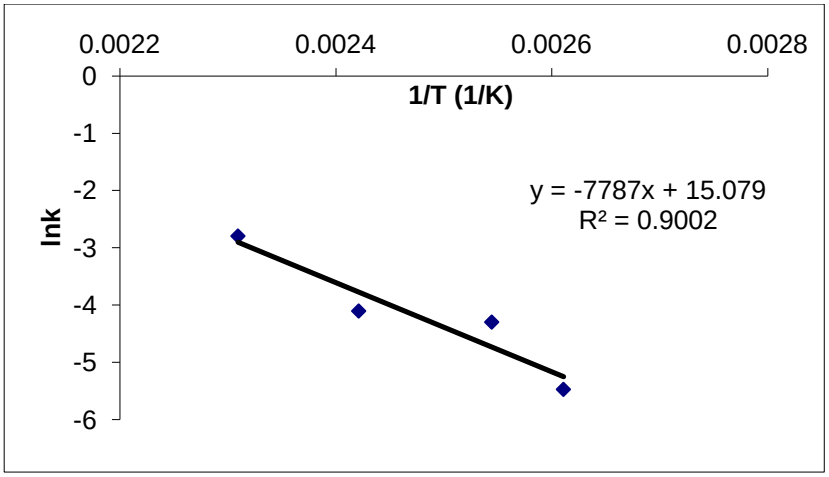

Figure 6.4. Arrhenius plot for hydrogenation of 9-ethylcarbazole catalysed using ruthenium black catalyst.

It is worth underlining that the obtained activation energies are only apparent activation energies. The true activation energy should be computed by adding the enthalpy of adsorption as a positive quantity to the apparent activation energy (7).

The apparent activation energy values of 57.9 kJ /mol (5 wt % Ru/Al_2O_3) and 64.7 kJ/mol (ruthenium black), agree well with the previously reported apparent activation energy of 58 kJ/mol for 9-ethylcarbazole hydrogenation in the molten state over the same supported catalyst (5 wt % Ru/Al_2O_3) in Chapter Four. This result implies that the presence of the cyclohexane does not significantly alter the reaction pathway. This reaction can be assumed to be controlled by the chemical process since hydrogenation reactions having much lower values of apparent activation energy were reported in the literature as taking place in the kinetic regime (18). For example, Proszenyak et al in (19) reported the apparent activation energy of hydrogenation of 4-(4-fluorobenzyl) pyridine over 10% Pd/carbon of 45.3 kJ/mol. In addition, the obtained values of apparent activation energy for 9-ethylcarbazole hydrogenation in the present work are in reasonable agreement with the values reported in the literature for hydrogenation of aromatics. Very recently, Ye et all (20) reported the apparent activation energy of 65.4 kJ/mol of hydrogenation of 9-

ethylcarbazole using Raney-Nickel catalyst. Apparent activation energy values (48-50 kJ/mol) were previously observed by Rautanen (21) and Jen (22) in hydrogenation of benzene and toluene on the commercial Ni/Al_2O_3 and Pd/C catalysts. The values of 52 kJ/mol of apparent activation energy were reported in hydrogenation of nitrogen containing aromatic compounds on sulfidised CoMo and NiMo catalysts (23). On the other hand, there are also reports of much higher apparent activation energies of aromatic hydrogenation reactions. For example, the apparent activation energy for hydrogenation of naphthalene on Pt supported on amorphous SiO_2-Al_2O_3, mesoporous SiO_2-Al_2O_3, SiO_2 and Al_2O_3 supports was reported in the range of 95-115 kJ/mol (24). Additionally, the value of activation energy of hydrogenation of diesel fuel on bimetallic Pt-Pd/ SiO_2-Al_2O_3 to be 92 kJ/mol (25). From the aforementioned literature review, it can be easily concluded that the apparent activation energy for hydrogenation of aromatic compounds varies in a wide range, depending on the catalyst used and the experimental set-up employed.

Nevertheless, our apparent activation energies are about 30 % lower when compared to 99.5 kJ/mol reported in the work of Soodoteh (16) for 9-ethylcarbazole hydrogenation in the liquid phase using decalin over commercial 5 wt % Ru/Al_2O_3. In the view of previously described results found in literature, this difference in values of apparent activation energy for the same reaction is not unusual. One could think that the lower apparent activation value in our case, could be the result of the reaction being limited by the transport of the hydrogen towards the active sites. However, the mass transport limitation is not very likely to be present in our work, since the experimental apparent activation energy is considerably higher than 6 kcal/mol (25.1 kJ/mol), which implies that the operation is in the reaction-controlled region (26). Thus, the difference in apparent activation energy between the values in the present work and those reported in (16) can be

ascribed to: differences in starting concentration of the reactant (5), type of solvents and catalysts used in these experiments.

The values of apparent activation energy of two catalytic systems studied (5 wt % Ru/Al_2O_3 and ruthenium black) are slightly different. It is well known that the path of the reaction and therefore the activation energy of the reaction depend on the type of active centres provided by the surface of the catalyst. Thus, the different apparent activation energies obtained for these two catalysts confirm the possibility of the presence of different types of active sites on their surfaces. The influence of the type of active sites of these catalysts on the reaction pathway was discussed in Chapter Five.

6.2.2. The influence of the reaction temperature

In the present work, the influence of the temperature (383.15-433.15 K) was evaluated in one hour reaction, utilizing 3 grams of 9-ethylcarbazole over 0.1 gram of 5 wt % Ru/Al2O3 or 0.15 gram of ruthenium black in 100 ml of cyclohexane under 70 bar of hydrogen pressure. The dependence of the conversion of the starting material on the reaction temperature is shown in Figure 6.5. The conversion values were divided by the amount of catalyst used to normalize the comparison between the two catalyst studied. The degree of hydrogenation increases monotonically with the increment in temperature in case of both catalytic systems studied. These means that the equilibrium state was not reached yet at the range of the temperatures studied. 5 wt % Ru/Al2O3 displayed higher reaction rates than ruthenium black in the whole temperature range studied, as shown in Figure 6.5.

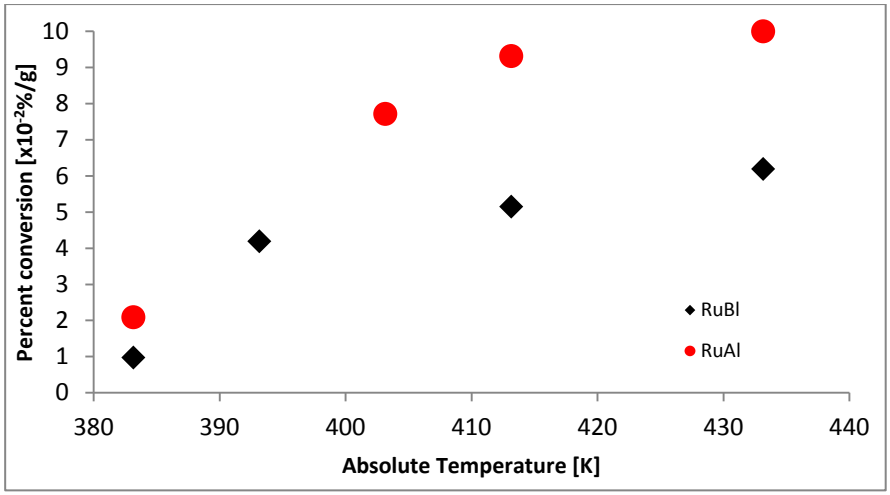

Figure 6.5. The effect of the increasing temperature on the conversion of the starting material on 5 wt % Ru /Al_2O_3 and Ru black catalysts. Percent conversion is referred to the amount of catalyst used.

The higher activity of the supported catalyst can be attributed to its higher dispersion and smaller particle size. In addition extra adsorption sites for the aromatic reagent can be provided in the region of metal-support interface (27) (28). Thus, the reaction takes place simultaneously on the surface of the metal and on the active sites of the support.

Increase in hydrogenation activity with temperature was previously observed in the hydrogenation of tetralin over Pt/Al_2O_3 catalyst (29) and toluene over Pt supported on carbon nanotubes (30). The conversion of the reactant over 5 wt % Ru/Al_2O_3 increased from 21% at 383 K up to a complete conversion at 433 K. Simultaneously, the conversion over ruthenium black catalyst increased from 15% at 383 K to 93% at 433 K.

In all of the reactions, the fully hydrogenated products were detected along with the partially hydrogenated intermediates as described in Chapter Four and Chapter Five. Thus, the type of products of 9-ethylcarbazole hydrogenation over 5 wt % Ru/Al_2O_3 or ruthenium black were identical, however the selectivity profiles displayed by these two catalytic systems differed noticeably. It should be noted that no traces of the products of ring opening/cracking reactions were detected up to 403 K, however small amounts < 1%

of 9-perhydrocarbazole (the product of hydrogenolysis of 9-ethyl-perhydrocarbazole) were detected at higher reaction temperatures (413 K and 433 K). It has been reported before in the literature that the hydrogenolysis of C-N bond in aliphatic compounds has higher rate than in aromatic compounds (23), thus the presence of this product in the reaction mixture can be easily explained.

The selectivity towards formation of fully hydrogenated isomers of 9-ethyl-perhydrocarbazole over both catalytic systems studied also increased with increasing temperature, see Figure 6.6 and Figure 6.10. In case of 5 wt % Ru/Al_2O_3, the selectivity towards fully hydrogenated products increased from 14 % at 383 K, up to 72% at 433 K. The selectivity towards the final product over ruthenium black catalyst increased from 9% at 383 K up to 40 % at 433 K. It was noted that in the range of temperatures studied, the supported catalyst was more selective towards the final product than the unsupported one.

Figure 6.6 shows the selectivity changes at different temperatures over 5 wt % Ru/Al_2O_3 catalyst. The main products at the lowest temperature (lowest conversion) studied are Pl 4 [H] and Pl 8 [H] obtained with the similar selectivity. The selectivity towards partially hydrogenated 9-ethyl-tetrahydrocarbazole decreases simultaneously with temperature, from 43 % at 383 K to 0.5 % 433 K. High selectivity of 9-ethyl-tetrahydrocarbazole at lower conversions of the starting material suggests that this compound is a primary product of the consecutive reaction as it was reported in Chapter Five. It has been observed previously in the literature, that the aromatic π-electrons play a major role in defining the trend of adsorption strength on the noble metals, especially on ruthenium nanoparticles (31). Therefore, it can be expected that the flat adsorption of the 9-ethylcarbazole on the surface of the metal will take place preferably to the adsorption of non-planar 9-ethyl-tetrahydrocarbazole. Thus, at lower temperatures with lower conversion, the accumulation

of 9-ethyl-tetrahydrocarbazole can be observed. The conversion of this intermediate increases rapidly, after the concentration of the substrate drops significantly.

The final product (sum Pl 12 [H]) consisted of three isomers of 9-ethyl-perhydrolcarbazole (A,B,C) as described in the previous chapter. In practice, the formation of structural isomers or conformers during hydrogenation of pi-conjugated systems depends on the conditions of the hydrogenation reaction as well as on the particle size. Generally, the least stable, more energetic isomers tend to form at lower temperatures, whereas higher temperatures favour equilibrium, which is the lower energy distribution of isomers (32).

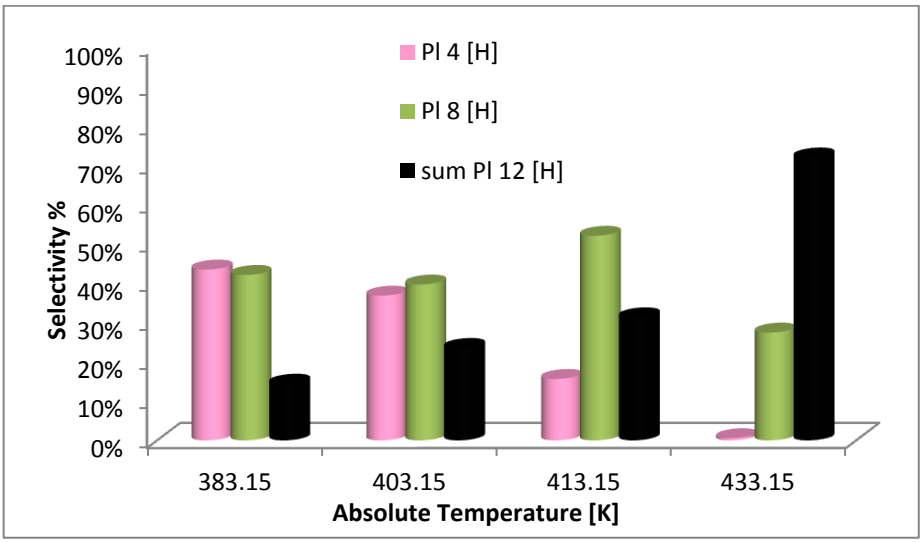

Figure 6.6. The effect of temperature on selectivity towards intermediate and final products of 9-ethylcarbazole hydrogenation over 5 wt % Ru/Al_2O_3 catalyst. Pl 4 [H] is 9-ethyl-tetrahydrocarbazole, Pl 8 [H] is 9-ethyl-octahydrocarbazole and sum Pl 12 [H] is the summation of the isomers of fully hydrogenated 9-ethyl-perhydrocarbazole.

It was also reported that the selectivity towards cis isomer increases as a particle size increases. Small particles were found to be less effective in producing cis-isomers according to the 'roll-on' model proposed by Inoue (33). The trans isomers were found to be more favourably produced over highly dispersed catalysts, because their formation requires a relatively longer stay of the precursor on the surface of the catalyst (33). The

ratio of isomers obtained in 9-ethylcarbazole hydrogenation over ruthenium catalysts was found to be a function of temperature. Figure 6.7 shows the distribution of the isomers in the fully hydrogenated product at four different temperatures studied. The structures of the isomers are depicted in Figure 6.8.

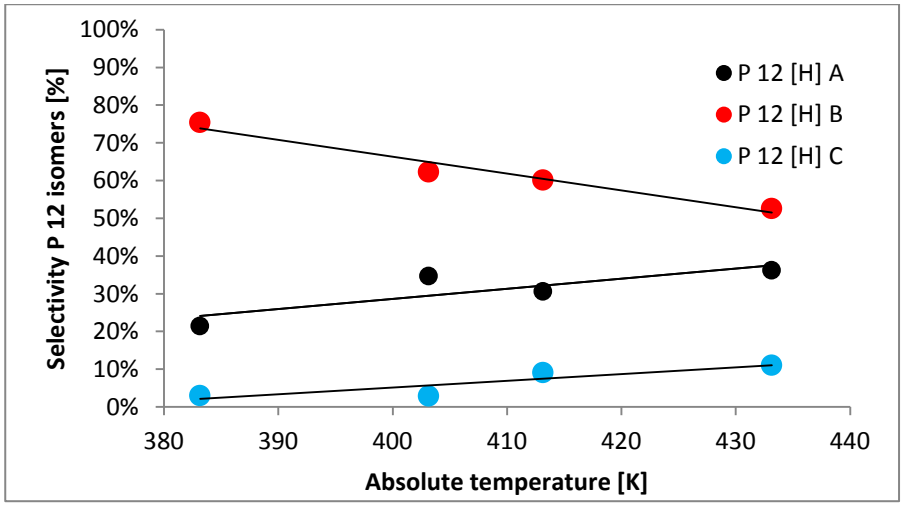

Figure 6.7. The selectivity distribution of the isomers in the fully hydrogenated product (9-ethyl-perhydrocarbazole) over 5 wt % Ru/Al_2O_3 catalyst at varied temperatures. The structures of the isomers of Pl 12 [H] are shown in Figure 6.8.

As it can be observed in Figure 6.7, that the main product of the reaction is isomer P 12 [H] B which has in majority a cis structure (see Chapter Four for NMR structure assignments results). It is noted however, that selectivity towards this isomer decreases with temperature from 75 wt % at 380.15 K down to 52 wt % at 433.15 K. This implies that isomer P 12 [H] B is a highly energetic product with a relatively low stability. It should be mentioned that the most stable intermediate of this reaction was found to be isomer P 12 [H] A. During extended times of reaction (up to 7 days), the main product found in the reaction mixtures was indeed isomer P 12 [H] A over both supported and unsupported catalysts, with selectivities of 95 % over the latter and 100% over the former. While the selectivity of the P 12 [H] B decreases, the selectivity towards the other isomers increases very slowly as the temperature increases. The decrease in selectivity towards the

main product can be explained by the isomerisation reaction of Pl 12 [H] B → Pl 12[H] A and P 12 [H] C described in Chapter Five and shown here again in Figure 6.8.

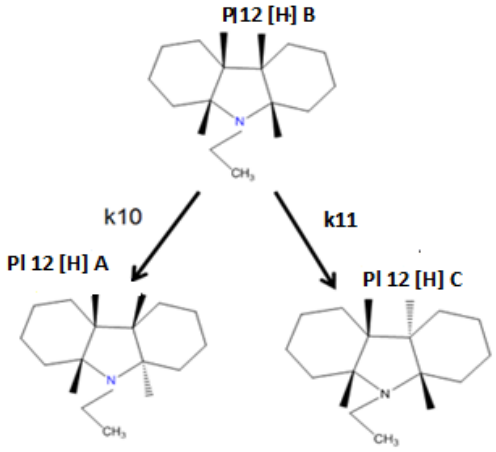

Figure 6.8. The proposed pathway of isomerisation reaction of 9-ethyl-perhydrocarbazole with numbered rate constants.

The experimentally obtained profiles of product distribution over time measured at four temperatures were used to model the reaction kinetics and the evolution of the selectivity with temperature. A kinetic model for the consecutive hydrogenation of 9-ethylcarbazole described in the previous chapter (Figure 5.7) was used to estimate the rate constant of each of the reaction steps. The kinetic parameters were obtained by solving the differential equations in accordance with the model as described in Chapter Three. The calculation of the rate constants of the isomerisation reactions over 5 wt % Ru/Al_2O_3 catalyst showed that the isomerisation generally takes place above 403 K with the rate constants lower than 0.01 [h^{-1}]. Only the isomerisation of P 12 [H] B into Pl 12 [H] A takes place at a significant rate (0.09 [h^{-1}]) starting at 433 K. It should be noted that the rate of isomerisation reaction is much slower relative to the rate of hydrogenation over both of the catalysts in the whole range of the temperature studied.

The calculated individual rate constants and the activation energies for each of the reaction step of 9-ethylcarbazole hydrogenation over 5 wt % Ru/Al_2O_3 catalyst are gathered in Table 6.1. below.

Table 6.1. Estimated first order rate constants and activation energies for individual steps in hydrogenation of 9-ethylcarbazole using 5 wt % Ru/Al_2O_3 catalyst. The dimension of rate constants is [h^{-1}]. The numbering of the rate constants is in accordance to the model shown in Figure 5.7. The highest rate constants at each of the temperatures are marked in red.

Temp [K]	k_0	k_1	k_2	k_3	k_4	k_5	k_6	k_7	k_8	k_9
383	1.17	0.18	0.44	0.47	0.12	0.65	0.07	0.01	0.00	0.06
403	2.71	0.39	1.97	0.01	0.35	1.38	0.24	0.04	0.07	0.13
413	3.16	0.33	1.76	0.94	0.46	2.49	0.13	0.06	0.18	0.00
433	9.64	2.69	2.94	3.38	0.00	3.69	0.48	0.01	0.80	0.00
E_a[kJ/mol]	56.4	69.2	50.6	51.8	60.6	49.5	49.6	N/A	N/A	N/A

The higher activation energy of the further conversion of 9-ethyl-octahydrocarbazole of 60.6 kJ/mol (see Table 6.1) when compared to the activation energy for the hydrogenation of 9-ethyl-tetrahydrocarbazole into 9-ethyl-octahydrocarbazole (49.5 kJ/mol) are in good agreement with the experimental observation of low consumption rate of 9-ethyl-octahydrocarbazole. The estimated apparent activation energy of direct formation of 9-ethyl-octahydrocarbazole is not high (51.8 kJ/mol), which suggests that this way of production of Pl 8 [H] is favourable over this catalyst. From the calculated rate constants, the most probable reaction pathways over supported ruthenium catalyst at each of the temperatures studied are depicted in Figure 6.9. As shown in Figure 6.9, at most of the temperatures studied, there are two active mechanisms of producing Pl 8 [H] stable intermediate.

Temperature [K]	Path of the reaction
383	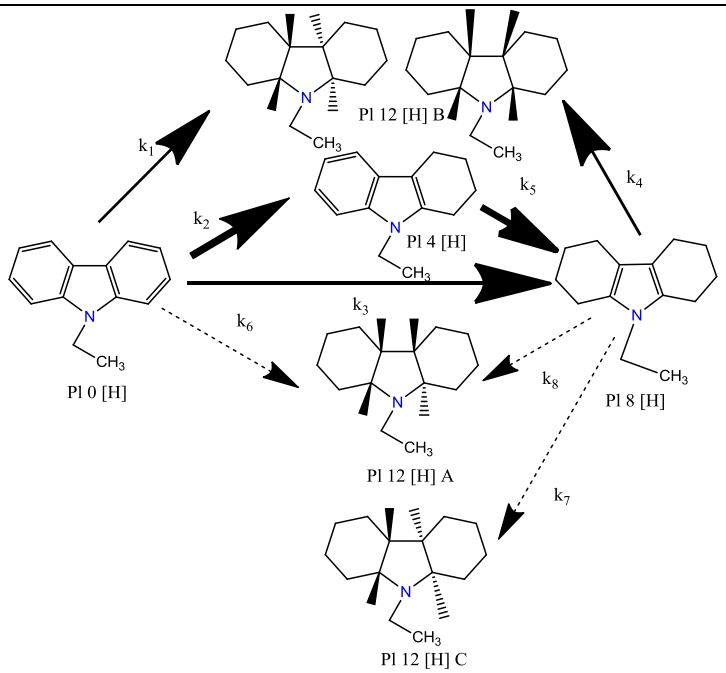
403	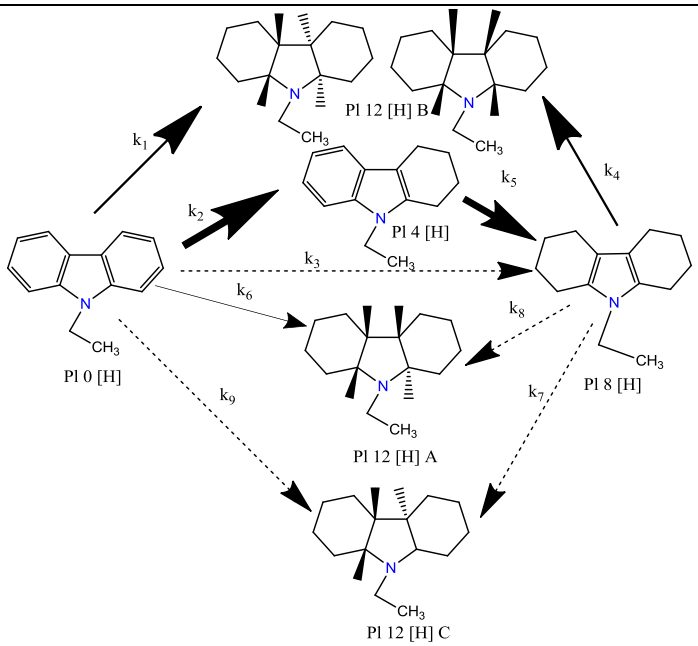

413	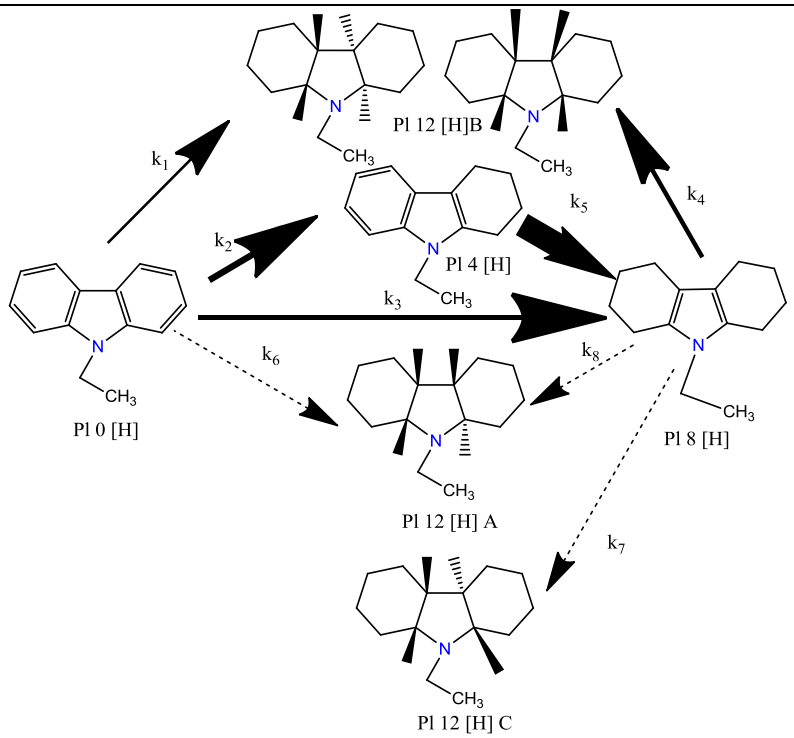
433	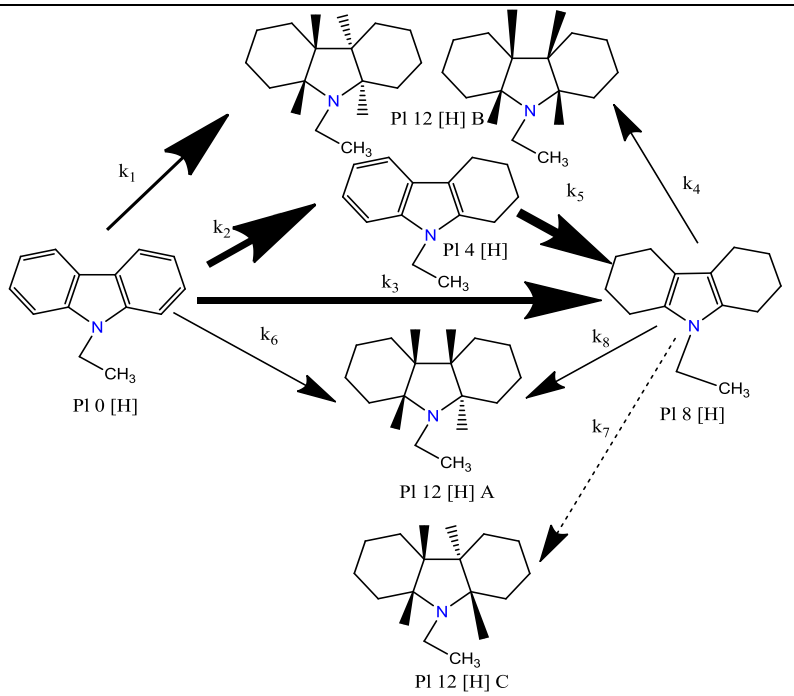

Figure 6.9.Predicted paths of the reaction based on the calculated rate constants at different temperatures for hydrogenation of 9-ethylcarbazole over 5 wt % Ru/Al_2O_3 catalyst. The thickness of the arrows is proportional to the value of the associated rate constants.

First is indirect path through Pl 4[H] and second is direct path from the substrate.

However, the rate of further conversion of 9-ethyl-octahydrocarbazole into the isomers of 9-ethyl-perhydrocarbazole is a minimum of 3 folds lower than the rate of its production which leads to the high accumulation of this intermediate in the solution. The rate of direct production of Pl 8 [H] is highest at the highest temperature studied and decreases as the temperature of the reaction decreases. It is noted that higher temperature may increase desorption of this intermediate from the catalysts surface. However, the selectivity towards Pl 8 [H] at lower temperatures (below 413 K) is around 40 %, than reaches the maximum of 52 % at 413 K and then decreases down to 27 % at 433 K (see Figure 6.6). It can be proposed that at higher temperatures, with lower concentrations of Pl 4 [H], the further conversion of Pl 8 [H] is facilitated, thus, lower selectivity towards this compound is observed at 433 K. This can be further explained by the possible competition for active sites between Pl 4 [H] and Pl 8 [H], since both of these compounds have tilted geometry and would preferably adsorb on the unsaturated sites of the catalyst via δ-adsorption.

Moreover, at all of the temperatures, the rate of direct production of Pl 12[H] B is much higher than the rate of direct production of isomers Pl 12 [H] A and Pl 12 [H] C. The rates of direct production of isomers Pl 12 [H] A and Pl 12 [H] C at lower temperatures are higher than the rates of their production from further conversion of 9-ethyl-octahydrocarbazole. At higher temperatures (from 413.15 K), the situation is reversed, and higher rate constant was calculated for direct production of isomers Pl 12 [H] A and Pl 12 [H] C directly from the substrate. Additionally, in the range of the temperatures studied, the direct formation of isomer P 12 [H] C takes place solely at lower temperatures. It could be observed that at the highest temperature, the conversion of starting material into Pl 4 [H] (indirect way) is partially replaced by the direct formation of Pl 8 [H] and the Pl 12 [H] A isomer (see Table 6.1. and Figure 6.9).

For comparison, similar profile of selectivity changes with temperature increase was obtained for the reactions performed over ruthenium black catalyst, which is shown in Figure 6.10.

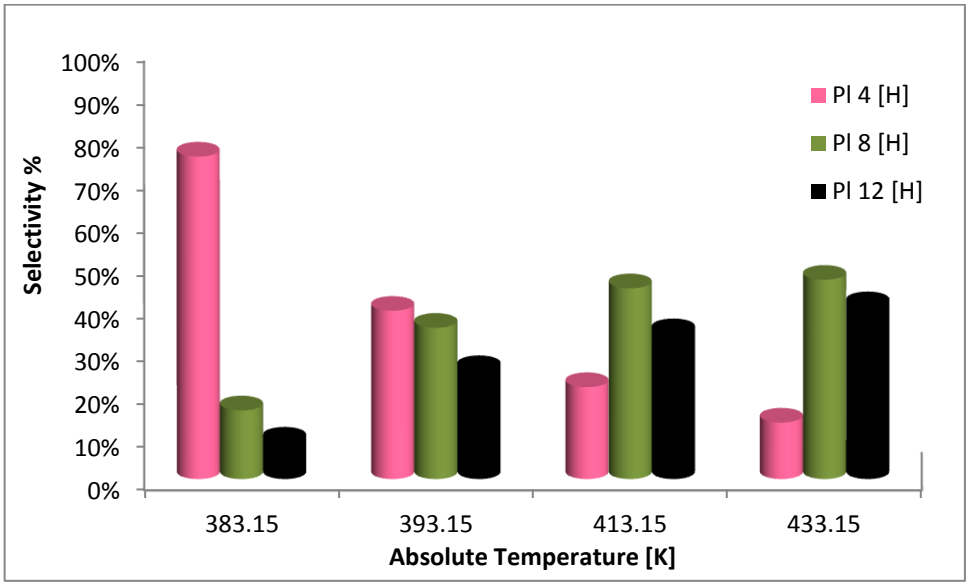

Figure 6.10. The effect of temperature on selectivity for intermediate and final products of 9-ethylcarbazole hydrogenation over ruthenium black catalyst. The acronyms for intermediates as described in Figure 6.6

Similarly to the results obtained over 5 wt % Ru/Al_2O_3 catalysts, the selectivity of ruthenium black catalyst towards the three isomers of 9-ethyl-perhydrocarbazole (A,B,C) increases with reaction temperature. Nevertheless, with unsupported catalyst, there is generally only one main product of the reaction at the lowest temperature studied (383 K) which is Pl 4 [H] reaching 75% of total reaction products. The selectivity towards Pl 8 [H] at the lowest temperature over ruthenium black is only 16%. This may suggest that there is mainly one indirect way of Pl 8 [H] production as in contrary to the observations made before over supported 5 wt % Ru/Al_2O_3. The selectivity of Pl 4 [H] decreases gradually down to 13% as the temperature increases to 433 K. The selectivity towards Pl 8 [H] increases steadily with temperature from 16% at 383 K up to around 40 % and from there on remains stable throughout the temperature range studied. It should be mentioned that the selectivity towards Pl 8 [H] decreased at higher temperatures over 5 wt % Ru/Al_2O_3

catalyst. Different behaviour of 9-ethyl-octahydrocarbazole over supported and unsupported catalysts may imply that the further conversion of this intermediate can be a structure sensitive reaction depending on the type of active sites present on the surface of the catalyst.

The distribution of the isomers of fully hydrogenated 9-ethyl-perhydrocarbazole was also studied over ruthenium black in the same range of temperature and the result is shown in Figure 6.11.

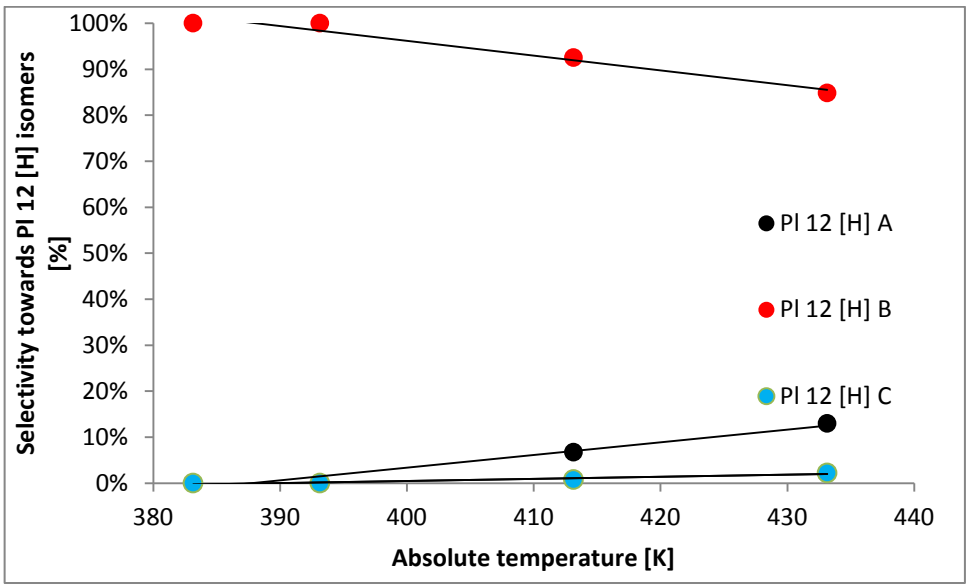

Figure 6.11 The selectivity distribution of the isomers in the fully hydrogenated product (9-ethyl-perhydrocarbazole) for the reaction performed over ruthenium black catalyst at varied temperatures. The acronyms were described previously.

Similarly to the previously discussed results for 5 wt % Ru/Al_2O_3 catalyst, the main isomer of 9-ethyl-perhydrocarbazole in the range of the temperatures studied is P 12 [H] B. This isomer is especially favoured at lower temperatures when it is almost exclusive product of the reaction. However, in case of ruthenium black this isomer represents over 90 % of the mixture of the final product up to 433 K. At 433 K, the selectivity decreases down to 84 %, as opposed to 52 % at the same temperature in case of supported 5 wt % Ru/Al_2O_3 (see Figure 6.7). The rate constants of Pl 12 [H] B

isomerisation into Pl 12 [H] A and Pl 12 [H] C were also calculated. The results showed that over ruthenium black, the only likely to occur isomerisation reaction is Pl 12 [H] B going into Pl 12 [H] A. However, it is important to note that this reaction takes place solely at 433 K with rate constant of 0.04 [h^{-1}] which is considerably lower than the rate constant of this isomerisation over 5 wt % Ru/Al_2O_3 at the same temperature (0.09 [h^{-1}]). At lower temperatures, the estimated rate constants (k_{10} and k_{11} from Figure 6.8) were zero, suggesting that the main source of the isomers Pl 12 [H] A and Pl 12 [H] C over ruthenium black catalyst can only be either direct hydrogenation of the starting material or further conversion of Pl 8 [H] intermediate. In contrast to the observations made over supported catalysts, over ruthenium black no isomerisation reactions were observed at lower temperatures.

The estimated rate constants of 9-ethylcarbazole hydrogenation over ruthenium black catalyst are gathered in Table 6.2.

Table 6.2. Estimated rate constants and activation energies for 9-ethylcarbazole hydrogenation over ruthenium black catalyst. The highest rate constants are marked in red. The unit of the rate constants is [h^{-1}].The numbering of the rate constants as depicted in Chapter Five, Figure 5.7.

Temp [K]	k_0	k_1	k_2	k_3	k_4	k_5	k_6	k_7	k_8	k_9
383	0.25	0.05	0.13	0.07	0.03	0.17	0.01	0.01	0.01	0.00
393	0.82	0.28	0.47	0.06	0.07	1.08	0.01	0.01	0.01	0.00
413	0.99	0.20	0.79	0.00	0.28	1.57	0.01	0.01	0.05	0.00
433	3.67	0.60	2.99	0.00	0.75	3.19	0.06	0.00	0.07	0.00
E_a[kJ/mol]	61.0	49.0	74.6	N/A	83.0	67.9	69.3	N/A	N/A	N/A

According to the data gathered in Table 6.2, there is a very significant improvement of the overall rate (k_0) of the reaction with the increase in temperature from 413 K and 433 K, but not much of the difference in k_0 between 393 K and 413 K. In addition, over ruthenium black catalyst the rates of direct production of Pl 8 [H] directly were very minimal at low temperatures and close to zero at higher temperatures (see Table 6.2). However, the

stepwise formation of Pl 8 [H] is present with significant rates in the whole temperature range studied over ruthenium black catalyst. Similarly to the observations made over supported catalyst, the rate constant of the production of Pl 8 [H] is higher than the rate constant of its further conversion over unsupported ruthenium black. Thus, in both of the catalytic systems, the formation of 9-ethyl-octahydrocarbazole is energetically more favourable than its further conversion into the fully hydrogenated product. This can explain the high stability of this intermediate over ruthenium based catalysts, especially over unsupported ruthenium black. It is worth noting that in contrary to ruthenium black, over of 5 wt % Ru/Al_2O_3 system the concentration of Pl 8 [H] was decreasing at higher temperatures (see Figure 6.6). As it could be expected, the activation energies of all of the intermediate reactions are much higher over unsupported catalyst, apart from the activation energy of conversion of substrate into Pl 12 [H] B. Because of the rather low activation energy of 49 kJ/mol, this isomer is the main product of the reaction in the range of the temperatures studied. It is clear that this reaction would be favourable over ruthenium black catalyst, due to the high percentage of the flat active sites present, which favour flat adsorption of the substrate. Therefore, the addition of hydrogen atoms takes place simultaneously to both of the rings, which are at the same proximity to the catalyst and are able to be activated at the same time.

Based on the calculated rate constants, the reaction pathways were developed which are shown in Figure 6.12. Additionally, the ratio between k_2 to k_0 at all of the temperatures gathered in Table 6.3 showed that over ruthenium black catalyst at lower temperatures, the reaction takes place via direct formation of the products and stepwise addition of the hydrogen atoms, whereas at higher temperatures the conversion of the starting material is more probably mainly taking place via consecutive addition of hydrogen atoms rather than through direct conversion into isomers of Pl 12 [H].

Temperature [K]	Path of the reaction
383	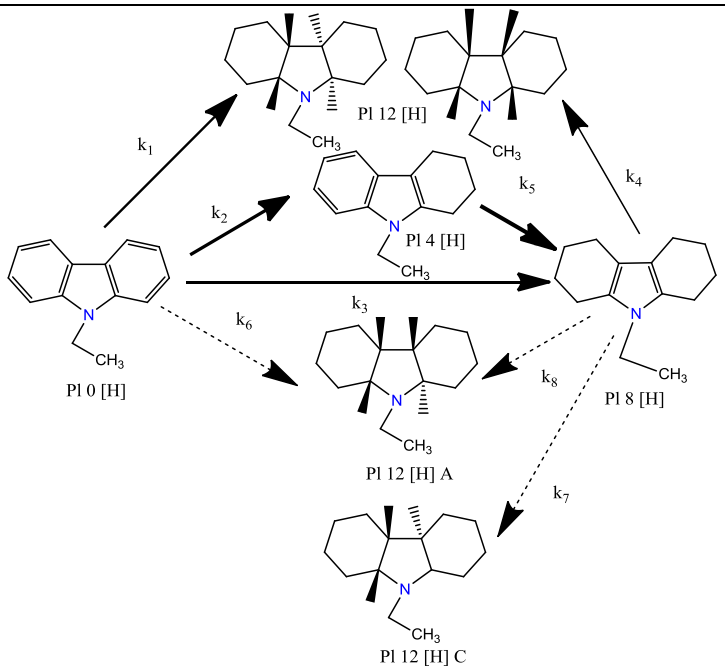
393	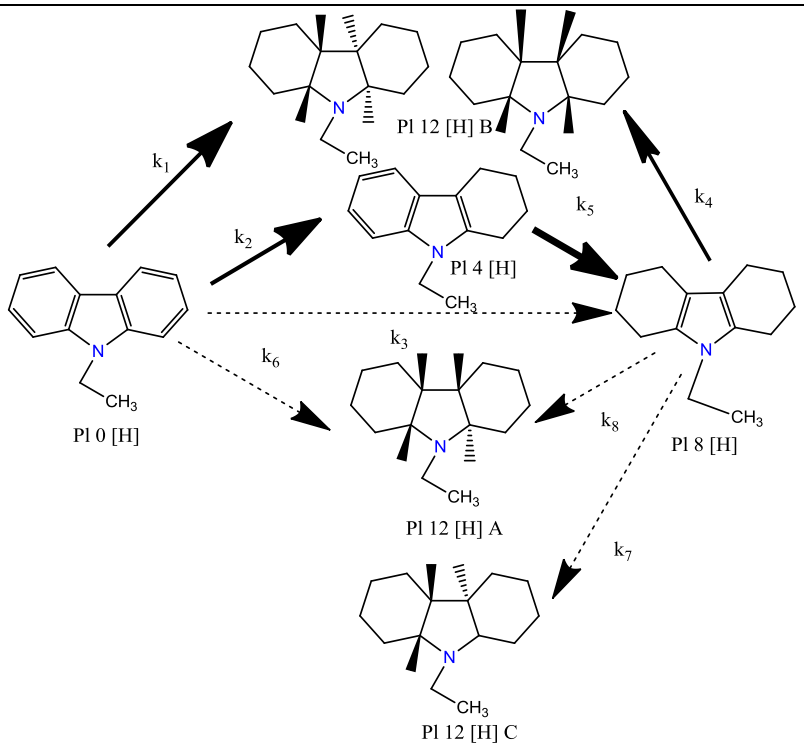

413	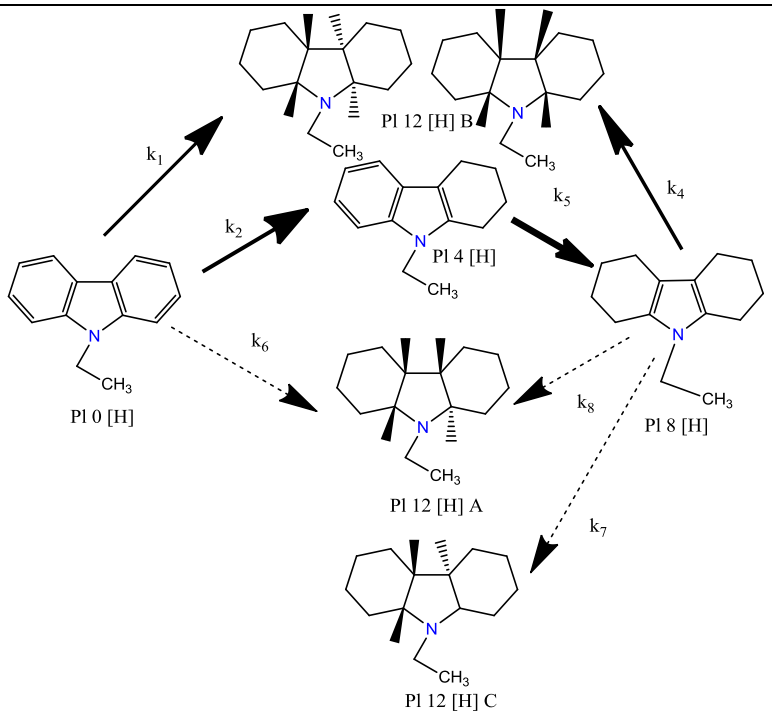
433	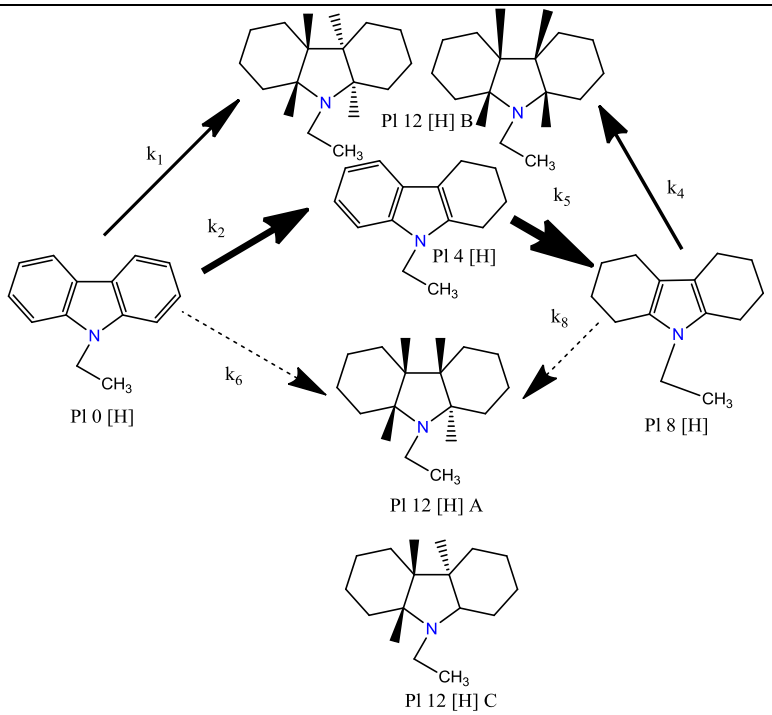

Figure 6.12. Predicted paths of the reaction based on the calculated rate constants at different temperatures for hydrogenation of 9-ethylcarbazole over ruthenium black catalyst. The thickness of the arrows is proportional to the value of the associated rate constants.

Table 6.3. The relationship between estimated rate constants of 9-ethylcarbazole hydrogenation over ruthenium black catalyst.

Temperature [K]	k_2/k_0
383.15	51%
393.15	58%
413.15	79%
433.15	81%

Regardless of the temperature of the reaction or the catalyst used, the rate constant of conversion of Pl 8 [H] into Pl 12 [H] B is always favoured over the conversion of Pl 8 [H] into Pl 12 [H] A or Pl 12 [H] C.

To sum up, the difference between the distributions of the isomers in the fully hydrogenated product over the two catalysts studied can be attributed to the type of the active sites present on the surface of the metal as it was discussed in the previous chapter. Regardless of the support presence, the main product observed over both of the catalysts, especially at low temperatures was Pl 12 [H] B. Over supported catalyst at higher temperatures this product isomerised into Pl 12 [H] A. However, the presence of isomer Pl 12 [B] as a main product of the reaction over supported catalyst is not surprising result, especially taking into consideration the possible geometries of this product which is a mixture of two isomers (see Chapter Four). Thus, it is expected that the majority of the product Pl 12 [H] B obtained over supported catalyst will have the structure having two rings hydrogenated in trans positions instead of cis positions.

The two side model described in Chapter Five is followed by the reaction at lower temperatures. The direct hydrogenation reaction associated with simultaneous multiple

additions of hydrogen to form isomer Pl 12 [H] B, which according to the model should take place on the flat surfaces has much lower activation energy over ruthenium black catalyst. This is a result of the fact that the flat π adsorption requires an ensemble of ruthenium atoms to adsorb. Such an ensemble is in majority on bigger particles, synthesized at higher temperatures. In addition, direct formation of all of isomers of Pl 12 [H] takes place only over supported catalyst. Over ruthenium black, mainly Pl 12 [H] B is made via direct pathway in the whole range of the temperatures studied, which agrees well with the model. In addition, the isomerisation reactions take place favourably over supported catalyst at higher temperatures. Isomerisation would also be expected to be favoured at higher conversions, due to the possible site-competition taking place between different intermediates and final products. It should be clear that the adsorption of a fully hydrogenated substrate is much easier on unsaturated sites, which are highly populated on supported nanoparticles. These results are also in agreement with the developed reaction model.

Nevertheless, there are also some variations from the model that can be observed. Firstly, the rate constants for direct formation of Pl 8[H] which is thought to be taking place on the flat surfaces is much lower over ruthenium black than over supported catalyst. Moreover, at high temperatures over 5 wt % Ru/Al_2O_3, the rate of direct formation of Pl 8 [H] increases. The two parallel mechanisms of producing Pl 8 [H] are active over supported catalysts in the whole range of the temperature studied, whereas over ruthenium black catalyst, the two mechanisms are only active at low temperature. At higher temperatures, the Pl 8 [H] is solely made via stepwise reaction over ruthenium black. In addition, there is a higher maximum accumulation of Pl 8 [H] observed over supported catalyst than over ruthenium black (60 % over the former versus 50 % over the latter). The higher accumulation of this intermediate over supported catalyst can be explained by the two

mechanisms of its formation being active over this catalyst as well as by the fact that it's direct formation and desorption tends to be more favourable over supported than over unsupported catalyst. From the results obtained in this chapter, it is clear that over ruthenium black catalyst, the direct formation of Pl 12 [H] B is more probable than the formation of Pl 8 [H] followed by its desorption from the surface. This observation is thought to be deviation from the model, in which direct formation of Pl 8[H] was expected to be favoured over unsupported catalyst, due to the preferable flat geometry of adsorption of 9-ethylcarbazole. Over 5 wt % Ru/Al_2O_3 catalyst, the direct formation of Pl 8 [H] seems to be favoured over the pathway following consecutive addition of hydrogen. This could be due to other mechanisms being activated at high temperatures or simply to the model being attained using data for the reaction at 130°C. This change of the reaction pathway could also be the result of the formation of carboceus species on the surface of the catalyst at higher temperatues that modified the active sites of the catalyst or poisoned them. The formation of coke from δ adsorbed aromatic compounds was reported previously in (34). Moreover, at 433 K, some dehydrogenation might have taken place on the surface of the catalysts, which influenced the reaction pathways. However, in general it can be stated that the developed model in Chapter Five, described well the hydrogenation of 9-ethylcarbazole in the wide range of temperatures.

6.2.3. The influence of hydrogen pressure

Pressure can modify the reaction pathway by applying geometric constraints on the substrate or on the catalyst (35). The influence of pressure was investigated in the batch process in a liquid phase reaction using 100 ml of cyclohexane, 3 g of 9-ethylcarbazole, 0.15 g ruthenium black /0.1 g 5 wt % Ru/Al_2O_3 in one hour reactions at fixed agitation rate. Increasing the hydrogen pressure from 30 bar up to 90 bar, resulted in increase in conversion from 11 % to 82 % in case of ruthenium black catalyst and from 47 % up to 99

% in case of 5 wt % Ru/Al_2O_3. The effect of hydrogen pressure on the conversion is shown in Figure 6.13.

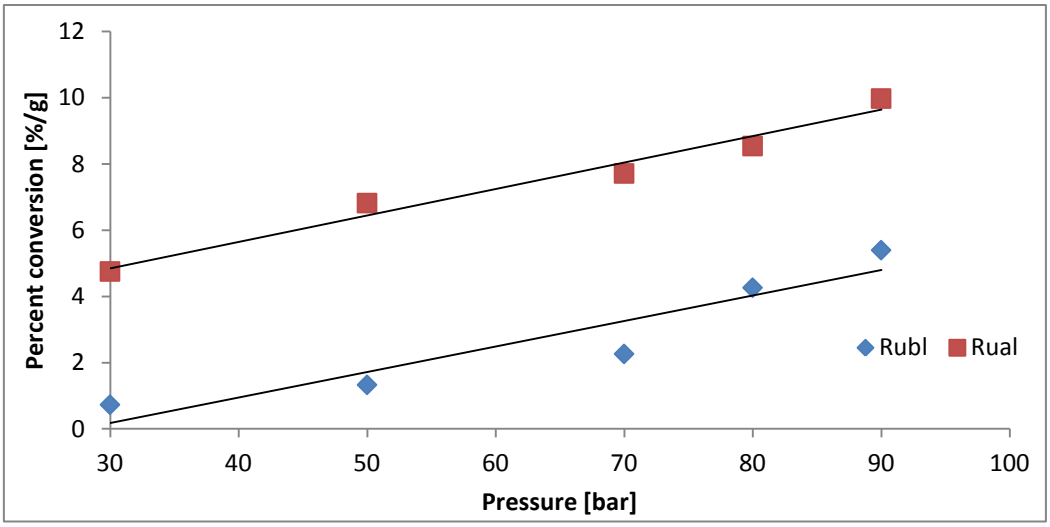

Figure 6.13. The effect of pressure on the conversion per gram of catalyst of 9-ethylcarbazole over 5 wt % Ru/Al_2O_3 and ruthenium black catalysts.

Since different amounts of catalysts were used, the conversion obtained was normalised to facilitate comparison between these two catalytic systems. As it can be seen in Figure 6.13, the highest yield (91 %) was achieved over supported catalyst at 90 bar, while at lower pressures (30 bar) the decrease of yield was observed down to 47 % over the same catalyst. With higher pressures, the concentration of hydrogen increases in both liquid phase and in the interface between liquid and solid catalyst, resulting in a higher rate of the reaction. Thus, at higher pressures/hydrogen concentration, the equilibrium shifts in favour of the forward reaction. Unsupported ruthenium black catalyst showed lower conversions than 5 wt % Ru/Al_2O_3 in the whole range of pressures studied. Similarly to supported catalyst, the highest yield over ruthenium black was obtained at the highest pressure of 90 bar (81%) and it decreased with decreasing pressure. However, overall maximum increase in conversion in the studied range of pressures was obtained over ruthenium black catalyst.

The increase of conversion with the increase of pressure is almost linear over both of the catalysts as can be seen in Figure 6.13. This result suggests that in the range of pressures

studied no saturation point of hydrogen in cyclohexane was reached. Therefore, in this range of hydrogen pressures, the reaction is controlled by the amount of hydrogen adsorbed and activated on the catalyst's surface. However, the trend of conversion versus pressure obtained in 9-ethylcarbazole hydrogenation over ruthenium based catalysts (see Figure 6.13) differs from the typical pressure versus conversion trends described in literature (5). The typical conversion versus pressure curve should contain an equilibrium pressure point above which the conversion is independent of the concentration of hydrogen. Under our testing conditions (30-90 bar), no such a limiting point was obtained. Further increase of pressure would probably allow reaching the equilibrium point, nevertheless such high pressures are not commercially feasible (5).

The selectivity changes with increased pressure are shown in Figure 6.14 and Figure 6.15. The selectivity change with increase pressure shows the same trend over both of the catalysts studied. It is apparent that the selectivity towards fully hydrogenated Pl 12 [H] isomers increases gradually with increased pressure. At low pressures the main product of the reaction over both catalysts is Pl 4 [H] (over 80 %), but its selectivity decreases with increased pressure. The decrease of the concentration of this intermediate is faster over supported catalyst, which has more exposed active sites of the metal. As it was mentioned before, the adsorption of the substrate is thought to be much stronger than the adsorption of Pl 4 [H] intermediate due to the electronic and geometry effects. Thus, with increased pressure, the conversion of the starting material increases and simultaneously it's coverage on the surface of the catalyst decreases. This results in higher amount of active sites available for further conversion of Pl 4 [H].

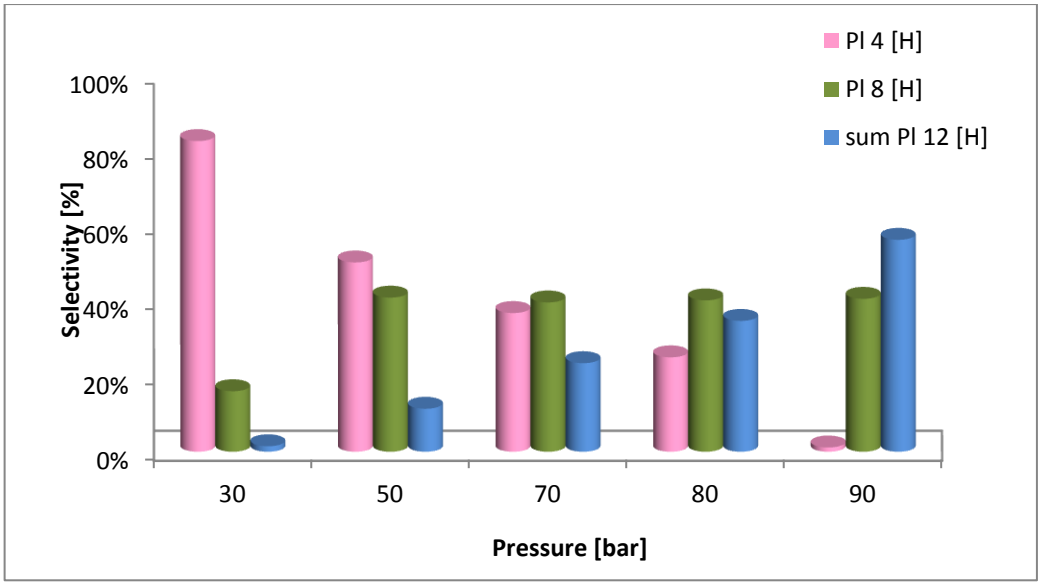

Figure 6.14. Product distribution of 9-ethylcarbazole hydrogenation over 5 wt % Ru/Al_2O_3 catalyst (t = 1h, 0.1g catalyst, 100ml cyclohexane, T= 403.15 K) as a function of pressure. The acronyms as explained previously.

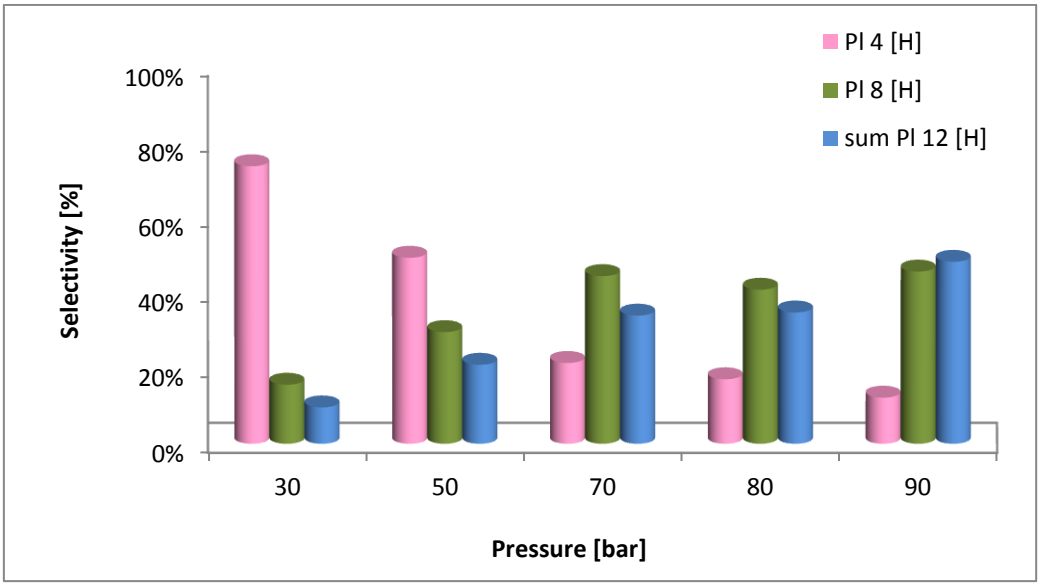

Figure 6.15. Product distribution of 9-ethylcarbazole hydrogenation over ruthenium black catalyst (t = 1h, 0.1 g catalyst, 100 ml cyclohexane, T = 403.15 K) as a function of pressure. The acronyms as explained previously.

At lower pressures, the selectivity towards Pl 8 [H] is lower over ruthenium black catalyst then on 5 wt % Ru/Al_2O_3, however at higher pressures the situation is inversed. Additionally, the selectivity towards this intermediate over 5 wt % Ru/Al_2O_3 catalyst (see

Figure 6.14) at low pressures reaches 16 % and then increases to the value of 40 % at 50 bar, which is stable up to 90 bar. The isomerisation reaction is more likely to take place at the highest pressure, due to the concentration of the starting material being low. Thus, under these conditions the re-adsorption of fully saturated Pl 12 [H] is easier. Similarly, over ruthenium black catalyst (Figure 6.15) at lower pressures, the selectivity towards this intermediate is 18% and at 70 bar increases to 45% and does not change up to 90 bar. It is worth noting that over 5 wt % Ru/Al_2O_3 catalyst, even under 90 bar of hydrogen pressure, the concentration of Pl 8 [H] remained unchanged even with almost complete conversion of Pl 4 [H]. On the other hand, in the study of the influence of the temperature in the present work, it was observed that over supported catalyst when Pl 4 [H] was fully converted, the concentration of Pl 8 [H] started to decrease. According to the model, the competition for highly unsaturated active sites (such as edges and corners) might be taking place between Pl 4 [H] and Pl 8 [H]. As it was shown previously, parallel adsorption of the residual inner aromatic ring of Pl 8 [H] on the catalyst surface is difficult as a result of steric interference between the two saturated 6 membered rings and the catalyst surface.

The effect of pressure change on the selectivity towards isomers in the fully hydrogenated product was also studied. In case of the reactions run over ruthenium black, the distribution of the isomers versus pressure does not differ much from the isomers distribution versus temperature showed in Figure 6.11. The mixture of isomers of 9-ethyl-perhydrocarbazole contains mainly (in around 90%) isomer Pl 12 [H] B in the whole pressure range studied. In case of the reactions run over supported catalyst, the distribution of the isomers in the final product of the reaction is slightly different than the profile obtained for this catalyst at varied temperatures showed in Figure 6.7. Over supported catalyst, at the lowest pressure studied (30 bar), the production of Pl 12 [H] A with the (selectivity of 72 %) was favoured. However, as the pressure increased, the selectivity

changed into preferable formation of Pl 12 [H] B. The selectivity towards this isomer increases with increasing pressure in contrary to the observation made at higher temperatures, where the selectivity towards this isomer decreased. Additionally, over 5 wt % Ru/Al_2O_3 catalyst, no isomerisation reaction was observed even at 90 bar. The increase of the concentration of the isomer Pl 12 [H] B is associated with the change of the reaction pathway enforced by the presence of the high concentration of hydrogen on the surface of the catalyst. It is noted that regardless of the pressure or the catalyst used, the lowest selectivity was always observed for isomer Pl 12 [H] C.

6.2.4. The influence of the solvent

The choice of the solvent has a crucial effect on selectivity, activity and the overall efficiency of the chemical process. In the present work, the influence of the solvent on the conversion and selectivity in liquid phase hydrogenation of 9-ethylcarbazole was investigated over ruthenium black catalyst. The aim of this study was to find the influence of the solvent on the stability of Pl 8 [H] intermediate and high selectivity towards Pl 12 [H] B isomer over ruthenium black catalyst. The influence of the solvent was examined in the 9-ethylcarbazole hydrogenation at 403.15 K, under 70 bar of hydrogen pressure in 7 hour reactions. The solvents employed were cyclohexane, 1,4 dioxane and ethanol. Physical properties of these solvents are listed in Table 6.4. The solvents used in the present studies are representatives of the three groups of solvents with varied polarity. Cyclohexane belongs to the truly non-polar solvents, 1, 4-Dioxane belongs to nondipolar solvents like benzene and ethanol is a polar solvent.

The highest solubility of the starting material was observed in ethanol, followed by 1,4-dioxane, whereas the solubility of 9-ethylcarbazole in cyclohexane was rather poor and had to be enforced by using ultrasonic bath. This is due to the fact that 9-ethylcarbazole

like most of the nitrogen heterocyclic compounds with similar structures (40) is considerably polar molecule.

Table 6.4. Physical properties of the tested solvents.

Solvent	**Polarity index** [36]	**Dipole moment**[37]	**Dielectric constant**
Cyclohexane	0.2	0	2.0[38]
1,4-Dioxane	4.8	0.5	2.2[38]
Ethanol	5.2	1.7	24.3[39]

Surprisingly, no reaction was observed in ethanol, despite a prolonged reaction time of 20 hours. This result can be explained by the fact that 9-ethylcarbazole as a polar reagent is favourably solvated in ethanol and therefore it is not readily adsorbed on the catalyst surface in the presence of a polar solvent. Additionally, it was observed previously in the literature that ethanol can absorb on the surface of the catalyst and change the nature of the active sites by modifying the coordinative unsaturation of the surface sites, which results in a decreased reaction rate (14). It is difficult to verify the actual reason for the lack of catalyst activity in the 9-ethylcarbazole hydrogenation in ethanol; however it is thought that it could be a result of the combination of the adsorption on the surface of the catalyst and the strong interaction of the solvent molecules with the reagent as it was mentioned before. Additionally, the solubility of hydrogen is inversely proportional to the polarity of the solvent, being higher in non polar solvents (41). This could also affect the rates of hydrogenation in ethanol.

Nevertheless, there were significant rates of reaction observed in both cyclohexane and 1,4-dioxane. The observed products of 9-ethylcarbazole hydrogenation in cyclohexane and

in dioxane had the same structures, however their distribution slightly differed. The conversion versus time obtained over ruthenium black catalyst in 1,4-dioxane and cyclohexane is shown in Figure 6.16.

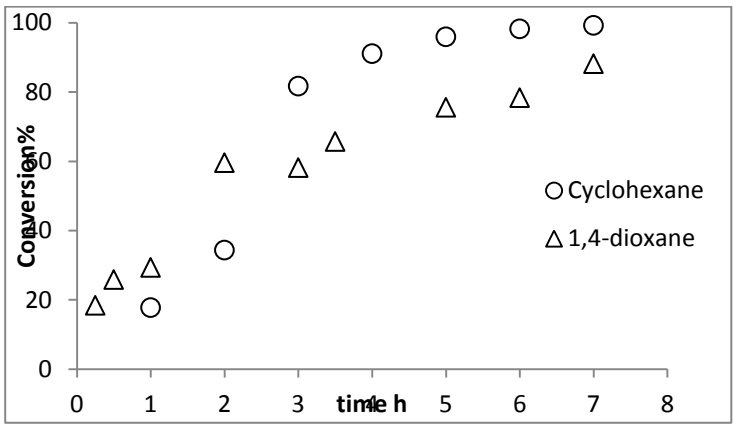

Figure 6.16. Solvent effect on conversion in 9-ethylcarbazole hydrogenation over ruthenium black catalyst at 403.15 K under 70 bar of hydrogen pressure.

As can be seen in Figure 6.16, it takes around 6 hours to convert almost fully 9-ethylcarbazole in cyclohexane (98 % conversion), whereas in 1,4-dioxane, only 88 % conversion is achieved in 7 hours. The initial conversion in 1,4-dioxane is higher than in cyclohexane, but as the reaction progressed, substantially more catalyst deactivation occurred in 1,4-dioxane. It has been reported before in the literature, that 1,4-dioxane undergoes hydrogenolysis and decomposition reactions at relatively low temperature in the presence of noble metal catalyst (42). Thus, the experiment was carried out at the standard reaction conditions but in the absence of the substrate to evaluate the stability of 1,4-dioxane. During GC-MS analysis of the resulting solution, traces of products of ring opening of 1,4-dioxane were indeed found. Thus, our experimental result of decrease in rate of the reaction in 1,4-dioxane can be explained by the ability of adsorbed 1,4-dioxane to suppress adsorption of the 9-ethylcarbazole.

The comparison of the selectivity towards reaction intermediates; 9-ethyl-tetrahydrocabazole, 9-ethyl-octahydrocarbazole and the sum of isomers of 9-ethyl-perhydrocarbazole is shown in Table 6.5 A,B,C.

Table 6.5. Products distribution versus time of 9-ethylcarbazole hydrogenation over ruthenium black catalyst, in cyclohexane and dioxane. A- distribution of Pl 4 [H], B-distribution of Pl 8 [H] and C-distribution of the sum of isomers of Pl 12[H].

A

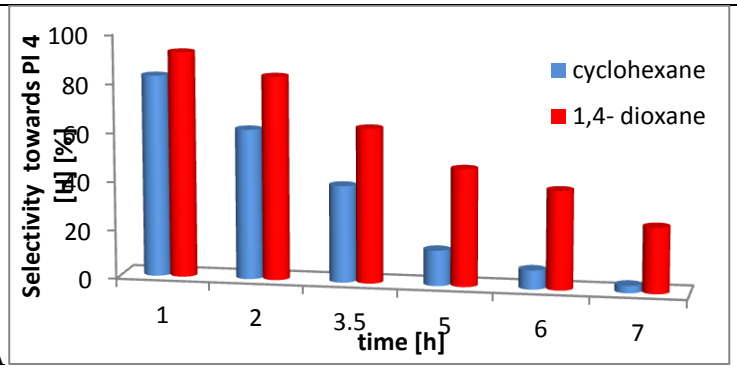

B

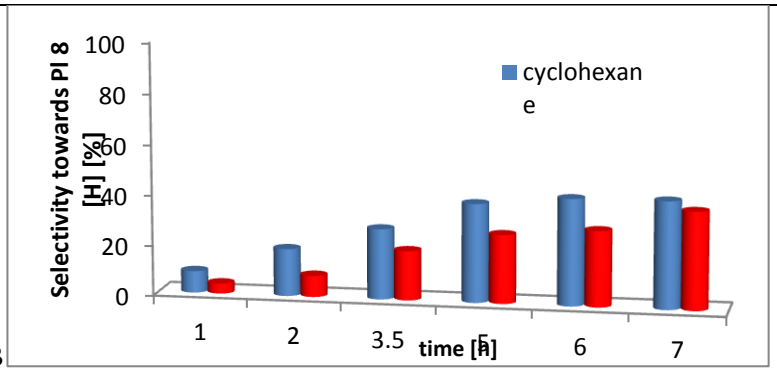

C

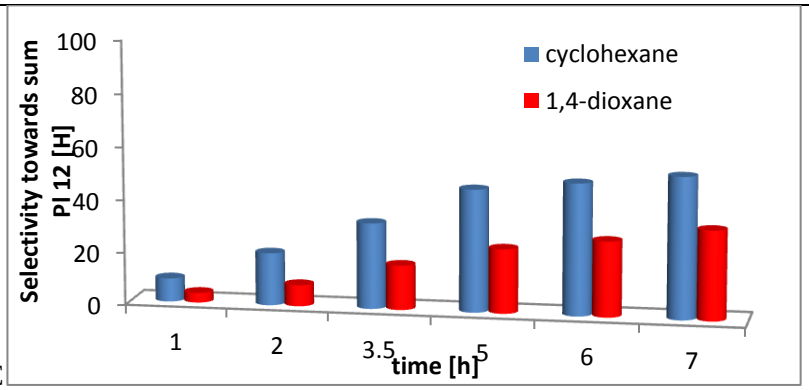

In general, the products distributions are very similar in both of the solvent probably due to the fact that these solvents have very similar dipole moment and dielectric constant, thus have very similar physical properties (see Table 6.4). The primary intermediate is 9-ethyl-tetrahydrocarbazole, concentration of which decreases in both of the solvents as the reaction progresses. However, the selectivity towards Pl 4 [H] (Table 6.5 A) is noticeably higher in 1,4-dioxane and also its rate of disappearance is slower in this solvent than in cyclohexane. This can be the result of the polarity differences between two solvents. It is possible that the solvent with higher polarity (1,4-dioxane) favours the solvation of Pl 4 [H] rather then it's adsorption on the surface of the catalyst. Therefore, the interaction between 1,4-dioxane and the intermediate is much stronger than the interaction of this intermediate with a non-polar cyclohexane. This can lead to the accumulation of Pl 4 [H] in the solution and diminishes its further conversion into Pl 8 [H]. As a result, lower selectivities towards Pl 8 [H] were observed in 1,4-dioxane than in cyclohexane as shown in Table 6.5 B. Additionally, higher selectivities towards the sum of isomers of Pl 12 [H] were obtained in cyclohexane. In both solvents, the final product was composed of the same isomers. The composition of the mixture of 9-ethyl-perhydrocarbazoles was analysed and the results for selected time spans of the reaction are gathered in Table 6.6.

In both solvents, the main isomer produced is Pl 12 [H] B, selectivity of which decreases as the reaction progresses probably due to isomerisation reactions described before. However, the decrease in selectivity towards this isomer is higher in cyclohexane, suggesting the rate of the isomerisation being higher in this solvent. The main difference between the composition of the final product is much lower selectivity towards isomer Pl 12 [H] C, observed in 1,4-dioxane.

Table 6.6. The comparison of the selectivity towards isomers of the final product of 9-ethylcarbazole hydrogenation over ruthenium black in cyclohexane and 1,4-dioxane.

Time [h]	Selectivity in cyclohexane [%]			Selectivity in 1,4-dioxane [%]		
	A	B	C	A	B	C
1	4.0	94.3	1.6	2.8	97.1	0
5	7.3	88.9	3.6	4.9	94.2	0.8
7	8.7	87.4	3.8	5.5	93.2	1.2

The overall influence of the solvent on hydrogenation of 9-ethylcarbazole studied by comparing the reaction selectivity and conversion of the catalyst show that higher rates of reaction were obtained in cyclohexane and decreased with increasing polarity of the solvent.

6.3. Conclusions

In summary, the kinetics of liquid-phase hydrogenation of 9-ethylcarbazole over 5 wt % Ru/Al_2O_3 and ruthenium black were studied. The reaction was found to follow a first order with respect to the concentration of the aromatic substrate and zero order in concentration of hydrogen gas. The apparent activation energy of 57.9 kJ /mol over supported catalyst and 64.7 kJ/mol over unsupported catalyst were obtained. The values of the apparent activation energies indicated lack of any transport limitation being involved in the process. Higher conversions in the whole range of the temperatures and pressures studied were observed over supported catalyst. The experimentally obtained product distributions versus time in the range of temperatures were modelled and the activation energies were calculated for the intermediate reactions involved. The temperature and

pressure was found to have an effect on the selectivity of the catalysts and the composition of the final product. Regardless of the presence of the support, the Pl 8 [H] intermediate was found to be the major intermediate on both of the catalysts. However, the further conversion of this intermediate was much faster over 5 wt % Ru/Al_2O_3 catalyst. The unsupported catalyst was found to be more selective in producing mainly one isomer of the fully hydrogenated 9-ethyl-perhydrocarbazole. On the other hand, Pl 8 [H] was found to be stable over this catalyst in the range of temperatures and pressures studied. The calculated activation energies of intermediate reactions over both catalysts showed that the activation energy of production of Pl 8 [H] was always lower than the activation energy of its further conversion. The pressure was found to have some effect on the conversion and the composition of the final product over both of the catalysts. However, no remarkable effect of pressure was noted on reaction selectivity over both of the systems studied. In addition, it was found that the activity of the catalyst is influenced by the polarity of the solvent.

From the point of view of using 9-ethylcarbazole as on board hydrogen carrier, it is clear that the rates of the hydrogenation reaction observed are far too slow even at high pressures and high temperatures. Additionally, pressures in the range of 70 bar and temperatures above 130 °C may not be commercially attractive in this application of the material. However, it was found that at lower pressures and lower temperatures, the rate of the reaction drops significantly, thus the time necessary for hydrogen upload proportionally increases. In addition, the final product of 9-ethylcarbazole hydrogenation consists of four different isomers. This implies that the dehydrogenation process may encounter problems due to the difficulties in readsorption of some of these isomers on the catalyst surface.

6.4. References

1. *Chemical kinetics.* **K. J. Laidler,** New York: McGraw-Hill Inc, 1965.
2. *Introduction to chemical kinetics.* **K. A. Connors,** New York: VCH Publishers, 1990.
3. **http://www.chm.davidson.edu.** [Online]
4. **http://en.wikipedia.org/wiki/Rate_equation.** [Online]
5. *Heterogenous catalysis for the synthetic chemist*. **R. L. Augustine,** New York: Marcel Dekker Inc, 1996.
6. *Reaction kinetics.* **M. J. Pilling, P. W. Seakings,** Oxford: Oxford Science Publications, 1995.
7. *Heterogenous catalysis principles and applications.* **G. C. Bond,** Oxford: Oxford University Press, 1974.
8. *Handbook of heterogenous catalysis Volume 1.* **G. Ertl, H. Knozinger, F. Schuth, J. Weitkamp.** Weinheim: Wiley-VCH Verlag GmbH.
9. *Influence of hydrogen pressure on selectivity in consecutive hydrogenation reactions.* **C. Niklasson, B. Andersson, N. H. Schoeoen,** Ind. Eng. Chem. Res., 1987, Vol. 26.
10. *The mechanism of the hydrogenation of unsaturated hydrocarbons on transition metal catalysts.* **G. C. Bond, P. B. Wells,** Adv. Catal., 1964, Vol. 15.
11. *Hydrogenation of benzene to cyclohexene on an unsupported ruthenium catalyst: effect of poisons.* **C. U. I. Odenbrand, S. T. J. Lundin,** J. Chem. Technol. Biotechnol., 1981, Vol. 31.
12. *Comperative studies of homogenous and heterogeneous catalyses: Part III.The hydrogenation of disubstituted cyclohexanes over Rh and Rh(PPh3)3cl.* **A. Yanagawa, Y. Suzuki, I. Anazawa,** J. Mol. Catal., 1985, Vol. 29.
13. *Competitive catalytic hydrogenation in the liquid phase on solid catalyst.* **C. L. Cerveny, V. Ruzicka,** Catal. Rev., 1982, Vol. 24.
14. *Heterogenous catalysis in organic chemistry. Competitive adsorption of solvents during alkene hydrogenation.* **R. L. Augustine, R. W. Warner, M. J. Melnick,** J. Org. Chem., 1984, Vol. 49.
15. *Catalysis in organic synthesis.***G. W. Roberts,** New York: Academic Press, 1976.
16. *Kinetics of H_2 recovery from dodecahydro-N-ethylcarbazole over a supported Pd catalyst.* **F. Sotoodeh, L. Zhao, K. J. Smith,** Appl. Catal. A, 2009, Vol. 362.
17. *Chemical kinetics and mechanism.* **M. Mortimer, P. Taylor,** Cambridge, Royal Society of Chemistry, 2002.
18. *Solvent effects in catalytic hydrogenation.* **R. A. Rajadhyaksha, S. L. Karwa,** Chem. Eng. Sci, 1986, Vol. 41.
19. *Hydrogenation of a 4-benzylpyridine derivative over supported precious metal catalysts.* **A. Proszenyak, B. Agai, L. Hegedus, F.Faigl,** Appl. Catal. A, 2004, Vol. 269.
20. *Kinetics of 9-ethylcarbazole hydrogenation over Raney-Ni catalyst for hydrogen storage.* **X. Ye, Y. An, G. Xu,** J. Alloys Compd., 2010, Vol. 509.
21. *Solvent effect in Liquid phase hydrogenation of toluene.* **P. Rautanen, J. A. Aittamaa, A. O. I. Krause,** Ind. Eng. Chem. Res, 2000, Vol. 39.
22. *The activity and stability of Pd/C catalysts in benzene hydrogenation.* **P-H Jen, Y-H Hsu, S. D. Lin,** Catal. Today, 2007, Vol. 123.
23. *Fundamental hydrodenitrogenation studies of polycyclic N-containing compounds found in heavy oils.1 5.6-Benzoquinone.* **J. Shabtai, G. J. C. Yeh, C. Russel, A. G. Oblad,** Ind. Eng. Chem. Res., 1989, Vol. 28.
24. *Hydrogenation of aromatics in Diesel fuels on Pt/MCM-41.* **A. Corma, A. Martinez, V. Martinez-Soria,** J. Catal., 1997, Vol. 169.

25. *Kinetic behaviour of hydrogenation of aromatics in diesel fuel over silica-alumina supported bimetallic Pt-Pd catalyst.* **T. Fujikawa, K. Idei, K. Ohki, H. Mizguchi, K. Usui,** Appl. Catal. A, 2001.
26. *Heterogenous Catalysis: Principles and Applications.* **G. C. Bond,** Oxford: Oxford University Press, 1987.
27. *The hydrogenation of toluene and o-m-and p-xylene over palladium II Reaction model.* **M. V. Rahaman, M. A. Vannice,** J. Catal., 1990, Vol. 127.
28. *Benzene hydrogenation over supported and unsupported palladium I Kinetic behaviour.* **P. Chou, M. A. Vannice,** J. Catal., 1987, Vol. 107.
29. *Kinetic study of naphtalene hydrogenation over Pt/Al_2O_3 catalyst.* **T. C. Huang, B. C. Kang,** 1995, Vol. 34.
30. *Pt catalyst supported on multi-walled carbon nanotubes for hydrogenation - dearomatization of toluene and tetralin.* **H. Kong, M. Zhou, G-D. Lin, H. B. Zhang,** Cat. Lett., 2010, Vol. 90.
31. *Kinetic study of hydrogenation of isoquinoline over supported ruthenium catalysts.* **H. Okazaki, M. Soeda, Y. Ikefuji, R. Tamura, I. Mochida,** Bull. Chem. Soc. Jpn., 1989, Vol. 62.
32. *Design and development of new carbon based sorbent systems for an effective containment of hydrogen.* **A. Cooper,** Anual progress Report (availiable online) : Air Products, 2006.
33. *O-xylene hydrogenation over supported ruthenium catalysts.* **P. Reyes, M. E. Konig, G. Pecchi, I. Concha, M. Lopez-Granados, J. L. G. Fierro,** Catal. Lett., 1997, Vol. 46.
34. *Liquid-Phase Hydrogenation of Naphthalene and Tetralin on Ni/Al_2O_3: Kinetic study.* **P. A. Rautinen, M. S. Lylykangas, J. R. Atimamaa, A. Outi, I. Krause,** Ind. Eng. Chem. Res., 2002, Vol. 41.
35. *Influence of hydrogen pressure on selectivity in consecutive hydrogenation reactions.* **C. Niklasson, B. Andersson, N-H Schoon,** Ind. Eng. Chem. Res., 1987, Vol. 26.
36. http://www.chemical-ecology.net/java/solvents.htm. [Online]
37. http://macro.lsu.edu/HowTo/solvents/Dipole%20Moment.htm. [Online]
38. *Solvent effects in liquid-phase reactions I. Activity and selectivity during citral hydrogenation on Pt/SiO2 and evaluation of mass transfer effects.* **S. Mukherjee, M. A. Vannice,** J. Catal., 2006, Vol. 243.
39. http://usm.maine.edu/~newton/Chy251_253/Lectures/Solvents/Solvents.html. [Online]
40. *Evaluation of the polarity and boiling points of nitrogen containing heterocyclic compounds by gas chromatography.* **I. L. Zhuravleva,** Russ. Chem. Bull., 2000, Vol. 49.
41. *Solubility of hydrogen in 10 organic solvents at 298.15, 322.15 and 373.15 K.* **E. Brunner,** J. Chem. Eng. Data, 1985, Vol. 30.
42. *Stability of 1,4 dioxane, tetrahydrofuran and ethanol under hydrogenation conditions over various catalysts.* **W. K. Schumann, O. M. Kutt, A. Baiker, G. Gut,** J. Chem. Tech. Biotechnol., 1989, Vol. 46.

7. Hydrogenation of 9-ethylcarbazole over supported and unsupported catalysts –influence of the catalytic system

7.1. Introduction

Active sites of the metal in heterogeneous metal catalysis may include flat sites, sites at the stepped surfaces and sites at the metal and metal oxide boundary on a supported catalyst (1). The properties of active sites (metal catalyst) and molecular structures (reactant) compose the main variables which determine the course of any catalytic reaction. In addition, structural effects are mutually interdependent, and can be divided into geometric and electronic effects (2). Electronic effects can be described in terms of metal active sites and reactants being either donors or acceptors of electrons in the reaction. On the other hand, geometric constrains affect the formation of the surface-complex (active site-reactant) (3). Beside these effects, the reaction outcome can be influenced by the thermodynamics, reaction conditions and mass transport limitations (4). The electronic structure of the metal has a major effect on its catalytic activity in a particular catalytic process. Transition metals posses rather complicated electronic structure with itinerant electrons originating from the valence s shell of the metal and more localized d band electrons, that are moving across the Fermi level (5). The bond is strongest when the antibonding state of the molecular bond is empty (5). Thus, shifting the d states above Fermi level will as a consequence shift up the antibonding states, leading to a smaller occupation resulting in stronger bond. However, as a general rule, the optimum catalyst for the reaction has to be a compromise between two extremes of very active and very noble surface according to a well-known ‘Sabatier-rule’ (1).

The selectivity and activity of a multipath reaction depends mainly on the energy differences between the activation energy barriers which can be induced by co-adsorbates

(6), small morphological changes (7), changes of the charge states of the metal, the nature of metal (8), the particle size and shape, the type of support (9), temperature and pressure. Additionally, strong evidence has been accumulated in the literature pointing at electronic interaction between metal and support called strong metal support interaction (SMSI), which alters the work function of the surface metal atoms and thus their chemisorptive and catalytic properties

In the present chapter, the reactivity of 9-ethylcarbazole in catalytic hydrogenation was comprehensively studied over ruthenium as well as other typical hydrogenation active noble metal and nickel catalysts in order to clarify the factors that influence the selectivity and activity of the catalyst in this reaction. The reaction pathways over different supported and unsupported catalysts were compared. The influence of the type of metal and support on the reaction selectivity and hydrogenation activity is discussed.

7.2. Materials and methods

The commercial catalysts were purchased from Sigma-Aldrich. The other catalysts were synthesized following the polyol process or mild chemical reduction as described in Chapter Three, paragraph 3.1. The hydrogenation reactions were performed according to the method described in Chapter Three, paragraph 3.4.3. Periodically, small samples were removed from the reactor for the composition analysis using a GC-MS (Agilent 6890GC-MS) as described in Chapter Three. All the catalysts were used without prior pretreatment. The used catalysts were characterized by TEM and BET techniques.

7.3. Results and discussion

7.3.1. Physical properties of the catalysts.

Under mild reaction conditions, hydrogenation of 9-ethylcarbazole in liquid phase was performed using various catalytic systems with different types of metal and supports. The catalysts tested in the present work are listed in Table 7.1 together with their physical properties. 5 wt % Rh on activated carbon (AC) was found to have elongated shapes apart from spherical, therefore the mean diameter was not determined. Figure 7.1 shows representative TEM images of Ru black, 5 wt % Rh on AC, 5 wt % Pd on AC, and 65 wt % Ni on SiO_2-Al_2O_3. More TEM images of the Ru black and ruthenium based systems can be found in the previous chapters.

Table 7.1. Physical characteristics of the catalysts used in the present work. AC- activated carbon,SiAl-silica-alumina, (s.d)-standard deviation.

Catalyst	***Preparation method***	***TEM size (s.d.) [nm]***	***BET [m^2/g]***
5 wt % Ru on AC	Commercial (COM)	3.01 (0.99)	809
5 wt % Ru on TiO_2	Chemical reduction (CR)	2.11 (0.55)	191
5 wt % Ru on TiO_2	Polyol (P)	3.11 (0.56)	180
5 wt % Ru on Al_2O_3	Commercial (COM)	9.08 (4.70)	83
5 wt % Rh on AC	Commercial (COM)	7.59 (4.50)	442
5 wt % Rh on Al_2O_3	Commercial (COM)	3.33 (1.41)	272
Ru black	Commercial (COM)	Aggregated	22
Pd black	Commercial (COM)	6.83 (2.04)	22
5 wt % Rh on AC (P) (various shapes)	Polyol (P)	-	-
5 wt % Pd on AC	Commercial (COM)	2.69 (0.61)	801
Pt black	Commercial (COM)	6.06 (3.16)	30
65 wt % Ni on SiAl	Commercial (COM)	7.51 (1.84)	96

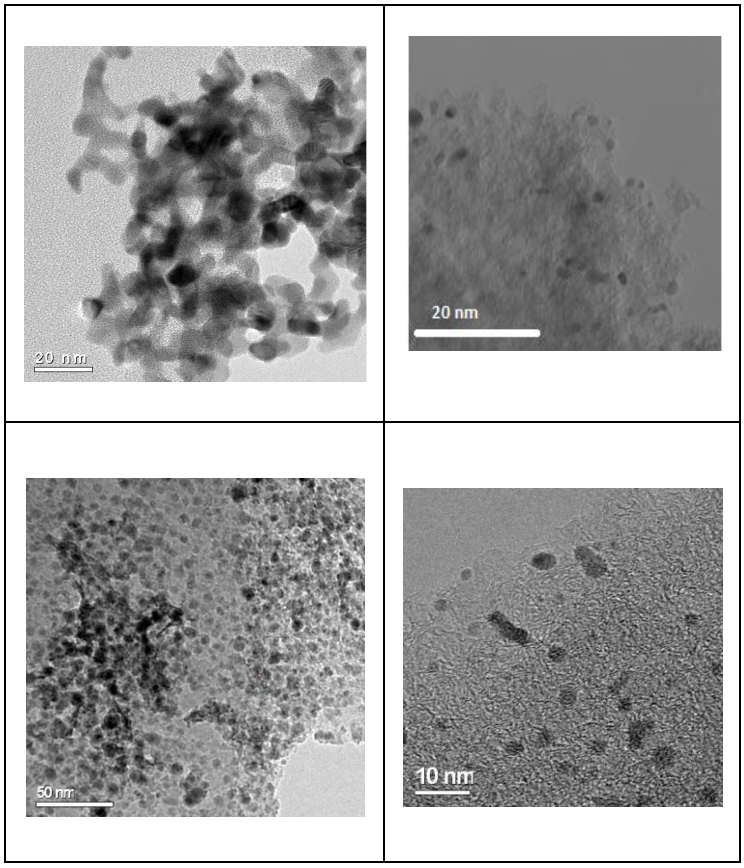

Figure 7.1 Top left- TEM image of ruthenium black nanoparticles, top right- TEM image of 5 wt % Rh on AC, bottom left 65 wt % Ni on SiO_2-Al_20_3, bottom right – 5 wt % Pd on AC.

7.3.2. Implications in the reaction selectivity over ruthenium black catalyst

The reaction products observed over ruthenium black catalyst under excess of catalyst (0.2 g of catalyst per 1 gram of substrate) were literally the same as the ones reported in Chapter Five obtained under harsher reaction conditions (0.15 g of catalyst and 3 g of substrate). Two partially hydrogenated products, namely 9- ethyl-tetrahydrocarbazole (Pl 4 [H]) and 9-ethyl-octahydrocarbazole (Pl 8 [H]) and four isomers of the fully hydrogenated products 9-ethyl-perhydrocarbazole (see reaction model in Figure 7.2 for structures of the products) were produced. Due to the problems encountered in the separation of the isomers of the fully hydrogenated 9-ethyl-perhydrocarbazoles (see Chapter Four, paragraph 4.3.6), for quantitative analysis, the two symmetrical isomers were treated together as a mixture with an acronym Pl 12 [H] B. The reaction model developed in Chapter Five which is shown again in Figure 7.2 was used to fit the experimental data. Generally, the mechanism

of hydrogenation of 9-ethylcarbazole over ruthenium based catalysts involves essentially concerted addition of activated hydrogen atoms from the catalyst's surface to the electron rich double bonds of the aromatic system, leading to several parallel reactions which are dependent on the catalytic sites available on a metal surface as it was reported in Chapter Five of the present work. The nature of the active sites present on the catalyst surface affects the adsorption mode of the intermediates of the reaction. Thus, on the planar surface, the adsorption is mainly through π -σ interaction of the aromatic system with d-band of the metal, however on the edge or corner site, the interaction is mainly σ- σ between the C=C double bonds of the aromatic system or lone pair of electrons on the nitrogen (less probable) of the intermediates, and d-band of the metal. From the findings of the previous chapters, stable intermediate, 9-ethyl-octahydrocarbazole (Pl 8 [H]) is formed in vast quantities when ruthenium based catalysts is used, but it is extremely stable solely over ruthenium black unsupported catalyst. In this chapter, regardless of an excess of unsupported ruthenium catalyst used, Pl 8 [H] was found to be extremely stable. It was shown in Chapter Five that this intermediate does not get readily converted over ruthenium black catalyst due to the majority of the active sites of this catalyst being flat, terraced sites. Due to the geometry of this intermediate, its adsorption on the flat surface of the catalyst for further conversion, is greatly hindered. As a result, 9-ethyl-octahydrocarbazole converts much faster into 9-ethyl-perhydrocarbazole only over catalysts having high proportion of unsaturated sites, such as edges and/or corners. On these sites, the adsorption of Pl 8 [H] is much favored. Thus, the main difference in selectivity between supported and unsupported ruthenium catalysts is the stability of the main intermediate Pl 8 [H]. From the gathered data obtained using ruthenium based systems, several issues were outlined, that require further investigation.

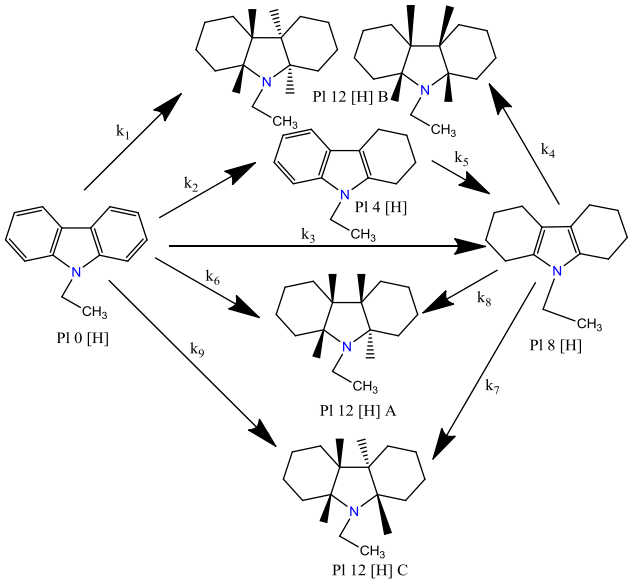

Figure 7.2 Model of the reaction pathway of hydrogenation of 9-ethylcarbazole hydrogenation over ruthenium catalysts Pl 0 [H] is 9-ethylcarbazole etc, Pl 12 [H] A is 9-ethyl-perhydrocarbazole isomer A, 12 [H] B is a mixture of two symmetrical stereoisomers of 9-ethyl-perhydrocarbazole and finally P 12 [H] C is 9-ethyl-perhydrocarbazole isomer C. The numbering of rate constants is in agreement with the numbering used for modelling of kinetics.

In order to optimize the effective catalyst for reversible hydrogenation of 9-ethylcarbazole, it should be considered whether Pl 8[H] intermediate is formed over other types of transition metals in the quantities similar to those observed over ruthenium catalysts. Furthermore, from the point of view of effective recovery of the spent fuel, it is important to determine factors that affect the possible stability of Pl 8 [H] over other noble metals. These factors may include type and presence of the support. It is also crucial to determine the influence of the different catalytic systems on the composition of the fully hydrogenated product.

7.3.3. Influence of the type of the transition metal used

The position of the metal in the periodic table is known to strongly affect the catalytic properties of the resulting catalysts based on that metal (10). In order to gain insight into the influence of the type of metal on the path of the reaction; commercially available unsupported Ru, Pd, Pt and Ni catalysts were tested. However, pure unsupported nickel catalyst showed no activity, partially because of the very large particle size (around 1

micron) and partially because of the magnetic properties of nickel (ferromagnetic element) which resulted in the catalysts interacting with the magnetic stirrer. As a result, it was decided to use the highest commercially available loading of nickel dispersed over a carrier (65 wt % Ni/SiO_2-Al_2O_3) to maximise the dispersion of nickel in the reaction solution.

It was anticipated that the reaction pathway and the type of intermediates might be different because of their differences in absorption strength on each of the metals tested. The catalytic activities calculated according to the formula listed in Chapter Three, Equation 3.1 together with the selectivities (Chapter three, Equation 3.3) towards all the intermediates and products for all the tested samples are gathered in Table 7.2. The catalytic activity of different unsupported metal catalysts in hydrogenation of 9-ethylcarbazole was found to follow the order: Ru>Pd>Pt>Ni. This order of activity corresponds to the values of d-band centres (in electron volt) (11) of the unsupported metals as follows: 1.41 (Ru) < 1.83 (Pd) < 2.25 (Pt) and decreases as the d-band centre increases. The changes in the energy centre of the valence d-band density of states at the surface sites can be correlated to the metal ability to form chemisorption bonds with the substrates (1). It should be noted that the activity of the metal catalyst in the reaction depends strongly on the adsorption of starting reactant on the metal surface. The adsorption strength of the starting material and the intermediates is directly related to the degree of filling of the antibonding adsorbate-metal d-states and the size of a coupling matrix element (V_{sd}) (5). In general, if the energy of antibonding states on the metal surface are below the Fermi level, these states are very likely to be occupied, leading to a weaker bond. The changes in the filling of the d-states of the metal in the periodic table are shown in Figure 7.3 (12). In addition, when the new compound is formed over the surface of the catalyst, the metal-metal bonds are broken. This introduces another factor describing

the energy of metal-metal bonds that is cohesive energy of the metal (12). 5 d metals including Pt have high values of cohesive energy, which adds up to their general nobleness. Thus, Pt is the least active of the unsupported metals studied here because it has the highest filling of the d-band and highest V_{sd}.

Table 7.2. Catalytic activity (after 1h of reaction) and selectivity of unsupported metal catalysts and 65 wt % Ni/SiO_2-Al_2O_3

Catalyst	*Catalytic activity [mM ETC· gram metal^{-1}·s^{-1}]*	*Selectivity (%)*					
		Pl4[H]	*Pl6[H]*	*P8[H]*	*P12[H]A*	*P12[H]B*	*P12[H]C*
Ru black	0.56	18	<1	30	2	50	<1
Pd black	0.55	50	-	3	6	40	1
Pt black	0.18	6	-	3	24	50	15
65 wt % Ni on SiO_2 Al_2O_3	0.16	64	2	3	12	17	2

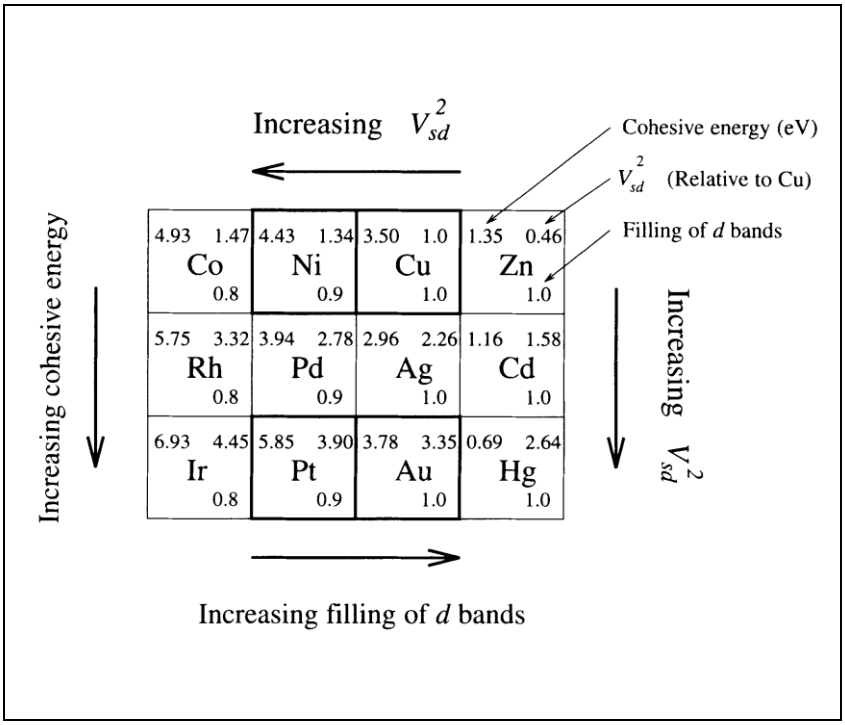

Figure 7.3. The values of cohesive energies, coupling matrix element and filling of the d-bands for transition metals with the general trends in the periodic table (12).

Independently of the metal used, the same intermediates were observed as previously identified in case of ruthenium catalysts (Figure 7.2). When 65 wt % Ni on SiO_2-Al_2O_3 was used, some Pl 6 [H] was detected, that probably was the product of stepwise addition of hydrogen atoms to Pl 4[H]. Since for this catalyst, the selectivity towards P 6 [H] was as

high as the selectivity towards Pl 8 [H], therefore it could not be neglected. As a result, for this catalyst the model showed in Figure 7.2 was altered by addition of this step in the indirect pathway of production of Pl 8 [H]. In contrast, over other metals we did not observed any Pl 6 [H] intermediate, apart from some traces (≤ 1%) over Ru catalysts. The reaction profiles obtained over catalysts based on different metals are showed in Figure 7.4 to Figure 7.7.The curves indicate very good fit of the experimentally obtained values to the model. The rate constants of each step that were used for fitting kinetic data under reaction conditions are summarised in Table 7.3. From the product distributions shown, it can be seen that the stable intermediate, 9-ethyl-octahydrocarbazole (Pl 8[H]) is only formed at significant amounts over ruthenium black catalyst (Figure 7.4). This catalyst also results in Pl 8 [H] accumulation in the reaction solution.

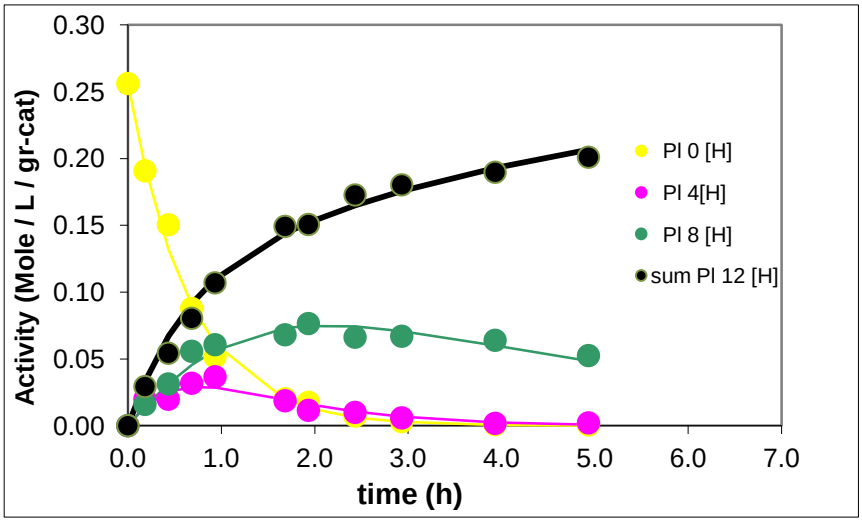

Figure 7.4 Time dependant product distribution obtained over Ru black catalyst in 5 hours of reaction at 130 °C and 70 bar of hydrogen together with modelled values illustrated as a solid lines.

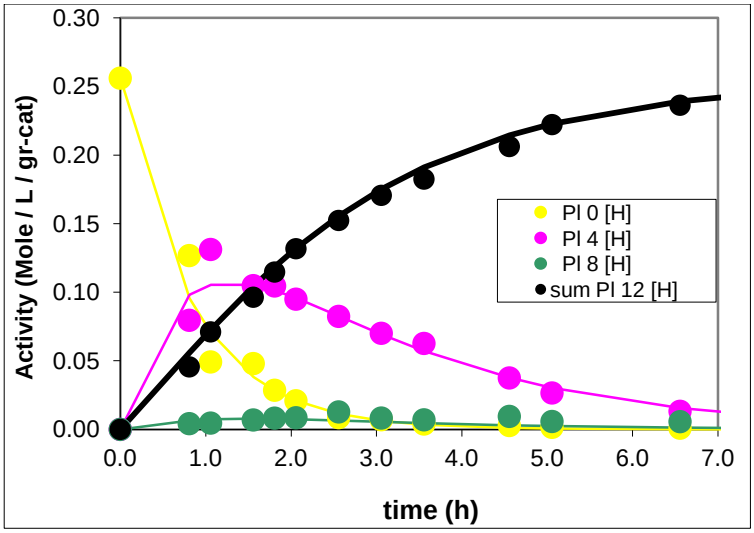

Figure 7.5. Time dependant product distribution obtained over Pd black catalyst in 6.5 hours of reaction at 130 °C and 70 bar hydrogen together with modelled values illustrated as a solid lines

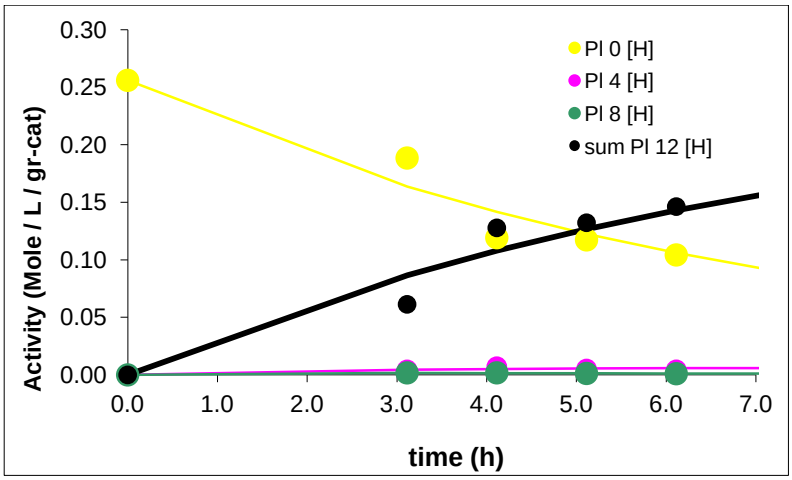

Figure 7.6 Time dependant product distribution obtained over Pt black catalyst in 6.5 hours of reaction at 130 °C and 70 bar hydrogen together with modelled values illustrated as a solid lines

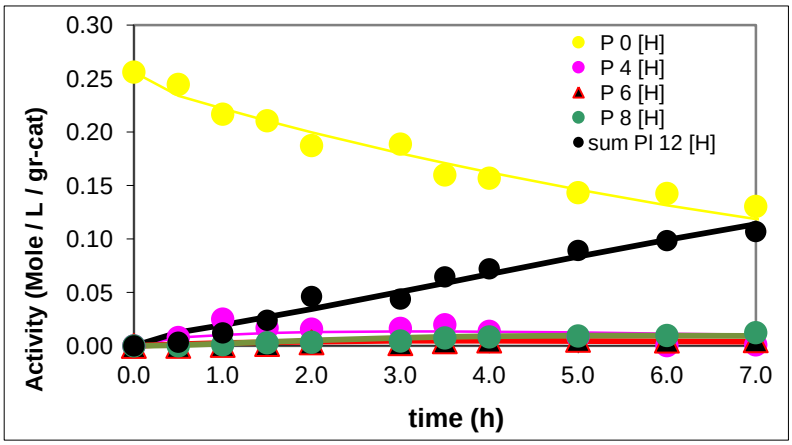

Figure 7.7 Time dependant product distribution obtained over 65 wt % Ni/ SiO_2-Al_2O_3 catalyst in 7 hours of the reaction at 130 °C and 70 bar hydrogen together with modelled values illustrated as a solid lines.

Pl 8 [H] was also detected in the reaction mixtures obtained over Pd and Ni catalysts, but in a much lower concentrations. In contrast, over Pt catalyst, this intermediate was produced in traces. It was found that the selectivity towards Pl 8 [H] is inversely proportional to the catalyst activity, which is shown in Figure 7.8.

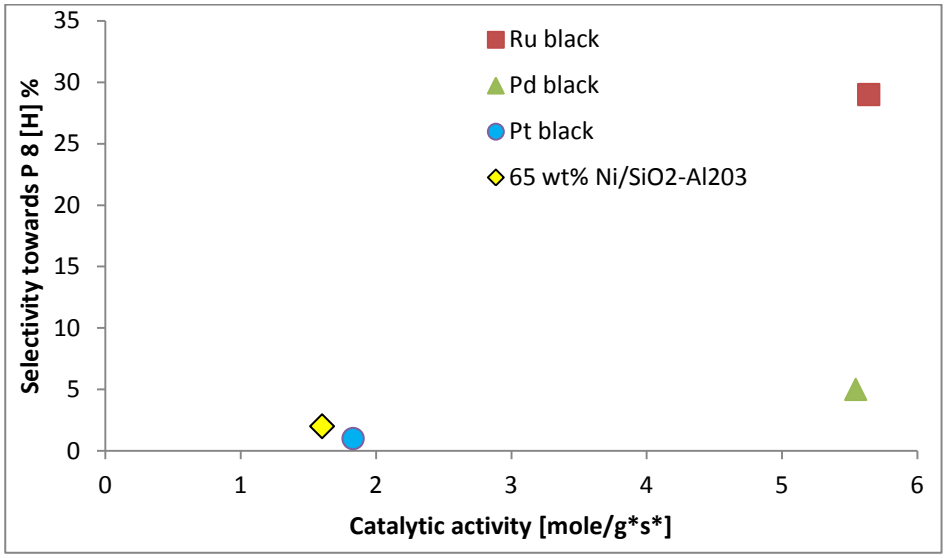

Figure 7.8. Selectivity towards P 8[H] versus catalytic activity of the catalyst after 1 hour of hydrogenation at 130 °C and 70 bar, using 1 g of 9-ethylcarbazole in 100 ml of cyclohexane and 0.2 g of catalyst.

As it can be seen from this plot, the more active the catalyst, the higher is the selectivity towards Pl 8 [H]. It is clear that selectivity towards this intermediate decreases with more electron rich metals. The calculated values of rate constants are listed in Table 7.3 that were used for fitting the experimental data into the model (see Figure 7.2)

Table 7.3 The calculated rate constant values for over various metals

Catalyst	k_0	k_1	k_2	k_3	k_4	k_5	k_6	k_7	k_8	k_9	k_{10}	k_{11}
Ru black	1.5	0.8	0.4	0.3	0.2	1.1	0.017	0.01	0.002	0.003	0.022	0
Pd black	1.2	0.263	0.9	0	6.1	0.5	0.038	0.001	0.003	0	0.093	0.015
Pt black	0.2	0.002	0	0.1	8.1	0.1	0.034	0.005	0	0.021	0.1	0
65 wt % Ni/SiO_2-Al_2O_3	0.1	0.028	0	0	0.6	0.7	0.026	0.17	0.011	0	0.004	0.6

It can be seen in Figure 7.9 that the k_0 decreases in order Ru<Pd<Pt<Ni. It is also apparent that only in case of ruthenium black catalyst, the rate of appearance of Pl 8 [H] is much higher than the rate of its further conversion. Over Pt black the ratio between the rate of

appearance and disappearance of Pl 8 [H] is the lowest in the whole group of metals studied.

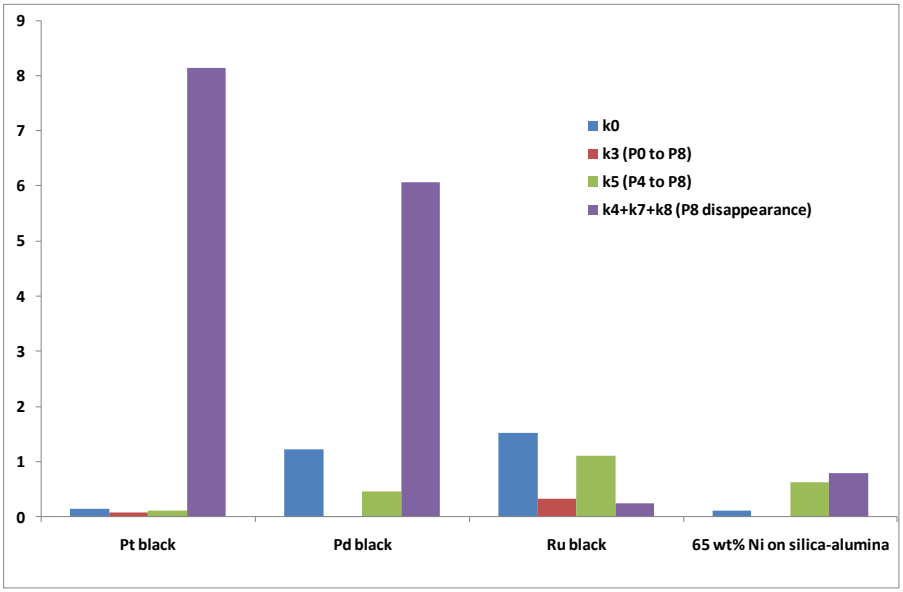

Figure 7.9. Comparison of the calculated rate constants of production and further conversion of 9-ethyl octahydrocarbazole.

Based on the ratios between the k_1, k_2 and k_0 listed in Table 7.4 it is evident that the direct formation of Pl 12 [H] B is most favourable only over ruthenium black catalyst. Over the other catalysts, the formation of this product takes place mostly via indirect pathway, through the formation of Pl 4[H] intermediate.

Table 7.4. Ratios between rate constants over catalysts tested. The numbering of the rate constants in accordance with the reaction model showed in Figure 7.2.

Catalyst	***k_1/k_0 [%]***	***k_2/k_0 [%]***
Ru black	52	27
Pd black	22	75
Pt black	1	6
65 wt % Ni/SiO_2-Al_2O_3	27	45

In addition, the values of k_0 were found to be inversely proportional to the value of the work function; the higher the work function, the lower the value of k_0 as depicted in Figure 7.10.

However it is clear from Figure 7.10 that the values for 65 wt % Ni/SiO_2-Al_2O_3 do deviate from the general pattern. This can be explained by the presence of support, which probably influences the activity of the catalyst.

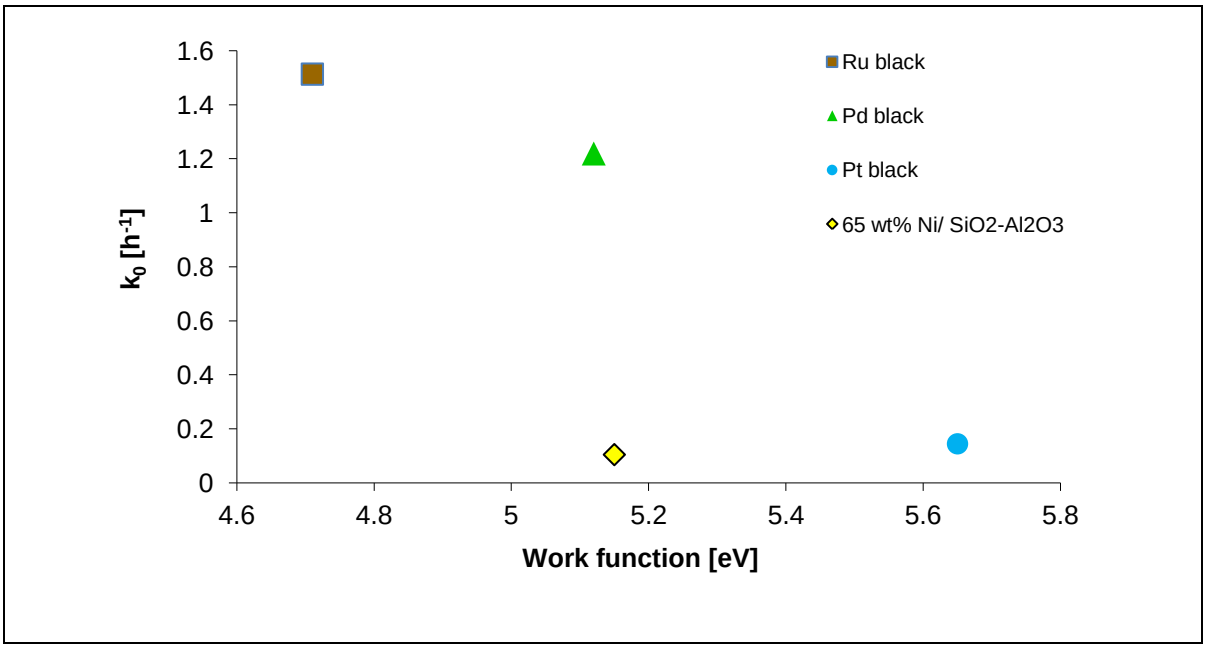

Figure 7.10. The calculated k_0 versus work function for tested catalysts.

In contrast, over Pd black the stable intermediate accumulated in the solution is Pl 4 [H] not Pl 8 [H]. Comparing the calculated rate constants over Pd catalyst, the rate of production of Pl 4 [H] is almost twice as high as the rate constant of its further conversion into Pl 8 [H]. This in turn means that the activation barrier for adsorption of this intermediate on palladium surface is high and therefore it gets accumulated in the solution As compared with Ru black, the selectivity towards Pl 4 [H] on Pd black is over 30% higher. Over Pt and Ni, no significant amounts of any of the intermediates were observed.

7.3.3.1. Variations in composition of the fully hydrogenated product over unsupported metals.

In order to experimentally obtain the most thermodynamically stable isomer of Pl 12 [H], a reaction was run with extended time (<7 days) using unsupported ruthenium black and supported 5 wt % Ru/rutile (CR). The result showed that the primary products of

the reactions were isomers Pl 12 [H] B but after the isomerisation process (showed in Figure 7.11) the composition of the final fully loaded compound displayed over 99 % selectivity towards isomer Pl 12 [H] A in case of supported catalyst and over 95 % selectivity towards the same product in case of ruthenium black. The composition of the fully hydrogenated mixtures, independently of the catalyst used, contained qualitatively the same four isomers as depicted in Figure 7.2. However, the distribution of the isomers and the rate of isomerisation reaction over each of the metals were slightly different. The compositions of the final product versus time for the catalysts studied are shown in Figure 7.12 A,B,C,D.

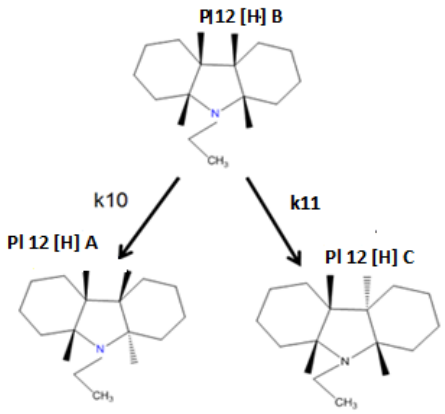

Figure 7.11. The mechanism of isomerisation of 9-ethyl-perhydrocarbazole over ruthenium based catalysts.

In the later stages of the reaction, some isomerisation of Pl 12 [H] B into Pl 12 [H] A is taking place over all of the catalysts studied (see k_{10} in Table 7.3). The isomer P 12 [H] C is produced mainly from further conversion of Pl 8 [H] or to the smaller extent by direct formation over ruthenium black catalyst. However, it should be noted that both of these reactions happen with a very slow rate. In addition, no isomerisation of Pl 12 [H] B into Pl 12 [H] C is taking place over ruthenium black. Thus, over this catalyst P 12 [H] C isomer appears as a minor product and its concentration does not increase significantly under the reaction conditions studied (Figure 7.12 A). In case of the reactions performed

over Pd black (Figure 7.12 B), the initially distinguished main product is also Pl 12 [H] B, however its concentration decreases more rapidly due to its isomerisation into Pl 12 [H] A. As it can be seen in Table 7.3, the k_{10} value over Pd black is higher than k_{10} value over Ru black catalyst. Similarly to the results over Ru black, the minor product over Pd black is isomer P 12 [H] C. However, it can be deduced from the calculated rate constants (gathered in Table 7.3) that unlike over Ru black, P 12[H] C isomer is mostly produced via isomerisation of P 12 [H] B over Pd black.

On the other hand, the 65 wt % Ni/SiO_2-Al_2O_3 and Pt black catalysts have very similar distributions of the isomers of 9-ethyl-perhydrocarbazole. Over both of these catalysts the main product is a mixture of P 12 [H] B and P 12 [H] A. Similarly to Ru black and Pd black, the minor product over Pt black (Figure 7.12 C) and over 65 wt % Ni/SiO_2-Al_2O_3 (Figure 7.12 D) is Pl 12 [H] C. However, in contrast to Ru black and Pd black, this product is observed at higher concentrations over Pt black and 65 wt % Ni/SiO_2-Al_2O_3 catalysts than over Ru black or Pd black catalysts. Moreover, unlike it was observed over Ru black and Pd black, the concentration of Pl 12 [H] C over Pt black and 65 wt % Ni/SiO_2-Al_2O_3 is not stable during the course of the reaction, but it steadily increases with time. It is apparent from Figure 7.12 D, that this product is mainly produced by isomerisation of P12 [H] B over 65 wt % Ni / SiO_2-Al_2O_3. In comparison, Pl 12 [H] C product is mainly produced directly from the substrate over Pt black catalyst. In addition, the isomerisation reaction of P12 [H] B takes place more rapidly and it is more pronounced on Pt and Ni than on Pd and Ru. This can be also observed by comparing the values of the rate constants of isomerisation reaction (k_{10} and k_{11}) gathered in Table 7.3.

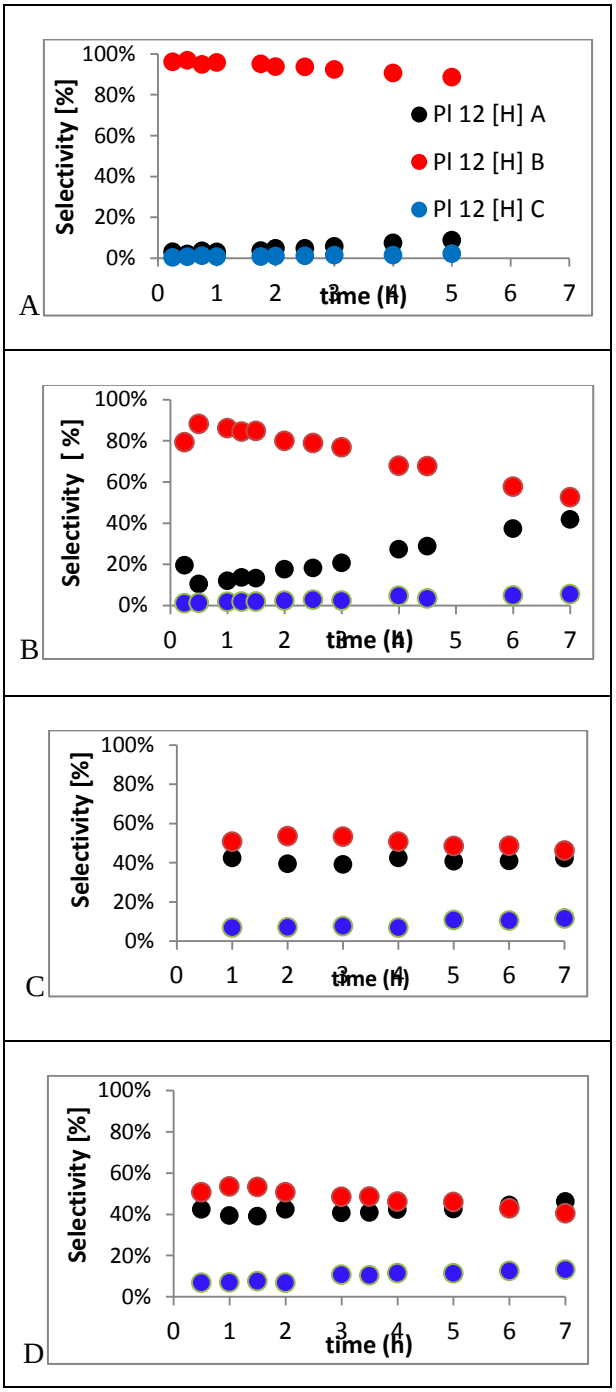

Figure 7.12 The concentrations versus time for the three 9-ethyl-perhydrocarbazole fractions at 130 °C, 70 bar obtained over :A) Ru black, B) Pd black, C) Pt black D) 65 wt % Ni/SiO_2-Al_2O_3.

7.3.4. The influence of the supported metal on the reaction rate and selectivity

After analysing the influence of the pure metal in the hydrogenation of 9-ethylcarbazole reaction, the focus was moved to the supported metals, since these catalysts are more commercially feasible due to much lower cost than their unsupported counterparts. Table

7.5 summarizes the catalytic activity and selectivity towards all the reaction products for Ru, Rh and Pd commercial catalysts all supported on activated carbon (AC). 5 wt % of Pt/ AC and 5 wt % Ni/AC were also tested under these reaction conditions; however no activity was displayed even with increased amount of catalyst to 0.3 g. Activated carbon was chosen for the support material to avoid the possibility of strong metal –support interaction (SMSI), which was reported previously for oxide supports (13).

Table 7.5. Catalytic activity and selectivity of supported catalysts after 1 h of hydrogenation reaction.

Catalyst	***Catalytic activity· 10^{-2}/mM ETC· g of metal^{-1}·s^{-1}]***	***Selectivity (%)***					
		P4[H]	***P6[H]***	***P8[H]***	***P12[H] A***	***P12[H] B***	***P12[H] C***
5 wt % Ru/ AC	27.77	1	-	32	44	19	3
5 wt % Rh/AC	13.11	0	-	6	50	38	6
5 wt % Pd /AC	4.69	58	Trace	1	24	13	4

As it can be seen in Table 7.5, the supported Ru and Rh showed very high activities, considerably higher than Pd. Similarly to the results for unsupported metals, the catalytic activity of the supported catalyst decreased in order Ru>Rh>Pd. The shift of d band position across the periodic table suggests that the metal in the right hand side of periodic table have lower d states energy as relative to the Fermi level which will consequently make the bonding with the adsorbate weaker, decreasing the conversion of the starting material and as a result, the overall activity of the catalyst.

From the data of activity and selectivity over unsupported catalysts (Table 7.2) and supported catalysts (Table 7.5), it is clear that ruthenium is the most active metal in this reaction. On the other hand, only ruthenium based catalysts lead to from accumulation of the Pl 8 [H] intermediate. These results show that the production and accumulation of 9-ethyl-octahydrocarbazole is mostly influenced by the type of the metal used, regardless of the presence, or absence of the support. It could be expected that stronger adsorption of Pl 8 [H] over Ru than other metals would lead to rapid consumption of this intermediate. However, the results obtained show the opposite. The unusual stability of Pl 8 [H] over

ruthenium catalysts could be attributed to the fact that Ru has different surface feature (hcp structure) with different surface characteristics than other metals (showing ccp structure) which facilitates the release of this intermediate, as discussed in the Chapter Five. In addition, the presence of the support does not affect the formation of Pl 8 [H], but only influences the stability of this intermediate, which tends to accumulate only when unsupported catalyst is used. The product distributions of the hydrogenation of 9-ethylcarbazole over 5 wt % Ru /AC, 5 wt % Rh/AC and 5 wt % Pd/AC are shown in Figure 7.13, Figure 7.14 and Figure 7.15 respectively.

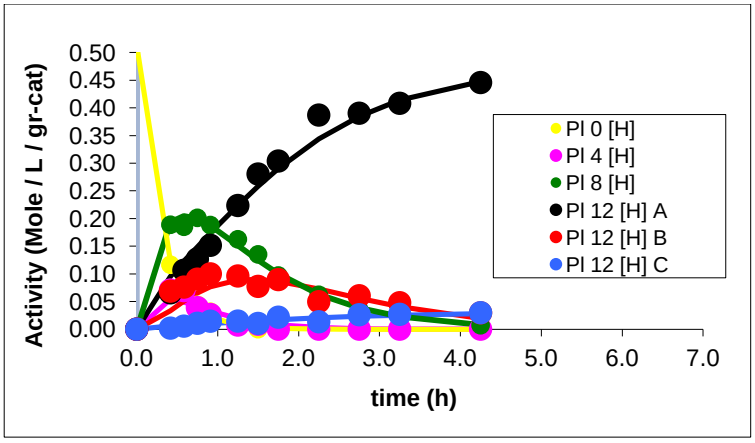

Figure 7.13 Time dependant product distribution obtained over 0.1 g of 5 wt % Ru/AC catalyst during 4.5 hours of the reaction at 130°C and 70 bar of hydrogen.

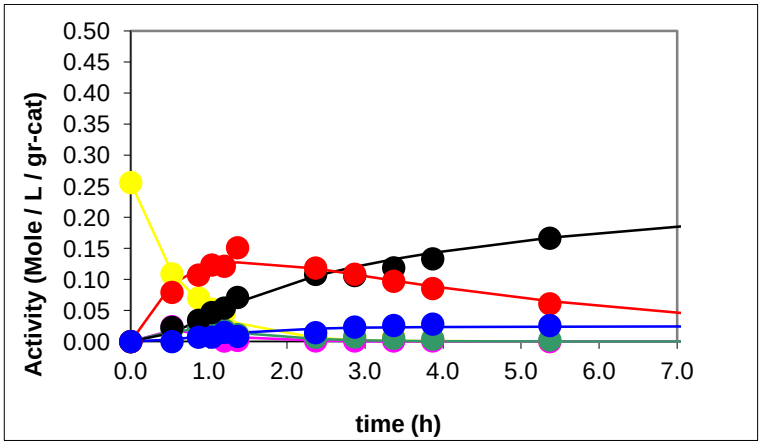

Figure 7.14. Time dependant product distribution obtained over 5 wt % Rh/AC catalyst in 5.5 hours of the reaction at 130 °C and 70 bar hydrogen together with modelled values illustrated as solid lines. The colours of the intermediates are the same as in Figure 7.13

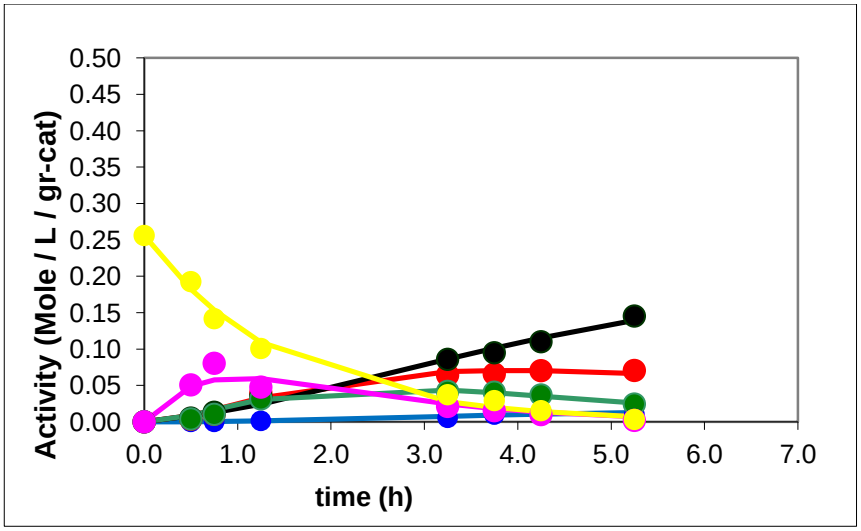

Figure 7.15. Time dependant product distribution obtained over 5 wt % Pd/AC catalyst in 5.5 hours of the reaction at 130 °C and 70 bar hydrogen together with modelled values illustrated as solid lines. The colours of the intermediates are the same as in Figure 7.13

The fitting curves indicate very good agreement of the model (see Figure 7.2) with the experimentally obtained data points for all of the supported catalysts tested. The rate constants of each step over 5 wt % Ru/AC, 5 wt % Rh/AC and 5 wt % Pd/AC catalysts used for fitting kinetic data into the model are summarised in Table 7.6.

Table 7.6. The calculated rate constant values for 5 wt % Ru/AC, 5 wt % Rh/AC and 5 wt % Pd/AC. *The amount of catalyst used was 0.1g instead of 0.2g.

Catalyst	k_0	k_1	k_2	k_3	k_4	k_5	k_6	k_7	k_8	k_9	k_{10}	k_{11}
5wt % *Ru/AC	3.4	0.6	1.6	1	0.001	3.7	0.22	0.001	1.058	0.002	0.13	0.003
5 wt % Rh/AC	3.0	1.4	0.59	0.62	0.92	1.3	0.28	0.53	0.433	0.11	0.13	0
5 wt % Pd/AC	0.33	0.049	0.22	0	0.008	0.24	0.03	0.005	9.449	0.03	0.027	0.015

Similarly to the previously observed results for unsupported catalysts (Figure 7.8), the selectivity towards Pl 8 [H] is inversely proportional to the catalyst activity, which is shown in Figure 7.16.

It is apparent that over the less electron rich metals like ruthenium or rhodium, the adsorption of the substrate is favoured, whereas on the other hand the re-adsorption of Pl 8[H] for further conversion is hindered**.** This leads to accumulation of this intermediate in the solution.

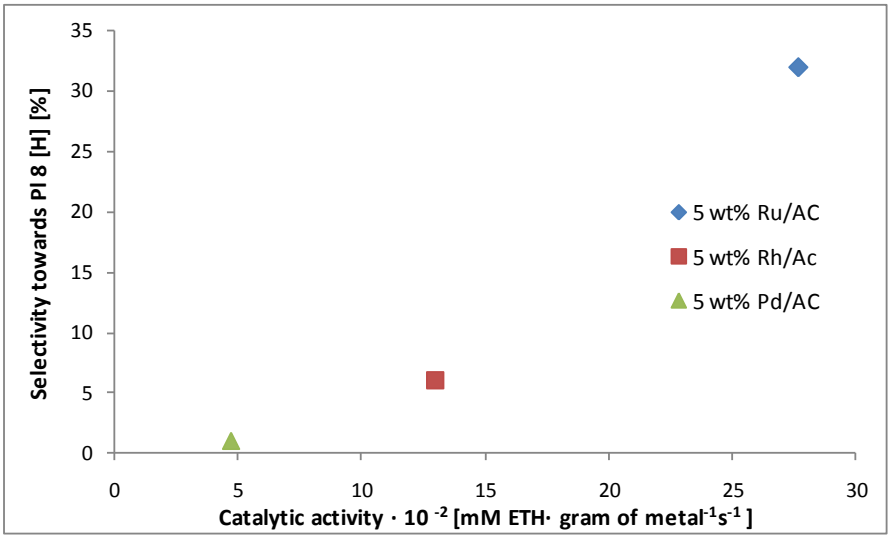

Figure 7.16 Selectivity towards Pl 8[H] versus catalytic activity of the catalyst after 1 hour of hydrogenation of 9-ethylcarbazole at 130 °C and 70 bar, in 100 ml of cyclohexane of supported catalysts.

Careful inspection of the k values listed in Table 7.6, shows that the calculated k_0 decreases in order Ru>Rh>Pd. Figure 7.17 shows the comparison of the calculated rate constants that are listed in Table 7.6. In Figure 7.17, it can be seen that over 5 wt % Ru / AC, the rate of appearance of Pl 8[H] is much higher than the rate of its further conversion. From the same figure, it is clear that the rate of production of Pl 8[H] over 5 wt % Pd / AC is much lower that the rate of its further conversion over this catalyst. The situation is similar when analysing the 5 wt % Rh / AC catalyst, however the difference between rates of appearance and disappearance of Pl 8 [H] is not as significant as in case of Pd based catalysts. It is worth noting from Figure 7.17 that the more probable way of producing Pl 8 [H] intermediate is via indirect pathway going through the Pl 4[H] intermediate, regardless of the metal type.

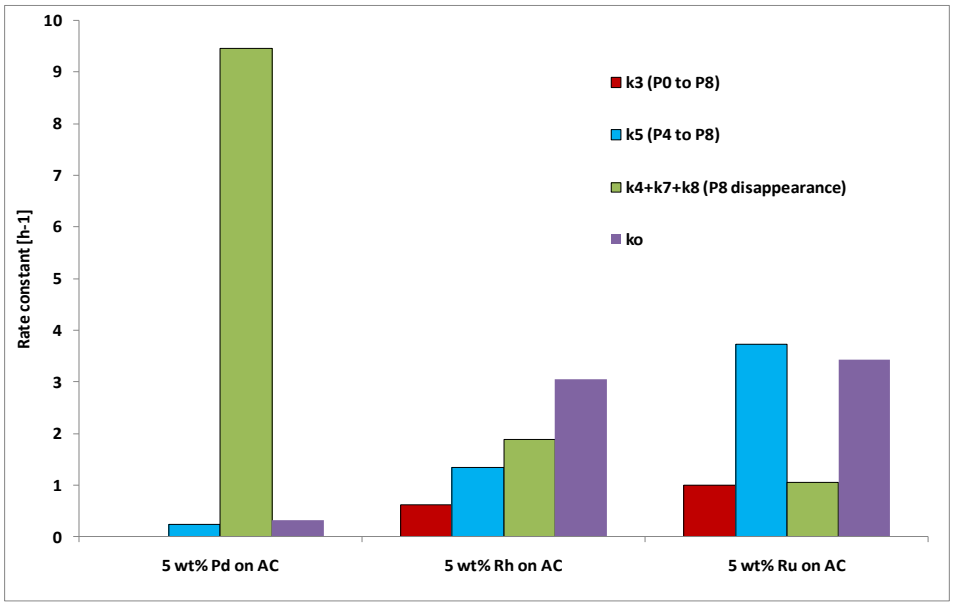

Figure 7.17. Comparison of the calculated k_0 together with rate constants of the production and disappearance of 9-ethyl-octahydrocarbazole over catalysts supported on activated carbon.

From comparing the rate constants listed in Table 7.6, it can be seen that over 5 wt % Ru / AC and 5 wt % Pd/AC, the reaction takes place mostly by consecutive addition of hydrogen atoms, whereas over rhodium based catalyst, the reaction takes place via direct hydrogenation of the substrate. No significant accumulation of any of the intermediate products was observed over rhodium based catalyst, however the total conversion of Pl 4 [H] and Pl 8 [H] is sluggish. On the contrary, the main intermediate over 5 wt % Pd / AC, similarly to the results over Pd black catalyst observed in the previous paragraph, was Pl 4 [H] (compare Figure 7.5 and Figure 7.15). This intermediate is produced in significant amounts over Pd catalysts, regardless the presence of the support. Comparing the maximum accumulation of Pl 4 [H] over Pd based supported and unsupported catalysts, it is apparent that the overall higher concentrations of Pl 4 [H] were obtained over unsupported catalyst. This result suggest that the type of active sites on the supported catalysts is more effective in further conversion of this intermediate. Additionally, supported Ru and Pd catalyst were found to be more active than their

unsupported counterparts. This can be explained by a better utilization of the metal which is in the form of smaller supported particles.

7.3.4.1. Variations in composition of the fully hydrogenated product over supported catalysts

The distribution of the isomers of the fully hydrogenated 9- ethyl-perhydroethylcarbazole was found to be similar for all of the carbon supported catalysts. The main product for supported catalysts is always Pl 12 [H] A not Pl 12 [H] B, which was the main isomer produced over unsupported Pd and Ru catalysts. As it was mentioned before, the P 12 [H] A was found to be the most thermodynamically stable isomer. It should be noted that for all of the carbon supported and unsupported Pd and Ru catalysts, the calculated rate constant for isomerisation of Pl 12 [H] B into Pl 12 [H] A is much higher than the rate constant of isomerisation of Pl 12[H] B into Pl 12 [H] C (compare Table 7.3 and Table 7.6). Moreover, the values of the isomerisation rate constants are higher in case of supported catalysts. Based on the results of supported and unsupported catalysts with different metals, it can be concluded that the composition of the final product might be mostly affected by the presence and type of the support. In addition, the selectivity towards intermediates and their type are likely to be governed by the kind of metal used, since both supported and unsupported ruthenium catalyst showed high concentration of relatively stable Pl 8 [H].

7.3.5. The influence of the support type and preparation method on performance of ruthenium catalysts

The performance of four different catalysts containing 5 wt % of Ru deposited on different carriers in hydrogenation of 9-ethylcarbazole was compared. These catalysts were synthesized by two different preparation methods; polyol (P) and mild chemical reduction

(CR) (as described in Chapter Three, paragraph 3.1). These catalysts were compared to the commercial samples (COM). Table 7.7 summarizes the catalytic activity and selectivity towards isomers of fully hydrogenated 9-ethyl-perhydrocarbazole calculated after 1 hour of the reaction. The catalytic activity was calculated according to the formula listed in Chapter Three, Equation 3.1.

Table 7.7. Catalytic activity and selectivity towards fully hydrogenated isomers after 1 hour of reaction at 130 °C, and 70 bar, using 1 g of substrate in 100 ml cyclohexane and 0.2 g of catalyst (for Ru on AC 0.1g was used to lower the conversion)

Catalyst	**Catalytic activity $\cdot 10^{-2}$ [mM ETC· gram of metal$^{-1}\cdot s^{-1}$]**	***Selectivity %***		
		Pl 12 A [H]	***Pl 12 B [H]***	***Pl 12 C [H]***
5 wt % Ru /AC (COM)	27.77	88	6	6
5 wt % Ru on rutile (CR)	13.88	21	64	15
5 wt % Ru on alumina (COM)	13.47	28	55	18
5 wt % Ru on rutile (P)	12.36	23	68	9

From the data in Table 7.7, the 5 wt % Ru/ AC (COM) catalyst showed to be much more active than its commercial counterpart with similar composition but dispersed on alumina support. This result cannot be readily explained, however better performance of the catalyst supported on activated carbon can be associated with its much smaller particle size and much higher BET surface area (see Table 7.1). It is also probable that the electronic interaction of the substrate/hydrogen could be different at the interface of materials with a change of support, which was previously reported by Hiyoshi et al. (14).

The distributions of the products and intermediates of the reactions obtained over supported ruthenium catalysts are gathered in Figure 7.18. The profile over 5 wt % Ru / AC was shown in Figure 7.13.

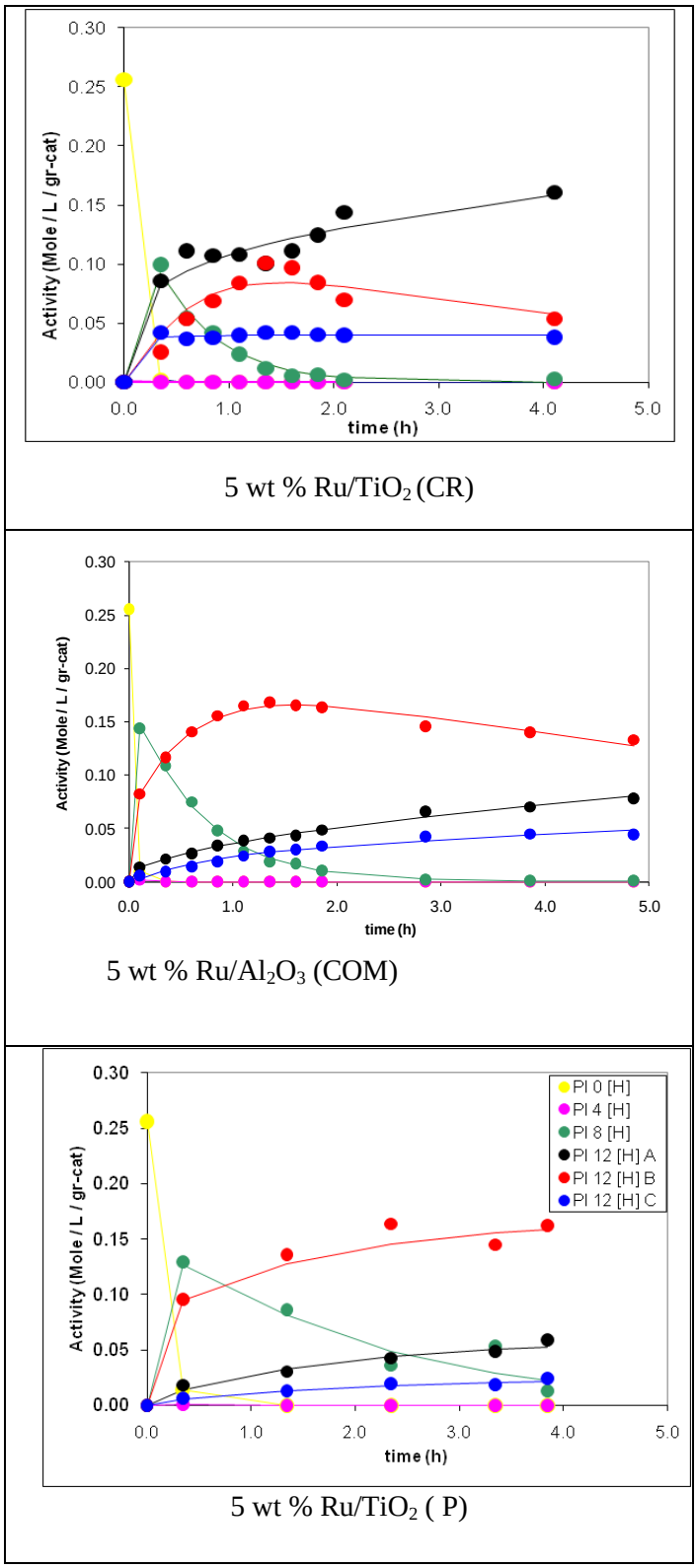

Figure 7.18. Distribution of the intermediates and products over ruthenium based supported catalysts. COM-comericial catalysts, P-catalysts synthesized by polyol process, CR-catalysts synthesized by chemical reduction.

Comparing the catalysts supported on TiO_2 (rutile) it is important to note that the support for both of these catalysts originated from the same batch of raw material. Therefore these

two catalysts differ solely by the synthesis method. Interestingly, the catalyst synthesized following mild chemical reduction showed better performance. This can be the result of the smaller particle size of this catalyst as well as its higher BET surface area (see Table 7.1). Smaller particle size of the chemically reduced catalyst can be explained by the low temperature of reduction at 90 °C, which prevents the particles from sintering. Higher temperatures of synthesis increase the mobility of surface atoms making the surface morphology of the nanoparticles more faceted (15) (16). In addition, it is apparent that the stability of Pl 8 [H] intermediate is higher over the catalyst synthesized at higher temperatures (polyol) with more flat active sites (see Table 7.1). Over 5 wt % Ru / TiO_2 (CR), the conversion of Pl 8 [H] takes around 2 hours as compared to over 4 hours in case of 5 wt % Ru/rutile (P) as showed in Figure 7.18.

Similarly to the previously reported results for other catalysts, the experimentally obtained distribution of intermediates and products over supported ruthenium catalysts fitted well to the model shown in Figure 7.2. The calculated rate constants over supported ruthenium catalysts are gathered in Table 7.8.

Table 7.8. The calculated values of rate constants for consecutive reactions obtained over supported ruthenium catalysts.*the amount of catalyst used was 0.1g instead of 0.2 g.

Catalyst	k_0	k_1	k_2	k_3	k_4	k_5	k_6	k_7	k_8	k_9	k_{10}	k_{11}
5wt % Ru/AC	3.42	0.60	1.6	1	0.001	3.7	0.22	0.001	1.1	0.002	0.13	0.003
5 wt % Ru/TiO_2	13	0.008	0.57	7.5	1.3	14.4	2.0	0.47	0.035	3.5	0	0.19
5 wt % Ru/Al_2O_3	12	0.93	0.65	9.2	1.1	16	1.4	0.22	0.19	0	0.068	0.033
5 wt % Ru/TiO_2	6.3	2.7	0.1	4.9	0.34	4.0	0.32	0.003	0.16	0.36	0	0.021

The k_0 rate constant of the most active catalyst which is listed in Table 7.8, (5 wt % Ru/AC) is lower than k_0 rate constant of other supported ruthenium catalysts. This could

be the result of the fact that smaller amount of this catalyst (0.1 g instead of 0.2 g for ruthenium supported on other supports) was used in the experiments. It should be noted that the calculated activity in Table 7.7 depends strongly on the amount of metal used. Comparing the rate constants of direct production of Pl 12 [H] isomers from the substrate (k_1, k_6 and k_9) with the rate constants of the stepwise addition of hydrogen atoms (k_2 and k_3), the reaction seems to have taken place in majority via a chain of consecutive reactions over supported ruthenium catalysts. In addition, the stepwise formation of Pl 8 [H] is more pronounced over 5 wt % Ru/AC catalyst, as it can be seen from comparison of the rate constants k_2 and k_3 in Table 7.8.

To sum up, in general, the reaction pathway undertaken by all of the tested supported ruthenium catalysts did not seem to be affected by the type of support or synthesis method used. Independently of the support used, the Pl 8 [H] appeared to be the main intermediate of the reaction over all ruthenium catalysts studied. The activity of the catalysts synthesized at higher temperatures was found to be lower. Overall, the stability of Pl 8 [H] is lower over supported than unsupported ruthenium catalysts.

7.3.5.1. Variations in composition of the fully hydrogenated product over supported ruthenium catalysts

Another main difference between ruthenium catalysts tested is the resulting composition of the final product Pl 12 [H]. For 5 wt % Ru/AC (COM), as it was mentioned before, the main product is almost entirely composed of isomer Pl 12 [H] A (with 88% selectivity). In case of other supported catalysts; the main product is isomer Pl 12 [H] B, with selectivities between 55 - 68 % of the total product composition. It can be noticed in Table 7.7. that almost identical compositions of the final Pl 12 [H] was obtained for both ruthenium catalysts supported on rutile. Thus, it is safe to conclude that

the composition of the final product is mainly influenced by the type of support present. In addition, no influence of the synthesis method or the particle size on the composition of the final product was observed. In general, the presence of support results in the composition of the Pl 12 [H] being scattered, probably due to higher rates of isomerisation reactions over small, highly defected nanoclusters as compared to the unsupported Ru black catalyst. Careful analysis of calculated rate constants listed in Table 7.8 allowed defining the more possible pathways of production of Pl 12 [H] isomers. Isomer Pl 12 [H] A is mainly produced directly from the substrate over all of the catalyst with an exception of 5 wt % Ru / AC, over which this product is created in the stepwise additions. It is interesting to note that isomer Pl 12 [H] B is produced almost exclusively via indirect pathway over 5 wt % Ru/rutile (CR), whereas over the 5 wt % Ru/rutile (P) the opposite is true, and this isomer is coming mostly from direct pathway. Isomer Pl 12 [H] C is produced mostly directly from the substrate, apart from 5 wt % Ru / Al_2O_3 (COM), when it is obtained solely via indirect pathway. These results show that the pathway of obtaining fully loaded product is affected by the type of the support and as a result, the composition of the final product is also governed by the type of support.

7.3.6. The influence of the synthesis method and support type on performance of rhodium based catalysts

Despite the fact that ruthenium is generally considered to be at best, an average catalyst in hydrogenation reactions (17) (18), our results showed clearly that ruthenium displays much higher activity as compared to other transition metals in hydrogenation of 9-ethylcarbazole. The lower, but comparable activity to ruthenium was displayed only by rhodium under our testing conditions. Rhodium based catalysts are interesting in our application because they showed much higher selectivity towards fully hydrogenated products than ruthenium along with moderate activity. Therefore, it is sensible to consider

the influence of the different factors on activity and selectivity of rhodium based catalyst. The selectivity and activity of two commercial catalysts; 5 wt % Rh on AC (described before) and 5 wt % Rh on alumina, were compared to 5 wt % Rh on AC synthesized via polyol reduction. The catalytic activity and selectivity towards all of the intermediates and products in 9-ethylcarbazole hydrogenation are gathered in Table 7.9.

Table 7.9. Comparison of the activity and selectivity of rhodium based catalysts. Reaction conditions: 0.2 g catalyst, 130 °C, 70 bar H_2, obtained in 1 hour of the reaction.

Catalyst	***Catalytic activity·10^{-2} [mM ETC· gram of metal^{-1} ·s^{-1}]***	***Selectivity (%)***				
		Pl 4[H]	***Pl 8[H]***	***Pl 12[H]A***	***Pl 12[H]B***	***Pl 12[H]C***
5 wt % Rh on AC (COM)	13.11	6	6	50	33	6
5 wt % Rh on Al_2O_3 (COM)	13.24	<1	5	29	62	3
5 wt % Rh on AC (P)	8.33	31	20	23	26	<1

From the results in Table 7.9, it is apparent that activity of commercial rhodium catalysts does not alter much with a change of support. This is in contrary to the observations made previously of ruthenium catalysts, where catalyst supported on activated carbon showed much higher activity than ruthenium supported on alumina (see Table 7.7). The activity of commercially available rhodium catalysts does not seem to depend on the size of the nanoparticles, since rhodium supported on carbon has more than twice as large particle size as rhodium supported on alumina (see Table 7.1), but their activity appears to be very similar. On the other hand, 5 wt % Rh/AC synthesized by the polyol process showed significantly lower catalytic activity. This result can be attributed to irregular shapes of these nanoparticles as shown in TEM image in Figure 7.1, which influence the type of active sites present. The active sites of this catalyst could also be blocked by the stabilizer

molecules, which could remain adsorbed on the metal surface despite the work up procedures applied. Nevertheless, this is unlikely as seen from the work of Oduro (19), who studied a very similar catalyst preparation method.

The experimental distributions of products and intermediates over rhodium based catalysts were fit to the model shown in Figure 7.2.As it can be seen from the results gathered in Figure 7.14, Figure 7.19 and Figure 7.20, the reaction pathway over rhodium catalysts was found to be described well with the proposed reaction model for ruthenium catalyst. This could be anticipated taking into consideration the positions of these two metals in the periodic table. As can be seen in Table 7.9, rhodium supported on carbon showed slightly higher selectivity towards production of Pl 4 [H] than rhodium supported on alumina. This result agrees well with the observations made for ruthenium catalysts (compare Figure 7.13 and Figure 7.18).

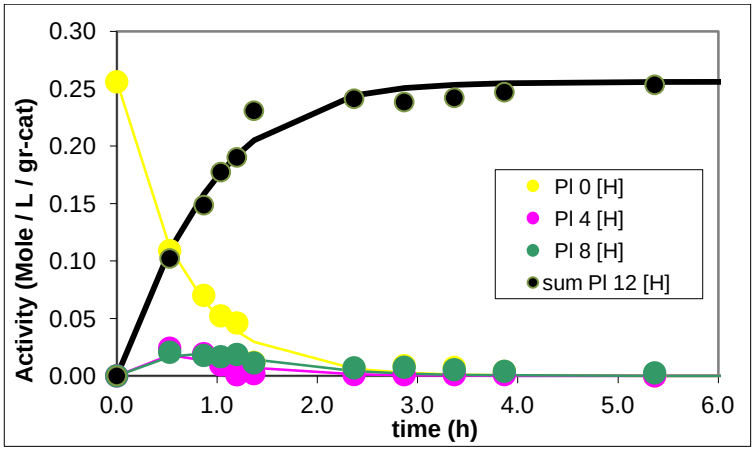

Figure 7.19. Time dependant products distribution over 5 wt % Rh/Al_2O_3 (COM) catalyst obtained in 5.5 hours of the reaction at 130 °C and 70 bar hydrogen together with modelled values illustrated as solid lines.

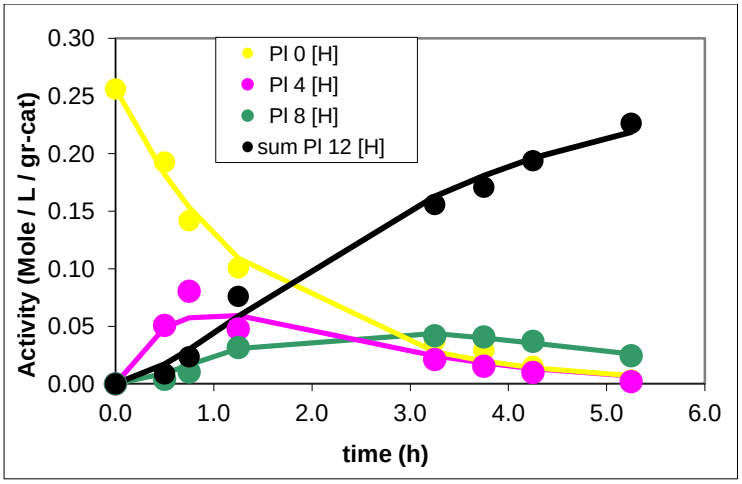

Figure 7.20. Time dependant product distribution obtained over 5 wt % Rh/AC (P) catalyst in 5.5 hours of the reaction at 130 °C and 70 bar hydrogen together with modelled values illustrated as solid lines

However, independently of the support used, both commercial rhodium catalysts showed similar selectivity towards Pl 8 [H] (see Table 7.9), unlike in the case of supported ruthenium catalysts, where 5 wt % Ru/AC showed higher concentrations of Pl 8 [H] in the solution (see Figure 7.13 and Figure 7.18). On the other hand, 5 wt % Rh on AC (P) shows significantly different behaviour than the commercial samples. Firstly, the selectivity towards Pl 4 [H] is higher than the selectivity towards Pl 8 [H] over this catalyst. This can be associated with the shape of the polyol synthesized rhodium nanoparticles which is not only spherical, but also elongated (see Figure 7.1). Other shapes than spherical may lack the active sites for further conversion of this intermediate and therefore it gets accumulated in the solution. The rate constants used to fit the experimental data into the model, are gathered in Table 7.10.

Table 7.10. The calculated rate constant values for 5 wt % Rh/Al_2O_3 (COM), 5 wt % Rh/AC (COM) and 5 wt % Rh / AC (P).

Catalyst	k_0	k_1	k_2	k_3	k_4	k_5	k_6	k_7	k_8	k_9	k_{10}	k_{11}
5 wt % Rh/Al_2O_3 (COM)	1.6	1.1	0.50	0	0.004	3.6	0	0.71	1.9	0	0.21	0.004
5 wt % Rh/AC (COM)	3.0	1.4	0.59	0.62	0.92	1.3	0.28	0.53	0.43	0.11	0.126	0
5 wt % Rh/AC (P)	1.1	0.073	0.52	0	0.87	1.0	0.09	0	0	0.43	0.046	3.7

Comparing the values of rate constants listed in Table 7.10, it can be concluded that regardless of the synthesis method or type of support, the 9-ethylcarbazole hydrogenation over rhodium based catalysts takes mostly the direct pathway. The direct synthesis of the Pl 8 [H] intermediate (k_3 in Table 7.10) takes place over 5 wt % Rh/AC (COM) and the direct synthesis of Pl 12 [H] A and Pl 12 [H] C take place with over both catalysts supported on activated carbon.

7.3.6.1. Variations in composition of the fully hydrogenated product over supported rhodium catalysts

The composition of the final fully saturated product is almost identical over both rhodium catalysts supported on carbon. The final product distribution versus time for 5 wt % Rh /AC (COM) is shown in Figure 7.21. Independently of the synthesis method used, the main product for rhodium supported on activated carbon catalysts similarly to 5 wt % Ru/AC is isomer Pl 12 [H] A. Based on the calculated rate constants gathered in Table 7.10, in the case of 5 wt % Rh /AC (P), this isomer is produced mostly directly from starting material.

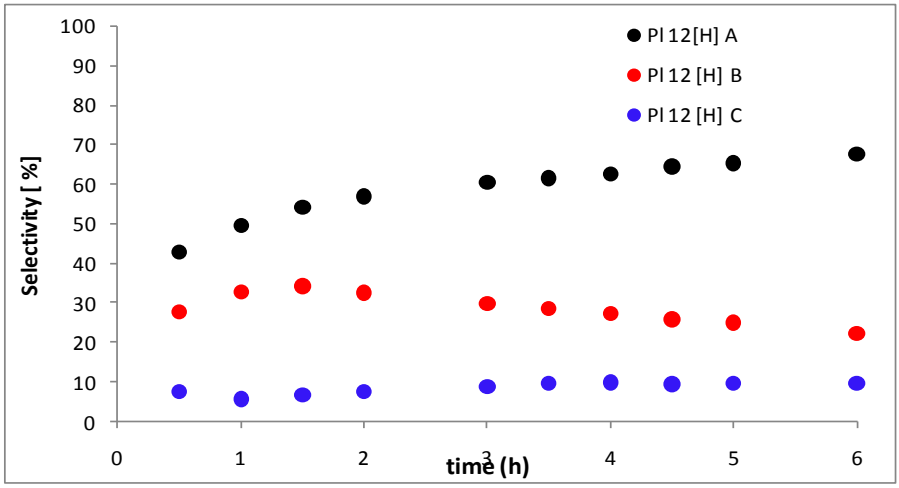

Figure 7.21. The concentrations versus time for the three 9-ethyl-perhydrocarbazole isomers at 130 °C, 70 bar obtained using 5 wt % Rh/AC (COM).

On the other hand, based on the rate constants gathered in Table 7.10, in the case of 5 wt % Rh/AC (COM), this product is made indirectly, from the Pl 8 [H] intermediate. In addition, over 5 wt % Rh/AC (COM) only isomerisation from Pl 12 [H] B into Pl 12 [H] A is likely to take place. On the contrary, over 5 wt % Rh /AC (P), the isomerisation reaction from Pl 12 [H] B into Pl 12 [H] C has much higher rate constant (see Table 7.10).

The composition of the final product over 5 wt % Rh / Al_2O_3 is significantly different. From the beginning of the reaction over 5 wt % Rh / Al_2O_3, the main product is Pl 12 [H] B (see Figure 7.22), similarly to the observations made for 5 wt % Ru/Al_2O_3. However, during the progress of the reaction, isomer Pl 12 [H] B undergoes isomerisation into Pl 12 [H] A. These results agree well with the previously made observation that the composition of the final product depends on the support used, not on the metal itself. Activated carbon support tends to favour the thermodynamically most stable isomer from the first minutes of the reaction. Whereas over alumina supported catalysts, the production of Pl 12 [H] B is more favoured. Based on the calculated rate constants, the isomerisation of Pl 12 [H] B into Pl 12 [H] C is very scarce over 5 wt % Rh / Al_2O_3 (COM), similarly to the results observed over 5 wt % Ru / Al_2O_3 (COM) catalyst.

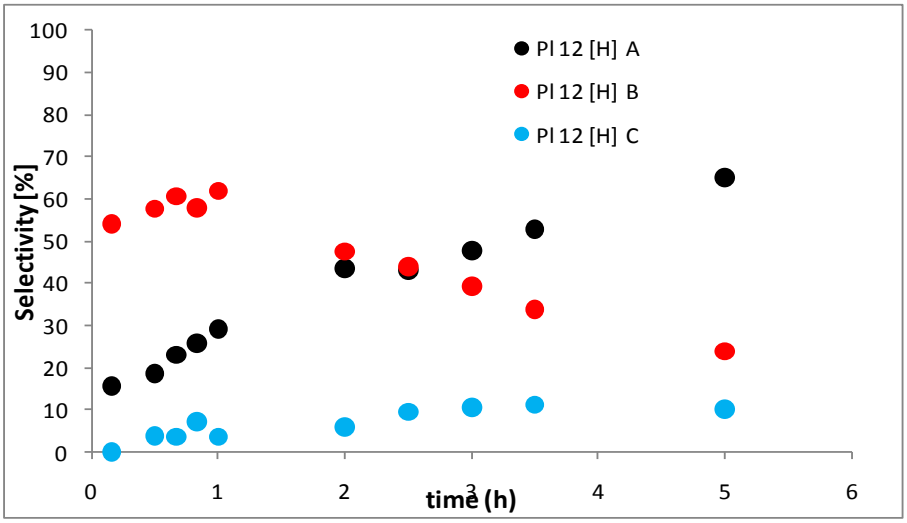

Figure 7.22. The concentrations versus time for the three 9-ethyl-perhydrocarbazole isomers at 130 °C, 70 bar using 5 wt % Rh / Al_2O_3 (COM).

7.4. Conclusions

The catalytic hydrogenation of 9-ethylcarbazole on the surface of metals involves a series of consecutive reactions of hydrogen addition to double bonds, most of them running parallel to each other. Independently of the catalyst used, the main products of the reaction are the same, excluding Ni based system, which additionally produces Pl 6 [H] intermediate. In addition, the main product of the hydrogenation always contains a mixture of stereoisomers, independently of the catalyst used. The isomerisation reaction towards the most stable product (Pl 12 [H] A) is always observed, regardless of the catalytic system used. However, it should be noted that the isomerisation reaction is more prominent over supported catalysts. From the point of view of spent fuel recovery, the production of a mixture of trans isomers of 9-ethyl-perhydrocarbazole in hydrogenation of 9-ethylcarbazole, would not be desirable due to the foreseen low rates of dehydrogenation of these isomers as compared to cis isomers of the fully hydrogenated compound.

The supported catalysts were found to be more active than the unsupported ones due to the higher dispersion and therefore better availability of active sites. The activity of the catalyst was found to be dependent on the synthesis method used in case of Ru and Rh

based systems. In addition, higher stability of intermediates (Pl 4 [H] or Pl 8 [H]) was observed over unsupported Pd and Ru than over their supported counterparts. The very stable intermediate, Pl 8 [H] was produced at high quantities only over ruthenium based catalysts; however some lower amounts were also detected over rhodium and palladium catalysts. In addition, this product was found to be stable only over ruthenium based catalysts. When comparing the stability of this intermediate over supported and unsupported ruthenium catalysts, Pl 8 [H] takes significantly much longer time for further conversion over unsupported catalyst. This can be due to the differences in the type of active sites on the surface Ru black catalyst. However, it is clear that the production and further conversion of this intermediate is governed solely by the type of metal. When metals other than ruthenium are used, the selectivity towards Pl 8 [H] decreases with more electron rich metals. In addition, the type of the support does not alter the main hydrogenation pathway; however it influences the concentrations of the intermediates. The highest concentration of Pl 8[H] was recorded over ruthenium supported on activated carbon. The type of support can also influence the composition of the isomers of the fully hydrogenated product.

To sum up, on the basis of the hydrogenation results, it can be stated that closely related metals such as ruthenium and rhodium were found to be the most active for hydrogenation of 9-ethylcarbazole, while palladium, nickel and platinum were not suitable for this hydrogenation. It is clear that ruthenium is the most active metal in this reaction however it suffers from relatively low selectivity, due to the production and accumulation of large quantities of the Pl 8 [H] intermediate. However, it is suggested that its selectivity could be improved by modifying its electronic structure by addition of a second metal, such as rhodium which showed a greater capacity to further hydrogenate the Pl 8 [H] intermediate. Further work would be necessary to fully clarify this point. In addition, for the application

as a hydrogen storage material, it is more favourable to impede the isomerisation reaction of cis to trans isomers in order to prevent the possible system reversibility problems brought about by geometrically hindered adsorption of trans isomers on the surface of the catalysts.

7.5. References

1. *Special sites at noble and late transition metal clusters.* **B. Hammer,** Top. Catal, 2006, Vol. 37.
2. *Structure effects in hydrogenation reactions on noble metal catalysts.* **P. Kacer, L.Cerveny,** Appl. Catal. A, 2002, Vol. 229.
3. *Handbook of heterogenous catalysis.* **M. Boudart, G. Ertl, H. Knozinger, J. Weitkamp,** VCH Weinheim, 1997.
4. *Heterogenous catalysis: Principles and applications.* **G.C. Bond,** Oxford University Press, 1987.
5. *A molecular view of heterogenous catalysis.* **C.H. Christensen, J.K. Norskov,** J. Chem. Phys, 2008, Vol. 128.
6. *Advancing the frontiers in nanocatalysis, biointerfaces and renewable energy conversion by innovations of surface techniques.* **G.A. Somorjai, H. Frei, J.Y. Park,** J. Am. Chem. Soc, 2009, Vol. 131.
7. *Regioselective catalytic hydrogenation of polycyclic aromatic hydrocarbons under mild conditions.* **P. P. Fu, H. M. Lee, R. G. Harvey,** J. Org. Chem, 1980, Vol. 45.
8. *Kinetic study on hydrogenation of isoquinoline over supported ruthenium catalysts.* **H. Okazaki, M. Soeda, Y. Ikefuji, R. Tamura, I. Mochida,** Bull. Chem. Soc. Jpn., 1989, Vol. 62.
9. *The reactivities of polyaromatic hydrocarbons in catalytic hydrogenation over supported noble metals.* **K. Sakanishi, M. Ohira, I. Mochida, H. Okazaki, M. Soeda,** Bull. Chem. Soc. Jpn, 1989, Vol. 62.
10. *Kinetic interpretation of periodic trends in heterogeneous catalysis.* **S. Kasztelan,** Appl. Catal. A. Genal, 1992, Vol. 83.
11. *Ligands effects in heterogenous catalysis and electrochemistry.* **T. Bligard, J. K. Norskov,** Electrochim. Acta, 2007, Vol. 52.
12. *Why gold is the noblest of all the metals.* **B. Hammer, J. K. Norskov,** Nature, 1995, Vol. 376.
13. *Strong metal -support interactions.* **S. J. Tauster,** Acc. Chem. Res., 1987, Vol. 20.
14. *Low temperature hydrogenation of tetralin over supported rhodium catalysts in supercritical carbon dioxide solvent.* **N. Hiyoshi, E. Mine, C.V. Rode, O. Sato, M. Shirai,** Appl. Catal. A., 2006, Vol. 310.
15. *Synthesis of silver nanoparticles using the polyol process and the influence of precursor injection.* **D. Kim, S. Jeong, J. Moon,** Nanotechnol, 2006, Vol. 17.
16. *Physical ceramics.***V. Chiang, T. Birnie, L. Kingery.** Wiley and Sons, 1997.
17. *Influence of the trace oxygen on the hydrogenation activity of Ru/Al_2O_3 catalyst.* **H. Seki, M. Ohshima, H. Kurokawa, H. Miura,** Reac. Kinet Mech Cat, 2010, Vol. 101.
18. *Stereoselective hydrogenation of tetralin to cis-decalin over a carbon-supported.* **N. Hiyoshi, E. Mine, C. V. Rode, O. Sato, M. Shirai,** Chem. Lett, 2006, Vol. 35.
19. *Towards ultra-selective hydrogenation and hydrogenolysis: A nano engineering approach to heterogenous catalyst design.* **W. O. Oduro,** University of Oxford, 2009. DPhil thesis.

8. Structure- reactivity correlation. Liquid phase hydrogenation of various heterocyclic compounds over ruthenium black catalyst

8.1. Introduction

The specific hydrogenation activity and selectivity of arenes are strongly affected not only by the catalyst used, but also by the structure of the substrate. As a result, in order to design new liquid organic carriers with improved kinetics and thermodynamics of reversible hydrogenation/dehydrogenation process, it is very important to understand the correlation between the structure of the carrier and its ability to hydrogenate/dehydrogenate. The reaction conditions, the amount, type and mobility of surface transition states and the intermediates can all strongly affect the activity in the hydrogenation reaction. In most of the hydrogenation reactions reported in the literature, the direct nature of the catalyst-reactant interaction is unknown. The selectivity in the hydrogenation of aromatic compounds is governed mainly by the adsorption mode of the substrate on the metal and therefore the position of the first hydrogenated bond (1). From the point of view of hydrogen storage applications, the hydrogenation (hydrogen loading step) must result in full conversion towards fully loaded product avoiding any competitive reactions taking place. Any side routes such as isomerization, cracking, or opening/contraction of the aromatic ring (2) would detriment the hydrogen capacity of the system as well as lead to very expensive purification procedures. Thus, the knowledge of the nature of correlations of catalyst and heterocyclic compound structure is crucial in order to rationally tailor the appropriate structure of future high capacity LOH.

In the previous chapters, a reversible hydrogen storage system based on 9-ethylcarbazole as a prototype of liquid organic carriers (LOH) was studied. It was found that the hydrogenation of 9-ethylcarbazole over commercial ruthenium black catalyst resulted in

the formation of a very stable intermediate; 9-ethyl-octahydrocarbazole (Pl 8 [H]), which decreased considerably the selectivity of the reaction towards fully loaded products. The formation of such stable intermediate products should be avoided in liquid organic hydrides storage systems in order to preserve the theoretical capacity of the material.

The focus of the following chapter is to investigate the influence of the structure of the heterocyclic compound on the formation of stable intermediates during hydrogenation (fuel recovery) process over a ruthenium black commercial catalyst. The structural features of the candidate carriers which could lead to undesired side reactions, poisoning of the catalyst's active sites, possible steric hindrance effects or slower overall hydrogen uptake kinetics will be remarked.

8.2. Experimental

8.2.1. Materials

All of the studied heterocyclic compounds, 1,4-dioxane and ruthenium black catalyst were purchased from Sigma-Aldrich. The structures of the compounds and their physical characteristics can be found in Chapter Three, Table 3.1. The physical properties of this catalyst can be found in Chapter 4, Table 4.1. XPS and TPR and HRTEM studies of Ru black catalyst together with metal area and dispersion are described in Chapter 5 together with HRTEM images of this catalyst. The selection of catalyst for study of the catalyst-LOH structure correlation was motivated by the fact that a stable intermediate was previously found to be formed over this catalyst during the hydrogenation of 9-ethylcarbazole. It would be of interest to find out if similar stable intermediates are formed over this catalyst during the hydrogenation of other heterocyclic compounds with slightly different structures.

8.2.2. Methods

A series of polycyclic heteroaromatic compounds with minor variations in chemical structures were hydrogenated in the liquid phase (using dioxane as a solvent) in a stainless steel batch-type Parr autoclave reactor according to the procedure described in Chapter Three. The hydrogenation reactions were performed in the conditions used previously for the hydrogenation of 9-ethylcarbazole that resulted in the production of a stable Pl 8 [H] intermediate, as described in Chapter Five. The structures of the final products and intermediates of the reactions were assigned based on their mass spectra and the database available with an Agilent 6890-5975E GC-MS system. The details of GC-MS analyses are described in Chapter Three.

8.3. Results and discussion

In the current chapter, the structures of the polycyclic heteroaromatic compounds were chosen in order to investigate the influence of the systematic variation of structural aspects of a reactant molecule on the compound's ability to be recharged with hydrogen (hydrogenated). The investigated structural factors include; difference in chain length and composition of the side chain, influence of partial hydrogenation of the substrate, substitution of the pyrrole ring (five membered ring) with pyridinic ring (six membered ring) and the influence of the presence and type of other heteroatom(s).

8.3.1. Influence of the length and composition of the side chain

The hydrogenation pathways of carbazole and 9-H-Carbazole -9-ethanol were compared with the results obtained for the 9-ethylcarbazole. All of these molecules have the same arrangement of 5-membered nitrogen-containing ring fused between two six-member aromatic rings. The only difference between these structures is the length and composition

of the side chain attached to the nitrogen. The structures of these compounds are gathered in Figure 8.1.

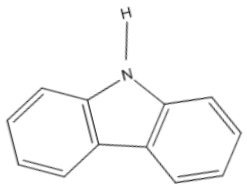	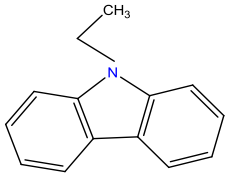	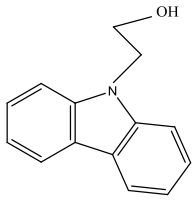
Carbazole	***9-ethylcarbazole***	***9H-carbazole-9-ethanol***

Figure 8.1. Chemical structures of heterocyclic polyaromatic compounds with different length and composition of the side chain attached to heteroatom.

8.3.1.1. Hydrogenation of carbazole

Carbazole has the shortest side chain that consists of a single hydrogen atom (see Figure 8.1). It has therefore the lowest molecular mass and the highest theoretical hydrogen uptake capacity of the three heterocyclic structures considered here. Carbazole is a non-basic nitrogen compound. Non-basic compounds were previously reported to be more difficult to hydrogenate than their basic counterparts (3). Carbazole has the highest melting point of 248 °C as compared to 60 °C for 9-ethylcarbazole or 78 °C for 9-H-Carbazole-9-ethanol. The melting point of the latter is increased by the presence of the –OH group (primary alcohol). The high melting point of carbazole will unavoidably create obstacle for solvent free-reversible hydrogenation under desirable/favourable conditions.

The following intermediates and products were found in the hydrogenation of carbazole over ruthenium black: tetrahydro-carbazole (Pl 4[H]), hexahydro-carbazole (Pl 6 [H]), octahydro-carbazole (Pl 8 [H]) and three stereoisomers of the fully hydrogenated perhydro-carbazole (Pl 12 [H]). It should be noted that the main isomer found was Pl 12 [H] C with selectivity reaching over 90 %. Similar products were previously observed in the hydrogenation of carbazole over supported ruthenium (4) and molybdenum catalyst (3). Moreover, the obtained products are similar to the products of 9-ethylcarbazole

hydrogenation over ruthenium black, with the exception of (Pl 6 [H]) which was produced in much lower quantities in the hydrogenation of the latter. Based on the concentration-time profiles obtained experimentally, the reaction model of hydrogenation of carbazole was developed as shown in Figure 8.2. The calculated rate constants for each of the intermediate reactions are gathered in Table 8.1. Comparing the rate constants gathered in Table 8.1, it can be seen that the preferred reaction pathway is undoubtedly the direct formation of the product Pl 12 [H] C.

Table 8.1. First order rate constants of hydrogenation of carbazole over ruthenium black catalyst

$\mathbf{k_0}$ **(h^{-1})**	0.57
$\mathbf{k_{0\text{-}12C}}$ **(h^{-1})**	0.30
$\mathbf{k_{8\text{-}12C}}$ **(h^{-1})**	0.029
$\mathbf{k_{0\text{-}4}}$ **(h^{-1})**	0.20
$\mathbf{k_{4\text{-}8}}$ **(h^{-1})**	0.30
$\mathbf{k_{6\text{-}12A}}$ **(h^{-1})**	0.03
$\mathbf{k_{0\text{-}6}}$ **(h^{-1})**	0.07
$\mathbf{k_{8\text{-}12A}}$ **(h^{-1})**	0.11
$\mathbf{k_{0\text{-}12B}}$ **(h^{-1})**	0.0
$\mathbf{k_{4\text{-}12C}}$ **(h^{-1})**	0.89

In accordance to the model in Figure 8.2 and the calculated rate constants, the hydrogenation of carbazole can take place directly, via adsorption on flat surface of the catalyst, resulting in the formation of the Pl 12 [H] C and Pl 12 [H] B isomers of perhydro-carbazole. Another parallel route is via the Pl 4 [H] intermediate, which leads to the formation of the Pl 12 [H] C isomer or the Pl 12 [H] A isomer via the Pl 8 [H] intermediate. The last possible hydrogenation pathway of carbazole is via Pl 6 [H] which can produce the fully loaded Pl 12 [H] A.

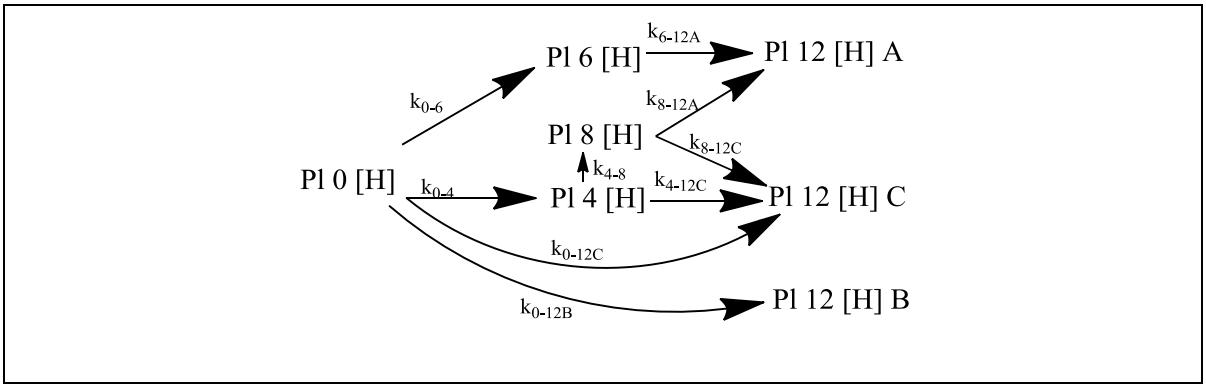

Figure 8.2. The developed model for hydrogenation of carbazole over ruthenium black catalyst together with indicated rate constants.

The experimental data showed very good agreement with the values predicted using the developed model for this reaction, which can be seen in the plot of product distribution over time plot shown in Figure 8.3. As it can be seen in this figure, the results confirm that the hydrogenation of carbazole is well described by the simplified first order kinetic model shown in Figure 8.2. The product distribution in time depicted in Figure 8.3 suggests that Pl 8 [H] is one of the main intermediates with moderate stability in this reaction. However, this octahydro-carbazole intermediate is considerably less stable as compared to the 9-ethyl-octahydrocarbazole intermediate in the hydrogenation of 9-ethylcarbazole. After extended periods of reaction time (20 hours) only nearly 4% of this intermediate was detected in the reaction mixture. On the contrary, in the hydrogenation of 9-ethylcarbazole, the concentration of Pl 8 [H] intermediate did not change up significantly to 30 hours of reaction and totaled around 40% of the reaction products.

The aromatic rings of carbazole have relatively strong affinity to the cation sites (5) and therefore the possible adsorption modes would be parallel or perpendicular to the metal surface. However, because the electron density on the aromatic ring and on the nitrogen atom is distributed evenly, carbazole is more probable to adsorb flat on the catalyst surface to maximize the interactions with the surface sites.

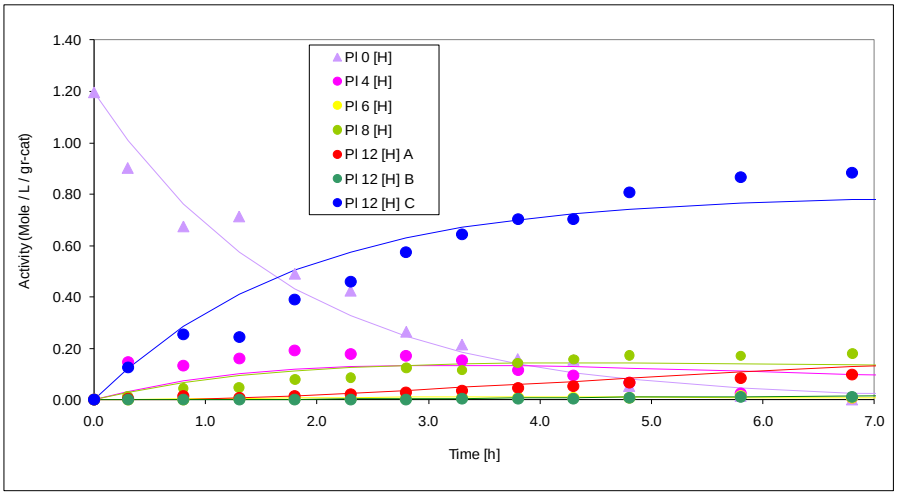

Figure 8.3. Product distribution in time for carbazole hydrogenation over ruthenium black catalyst. The acronyms of the intermediates as explained in the text.

However, once the aromaticity is broken by hydrogenation of at least one double bond in the ring, the lone pair of electrons becomes more localized on the nitrogen atom, making it more available for binding to the metal surface (6). In addition, there is no stereochemical barrier from side chains around nitrogen in the carbazole structure and its intermediates to hinder the interaction between the approaching molecule and the catalyst active sites. Therefore, the mode of adsorption may change from parallel adsorption of substrate into perpendicular adsorption of the intermediate on the surface of the metal catalyst. The perpendicular adsorption of the Pl 8 [H] intermediate on the catalyst surface via interaction of a lone pair of electrons will then be more strongly binded in the case of octahydro-carbazole than it was in the case of 9-ethyl-octahydrocarbazole. This can explain the lower kinetic stability of octahydro-carbazole as opposed to 9-ethyl-octahydrocarbazole. In addition to the consecutive hydrogenation of carbazole, no other reactions such as bond scission or/and ring opening were observed. However, similarly to the observation made in case of 9-ethylcarbazole over ruthenium black, the isomerization reactions of the fully saturated Pl 12 [H] products were noted, however the rate constants of these reactions were not significant and hence not reported in Table 8.1.

8.3.1.2. Hydrogenation of 9 H-carbazole-9 ethanol

9-H-carbazole-9 ethanol has the longest side chain attached to nitrogen that consists of CH_2-CH_2-OH. Because of the presence of the –OH group, it is easily soluble in polar solvents and has higher melting and boiling point than the 9-ethyl-carbazole. However, in contrast to carbazole, the melting point of 9 H-carbazole-9 ethanol (78 °C), would still make the reversible hydrogenation in the molten state possible. Unfortunately, the length of the side chain decreases its theoretical hydrogen uptake capacity (5.4 wt %) as compared to that of carbazole (6.7 wt %) or 9-ethylcarbazole (5.8 wt %).

The identified products in hydrogenation of 9 H-carbazole-9-ethanol suggest that the reaction mechanism relied also on the consecutive addition of hydrogen atoms to the double bonds in the ring. The following products have been found in the reaction solution: 9 H-tetrahydrocarbazole-9-ethanol (Pl 4 [H]), 9 H hexahydrocarbazole-9-ethanol (Pl 6 [H]) 9 H octahydrocarbazole-9-ethanol (Pl 8 [H]) and only one isomer of the fully hydrogenated 9 H-perhydrocarbazole-9-ethanol (Pl 12 [H]). Based on the concentration versus time plots of the substrate and the intermediates, the model for hydrogenation of 9-H-carbazole-9-ethanol was developed and it is shown in Figure 8.4. The calculated rate constants for each of the intermediate reactions are gathered in Table 8.2.

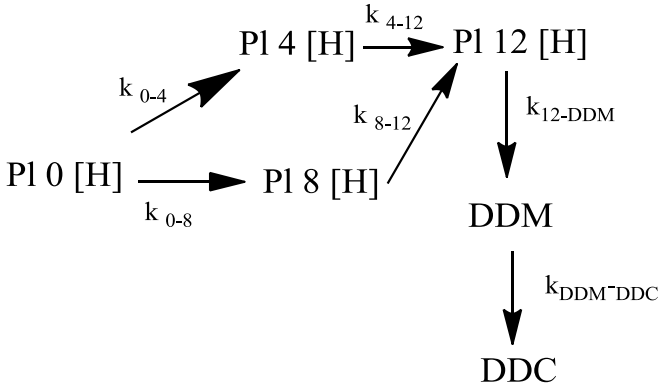

Figure 8.4. Reaction model of 9-H-carbazole-9-ethanol over ruthenium black. DDM - 9-H-dodecahydro-methyl-carbazole-9-ethanol and DDC-9-H-dodecahydro-carbazole-9-ethanol.

According to the developed model, there are two parallel routes for the hydrogenation reaction; one is hydrogenation of the substrate to form Pl 12 [H] via the Pl 8 [H] intermediate. This intermediate has an analogue structure to the structure of 9-ethyl-octahydrocarbazole. It is believed that Pl 8 [H] is produced via flat adsorption on the catalyst surface and through simultaneous hydrogenation of both of the rings, leaving the pyrrolic ring untouched. Due to the geometrical constraints of the structure of this intermediate, its re-adsorption on the surface of ruthenium black catalyst is hindered and as a result the rate constant of conversion of Pl 8 [H] to Pl 12 [H] is much lower than the rate constant of Pl 8 [H] production (see Table 8.2). The alternative hydrogenation pathway of 9 H-carbazole-9-ethanol is via the formation of the Pl 4 [H] intermediate. The Pl 4 [H] intermediate is rapidly converted into the final product and the rate constant of this reaction is one order of magnitude higher than the rate constant of production of Pl 12 [H] from Pl 8 [H].

Table 8.2. First order rate constants for hydrogenation of 9H-carbazole-9-ethanol over ruthenium black catalyst.

k_0 [h^{-1}]	1.3
k_{0-4} [hr^{-1}]	0.78
k_{0-8} [h^{-1}]	0.54
k_{8-12} [h^{-1}]	0.10
k_{4-12} [h^{-1}]	1.02
k_{12-DDM} [h^{-1}]	0.04
$k_{DDM-DDC}$ [h^{-1}]	0.62

As it can be seen in Figure 8.4, apart from the products of the consecutive hydrogenation, two other compounds namely; 9-H-dodecahydro-carbazole-9-ethanol (DDC) and 9-H-dodecahydro-methyl-carbazole-9-ethanol (DDM) were identified in the reaction solution. These compounds are the products of stepwise hydrogenolysis of the side chain attached to nitrogen in 9 H-perhydro-carbazole-9-ethanol. The possible pathway of the

Pl 12 [H] hydrogenolysis with the structures of products is shown in Figure 8.5. It is interesting to note that the hydrogenolysis of the side chain takes place only after the complete saturation of the aromatic rings. The terminal -OH may play a role in enhancing the adsorption of the side chain of the molecule on the surface of the catalyst and therefore increase hydrogenolysis reactivity (7). In the hydrogenolysis of 9H-carbazole-9-ethanol, the rupture of C-C bonds and of the C-N bond takes place. The dissociation energy of C-C and C-N are almost identical (± 80 kcal/mole) (8), therefore the order of the bond rupture is probably dictated by steric effects and it is possible that these reactions take place simultaneously/competitively or as a consecutive/stepwise reaction (see

Figure 8.5). However, in our model, we have considered only the step-wise hydrogenolysis from Pl 12 [H] to DDC to DDM, since the fitted rate constants for the other reactions were close to zero.

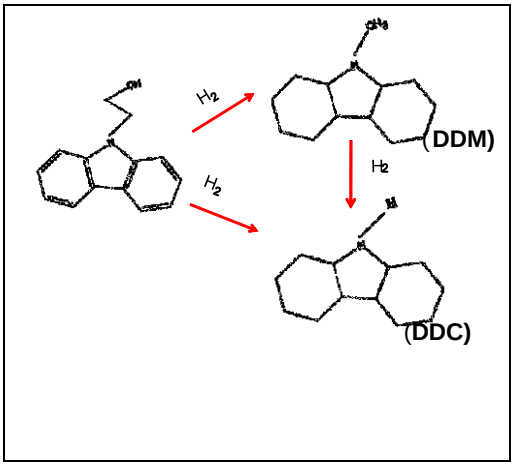

Figure 8.5. The possible reaction pathways of hydrogenolysis of the side chain of 9-H-perhydro-carbazole-9-ethanol over ruthenium black catalyst. The acronyms are explained in the text.

The hydrogenation of 9 H-carbazole-9-ethanol over ruthenium black catalyst showed very good agreement with the developed first order reaction model as it can be seen in Figure 8.6.

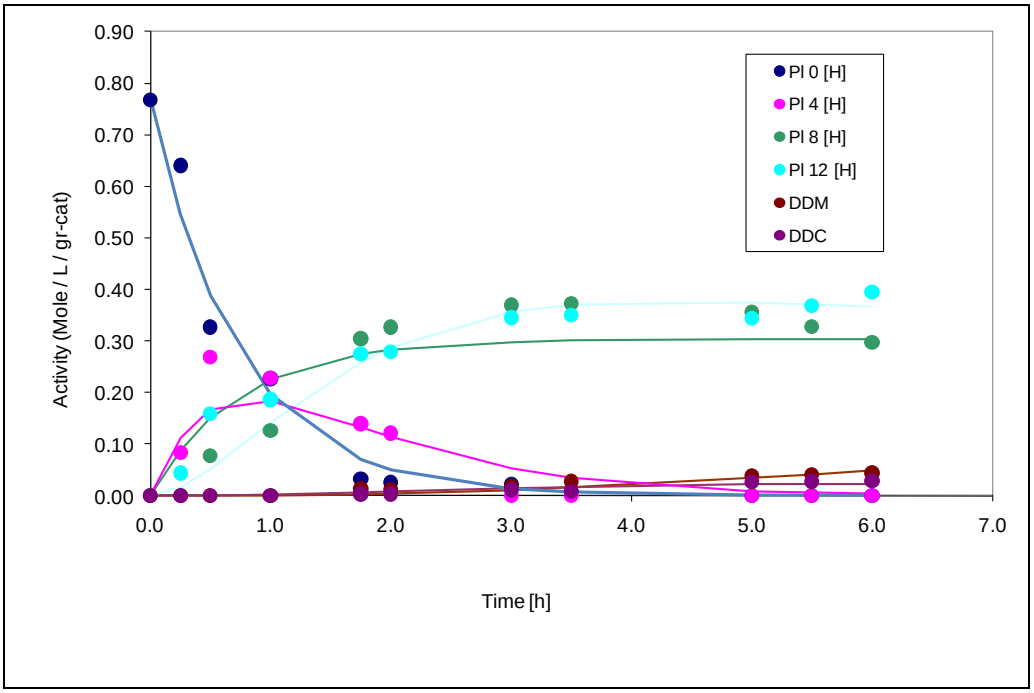

Figure 8.6. Product distribution over time for hydrogenation of 9H-carbazole-9-ethanol over ruthenium black catalyst.

8.3.1.3 Side chain impact-conclusions

The hydrogenation reactions of three compounds with systematic change of the length of the side chain attached to nitrogen have been studied, namely; carbazole (CARB), 9-ethylcarbazole (ETHC) and 9H-carbazole-9-ethanol (CARB-ETH). The resulting conversions and selectivities at the initial stage of the reaction (2h) and extended reaction time (20 h) are compared in Table 8.3.

Table 8.3. Comparison of the results of liquid phase hydrogenation of heterocyclic compounds with various lengths and compositions of the side substituents. The selectivity towards Pl 12 [H] is the sum of selectivities towards Pl 12 [H] isomers- where applicable.

Molecule	***Time [h]***	***Conversion[%]***	***Selectivity [%]***				
			Pl 4 [H]	***Pl 6[H]***	***Pl 8[H]***	***Pl 12 [H]***	***Other***
CARB	2	59	31	0	12	57	-
	20	100	0	1	4	95	-
ETHC	2	45	83	Trace	8	9	-
	20	100	2	Trace	44	54	-
CARB-ETH	2	97	16	1	43	38	2
	20	100	0	1	5	34	60

From the results obtained, the activity towards hydrogenation appears to be the highest for the molecule with the longest chain. However, comparing carbazole and 9-ethylcarbazole both with alkane type of chain, the highest conversion was achieved by carbazole, probably due to the significantly lower steric hindrance effects. This result agrees well with the reports in the literature describing the considerably decreased reactivity of carbazoles with alkyl substitution adjacent to the heteroatom as compared to unsubstituted carbazole (9) (10). As depicted in Table 8.3, the products of the hydrogenation reactions are virtually the same for all of the compounds, regardless of the length or composition of the side chain. In addition, Pl 6 [H] is always a minor product with a selectivity ≤1% of the total reaction mixture. Moreover, the Pl 8 [H] intermediate is formed at significantly higher quantities and accumulates in the solution only in the hydrogenation of molecules with longer side chain. It is probable that the presence of –OH group facilitates the re-adsorption of this intermediate for further conversion at prolonged time. Furthermore, the hydrogenolysis of the fully loaded products takes place following the hydrogenation of CARB-ETH. It is believed that the substituent with –OH group can act as a secondary coordination site to the active sites on the surface of the metal. Similar effect was observed in carbethoxypyrroles (11). Overall, it was shown that the side chain can influence the thermodynamic stability of the substrates and products by inducing a steric hindrance effect. The nature of the substituent can also change the preference in the reaction network by modifying the adsorption mode of the substrate.

8.3.2. Influence of the partial ring saturation- hydrogenation of 1,2,3,4-tetrahydrocarbazole

1,2,3,4-tetrahydrocarbazole dearomatization is typically involved as a sequential reaction step in carbazole hydrogenation, as it was described before. In this paragraph, the focus

will be to evaluate experimentally the influence of partial hydrogenation of one of the fused rings on the activity of the molecule towards hydrogenation as well as the effect of absence of carbazole substrate in the hydrogenation pathway of 1,2,3,4-tetrahydrocarbazole.

As it was mentioned before, with the addition of a hydrogen atom to at least one of the aromatic carbon bonds, the aromaticity of the system is destroyed and the molecule is activated for hydrogenation. However, the hydrogenation of carbazole which is a non-basic compound into 1,2,3,4-tetrahydrocarbazole, makes the lone electron pair more localized on nitrogen rather than donated to a Π-conjugated system. Thus, 1,2,3,4-tetrahydrocarbazole is more basic than carbazole. The products of hydrogenation of 1,2,3,4-tetrahydrocarbazole were as follows; octahydrocarbazole (Pl 4 [H]) and three isomers of fully saturated perhydrocarbazoles (Pl 8 [H]). However, the concentration of Pl 8 [H] B was found to be below 1%, thus its formation was not taken into account in the developed reaction model in Figure 8.7. In addition, the concentration of isomer Pl 8 [H] C was also low (around 5%) As compared to the previously described hydrogenation of carbazole, no hexahydrocarbazole (Pl 2 [H]) was detected in the absence of carbazole. This could have been expected as this compound was found to be produced only from the starting material in the hydrogenation of carbazole according to the fitted kinetic model. In addition, in hydrogenation of carbazole, fully saturated isomer Pl 8 [H] C was found to be produced solely from the starting material as depicted in Figure 8.2. In comparison, in the hydrogenation of 1,2,3,4-tetrahydrocarbazole, the rate constant of this reaction was very low, thus this reaction was not taken into account in our reaction model. The developed model for 1, 2, 3, 4-tetrahydrocarbazole hydrogenation over ruthenium black catalyst is shown in Figure 8.7.

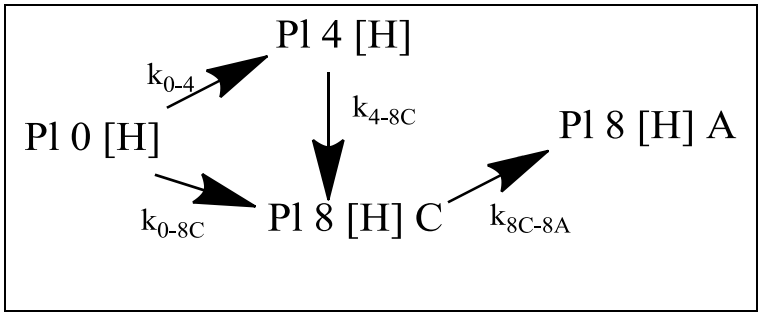

Figure 8.7. Reaction pathway of hydrogenation of 1,2,3,4-tetrahydrocarbazole over ruthenium black catalyst.

The rate constants are gathered in Table 8.4.

Table 8.4. First order rate constants for hydrogenation of 1,2,3,4-tetrahydrocarbazole over ruthenium black catalyst.

k_0 [h^{-1}]	0.84
k_{0-8C} [h^{-1}]	0.003
k_{0-4} [h^{-1}]	0.84
k_{8C-8A} [h^{-1}]	0.003
k_{4-8C} [h^{-1}]	3.0

The results confirmed that the production of intermediates and the final compounds was well described by the first order simplified reaction network (Figure 8.7.) as shown in Figure 8.8. The rate of hydrogenatation of 1,2,3,4-tetrahydrocarbazole was found to be much faster than that of carbazole. In the first hour of the reaction, the conversion of carbazole was only 43%, whereas in the same time the conversion of 1,2,3,4-tetrahydrocarbazole reached 75%. The higher conversion of 1,2,3,4-tetrahydrocarbazole in comparison with carbazole can be explained by the absence of resonance stability in one of the benzoid rings conjugated with the middle 'pyrrole' ring which renders the molecule more susceptible towards the hydrogenation reaction. In addition, carbazole adsorbs much stronger than 1,2,3,4-tetrahydrocarbazole on the catalyst surface (5) (12). A less stable adsorption mode can sometimes lead to increased hydrogenation rates. The five-membered nitrogen containing compounds with one aliphatic ring like 1,2,3,4-tetrahydrocarbazole were reported to absorb at an angle of 30° away from the metal atom (12), which is a

considerable less stable adsorption mode as compared to the parallel flat adsorption of 9-ethylcarbazole on the catalysts surface.

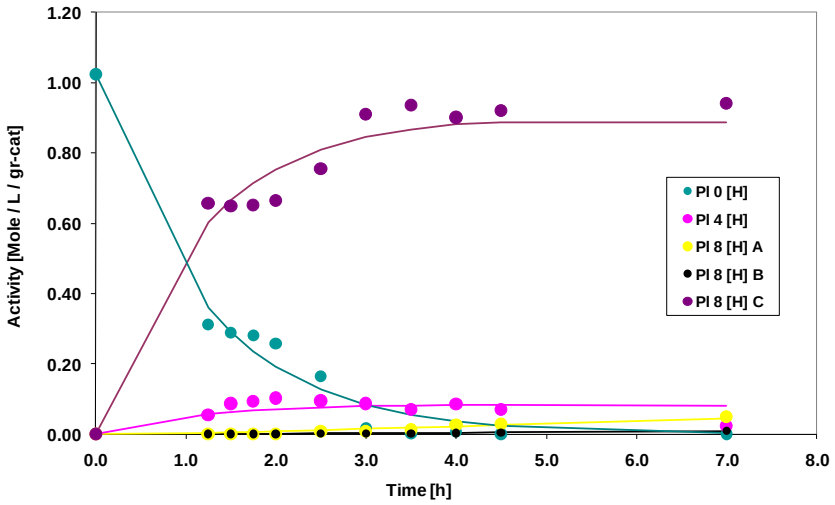

Figure 8.8. Product distribution over time for hydrogenation of 1,2,3,4-tetrahydrocarbazole over ruthenium black catalyst.

The higher rate of hydrogenation of partially saturated intermediates was also reported in the study of naphthalene (13). When it comes to selectivity, higher selectivity towards fully hydrogenated compounds was recorded for 1,2,3,4-tetrahydrocarbazole. Additionally, the partially saturated molecule showed lower selectivity towards the formation of the intermediate with intact middle "pyrrole" ring as compared to carbazole. Morover, the isomerisation of fully hydrogenated product 8 [H] C to 8 [H] A is more pronounced when the starting material is partially saturated (or in absence of carbazole).

8.3.3. Substitution of pyrrole ring with pyridinic ring- hydrogenation of acridine

In comparison to the structure of carbazole (see Figure 8.9), acridine has the pyrrole ring of carbazole replaced with a pyridinic ring fused between two benzenoid rings. The basic properties of acridine origin from the fact that the lone pair of electrons on the nitrogen is not delocalised in the aromatic ring and therefore it is more available for donation to a

Lewis acid (14). The hydrogenation of acridine progressed very rapidly as compared to the previously studied compounds and around 90% of conversion of the substrate was obtained in only 30 minutes of reaction. The fast rates of hydrogenation of acridine were reported before in several papers (1)(15) (16) (3) (17) and they were attributed to the basic nature of this compound.

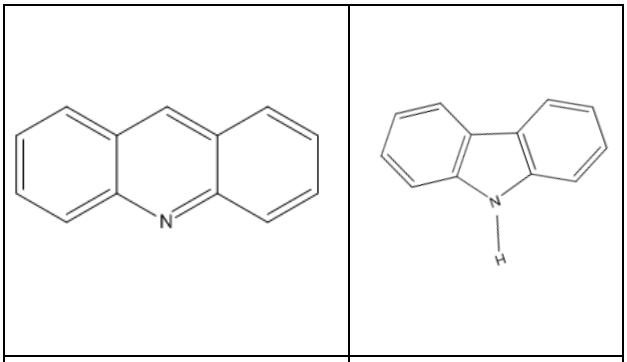

acridine	***carbazole***

Figure 8.9. Comparison of the structures of acridine and carbazole

Because of the localized character of the nitrogen lone pair of electrons, acridine is able to absorb promptly and effectively on the catalyst surface and occupy large number of active sites simultaneously. This leads to much higher conversions in catalytic hydrogenation. The main products observed during liquid phase hydrogenation of acridine over ruthenium black catalysts were: Pl 2 [H] - dihydroacridine, Pl 4 [H]- tetrahydroacridine, Pl 8 [H]-octahydroacridine, and three stereoisomers of the fully hydrogenated Pl 12 [H] – perhydroacridine. It should be noted that in the hydrogenation of the analogues of carbazole with pyrrole ring, dihydro (Pl 2 [H]) intermediates were never observed. The dihydroacridne is formed from partial saturation of the pyridinic ring. The formation of the dihydro intermediate product in case of basic compounds is governed by the preferential adsorption on the catalyst surface via the lone pair of electrons in nitrogen instead of via the electron deficient heteroaromatic rings. The formation of dihydoroacridine was previously reported in hydrogenations over $NiMo/Al_2O_3$ catalyst (15) , Raney nickel (17) and supported Pd and Pt catalysts (1). Additionally, no traces of hexahydroacridine (Pl

6[H]) were observed despite the fact that considerable amount of this intermediate were observed in the hydrogenation of carbazole. This suggests that the basic properties of nitrogen are influential in selectivity in hydrogenation over ruthenium black catalyst. In addition, the Pl 8 [H] intermediate was detected, which is a product of hydrogenation of two adjacent benzenoid rings, therefore it has virtually the same structure as octahydocarbazole (Pl 8 [H]). Based on the product distribution versus time for the hydrogenation of acridine over ruthenium black catalyst, a reaction model was developed which is shown in Figure 8.10

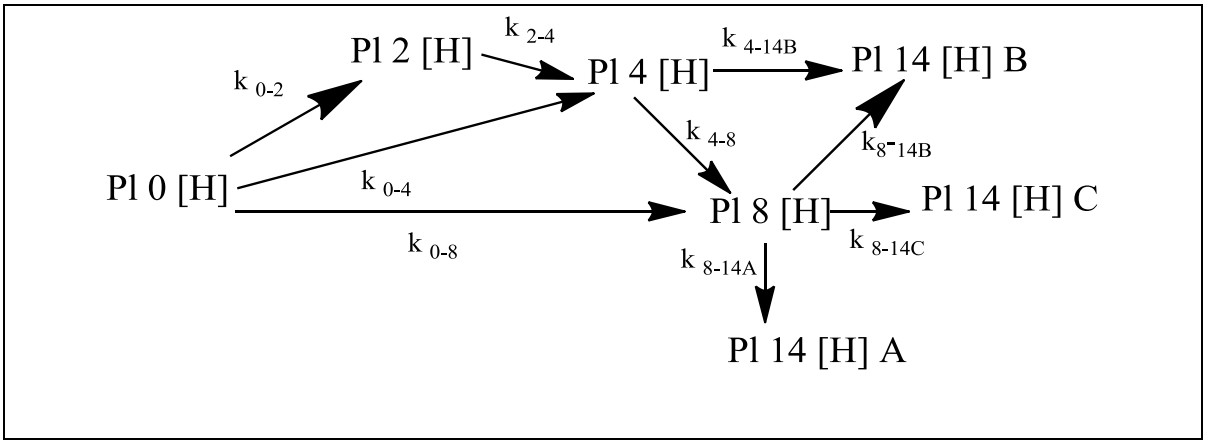

Figure 8.10. Reaction model for hydrogenation of acridine over ruthenium black catalyst

The calculated rate constants of the intermediate reactions are gathered in Table 8.5.

Table 8.5. Calculated rate constants of hydrogenation of acridine over ruthenium black catalyst.

k_0 [h^{-1}]	2.9
k_{0-2} [h^{-1}]	0.29
k_{0-4} [h^{-1}]	1.7
k_{2-4} [h^{-1}]	0.60
k_{4-8} [h^{-1}]	1.5
k_{0-8} [h^{-1}]	0.88
k_{8-14B} [h^{-1}]	0.32
k_{8-14A} [h^{-1}]	0.077
k_{8-14C} [h^{-1}]	0.014
k_{4-14B} [h^{-1}]	0.75

It is clear from the reaction model (Figure 8.10) that the substitution of the pyrrole ring (five membered ring) with piridinic ring (six membered ring) results in the hydrogenation reaction being more complex and involving additional reaction steps and intermediates.

The developed simplified first order reaction model for acridine hydrogenation over ruthenium black catalysts depicted in Figure 8.10, agreed well with the experimentally obtained concentration changes in time (Figure 8.11). As it can be seen from Figure 8.11, in the hydrogenation of acridine, the main intermediate observed was the octahydro intermediate (PL 8 [H]) with both benzenoid rings saturated. Additionally, Pl 8 [H] accumulated in the solution, similarly to the results reported for hydrogenation of 9-ethylcarbazole, described in the previous chapters. On the contrary, in the hydrogenation of carbazole, the Pl 8 [H] intermediate was formed in much smaller quantities and it did not accumulate in the solution but instead was rapidly converted to the final products.

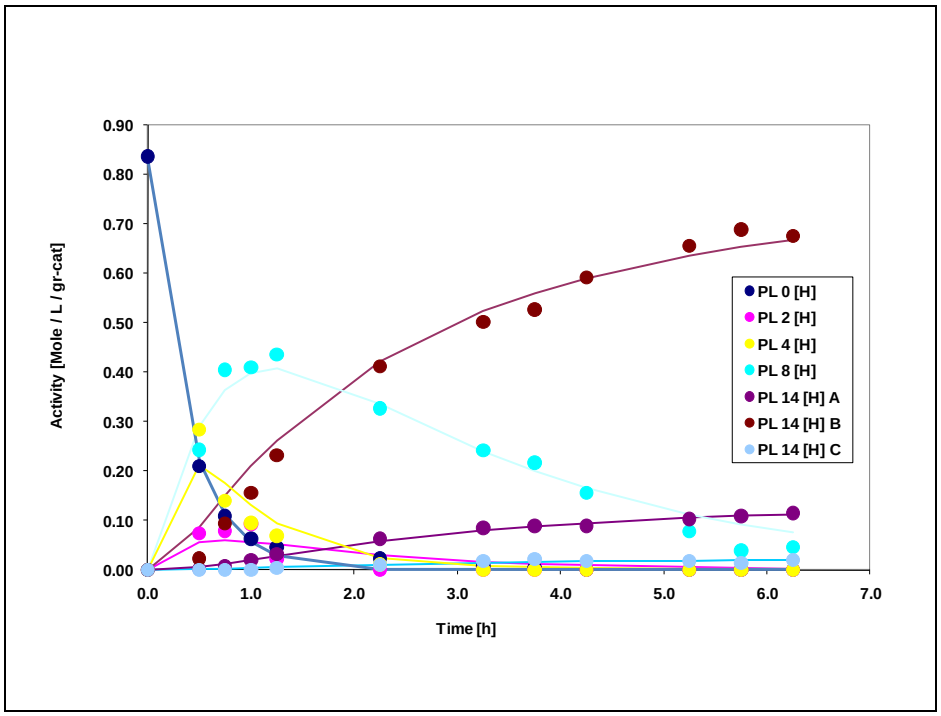

Figure 8.11. Product distribution over time for hydrogenation of acridine over ruthenium black catalyst.

Comparing the rate constants of the intermediate reactions, in case of carbazole, the rate constant for formation of Pl 8 [H] was two times higher than the rate constant of its further

hydrogenation (see Table 8.1) whereas in the case of hydrogenation of acridine, the rate constant of Pl 8 [H] production is more than five times higher much than the rate constant of its disappearance (see Table 8.5). Similar observations were made in the case of hydrogenation of 9-ethylcarbazole over ruthenium based catalysts described in the previous chapters. It is believed that the further conversion of Pl 8 [H] is hindered by the presence of the two fully saturated banzenoid rings, which make the re-adsorption of this intermediate on the catalyst surface difficult.

To sum up, the rate of hydrogenation of a basic nitrogen heterocycle (acridine) is higher than the rates of hydrogenation of non-basic compound (carbazole) over ruthenium black catalyst. It was previously reported by Sun et al. (18) that the energy levels of LUMO and HOMO for basic heterocyclic compounds are lower than those for corresponding non-basic compounds. Therefore, the transfer of electrons from the aromatic substrate to the catalysts surface is energetically more favourable for basic nitrogen compounds. As a result, since ruthenium is a rather electron deficient metal, basic compounds show higher reaction rates over this catalyst. Moreover, the reaction pathway of hydrogenation of acridine is more complex as compared to the pyrrole analogues studied previously and contains Pl 2 [H] as an additional stable intermediate. The main intermediate product is Pl 8 [H] octahydroacridine which accumulates in the reaction solution similarly to the observation made for the hydrogenation of 9-ethylcarbazole, where the main stable intermediate product had a similar structure. However, the Pl 8[H] intermediate in the case of hydrogenation of acridine is less stable than in the case of hydrogenation of 9-ethylcarbazole over the same catalyst. In addition, the main product of hydrogenation of acridine has three isomers, however no isomerisation reaction between them was observed. Moreover, no ring opening or hydrogenolysis products were identified via GC-MS analysis.

8.3.4. Influence of the type of the heteroatom in the pyrrole ring

In order to determine the influence of the type of the heteroatom in the pyrrole ring on the reactivity of the potential carrier material towards hydrogenation over ruthenium black catalyst, three representative compounds were chosen, namely: furan (O-heteroatom), dibenzothiophene (S-heteroatom) and fluorene (no heteroatom), the structures of which are shown in Figure 8.12.

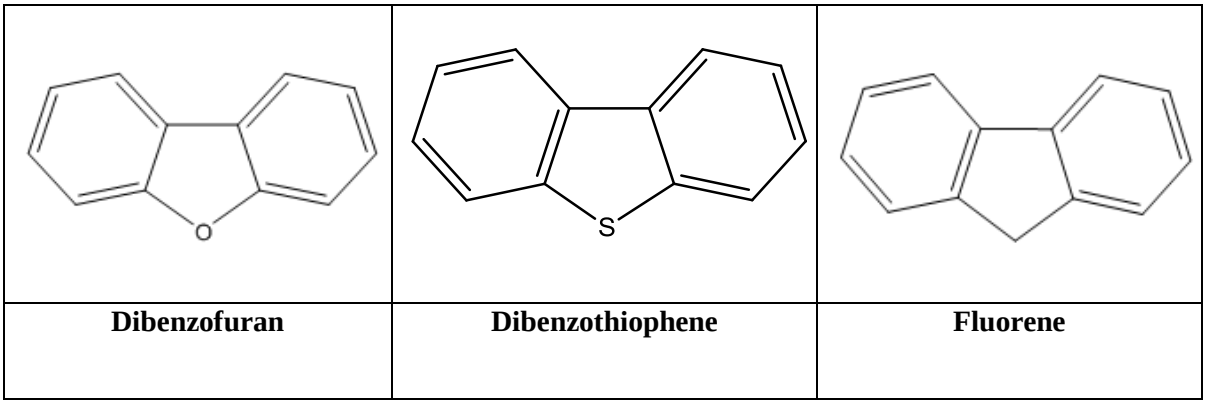

Dibenzofuran	Dibenzothiophene	Fluorene

Figure 8.12. Structure of model heterocyclic compounds studied.

The hydrogenation properties of these compounds will be compared to carbazole (nitrogen- heteroatom), described previously. In general, the introduction of the heteroatom apart from changing the bond lengths and distorting the geometry, can result in a reduction of the π-electron density in the aromatic ring, if the introduced heteroatom is more electronegative than carbon (N, O, S). One of the factors influencing the hydrogenation activity of the molecule is its aromaticity. The aromaticity of the heterocycles decreases in order of substituted heteroatoms as follows S > N >O (19). High aromaticity of thiophene analogues can be explained by equal electronegativity of sulphur as compared to carbon as well as its covalent radius only slightly higher than that of carbon.

8.3.4.1. Hydrogenation of Dibenzofuran

Dibenzofuran is a heteroaromatic compound (aromatic ether) which can be classified as basic, due to the fact that it contains a lone pair of electrons residing in a p orbital of oxygen that is not involved in the formation of the aromatic electron cloud. The remaining lone pair of electrons of oxygen is delocalized as a part of aromatic cloud (20). Dibenzofuran has a relatively low melting point of 81-85 °C, which makes the solvent-free reversible hydrogen charge and discharge possible under moderate conditions.

In the hydrogenation of dibenzofuran over ruthenium black catalyst, the following products were identified; tetrahydro-dibenzofuran (Pl 4 [H]), octahydro-dibenzofuran (Pl 8 [H]), and two isomers of the fully saturated isomers of perhydro-dibenzofuran (Pl 12 [H]). In addition to these products, three other compounds were found which are the products of the furan ring opening reaction (hydrogenolysis of perhydrodibenzofurans) namely: bicyclohexyl (BCH), bicyclohexyl-2-one (BCHO) and cyclohexylcyclohexanol (CHCH). The structures of the products of ring opening of perhydrodibenzofurans are shown in Figure 8.13. The absence of biphenyl and its analogues suggests that the furan ring opening and oxygen removal took place after hydrogenation of the adjacent rings was completed. Generally, if the oxygen is inserted into an aromatic ring, hydrogenation of this ring is essential prior to the C-O scission (21). The hydrogenation of two double bonds followed by ring cleavage was previously reported in the hydrogenation of furan over platinum catalyst (22). However, it was found in the literature that over presuldified NiMo/γ-Al_2O_3 catalyst, the oxygen removal took place prior to the hydrogenation reaction, via direct reaction (23). This can be due to the presence of Lewis type active sites on the surface of the sulphided catalyst, as it was reported in case of hydroprocessing of nitrogen-containing compounds over Ni-Mo and Ni-W mixed oxide catalysts (24).

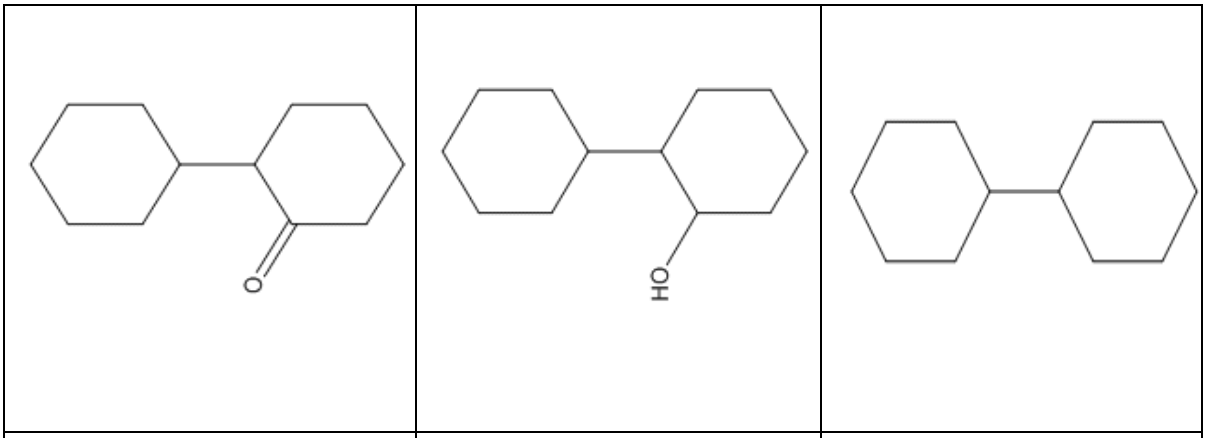

Bicyclohexyl 2-one	*Cyclohexyl cyclohexanol*	*Bicyclohexyl*

Figure 8.13. The structures of ring opening reaction of dibenzofuran over ruthenium black catalyst.

Based on the experimentally obtained product distributions versus time in the hydrogenation of dibenzofuran over ruthenium black catalyst, the simplified first order model of the reaction was developed and is shown in Figure 8.14. The products of hydrogenolysis were treated as a sum to simplify the model, since reaction of ring opening of furan in hydrogenation of dibenzofuran is not the main focus of this work. The calculated rate constants are gathered in Table 8.6.

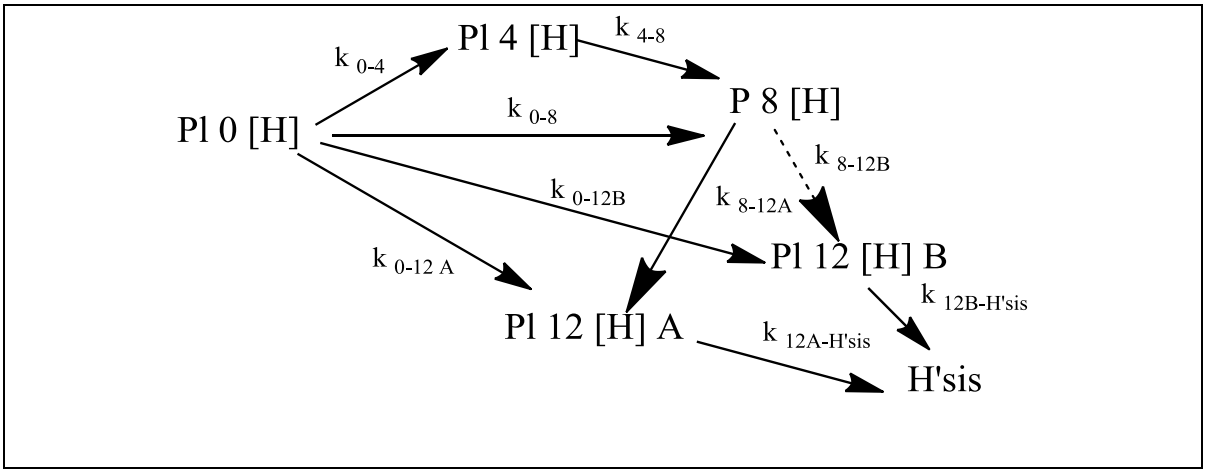

Figure 8.14. Simplified first order model of hydrogenation of dibenzofuran followed by hydrogenolysis of C=O bonds of perhydrodibenzofuran. H'sis-sum of hydrogenolysis products.

The experimental product distribution was found to be described well by the above developed model, as can be seen in Figure 8.15. The rate of hydrogenation of dibenzofuran is almost twice as high as the rate of hydrogenation of carbazole reported previously. This is the result of a higher electronegativity of oxygen than nitrogen, which decreases the

aromaticity of the dibenzofuran versus carbazole. When it comes to selectivity, dibenzofuran, similarly to carbazole, produced the Pl 8 [H] intermediate in considerable amounts.

Table 8.6. Calculated first order rate constants of intermediate reactions of hydrogenation of dibenzofuran over ruthenium black catalyst. Hiss- sum of hydrogenolysis products.

$k_0[h^{-1}]$	1.7
$k_{0\text{-}4}\,[h^{-1}]$	0.79
$k_{4\text{-}8}\,[h^{-1}]$	0.61
$k_{0\text{-}8}\,[h^{-1}]$	0.23
$k_{0\text{-}12B}\,[h^{-1}]$	0.37
$k_{8\text{-}12A}\,[h^{-1}]$	0.96
$k_{8\text{-}12B}\,[h^{-1}]$	0.0012
$k_{12B\text{-}Hsis}\,[h^{-1}]$	6.2
$k_{0\text{-}12A}\,[h^{-1}]$	0.26
$k_{12A\text{-}Hsis}\,[h^{-1}]$	0.054

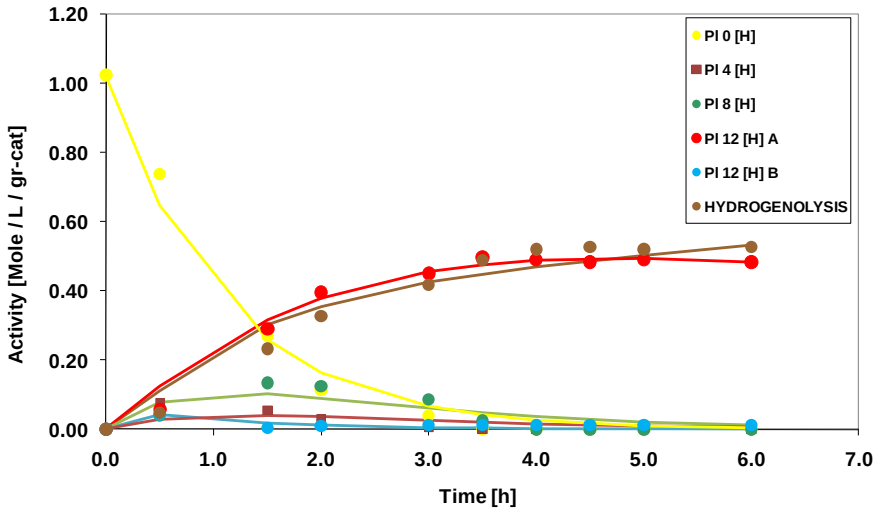

Figure 8.15. Product distribution over time for hydrogenation of dibenzofuran over ruthenium black catalyst.

Furthermore, octahydrodibenzofuran does not accumulate in the solution as similar to octahydrocarbazole. However, the octahydrodibenzofuran intermediate is converted much

faster than octahydrocarbazole (3.5 hours versus over 6 hours). Additionally, the rate constant of formation of octahydrodibenzofuran is lower than the rate constant of its further conversion (see Table 8.6). As compared to the products of carbazole hydrogenation over the same catalyst, no Pl 6 [H] was observed in the case of dibenzofuran hydrogenation. In addition, the hydrogenation of dibenzofuran resulted in the production of two stereoisomers of the fully hydrogenated perhydro- products, as opposed to three stereoisomers that were observed in the hydrogenation of carbazole. Unlike the nitrogen containing liquid organic hydrides reported previously, oxygen containing perhydrodibenzofuran underwent ring opening reactions over the same catalyst and under the same reaction conditions. Therefore, based on our results, it can be concluded that C-O single bonds in the fully saturated cyclic products are more susceptible to rupture than C-N bonds under the same reaction conditions over ruthenium black catalyst.

Regardless the fact that the rates of hydrogen loading into dibenzofuran are higher than in the case of hydrogenation of carbazole, the commercial application of dibenzofuran in hydrogen storage can be strongly inhibited by the possibility of a ring opening reaction. The presence of hydrogenolysis affects drastically the fuel recovery process, making the reversible hydrogenation impossible over ruthenium black catalyst. Nevertheless, there are reports in the literature stating that ruthenium has a promoting effect on hydrogenolysis of C-O bond (25). It is therefore believed that the ring opening of perhydrodibenzofuran can be eliminated by using catalyst based on other noble metals, which are known to display strong hydrogenation activities and simultaneously hinder bond rupture such as Pt, Re or Ir (25). Further experimental work would be necessary to verify this point.

8.3.4.2. Hydrogenation of dibenzothiophene

Similarly to dibenzofuran, dibenzothiophene can be considered a basic compound due to the availability of the lone pair of electrons on the sulphur atom. It has a melting point of

97°C which is higher than that of dibenzofuran, however solvent free reversible storage of hydrogen would be possible using this compound under feasible reaction conditions.

Unfortunately, despite the extended reaction times (24 hours) and two fold increase of the catalyst amount used, no hydrogenation of dibenzothiophene took place under the reaction conditions studied. GC-MS analysis of the hydrogenated mixture revealed only the intact substrate material. This can be attributed to irreversible adsorption of sulphur on the surface of the unsupported ruthenium metal, which poisoned the small density of active sites on the surface of the metal. It is well known that dibenzofuran preferably reacts with hydrogen by direct desulfonization pathway rather than hydrogenation pathway (21) (24) (26). It is believed that the poisoning of the active sites took place right after the beginning of the reaction by irreversible adsorption of the products of direct desulfurization as it was reported in (27). This result was not surprising taking into consideration that deactivation of noble metal catalyst in the presence of sulphur containing species is a well known phenomenon (28).

8.3.5. Hydrogenation of fluorene

Fluorene has been considered a good candidate for liquid organic hydrides in the autothermal hydrogen storage mode (29) Fluorene is the only policyclic compound studied containing five membered and six membered rings without any heteroatoms in the structure. The hydrogenation of fluorene was studied here to find the influence of the presence of heteroatom on the reaction pathway and the rate of hydrogenation.

The hydrogenation of fluorene over ruthenium black catalyst involves typical sequential saturation of aromatic rings. The major products of this reaction were: the primary product- hexahydrofluorene (Pl 6 [H]), two isomers of decahydrofluorene (Pl 10 [H]) and one isomer of the fully hydrogenated perhydrofluorene (Pl 12 [H]). No other products of any ring opening or isomerisation reactions were observed. Similar products in the

hydrogenation of fluorene over supported Ru, Pd, Pt and Rh were obtained by Sakanishi et al. (1). However, no decahydro intermediates were reported over NiW/Al_2O_3 catalyst (30), which shows the effect of the type of the catalytic system on the reaction pathway. Based on the experimentally obtained concentration changes of the reaction products and intermediates in time, a simplified first order reaction model was developed as shown in Figure 8.16.

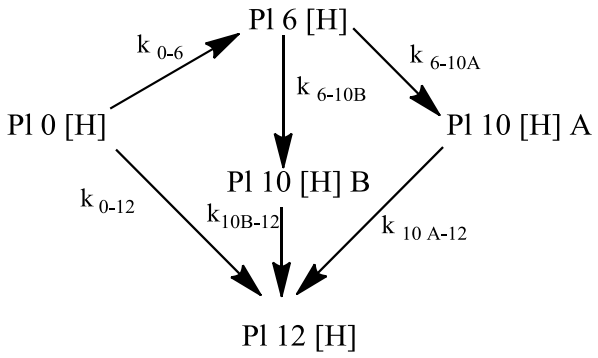

Figure 8.16. Simplified first order model of hydrogenation of fluorene over ruthenium black catalyst.

The calculated rate constants of the intermediate reactions shown in Figure 8.16, are gathered in Table 8.7. As it can be seen from Table 8.7, the conversion of starting material towards Pl 6 [H] has the highest rate constant, almost one order of magnitude higher than that of its conversion to perhydrofluorene Pl 12 [H]. It is clear that this primary product of hydrogenation is a stable intermediate of the reaction. It is formed by hydrogenation of one of the benzenoid rings adjacent to the five membered ring. The readsorption of the hexahydro-intermediate for consecutive saturation is probably sterically hindered by the fully saturated six-membered ring. In the present work, the Pl 6 [H] intermediate was only observed in the hydrogenation of carbazole. It is interesting to note that in the absence of heteroatom in the five membered ring, the octahydro-intermediate is not formed. This intermediate was previously observed in all of the heterocyclic compounds studied.

Instead, in the hydrogenation of fluorene, we have observed the production of decahydro-fluorene (Pl 10 [H]) as a stable intermediate.

Table 8.7 Calculated first order rate constants of intermediate reactions of hydrogenation of fluorene over ruthenium black catalyst.

k_0 (h^{-1})	0.2
k_{0-6} (h^{-1})	0.19
k_{0-12} (h^{-1})	0.012
k_{6-10A} (h^{-1})	0.02
k_{6-10B} (h^{-1})	0.028
k_{10A-12} (h^{-1})	0.045
k_{10B-12} (h^{-1})	0.11

Decahydro- intermediates have not been observed in the heteroaromatic structures analysed in this work. Moreover, in hydrogenation of fluorene, there are two isomers of Pl 10 [H] formed by readsorption of the Pl 6 [H] intermediate on the catalyst surface. In addition, only one isomer of the fully saturated perhydrofluorene was indentified, similarly to the observation made in hydrogenation of 9 H-carbazole-9-ethanol. Even after 24 hours of extended reaction, the total conversion of fluorene was not reached. This is very slow as compared to the hydrogenation of carbazole, where full conversion was reached in a little over 6 hours. In fact, the rate of hydrogenation of fluorene was the slowest of all the molecules studied, possibly due to the higher resonance energy of fluorene. Therefore, a cost effective recyclability of fluorene fuel would be a challenging task. The developed first order model shown in Figure 8.16, fitted the experimental data well (see Figure 8.17). It can be seen from this profile that Pl 6 [H] is a stable intermediate in this reaction that accumulates in the solution probably due to geometrical constraints.

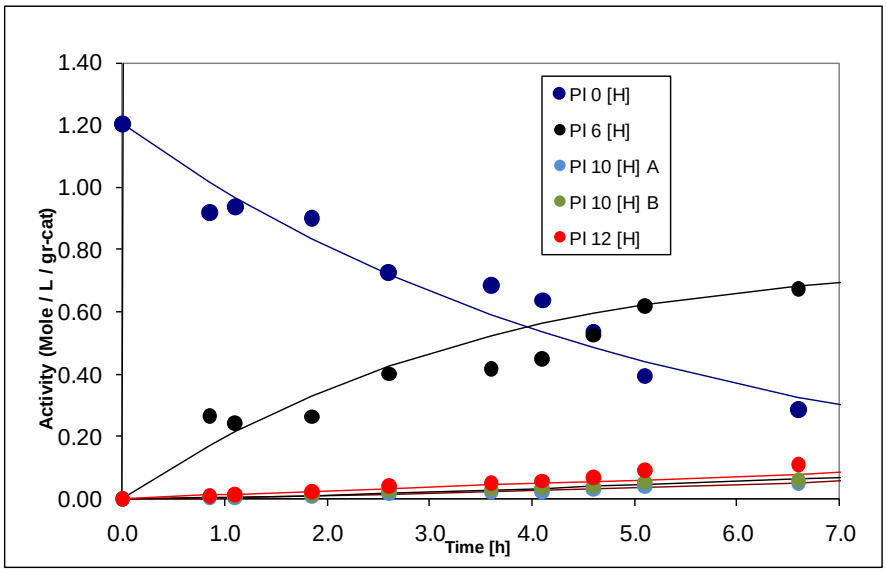

Figure 8.17. Product distribution over time for hydrogenation of fluorene over ruthenium black catalyst.

8.3.6. Influence of the presence and type of heteroatom- conclusions

The rate of hydrogenation is considerably enhanced by the presence of a heteroatom in the structure. The obtained conversions decreased in order dibenzofuran > carbazole > fluorene. Dibenzothiophene was found to poison the catalyst via irreversible adsorption on the catalyst surface via lone pair of electrons on sulphur. Despite high activity of oxygen containing compounds towards hydrogenation, it was found that C-O bonds present in the furan ring are susceptible to rupture which results in a ring opening reaction and oxygen removal. The side cracking reactions have detrimental effect on the recyclability of the liquid organic hydride and therefore should be avoided. Hydrogenolysis and ring opening were not observed in carbazole and fluorene. Moreover, the selectivity of the reaction was governed by the type of the heteroatom present, thus slightly different intermediates were formed in hydrogenation of carbazole, dibenzofuran and fluorene. The amount of isomers of the fully saturated compound was also influenced by the type of the heteroatom and decreases in order carbazole>dibenzofuran>fluorene. In addition, the stable intermediate Pl 8 [H] was only produced during the hydrogenation of heterocyclic compounds, however this intermediate was not always stable at prolonged time. In the hydrogenation of

homocyclic fluorene, no formation of Pl 8 [H] was observed, however the Pl 6 [H] intermediate was found to be stable in this reaction. This can be explained by the preferable modes of adsorption of substrates and intermediates.

8.4. Conclusions of structure-reactivity correlation

The activity in the hydrogenation reaction is governed by both; the type of the substrate and the electronic structure and properties of the surface of the catalyst. The comparison of the calculated rate constants values for all of the hydrogenation reactions studied is shown in Table 8.8. As it can be seen from these results, the highest rate was obtained by acridine. This is due to the lower electron density of the pyridine ring as compared to the pyrrole ring. Therefore, the adsorption of acridine is more efficient on the ruthenium surface. Additionally, the rate of hydrogenation reaction is greatly improved by the substitution of carbon with an oxygen or a nitrogen atom in the five membered ring. This is clear comparing the rate constants of carbazole, dibenzofuran and fluorene listed in Table 8.8.

Table 8.8. Comparison of the rate constants of studied candidate molecules for hydrogen storage.

Compound	***Rate coefficient k_0 [h^{-1}]***
Acridine	2.9
Dibenzofuran	1.7
9H-carbazole-ethanol	1.3
Tetrahydro-carbazole	0.8
Carbazole	0.6
9-ethylcarbazole	0.3
Fluorene	0.2

However, it should be noted that higher rates were obtained with oxygen substitution than with the nitrogen one. The presence of the oxygen not only in the five membered ring but also in the side substituent chain increases the hydrogenation activity of the molecule. This

can be explained again by the charge redistribution caused by the presence of oxygen, which makes the aromatic ring electron deficient. Moreover, it was found that partial saturation of the aromatic molecule increases drastically the rate of hydrogenation. When it comes to the influence of the substituent on the hydrogenation reactivity, comparing only carbazole and 9-ethylcarbazole, higher rates are attained by the former. This is due to the steric hindrance effect during flat adsorption on the catalyst surface that is imposed by the ethyl- substituent on nitrogen, which decreases the rate of reaction. The lowest hydrogenation activity, as expected, was observed in the hydrogenation of fluorene. The lack of a heteroatom in the structure of fluorene results in higher resonance stabilization of this compound and therefore lower reactivity in the hydrogenation reaction. In the case of dibenzothiophene, the catalyst was poisoned and no activity was observed even with increased amounts of catalyst used.

The structure of the aromatic compound affects the elementary steps of the reaction on the surface of the catalyst. Thus, the selectivity of the hydrogenation is influenced by the manner in which the bonds are formed between the catalyst and the surface. It can be said that the consecutive hydrogenation of polyaromatic compounds can be promoted or hindered depending on the geometry and reactivity of the intermediate. In the present work, it has been observed that the dihydro-intermediate (Pl 2 [H]), has only appeared during the hydrogenation of acridine which contains a six membered pyridine ring fused between two benzenoid rings. The production of this intermediate in the hydrogenation of basic acridine is influence by the preferential interaction of this compound with the metal surface using the side-on nitrogen down adsorption mode and the lone pair of electrons localized on the heteroatom. In case of non-basic compounds like carbazole, the adsorption tendency is more through the electron rich heteroaromatic ring as reported by Ho (31). During the hydrogenation of these compounds, the formed Pl 2 [H] is too unstable to

become a primary intermediate and therefore further addition of hydrogen must take place almost simultaneously, without any desorption of the intermediate from the catalyst surface.

The tetrahydro-intermediate (Pl 4 [H]) is produced only in the hydrogenation of heterocyclic compounds regardless the basicity properties or number of atoms in the middle ring (pyrrolic, furan or pyridinic rings). Similarly, the formation of the octahydro-intermediate (Pl 8 [H]) is mainly a result of further saturation of the Pl 4 [H] intermediate. Therefore Pl 8 [H] is also formed only in the hydrogenation of heterocyclic compounds.

The formation of the Pl 8 [H] intermediate is thought to take place following the adsorption of Pl 4 [H] with the aromatic ring lying flat on the metal surface and the aliphatic ring in an angle. However, the Pl 8 [H] intermediate was found to accumulate in the solution during the hydrogenation of 9-ethylcarbazole, 9 H-carbazole-ethanol and acridine. Based on the obtained results, it is believed that the stability of Pl 8 [H] in these reactions is determined mainly by steric factors. The saturation of the central ring of acridine is sterically hindered by the presence of two adjacent fully saturated six membered rings especially taking into consideration the majority of flat active sites on ruthenium black catalyst. The stability of 9-ethyl-octahydrocarbazole and 9H-octahydrocarbazole-9-ethanol is the result of the steric hindrance induced by the chain substituent on nitrogen atom. On the other hand, from the product distribution of the hydrogenation of carbazole showed in Figure 8.3, it seems that possibly some edgewise adsorption is likely to take place due to the presence of the products with partially saturated central ring. As a result, there is lower accumulation of this intermediate in the hydrogenation of carbazole. The product distribution of dibenzofuran (Figure 8.14) showed the formation of considerable amounts of Pl 8 [H], but further conversion of octahydrodibenzofuran to perhydrodibenzofuran was much quicker than in the case of

octahydrocarbazole. Therefore, it seems that due to the difference in electronegativity of oxygen and nitrogen, the edgewise adsorption of octahydrodibenzofuran is more favourable than that of octahydrocarbazole.

In the hydrogenation of homocyclic fluorene, the stable intermediate was Pl 6 [H], which is the result of subsequent hydrogenation of the aromatic rings in the structure. The further conversion of this intermediate is hindered by the steric hindrance of the fully saturated six membered ring, which hampers the flat re-adsorption of Pl 6 [H] on the surface of the catalyst.

Decahydro-intermediates were only present in the hydrogenation of fluorene, which shows that the mode of absorption of the intermediates and products on the surface of the catalyst is strongly affected by the presence of heteroatom in the central ring.

The presence of side reactions, the isomerisation of the main fully loaded products to more thermodynamically stable forms, was observed in the case of hydrogenation of 9-ethyl-perhydrocarbazole. Additionally, the presence of the oxygen in the structure results in the presence of side reactions.

In general, for the hydrogen storage in liquid organic hydrides to be economically feasible, the efficient recycling of the spent fuel has to be optimised at the minimum cost. Based on the gathered results and available data from the literature, the optimisation of the structure of the heterocycle appears to be a very challenging task. The biggest difficulty lays in the fact that the structure has to favour the hydrogen release step without compromising the thermodynamics and kinetics of hydrogenation.

From the point of view of fuel recovery step, acridine seems to be the best candidate, due to the favourable kinetics and thermodynamics of hydrogenation and at the same time, high hydrogen uptake capacity of 7.2 wt %. However, the dehydrogenation of acridine has been reported in the literature to be difficult and mostly resulting in poor yields despite

high catalyst content and elevated temperatures used (32). Generally, the hydrogen uptake is favoured in six membered rings. However, hydrogen release is favoured in five membered rings. In addition, the structure of acridine with three six membered fused rings results in the formation of vast majority of intermediates and isomers of these intermediates, further complicating both hydrogenation and dehydrogenation processes.

In the case of dibenzofuran, which has got a five membered ring fused between two benzenoid rings, the number of of possible intermediates and products is lower than in case of acridine. Moreover, the presence of the five membered ring and oxygen in the cycle decreases the endothermicity of dehydrogenation. However, it has been shown in the present work that in spite of reasonable kinetics and thermodynamics of hydrogenation, the hydrogen uptake of dibenzofuran results in a hydrotreating reaction, making the reversible process economically not feasible.

Moving towards compounds with nitrogen containing heterocycles (see Table 8.8), carbazole could be considered a reasonable candidate, with equal hydrogen uptake capacity and slightly worse kinetics and thermodynamics of hydrogenation than dibenzofuran. Dehydrogenation of the mixture of perhydrocarbazole was reported to be facile at moderate temperatures of 125°C, but with low selectivity towards carbazole (33). In addition, the melting point of carbazole (246°C) prohibits the solvent free reversible hydrogenation. A significantly lower melting point can be obtained by introducing the ethyl-substituent on the nitrogen atom in the pyrrole ring of carbazole, resulting in the formation of 9-ethylcarbazole structure. The dehydrogenation of the mixture of isomers of 9-perhydroethylcarbazole takes place at more moderate conditions resulting in a high yield of 9-ethylcarbazole. However, the introduction of the side substituents has detrimental effect on the theoretical hydrogen capacity of the material. In addition, the hydrogenation activity of 9-ethylcarbazole is hindered by the formation of the Pl 8 [H] stable

intermediate. Unfortunately, overall no clear direction in the structure design can be outlined.

In general, the structure of the compound should be optimised so that the calculated Gibbs free energy (ΔG) would be minimized at reasonably low temperatures. However, too low temperatures might result in the hydrogenation step being difficult and too high can make dehydrogenation reaction difficult. It is clear from our results that from the point of view of recyclability, the six member rings are preferable to five member rings. In addition, the presence of nitrogen heteroatom in the structure does not result in rapid hydrotreating reactions as in the case of oxygen containing heterocycles. The presence of the nitrogen in the heterocycle also does not result in catalyst poisoning. The attachment of the substituent on nitrogen depending on its structure can either increase or decrease the hydrogenation activity of the substrate. In addition, it decreases the melting point of the molecule. However, it should be taken into account that the presence of substituents decreases the hydrogen uptake capacity of the system, as well as it induces a steric hindrance effect in the hydrogenation reaction. Because of the storage density of hydrogen is very important, further research should be focussed on finding liquid organic carriers with higher hydrogen capacity (> 7.5 wt %), preferably containing six member rings with nitrogen heteroatoms. However, it can be expected, based on the obtained results that hydrogenenation of such structures would most likely result in the formation of several products and intermediates that would in turn hinder the dehydrogenation process. The multiplicity of the side reactions can also become a problem. Therefore development of highly active and selective catalyst would be crucial for the future research.

8.5. References

1. *The reactivities of polyaromatic hydrocarbons in catalytic hydrogenation over supported noble metals.* **K. Sakanishi, M. Ohira, I. Mochida, H. Okazaki, M. Soeda,** Bull. Chem. Soc. Jpn, 1989, Vol. 62.

2. *The chemistry of selective ring-opening catalysts.* **H. Du, C. Fairbridge, H. Yang, Z. Ring,** Appl. Catal., 2005, Vol. 294.

3. *Hydrodenitrogenation of a mixture of basic and non-basic polynuclear aromatic nitrogen compounds.* **M. Nagai, T. Masunaga,** Fuel, 1987, Vol. 67.

4. *Kinetics of hydrogen uptake and release from heteroaromatic compounds for hydrogen storage.* **F. Sotoodeh, K.J. Smith,** Ind. Eng. Chem. Res., 2010, Vol. 49.

5. *Quantum chemistry of adsorption and hydrogenation of DBT and carbazole on NiMoS using ZINDO / I method.* **A. Duan, J. Gao, C. Xu, D. Wang, Z. Zhao, T. Dou, K.H. Chung,** Mol. Simul., 2007, Vol. 33.

6. *Pyrrole hydrogenation over Rh (111) and Pt (111) single-crystal surfaces and hydrogenation promotion mediated by 1-methylpyrrole: A kinetic and sum - frequency generation vibrational spectroscopy study.* **C. J. Kliewer, M. Bieri, G. A. Somorjai,** J. Phys. Chem. C, 2008, Vol. 112.

7. *Deep hydrotreating of middle distillates from crude and shale oils.* **M. V. Landau,** Cat. Today, 1997, Vol. 36.

8. *Catalytic hydrogenolysis on metals.* **J. H. Sinfelt,** Cat. Lett., 1991, Vol. 9.

9. *Organic nitrogen compounds in gas oil blends, their hydrotreated products and the importance to hydrotreatment.* **P. Zeuthen, K.G. Knudsen, D.D. Whitehurst,** Cat. Today, 2001, Vol. 65.

10. *The reactions of hydrogen with derivatives of pyrrole II.* **J. L. Rainey, H. Adkins,** J. Am. Chem. Soc, 1939, Vol. 61.

11. *The reduction of the carbazole nucleus. Some derivatives of hydrocarbazoles.* **H. Dressler, E. M. Baum,** J. Am. Chem. Soc., 1960, Vol. 26.

12. *The energetics of tetrahydrocarbazole aromatization over Pd (111): A computational study.* **P. Crawford, R. Burch, C. Hardacre, K.T. Hindle, P. Hu, D. W. Rooney,** J. Chem. Phys., 2008, Vol. 128.

13. *Preeliminary study on mechanism of naphtalene hydrogenation to form decalins via tetralin over Pt/TiO_2.* **K. Ito, Y. Kogasaka, H. Kurokawa, M. Ohshima, K. Sugiyama, H. Miura,** Fuel Proc.Tech, 2002, Vol. 79.

14. *Reactivities, reaction networks and kinetics in high-pressure catalytic hydroprocessing.* **M. J. Girgis, B. C. Gates,** Ind.Eng.Chem.Res, 1991, Vol. 30.

15. *Comaprison of hydrodenitrogenation of model basic and nonbasic nitrogen species in a trickle bed reactor using comercial NiMo/Al_2O_3 catalyst.* **D. Ferdous, A. K. Dalai, J. Adjaye,** Energy Fuels, 2003, Vol. 17.

16. *Active sites of a reduced molybdena-alumina catalyst. A transient study of hydrodenitrogenation of carbazole and acridine.* **M. Nagai, T. Masunaga.** Bull. Chem. Soc. Jpn., 1989, Vol. 62.

17. *The selective hydrogenation of derivatives of pyrrole, indole, carbazole and acridine.* **H. Adkins, H. L.Coonradt,** J. Am. Chem. Soc., 1940, Vol. 63.

18. *Correlating the electronic properties and HDN reactivities of organonitrogen compounds: an ab initio DFT study.* **M. Sun, A.E. Nelson, J. Adjaye,** J. Mol. Catal. A, 2004, Vol. 222.

19. *Aromaticity in heterocyclic compounds.* **R. R. Grupta, T. M. Krygowski, M. K. Cyranski.**Springer-Verlag Berlin Heidelberg, 2009.

20. *A FT-IR study of the adsorption of indole, carbazole, benzothiophene, dibenzothiophene and 4,6-dibenzothiophene over solid adsorbents and catalysts.* **M. A. Larrubia, A. Gutierrez-Alejandre, J. Ramirez, G. Busca,** Appl. Catal. A, 2002, Vol. 224.

21. *Catalytic hydrogenation of model nitrogen, sulfur and oxygen compounds.* **L. D. Rollman,** J. Catal., 1977, Vol. 46.

22. *Catalytic hydrogenation of furan and substituted furans on platinum.* **H. A. Smith, J. F. Fuzek,** J. Am. Chem. Soc, 1949.

23. *Hydrodeoxygenation of dibenzofuran and related compounds.* **S. Krishnamurthy, S. Panvelker,Y. T. Shah,** AlChE J., 1981, Vol. 27.

24. *Structure-activity relationships in hydroprocessing of aromatic and heteroaromatic model compounds over suldified NiO-MO_3 / gamma Al_2O_3 and NiO-WO_3 / gamma Al_2O_3 catalyst; chemical evidence for the existance of two types of catalytic sites.* **C. Moreu, C. Aubert, R. Durand, N. Zmimita,P. Geneste,** Catal. Today, 1988, Vol. 4.

25. *Catalytic functionalities of supported sulfides. IV C-O hydrogenolysis selectivity as a function of promoter type.* **J. Shabtai, N. K. Nag, F. E. Massoth,** J. Catal., Vol. 104.

26. *Deep HDS of diesel fuel: chemistry and catalysis .* **T.C.Ho,** Catal.Today, 2004, Vol. 98.

27. *Factors controlling the development of the HYD route of desulfurization of DBT over gamma alumina supported Pt and Pd catalyst.* **V. G. Baldovino-Meldano, P. Ely, E. M. Gaigneaux, S. A. Giraldo, A. Centeno,** Cat. Today, 2010, Vol. 150.

28. *Aromatic hydrogenation catalysis: A review.* **A. Stanislaus, B. H. Cooper,** Catal. Rev, Vol. 36.

29. *IV.B.2. Hydrogen storage by reversible hydrogenation of liquid-phase carriers.* **A. Cooper, A. Scott, D. Fowler, J. Cunningham, M. Ford, F. Wilhelm, V. Monk, H. Cheng, G. Pez.**. Air Products-report, 2008.

30. *Catalytic hydrogenation and hydrocracking of fluorene: reaction pathways, kinetics, and mechanism.* **A. T. Lapinas, M. T. Klein, B. C. Gates,** Ind. Eng. Chem. Res, 1991, Vol. 30.

31. *Hydrodenitrogenation catalysis.* **T. C. Ho,** Catal. Rev. Sci. Eng., 1988, Vol. 30.

32. *Acridines.* **R. M. Acheson.** Interscience Publishers, 1973.

33. U.S.Patent 7101530. **G. Pez, R. Aaron, A.C. Cooper, H. Cheng,** *Freepatentsonline, 2006*

Chapter 9. Conclusions

Liquid organic hydrides (LOH) are considered for use in reversible hydrogen storage because they present several advantages over other known hydrogen storage systems. However, to make the economics feasible of this approach for a large scale application, development of efficient and cheap methods of recyclability of the spent material is critical.

In the present work, the hydrogenation of 9-ethylcarbazole as a prototype of liquid organic hydride (LOH) was studied in detail, in order to shed a light on the possible difficulties that might be encountered during hydrogen re-charging step. In the first part of the work, the direct and integrated system based on hydrogenation of 9-ethylcarbazole in the molten state was presented. The successful reversible hydrogenation of the substrate was demonstrated under moderate operating conditions. Several synthetic as well as commercially available catalysts based on noble metal and nickel were experimentally screened. A very active catalyst, nominal 5 wt % Ru/Al_2O_3 was synthesized by means of mild chemical reduction, which showed better performance than its commercially available counterparts. In addition, the selectivity and the activity of the hydrogenation reaction was found to be dependent on the type of the metal and support used. Moreover, the structures of all of the reaction products and intermediates of hydrogenation of 9-ethylcarbazole over ruthenium catalyst were assigned for the first time using combined GC-MS and NMR analysis. It was shown that the final fully saturated product is a mixture of symmetric and asymmetric isomers. The obtained structures of the most stable intermediates and products of the reaction agreed well with the theoretically predicted structures using DFT calculations. These structures proved that the hydrogenation of the 9-ethylcarbazole was not taking place as a simple concerted reaction, but involved several simultaneous reactions including isomerization steps. Consequently, the detail study of the

reaction mechanism of 9-ethylcarbazole hydrogenation was conducted over ruthenium based catalysts, which were found to be most active in the preliminary studies. The study of the reaction pathway was conducted in solvent phase due to some technical difficulties. The kinetic model of the hydrogenation reaction over ruthenium based catalysts was developed which fitted well with the experimentally obtained data. The developed reaction model accounted for different type of active sites present on the supported and unsupported ruthenium catalysts. The activity and selectivity was found to depend directly on the type of the active sites on the surface of the catalyst. The highest activity and selectivity was obtained by 5 wt % Ru/Al_2O_3 produced by chemical reduction. Due to the fact that this catalyst contained small and defective metal particles, the majority of the active sites present were highly unsaturated sites such as edges and corners. On this type of active sites, the consecutive addition of hydrogen atoms was found to take place effectively without formation of any considerable amounts of any stable intermediates. On the contrary, over the surface of unsupported particles of commercial ruthenium black catalyst, containing mainly flat active sites, the hydrogenation of 9-ethylcarbazole was sluggish and the selectivity obtained was very poor due to the formation of a stable intermediate 9-ethyl-octahydrocarbazole (Pl 8 [H]). The enthalpies of adsorption calculated using DFT methods showed that the enthalpy of adsorption of Pl 8 [H] intermediate is decreased due to the steric constraints imposed by the terraced sites on the surface of ruthenium black. The adsorption of this intermediate on the flat surfaces was found to be further reduced by the presence of ethyl substituent on the nitrogen atom. On the other hand, the calculated energy of adsorption of this intermediate on the highly unsaturated sites was found to be much higher than on the planar surfaces. Thus, it was showed that unsupported ruthenium catalyst with the majority of planar active sites is effective for the initial hydrogenation of 9-ethylcarbazole to intermediate due to enhanced

adsorption of polyaromatic structure with terrace sites, however, further hydrogenation to fully hydrogenated products is hindered by the accumulation of this stable intermediate in the solution. The formation of a stable intermediate with lower nominal hydrogen uptake, results in purifying problems during spent fuel recovery process. On the contrary, the selectivity towards symmetric isomer of the fully loaded product was found to be higher on the unsupported catalyst with majority of flat active sites. Because of the fact that the low coordination sites imposed less steric hindrance to subsequent hydrogen additions to Pl 8 [H], this intermediate was able to add hydrogen atoms to either sides of the molecule, leading to the formation of additional asymmetrical Pl 12 [H] products. Taking into consideration the dehydrogenation process, the formation of single isomer of the fully loaded compound is more desirable. Different geometries and energetic of stereoisomers could cost selectivity and activity problems in reversible process. Thus, based on the obtained results, it can be concluded that the optimization of an active catalyst for efficient re-hydrogenation of 9-ethylcarbazole based fuel should be focused on obtaining the right balance between terraced and low coordination sites on the catalyst. In addition, it was found from the XPS study that the possible modes of adsorption of the substrate and intermediates on the surface of the catalyst can be influenced by tailoring the electron density of the metal. Taking into consideration the clear difference between the activity and selectivity in hydrogenation of 9-ethylcarbazole over supported and unsupported catalyst, the reaction kinetics were studied over these two types of catalysts. The 9-ethylcarbazole hydrogenation was found to follow a first order with respect to the concentration of the aromatic substrate and zero order in concentration of hydrogen gas. The apparent activation energies of 57.9 kJ /mol over 5 wt % Ru/Al_2O_3 catalyst and 64.7 kJ /mol over ruthenium black catalyst were obtained. The experimentally obtained product distributions versus time in the range of temperatures were modelled for both of the

catalysts and the activation energies were calculated for the intermediate reactions involved in the hydrogenation of 9-ethylcarbazole. The temperature and pressure was found to influence the selectivity of the catalysts and the composition of the final product. The calculated activation energies of intermediate reactions over both catalysts showed that the activation energy of production of Pl 8 [H] stable intermediate was always lower than the activation energy required for its further conversion. Overall, it was found that the lowest optimal condition for this reaction to take place at reasonable rate over the most active catalyst studied in this work was 70 bar of hydrogen pressure and 130 °C. These conditions are highly energetically demanding taking into consideration fuel recovery on the large scale. Thus, influence of the type of the metal and support on the reaction selectivity and hydrogenation activity of the substrate were investigated in order to gain more detailed knowledge of the catalyst - reaction pathway/activity correlation in hydrogenation of 9-ethylcarbazole. From the results obtained over various catalysts, the type of products and intermediates was found to be constant regardless of the metal or support used. The isomerisation reaction of the fully loaded product was more prominent over supported catalysts. Additionally, regardless of the metal used, the supported catalysts were found more active than their unsupported counterparts. The production and stability of the Pl 8 [H] intermediate was found to be determined solely by the type of the metal present in the catalyst. The hexagonal close packed Ru metal giving unique surface feature resulted in weaker adsorption of Pl 8 [H] intermediate on the catalyst's surface as compared to other cubic close noble metals, hence accounting for its high stability in the solution. In addition, further conversion of this intermediate was found to be easier over supported catalysts. Furthermore, the type of support did not alter the pathway of the reaction but was found to have an influence on the relative concentration of intermediates and the composition of the fully saturated product. Last but not least, the correlation of the

structure of the LOH on the activity and selectivity in hydrogenation reaction was also examined. It was found that the hydrogenation activity is higher for structures containing centrally fused six membered ring than those involving five-membered ring. Moreover, the presence of the heteroatom increased drastically the rate of the hydrogen loading reaction. In addition, the presence of the substituent on the nitrogen ring decreased the hydrogenation activity of the molecule by imposing steric hindrance effect in the interaction between substrate and metal, prohibiting the former from adsorption. Moreover, the presence of oxygen in the ring or substituent increased the rate of hydrogenation over ruthenium black catalyst. However, on the other hand, oxygen heteroatom can lead to unfavourable reactions for efficient recovery of the spent fuel such as hydrogenolysis, ring opening and heteroatom removal (hydrodeoxygenation). The stable intermediate Pl 8 [H] with unsaturated ring was found to be produced only over defined heterocyclic structures and its stability was influenced by the electonegativity of the heteroatom, or/and steric hindrance effects.

Overall, based on this study, it is clear that storing hydrogen in polyaromatic compounds is not a straightforward method, but rather very complex approach. Therefore, it does not seem to be a direct solution for mobile applications onboard of the vehicles that could compete with well established methods such as high pressure cylinders in the near future. The use of LOH for reversible hydrogen storage gives a number of related problems, most of them underlined in the present work. Considering the optimisation of the spent fuel recovery process, the hydrogenation of fused aromatic rings with good theoretical hydrogen storage values requires harsh reaction conditions which may not be economically feasible on a large scale. In addition, the weight capacities of these organic carriers are not high enough to be able to reach the DOE system targets for mobile applications. It could be expected that simply increasing the number of fused rings could increase the possible

hydrogen uptake capabilities. However, it should be noted based on the presented results that the hydrogenation of such complex structures with a number of fused rings increases complexity of the pathway of reversible reaction as well as increases the number of possible side reactions such as ring opening / isomerisation. Additionally, depending on the catalyst, as it was shown here, the hydrogenation reaction can result in formation of a stable intermediate or intermediates, which would decrease the theoretical hydrogen uptake leading to expensive purification procedures. Beside all these pointed out difficulties, the design of the high capacity LOH would require additional consideration of the following points; the toxicity of the compound, safety of use, its biodegradability and thermal decomposition as well as inexpensive production routes using biomass. Taking all of these issues into account it is believed that optimisation of the effective catalytic system for such reactions would appear exceedingly challenging for wide spread applications, especially in transportation sector. Nevertheless, it would be more likely that hydrogen storage strategy based on LOH may find niche applications in smaller portable technologies such as mobile phones, laptops, or electric bicycles, scooters or jet- ski or stationary use in the power stations.

However, in order to achieve further progress toward commercialization of this hydrogen storage strategy, there is still a lot of work to be done, especially in designing effective catalytic systems for reversible hydrogenation. Therefore, future work should be focused on studying the activity and selectivity of novel bimetallic or core-shell catalysts in the hydrogenation of the model compounds. In addition, active search for new LOH structures preferably containing nitrogen heteroatom, displaying feasible kinetics and thermodynamics of reversible hydrogenation should be continued. Additionally, an interesting approach would be to carefully design and synthesise new organic carriers

following the obtained fundamental understanding of interactions between organic molecules and catalyst surfaces.